Proceedings of International Conference
Applications of Structural Fire Engineering
Prague, 19-20 February 2009

Session 4

Concrete Structures

BASIC APPROACH FOR THE DIAGNOSIS OF CONCRETE AFTER FIRE EXPOSURE

Emmanuel Annerel [a], Luc Taerwe [b]

[a,b] Ghent University, Laboratory Magnel for Concrete Research, Ghent, Belgium

INTRODUCTION

Generally, concrete structures have a very good fire resistance. Although damage to the concrete gradually appears with increasing temperature, it is possible to repair the structure after an adequate assessment. To do this in a systematic way, knowledge is necessary concerning residual material properties and methods to assess this strength. The residual strength varies between additional strength loss due to internal expansion reactions and strength recovery due to possibly rehydration processes ([1], [2] and [3]). Since the residual strength is temperature dependent, methods may be used to assess the strength indirectly by measuring the alteration in the material as function of the temperature. [1] and [2] illustrate how cracks appear and the colour of the concrete changes from red (300-600°C) to whitish grey (600-900°C) and buff (900-1000°C). Once these temperatures are obtained, simple calculations based on EN1992-1-2 [4] may be used to determine the residual capacity of concrete elements, as elaborated in [5].

1 RESIDUAL STRENGTH

Table 1 summarizes the mix design of a self-compacting concrete (SCC), a traditional vibrated concrete with siliceous aggregates (TC) and calcareous aggregates (TCk), as well as a high strength concrete (HPC). One hundred fifty millimetre cubes are cured for 4 weeks in an air-conditioned room at a RH >90% and a temperature of 20±1°C, after which they are stored at 60% RH and 20±1°C for drying until testing age (> 17 weeks). Two cubes are heated for each of the examined temperature levels (till 800°C), occurring at a heating rate of 3.5°C/min. The target temperature is kept constant for 750 minutes. The cubes are allowed to cool slowly in the oven, after which they are immediately tested for compression. *Fig. 1* shows how the results are situated around the curves mentioned in EN 1992-1-2 [4]. Tests are executed to determine the influence of the heating rate, duration at target temperature (350°C, 550°C) and cooling method on the residual strength immediately after cooling [1]. The heating rate is changed to 10°C/min for TC and 20°C/min for SCC. The duration at the target temperature is altered to 3600 minutes and the cooling regime is modified into a rapid cooling by quenching under water. Results show that only the cooling method is an important parameter to consider, resulting in an extra drop of the residual strength of 30-35%.

Table 1. Concrete mix design

	SCC siliceous	TC siliceous	TCk calcareous	HPC siliceous
sand [kg/m³]	782	640	663	650
gravel 2-8 mm [kg/m³]	300	525	-	530
gravel 8-16 mm [kg/m³]	340	700	-	720
limestone 2/6	-	-	450	-
limestone 6/20	-	-	759	-
portland cement I 52.5 [kg/m³]	400	350	350	400
water [kg/m³]	192	165	165	132
limestone powder [kg/m³]	300	-	-	-
superplasticizer 1 [l/m³]	2.90	-	-	-
Superplasticizer 2 [l/m³]	-	-	-	16.5
W/C [-]	0.48	0.47	0.47	0.33
compressive strength 28d [N/mm²]	65.9	56.5	60.3	77.3

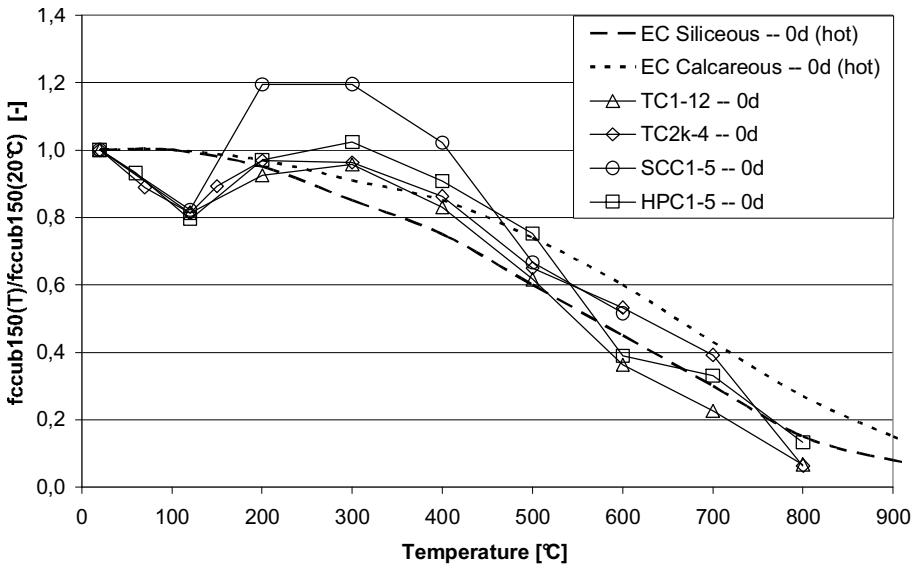

Fig. 1. Residual compressive strength

Besides the test conditions, storage after heating influences the residual strength. One hundred and fifty millimetre cubes TC2k are heated to different target temperatures according to the standard conditions as mentioned before. Furthermore, TC1 cylinders (Ø113mm x 320 mm) are heated at a rate of 1°C/min, kept for 750 minutes at target temperature and slowly cooled in the oven. *Fig. 2* shows an additional strength decrease above 200°C compared to the strength loss due to heating (*Fig. 1*) of about 20% when testing the cubes and cylinders after a period (28 days; 12 weeks) of storage at RH 60% and 20±1°C. These experiments have been repeated for 350°C and 550°C, after which they were stored under water and ambient air [1]. Again an additional strength decrease of 20-30% was observed around 7 days of storage, from where the strength slowly recovers. Strength recovery of up to 10% was found when storing for 56 days under water.

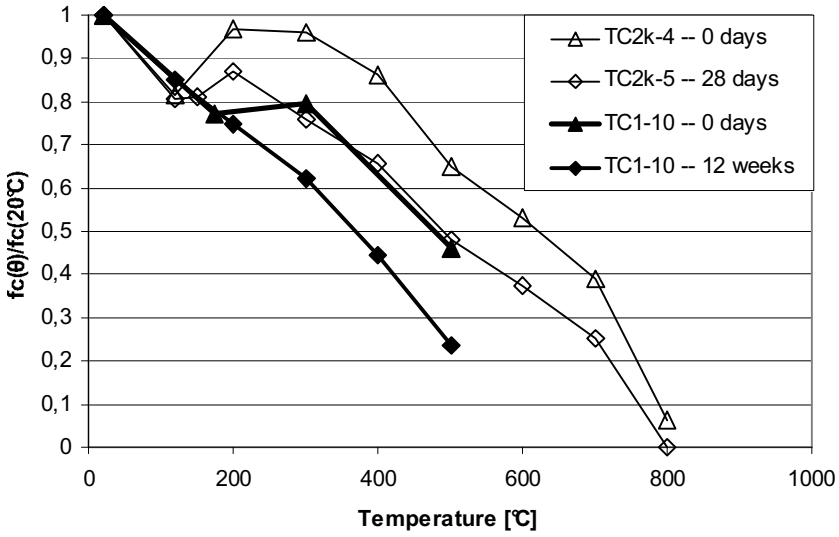

Fig. 2. Further strength decrease of TC2k cubes and TC1 cylinders due to storage in ambient air after heating

2 ASSESSMENT OF THE TEMPERATURE PROFILE

2.1 Colorimetry

The colour is measured with an X-rite SP60 spectrophotometer (aperture 8 mm) according to the CIE Lab-colour space. In this colour system 'L' is the lightness with values between 0 (black) and 100 (white), while 'a' is spread between magenta (positive values) and green (negative values) and 'b' is positioned between yellow (positive values) and blue (negative values). *Fig. 3* shows how the colour measured on cast surfaces describes an elliptical path in the a*b*-colour space. However, differences are noticeable between the 4 concrete types. The measurements are executed immediately after cooling down to ambient temperatures and before the compression test (*Fig. 1*). When storing these cubes under RH 60% and at temperatures of 20±1°C for several weeks, a shift towards the inner part of the ellipse is found [1]. This shift can probably be attributed to the moisture absorption, because a linear relationship between the colour change (L, a, b) and the weight increase exist with a R^2 of 0.7-0.8. Further studies are executed on TC and SCC discs cut from drilled cores, after polishing and masking of the colourful aggregates [1]. These colour alterations provide information to identify the temperature reached inside the concrete after fire exposure.

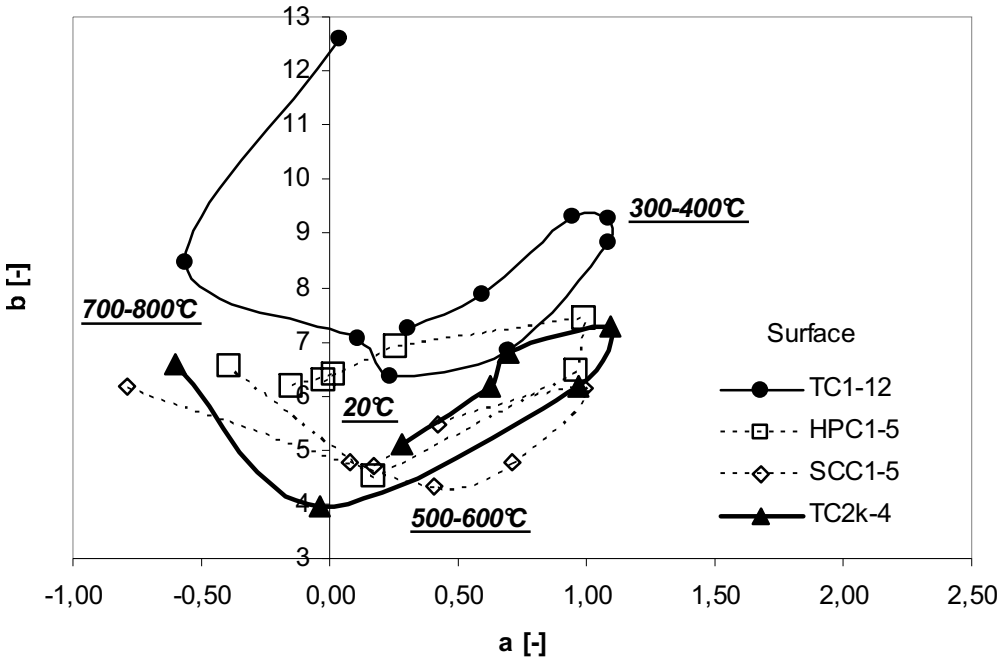

Fig. 3. Colour development at concrete surface

Fig. 4 shows the colour paths described by some heated siliceous aggregates. They are named after their initial colour which is visible when wetting the aggregates. Generally, these aggregates alter in colour towards a reddish tint above 300°C due to the oxidation process of the iron. However, knowledge about the exact colour path could provide more detailed information on the temperature distribution inside a concrete element. The link to the aggregates composition is important, since once changed to red, it is difficult to distinct the different aggregates.

From a batch of siliceous gravel, aggregates which are most present are selected. These aggregates are grinded to powder, after which their composition is determined with EDX under a SEM in low vacuum mode at 200x magnification (*Table 2*). Group 1 is determined by silicon Si with a mutual ratio of around 97 %. Group 2 consists of the same ions (Al, Si, K and Fe) in comparable proportion. The aggregates of group 3 shows higher mutual percentage of calcium Ca, but lower for

silicon Si. Group 4 is characterised by the presence of magnesium Mg. The powders are heated for 3 hours in an electric oven for different target temperatures at a rate of about 30°C/min. The target temperature is raised successively by 50°C: 120°C, 200°C, 250°C, 300°C, …, 1100°C and 1150°C. Between two heating regimes, the colour of the powders is measured with an X-rite SP60 spectrophotometer. The colour of group 1 and 2 alter gradually towards a more orange tint with a maximum at 700°C. From there, the colour changes back to a more grey tint and even white above 1000°C. The path of group 3 is more complicated: a jump is recognisable at 250°C with further increase till 450°C, from where the colour turns halfway back till approximately 700°C. At 1100°C, the aggregate 'blue' is coloured white, while the aggregate 'brown' has turned into orange. Group 4 keeps travelling to an orange tint till around 950°C, from where it turns back in a loop. This green aggregate also shows a jump at 250°C, which is supposed to be caused by the oxidation of the iron oxides. This assumption seems to be right since the aggregates with the largest amount of iron (green, brown) do show a larger colour jump. However, even for the aggregates with no detection of iron (white, blue), a smaller jump is visible. *Fig. 4* illustrates also the colour shift of calcareous aggregates. Although the colour changes from black over blue to white (>700°C: decarbonation), the displacements are small compared to siliceous aggregates.

Table 2. EDX results

	Group 1		Group 2		Group 3		Group 4
At %	white	white-yellow	yellow-brown	brown-iron	brown	blue	green
MgK	-	-	-	-	-	-	2.55
AlK	1.29	-	3.73	7.12	2.24	-	4.92
SiK	97.30	96.76	90.43	86.93	72.40	56.28	85.03
KK	-	-	3.74	4.01	-	-	-
CaK	1.42	-	-	-	22.17	43.73	-
FeK	-	3.24	2.12	1.95	3.21	-	7.51

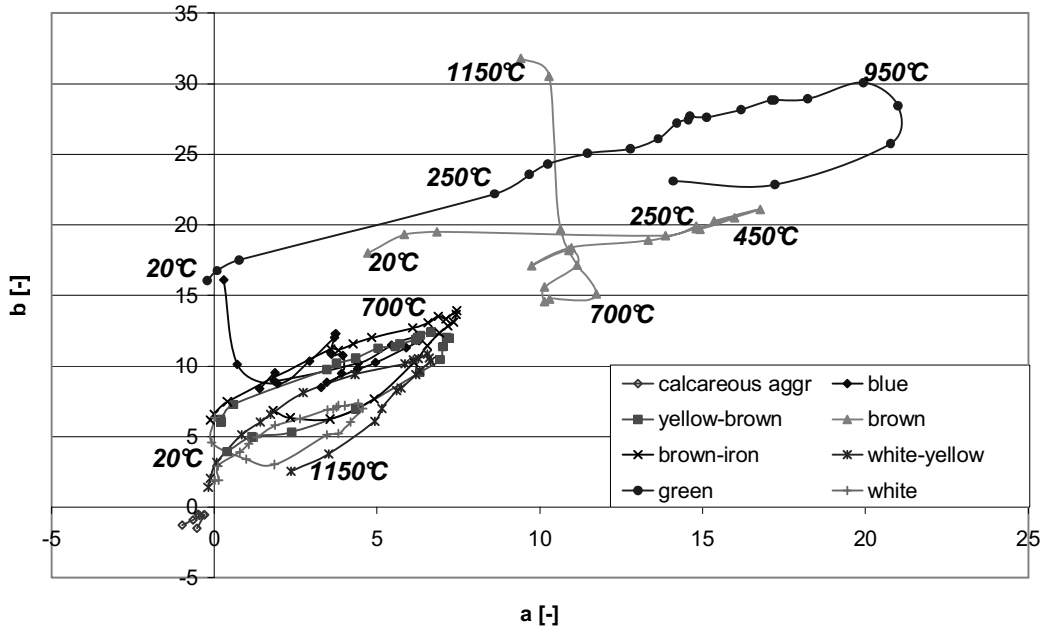

Fig. 4. Colour path of aggregates

2.2 Water immersion

Heating of concrete introduces stresses, resulting in cracks. Meanwhile, chemical alterations, such as dehydration and decarbonation, lead to the disappearance of the hydration products, which increases the pore space (*Fig. 5*) [6]. Hence, these two effects cause an increase of the porosity when heating concrete. Remark that immersion of concrete under water will fill the pores and cracks with water. Then, the weight increase can be used to assess the internal damage due to heating.

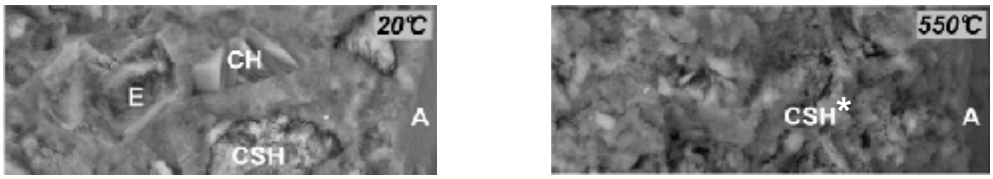

Fig. 5. ESEM images of ordinary Portland concrete at 20°C and heated up to 550°C. (E = ettringite, CH = portlandite, A = aggregate, CSH* = fire altered CSH)

The total water absorption can be defined as the difference in weight after storage under water and a reference weight, for instance the weight at uniform target temperature ($M_{0d,hot}$). After already 7 days, the weight increase flattens. Under in situ circumstances, $M_{0d,hot}$ can be determined from the drilled core by drying it till constant mass. Drying is necessary to eliminate the moisture absorbed due to climatic exposure. Notice that the heated sample itself functions as reference, which is more convenient than searching for an adequate reference concrete that has not been exposed to fire. New made hydration products which may fill some small cracks and thus may hinder the water absorption are neglected in this method. In laboratory conditions, this reference weight is measured during the test when the concrete is at target temperature or after cooling down to 60°C (*Fig. 6*). *Fig. 7* illustrates the water immersion of half cubes (TC1-8, TC2k-1) and small discs (TC1-10) with Ø80mm and 15mm height. These results are transformed in percentages by dividing with the reference weight $M_{0d,hot}$. For the discs, different cooling methods are used: 1) slowly cooling in the oven ('L, oven'); 2) cooling outside the oven at ambient air ('L, 20°C'); 3) cooling by quenching into water ('Water'). The results on half cubes and small discs are comparable, as is visible on the graph for the water absorption of specimens slowly cooled in the oven.

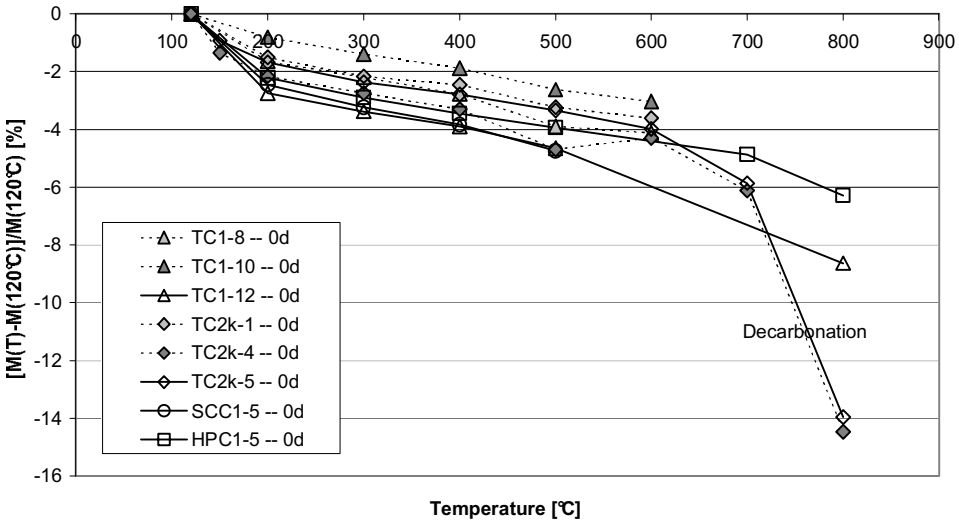

Fig. 6. Weight loss due to heating

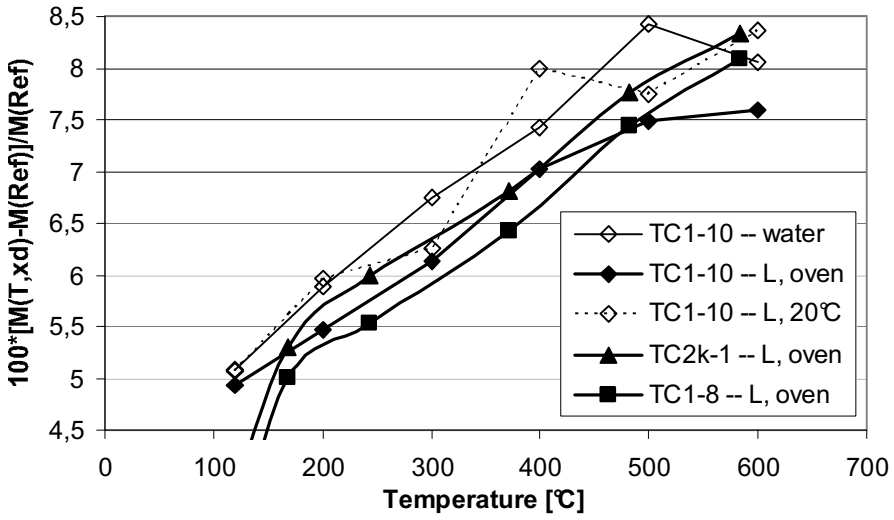

Fig. 7. Water immersion

3 SUMMARY

- The residual strength is mainly influenced by the temperature during heating, the way of cooling and the time of storage after fire.
- Colour analysis and water immersion provide an adequate basis to assess the temperature history of concrete.

4 ACKNOWLEDGMENT

The authors would like to thank the Fund for Scientific Research in Flanders (FWO) for the financial support through the research grant "Damage assessment and estimation of the residual strength of concrete members after exposure to fire". The authors are thankful for the help of TNO Delft and TU Delft (Netherlands) for their contribution to the microscopic research.

REFERENCES

[1] Annerel E., Taerwe L., Approaches for the Assessment of the Residual Strength of Concrete Exposed to Fire. *Proceedings of the International Workshop, Fire Design of Concrete Structures, From Materials Modelling to Structural Performance,* Coimbra, 8th and 9th November, 2007, pp. 489-500

[2] Fib TG 4.3.2, *fib bulletin 46: Fire design of concrete structures – structural behaviour and assessment, state-of-the art report*, july 2008, 209 p.

[3] Fib TG 4.3.1, *fib bulletin 38: Fire design of concrete structures – materials, structures and modelling, state-of-the art report*, april 2007, 97 p.

[4] EN 1992-1-2: 2004 - *Eurocode 2: Design of Concrete Structures – Part 1-2: General Rules – Structural Fire Design*, CEN, Brussels, 2004, 97 p.

[5] Taerwe L., Poppe A.-M., Annerel E., Vandevelde P., Structural Assessment of a Pretensioned Concrete Girder after Fire Exposure. *Proceedings of the 2nd fib Congress,* Napels, 5-8 june, 2006

[6] Liu X., *Microstructural investigation of self-compacting concrete and high-performance concrete during hydration and after exposure to high temperatures*, PhD thesis, Ghent University, 2005-2006, 174 p.

HEATING-INDUCED PRESTRESS VARIATION IN UNBONDED POST-TENSIONED CONSTRUCTION

Potential Consequences for Post-Fire Performance

Luke Bisby [a], Kevin MacLean [b], Colin MacDougall [c]

[a] University of Edinburgh, BRE Centre for Fire Safety Engineering, Edinburgh, Scotland, UK
[b] Read Jones Christoffersen Ltd., Toronto, Canada
[c] Queen's University, Department of Civil Engineering, Kingston, Canada

1 INTRODUCTION

Unbonded post-tensioned (UBPT) concrete is a popular form of construction that allows for rapid erection of economical and sustainable buildings. UBPT buildings are more efficient than non-prestressed concrete construction and make optimal use of the structural materials from which they are constructed [1]. However, this efficiency also causes concerns associated with the performance of UBPT structures at elevated temperatures. In particular, prestressing steel is much more sensitive to temperature than mild steel reinforcement, and it suffers proportionally greater losses in strength and stiffness as temperatures increase. Experimental results from few, limited large-scale furnace tests on isolated UBPT slabs have recently led to concern, and considerable debate, regarding their performance in fire [2]. However, while available tests are instructive, in many important respects their results may not be representative of the performance of real UBPT structures in fire.

Current design requirements for UBPT floors are based on a fundamentally limited understanding of full structural response in fire. Available fire tests on UBPT members have either been furnace tests on isolated beams or slabs [2,3,4], with their numerous, well-documented shortcomings, or are so old as to be of limited relevance to today's advanced concretes and construction methods [4]. There are a number of factors that may be important for UBPT systems in fire that have not yet been identified or adequately considered. In particular, because UBPT structures are typically continuous across multiple bays, sometimes with two-way action within a floor plate and with higher span-to-depth ratios than reinforced concrete slabs, furnace tests on isolated, simply-supported, one-way members with short unbonded lengths cannot be considered as representative (or necessarily conservative). Tendon continuity, compression and tension membrane actions, restraint, spalling, thermal deformations, and non-uniform heating and cooling can all be expected to play important roles in real UBPT structures, both during and after a fire.

Experiments and modelling aimed at predicting the effects of localized heating on UBPT tendons and the potential consequences for the post-fire response of UBPT members are presented in this paper. The issues discussed are related to creep of the stressed tendons at high temperature and are specific to UBPT construction – arising as a consequence of continuity of unbonded tendons, with varying cover, over multiple bays of a structure (some of which may not be heated during a fire).

2 BACKGROUND AND OBJECTIVES

For a given metal, transient creep strains increase with time, temperature, and stress. Since both stress and temperature may be high in the tendons of a fire-affected, post-tensioned structure, large creep strains may develop in shorter times than are normally considered in structural engineering. In the absence of other effects, these creep strains will, along with changes in the elastic properties of the prestressing and thermal expansion, reduce the effective prestress in the structure. This will affect the capacity of the structure both during heating and, since creep strains are irrecoverable on cooling, after a fire. They may also contribute to tendon rupture in extreme cases of localized heating (due to localized cover spalling during fire for example). Creep strains in steel tendons under transient temperature and stress conditions therefore need to be accurately quantified before realistic fire testing or modelling of UBPT members can be performed with confidence.

Data on the creep behaviour of modern post-tensioning tendons under high-stress, high-temperature conditions is scarce, and no high temperature creep data are apparently available for tendon stresses in excess of 690 MPa [5], despite the fact that in-service stress levels in UBPT members may be in the range of 1000-1200 MPa [1]. The objectives of the research presented herein were to: (1) develop a better understanding of, and ability to model, the creep behaviour of prestressing tendons at elevated temperature subjected time-varying stress and non-uniform heating; (2) study the effects of varying the concrete cover and heated length ratio (i.e., the ratio of the heated length of tendon to the overall length of tendon) on the observed/predicted reductions in prestressing force for a typical UBPT flat-plate slab both during and after a fire; and (3) highlight potential concerns for the performance of real UBPT structures during and after a fire.

3 EXPERIMENTS ON LOCALLY-HEATED PRESTRESSING TENDONS

Experiments were performed on locally-heated, prestressed, unbonded, restrained tendons to measure the changes in stress under localized heating and cooling regimes. These tests have been described in detail by MacLean et al. [6]. *Fig. 1* shows the testing apparatus used. A single tendon 6300 mm long was passed through a 610 mm long tube furnace and stressed in a fixed-abutment prestressing bed to a target initial stress of 1000 MPa (after losses). The restrained tendon was then locally heated using one of a number of preselected ramp-soak-cool regimes. The ramp rate for all tests was 10°C/min, chosen to represent typical heating rates for tendons in UBPT concrete slabs. Soak temperatures of 200, 300, 400, 500, and 700°C were held for between 5 and 90 minutes before slow cooling to room temperature. Load cells at both ends of the tendon were used to measure prestress variation, and temperatures were continuously recorded along the tendons' length.

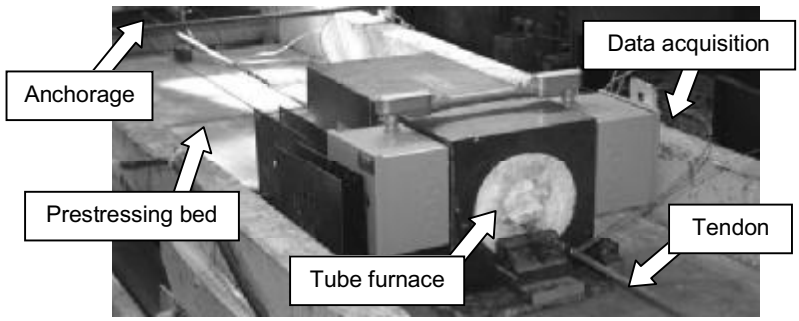

Fig. 1. Experimental apparatus used in relaxation tests on locally-heated unbonded steel prestressing tendons

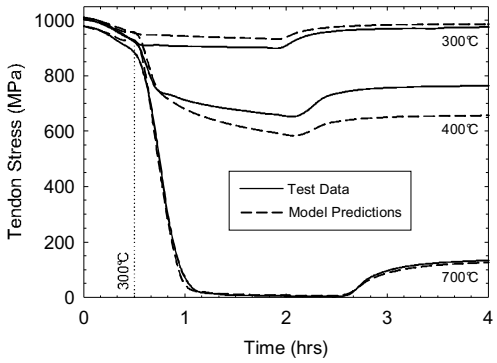

Fig. 2. Comparison of observed and predicted variation in tendon stress levels with localized heating (ramp-soak-cool) to various soak temperatures [8]

As an example of the data obtained during these tests, *Fig. 2* shows the measured variation in tendon stress with exposure to one of three ramp-soak-cool regimes (to 300, 400, or 700°C). The

initial reductions in tendon stress are essentially linear, and are due to thermal expansion of the tendon in the heated region. However, at temperatures above 300°C, the stress reductions accelerate (due to creep/relaxation), causing considerable reductions in effective prestress. The irrecoverability of effective prestress for exposure temperature above 300°C is also clearly evident in this figure.

4 MODELING HIGH-TEMPERATURE CREEP/RELAXATION OF STEEL TENDONS

The transient variation in tendon stress noted in the tests presented above can be predicted using an appropriate computational model which accounts for the spatial and temporal variation in temperature along the length of a heated tendon inside a concrete slab. Such a model has been developed by the authors and is presented in detail by Gales et al. [7]. The analysis procedure divides the tendon into a series of longitudinal thermal regions of assumed constant temperature during a given time step. At the beginning of the analysis, the stress in the tendon is known from the service prestress condition. Given the known time-temperature history of each thermal region along the length of the tendon (taken as measured temperatures from tests [6] or from a simple heat transfer analysis of the structure under consideration [8]) the continuous thermal exposure is discretized into finite time steps of small duration. The changes in strain of each thermal region due to thermal expansion, degradations in elastic properties, and creep can be computed using steady-state high-temperature creep models and parameters available in the literature [7]. The change in length of each thermal region during a given time step can therefore be determined, and the changes in length of all regions subsequently summed over the length of the tendon to determine the stress change required for no net change in length (using temperature-dependent elastic properties). By repeating this procedure at multiple time steps, the full stress-time history can be predicted.
In addition to showing experimental stress-time histories for the tests by MacLean et al. [6], *Fig. 2* includes predictions made using the authors' computational model [7]. The agreement between the test data and model predictions is satisfactory, with the model being conservative in the critical temperature range between 300 and 700°C. It must be stressed that the model is based on an extrapolation of creep parameters derived from steady-state testing up to only 690 MPa [5]. Additional tests are needed to verify the use of these parameters at initial stress levels of 1000 MPa or more, as can be expected under service loading in UBPT structures [1].

5 POTENTIAL CONSEQUENCES: TYPICAL UBPT FLAT SLAB

Given the wide variety of possible forms of UBPT construction, it is difficult to make generalizations regarding their performance in fire. However, for the purposes of illustrating the potential importance of irrecoverable creep-induced tendon stress reductions for locally-heated multiple span tendons in UBPT slabs, a series of analyses were performed using the previously described computational model in conjunction with a typical UBPT flat-slab structure; this is shown in *Figs. 3* and *4* (from Example 3-37 of the CPCI design manual [9], which can be consulted for complete details of the design and reinforcement details).

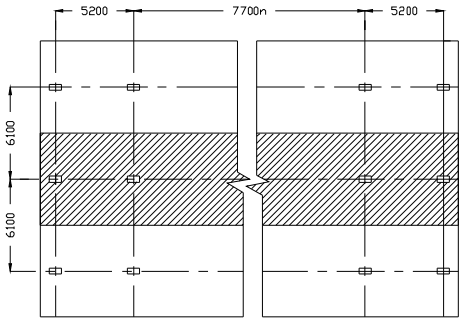

Fig. 3. Example slab with '*n*' interior spans (plan view)

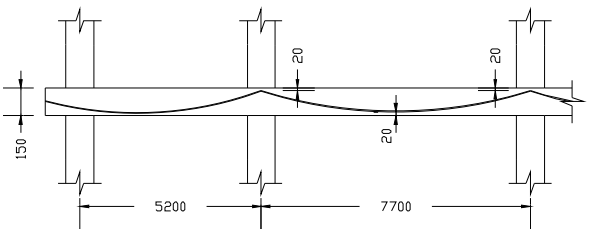

Fig. 4. Example slab end span and interior span (partial elevation view)

The spatial and temporal variation in tendon temperatures along its entire length were determined using a simple one-dimensional heat transfer analysis programmed previously by Bisby [8], and the transient variation in tendon stress was determined using the previously described computational model. During parametric analyses the total tendon length was varied by changing the number of internal bays in the structure while maintaining the same interior and exterior bay dimensions and tendon profiles. The heated length ratio was varied by changing the number of internal bays exposed fire (from below) according to the ASTM E119 [10] standard fire curve. Note that the parabolic tendon profile causes a continuously varying tendon temperature, with higher temperatures in regions with smaller concrete cover.

Fig. 5 shows the predicted variation in tendon stress for three arbitrarily selected heated length ratios: 3 spans with only the interior span heated, 5 spans with one interior span heated, and 5 spans with all three interior spans heated. Also shown in *Fig. 5* are the predicted tendon stress profiles that would be generated if only thermal expansion were considered (i.e., by ignoring creep strains and degradation of elastic properties); the importance of properly accounting for transient effects when modelling these structures is clear. It is also clear that larger heated length ratios show a slightly larger reduction in prestress during heating – due to greater overall thermal expansion of the tendon – although the irrecoverable component is less for these cases (since thermal strains are recoverable). This implies that larger heat length ratios may be more critical *during* a fire, but smaller heated length ratios may be more important in for residual prestress *after* a fire.

Fig. 6 shows the effect of the heated length ratio on the reduction in prestress during fire at 45 minutes, 60 minutes, and 75 minutes. This figure confirms that the influence of the heated length ratio in causing tendon stress reductions is minor during heating, and also highlights the speed with which tendon stress reductions might realistically occur in a fire – again stressing the importance of properly accounting for prestress reductions when modelling (or testing) UBPT structures in fire. More recent work [11] has shown that smaller heated length ratios may lead to tendon rupture.

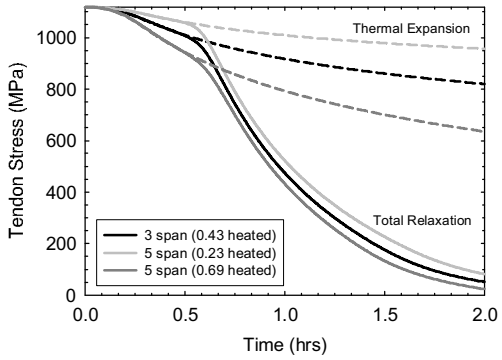

Fig. 5. Predicted variation in tendon stress with for the example structure (effect of heated length ratio)

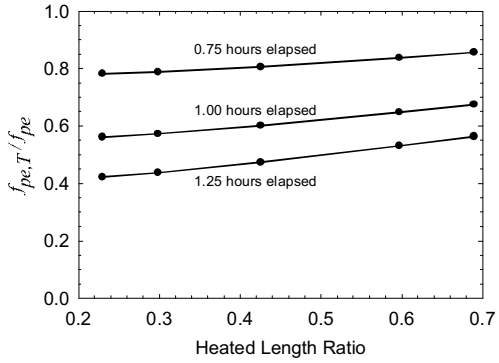

Fig. 6. Predicted effect of heated length ratio on tendon stress levels for the example structure (during exposure to an ASTM E119 [10] fire)

Adequate fire resistance of UBPT structures is currently ensured during the design process by providing sufficient concrete cover to maintain the temperature of the prestressed reinforcement below reasonable limits [1]. Typical specified covers may range between 20 (0.5 or 1 hrs rating) to 80 mm (4 hrs rating), depending on the jurisdiction and on local requirements. To highlight the importance of actually achieving design concrete covers for assuring adequate fire performance, and also to conceptually illustrate the potential consequences of loss of cover due to localized spalling, *Fig. 7* shows the effects of varying the concrete cover at midspan between 10 and 30 mm for the example structure (shifting the tendon profile up or down during the heat transfer analysis) with one internal bay exposed to an ASTM E119 [10] fire.

As expected, *Fig. 7* shows that concrete cover to the prestressed reinforcement has a profound impact on the transient variation in tendon stress, both during and after a fire. For example, after

one hour of fire exposure, the total reductions in tendon stress (from an initial tendon stress value of 1116 MPa, or 60% of ultimate) are 180, 617, and 1028 MPa for 30, 20, and 10 mm concrete cover respectively. Perhaps just as importantly, the irrecoverable portion of the prestress loss for these three cases is 76, 478, and 849 MPa respectively, showing the importance of the above considerations for engineers involved in structural evaluations of fire-damaged UBPT structures, even when damage appears localized.

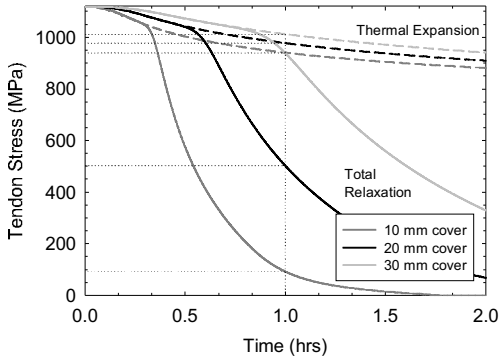

Fig. 7. Predicted variation in tendon stress with for the example structure (effect of concrete cover to the prestressed reinforcement)

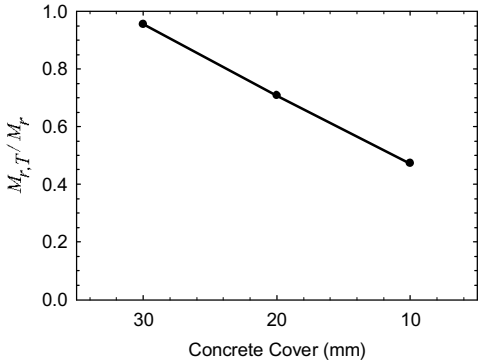

Fig. 8. Predicted variation of post-fire residual midspan positive bending moment capacity with different concrete covers for the example structure (after one hour of fire exposure)

Given that localized heating of UBPT tendons results in irrecoverable reductions in tendon stress both during and after a fire, an obvious question is: what might be the consequences of this for failure of the structure during a fire (when subjected to fire design loads only) or after a fire (when the full design loads must be considered)? Structural performance during a fire depends on many factors that have not been considered in the current analysis. In particular, membrane actions and thermal deformations of the slab must be considered in any rational analysis of the capacity of a real UBPT structure during fire – this is beyond the scope of the current paper and is not treated here.
However, for the purposes of illustration, *Fig. 8* illustrates the potential consequences of localized heating for the post-fire (residual) cross-sectional flexural capacity of the example UBPT slab (at midspan) according to Canadian UBPT slab design guidelines [12]. Very briefly, for a partially-prestressed beam or slab strip, the moment capacity at ultimate limit state can be expressed as sum of the respective moment contributions from the tensile non-prestressed (A_s), prestressed (A_{ps}), and compressive non-prestressed (A_s') reinforcement, about the compressive stress resultant, giving:

$$M_r = \phi_s A_s f_s \left(d_s - \frac{\beta_1 c}{2} \right) + \phi_{ps} A_{ps} f_{pr} \left(d_p - \frac{\beta_1 c}{2} \right) - \phi_s A'_s f'_s \left(d'_s - \frac{\beta_1 c}{2} \right) \quad (1)$$

where ϕ_s, ϕ_{ps}, and ϕ_s' are code-specified material resistance factors, β_1 is a code-specified concrete stress block parameter, d represents the distances of the respective reinforcements from the extreme compression fibre, f represents the stresses in the respective reinforcements at the ultimate condition, and c represents the depth to the neutral axis, determined from force equilibrium at a section as:

$$c = \frac{\phi_s A_s f_s + \phi_{ps} A_{ps} f_{pr} - \phi_{ps} A'_s f'_s}{0.85 \phi_c f'_c b \beta_1} \quad (2)$$

All of the terms in *Eq. 2* are known or can be determined directly, with the exception of tendon stress at ultimate, f_{pr}. For UBPT structures this value is partially dependent on the strain in the concrete at the level of the tendon caused by member deflections, and therefore consists of two

components: (1) the stress created by prestressing operations *after all loses* (the effective prestress force), f_{pe}, and (2) the increase in stress created by member deflection, Δf_{pr}, so:

$$f_{pr} = f_{pe} + \Delta f_{pr} \tag{3}$$

Rational determination of Δf_{pr} is complicated even at ambient temperature because it depends on many factors, including: patterned loading, the span-to-depth ratio, and the amount of bonded non-prestressed reinforcement present. The Canadian code [12] uses an empirical expression defining tendon stress at ultimate in a UBPT concrete member. Tendon stress is defined as:

$$f_{pr} = f_{pe} + \frac{8000}{l_e}(d_p - c_y) \le f_{py} \quad \text{(MPa)} \tag{4}$$

where l_e is the total tendon length between anchorages divided by the minimum number of plastic hinges required to create a failure mechanism in the span being designed, and c_y is the neutral axis depth determined assuming the yield stress of f_{py} in the tendons. The above equations were used to derive the data shown in *Fig. 8*, which shows the importance of reductions in tendon prestress levels after a fire-affected structure has cooled to room temperature and is expected to resist its full factored design load. While this simple illustration should obviously not be considered a rigorous treatment of the problem, it nonetheless confirms the importance of careful consideration of the effects of localized heating of prestressing tendons, particularly given that changes in prestress will manifest themselves not only in the fire damaged region, but also in areas of the structure which may have remained remote from the fire.

6 ACKNOWLEDGMENT

The Authors would like to acknowledge the support of the Natural Sciences and Engineering Research Council of Canada, Queen's University, and Dr. Ivan Campbell.

REFERENCES

[1] Khan, S. & Williams, M., *Post-Tensioned Concrete Floors*, Laxton's, 1995.

[2] Kelly, F. & Purkiss, J., Reinforced concrete structures in fire: a review of current rules, *The Structural Engineer*, 86(19): 33-39, 2008.

[3] Ellobody, E. & Bailey, C., Testing and modelling of bonded and unbonded post-tensioned concrete slabs in fire. *Proc. 5th Int. Conf. on Structures in Fire*, Singapore, pp. 392-405, 2008.

[4] Lee, D. & Bailey, C. The behaviour of post-tensioned floor slabs in fire conditions, *Proc. Int. Congress on Fire Safety in Tall Buildings*, Santander, Spain, pp.183-201, 2006.

[5] Harmathy, T. & Stanzak, W., *Elevated-temperature tensile and creep properties of some structural and prestressing steels*, National Research Council, Ottawa, Canada, 1970.

[6] Maclean, K., Bisby, L. & MacDougall, C., Post-fire assessment of unbonded post-tensioned slabs, *ACI-SP 255*, American Concrete Institute, USA, 2008.

[7] Gales, J., Bisby, L., MacDougall, C. & MacLean, K., Transient high-temperature stress relaxation of prestressing tendons in unbonded construction, *Fire Safety J.*, in press, 2009.

[8] Bisby, L., *Fire Behaviour of Fibre-Reinforced Polymer (FRP) Reinforced or Confined Concrete*, Ph.D. Thesis, Civil Engineering, Queen's University, Kingston, Canada, 2003.

[9] CPCI, *Design Manual*, Canadian Prestressed Concrete Institute, Ottawa, Canada, 1996.

[10] ASTM, *Test Method E119-01: Standard Methods of Fire Test of Building Construction and Materials*, American Society for Testing and Materials, West Conshohocken, PA, USA, 2001.

[11] Gales, J., Bisby, L. & MacDougall, C., Irrecoverable prestress loss in unbonded post-tensioned concrete slabs in fire, *Fire & Materials*, San Francisco, USA, 2009.

[12] CSA, *Design of Concrete Structures*, Canadian Standards Association, Ottawa, Canada, 1994.

FIRE RESISTANCE OF AXIALLY LOADED SLENDER CONCRETE FILLED STEEL TUBULAR COLUMNS

Development of a three-dimensional numerical model and comparison with Eurocode 4

Ana Espinós, Antonio Hospitaler, Carmen Ibáñez, Manuel L. Romero

Instituto de Ciencia y Tecnología del Hormigón (ICITECH)
Universidad Politécnica de Valencia, Camino de Vera s/n, 46022 Valencia (Spain)
aespinos@mes.upv.es, ahospitaler@cst.upv.es, caribus@etsii.upv.es, mromero@mes.upv.es

INTRODUCTION

Filling hollow steel columns with concrete is an interesting way for improving their fire resistance [7]. The temperature at the surface of a hollow structural section without external protection increases quickly during the development of a fire. On the other hand, if the steel tube is filled with concrete, while the steel section loses gradually its resistance and rigidity, the load is transferred to the concrete core, that heats up more slowly, thus increasing the fire resistance of the column.

Besides its structural function, the steel tube acts as a radiation shield to the concrete core, what, combined with a steam layer in the steel-concrete boundary, leads to a lower temperature rise in the concrete core when compared to exposed reinforced concrete structures [7].

During a fire, the temperature distribution in the cross-section of a CFT column is not uniform: steel and concrete have very different thermal conductivities, what generates a behaviour characterized by noticeable heating transients and high temperature differentials across the cross-section. Due to these differentials, CFT columns can reach high fire resistance times without external fire protection [7]. However, it is necessary to resort to numerical models in order to predict accurately these temperature profiles along the fire exposure time [8], [9].

In this work, the finite element analysis package ABAQUS [1] was employed to model the behaviour of slender axially loaded CFT columns exposed to fire. With this software, a sequentially coupled nonlinear thermal-stress analysis was conducted. The results of the simulations were compared with a series of fire resistance tests available in the literature [11], as well as with the predictions of the Eurocode 4 [6] simplified calculation model.

1 DEVELOPMENT OF THE NUMERICAL MODEL

- Finite element mesh

A three-dimensional numerical model was developed in ABAQUS [1], with variable parameters such as the length of the column (L), the external diameter (D), the thickness of the steel tube (t) and the thermal and mechanical material properties. It consisted of two parts: the concrete core and the steel tube. Due to symmetry on the geometry and boundary conditions, only a quarter of the column was modelled.

The three-dimensional eight-node solid element C3D8RT was used to mesh the model. It is an eight-node thermally coupled brick, with trilinear displacement and temperature, reduced integration and hourglass control. The mesh density was controlled to have a maximum element size of 2 cm, what proved to be sufficient to predict with enough accuracy the thermal and mechanical behaviour of the CFT columns under fire.

- Material properties

The numerical model took into account the temperature dependent thermal and mechanical properties of the materials. For concrete, Lie's model [12] was employed, provided that it proved to be the one that best predicted the behaviour of the concrete infill in CFT columns, as said by Hong & Varma [9]. The mechanical model implemented in ABAQUS employed the hyperbolic Drucker-Prager yield surface. The thermal properties for concrete at elevated temperatures were extracted from EN 1992-1-2 [4]. For steel, the temperature dependent thermal and mechanical properties recommended in EN 1993-1-2 [5] were adopted. The isotropic multiaxial plasticity model with the Von Mises yield surface was employed.
The values of the thermal expansion coefficient for concrete and steel recommended by Hong and Varma [9] were employed: α_s = 12 x 10-6 ºC-1, α_c = 6 x 10-6 ºC-1. The moisture content of the concrete infill was not modelled in this research, what lies on the safe side.

- Thermal analysis

For conducting the thermal analysis, the standard ISO-834 [10] fire curve was applied to the exposed surface of the CFT column model as a thermal load. The thermal contact in the steel-concrete boundary was modelled by employing the "gap conductance" and "gap radiation" options. For the governing parameters of the heat transfer problem, the values recommended in EN 1991-1-2 [3] were adopted.

2 VALIDATION OF THE NUMERICAL MODEL

The three-dimensional numerical model was validated by comparing the simulations with experimental fire resistance tests [11] and with the EC4 simplified calculation model [6].

2.1 Comparison with experimental results

The numerical model was employed to predict the standard fire behaviour of a series of CFT column specimens listed in *Table 1*. These specimens were tested at the NRCC, and their results published by Lie & Caron [11]. All the specimens tested were circular, filled with siliceous aggregate concrete and subjected to concentric compression load. Their total length was 3810 mm, although only the central 3048 mm were directly exposed to fire. Because of the loading conditions, all the tests were assumed as fix-ended.

Table 1. List of CFT columns analyzed, from the NRCC research report [11]

Column specimen	D (mm)	t (mm)	f_y (N/mm^2)	f_{ck} (N/mm^2)	N (kN)	$\mu = N / N_{pl,Rd}$	FRR (min)
1	141	6.5	401.93	28.62	131	8.90%	57
2	168	4.8	346.98	28.62	218	15.37%	56
3	219	4.8	322.06	24.34	492	26.19%	80
4	219	4.8	322.06	24.34	384	20.44%	102
5	219	8.2	367.43	24.34	525	18.88%	82
6	273	5.6	412.79	26.34	574	17.08%	112
7	273	5.6	412.79	26.34	525	15.63%	133
8	273	5.6	412.79	26.34	1000	29.76%	70

For each simulation, the axial displacement at the top of the column versus the fire exposure time was registered, comparing this curve with the one obtained in the fire resistance test [11]. *Fig. 1* shows an example of the comparison between both curves for one of the specimens studied.

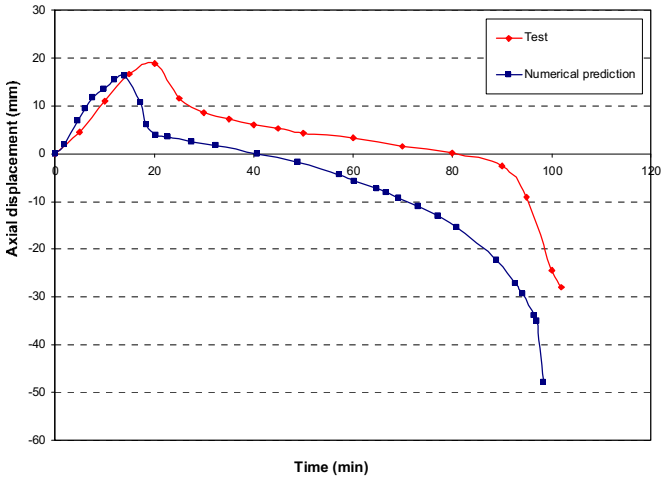

Fig. 1. Comparison between calculated and measured axial displacement, for test no. 4

From this curves, the fire resistance rating (FRR) was obtained for each one of the specimens under study. The failure criteria from EN 1363-1 [2] were adopted. This standard establishes that the failure time is given by the most restrictive from the following two limits: maximum axial displacement and maximum axial displacement velocity. By applying these criteria, the values in *Table 2* were obtained. As it can be seen in *Fig. 2*, most of the values obtained lie in the region of the 15% error, apart from two values, corresponding to column specimens no. 1 and 2, which have the smallest diameters.

The maximum axial displacement (δ_{max}) was also obtained for each of the column specimens studied. *Table 2* shows the calculated and measured values, which are plotted in *Fig. 3*, were it can be seen again that most of the cases lie in the region of the 15% error, apart from specimens no. 3 and 8, corresponding to those with a higher loading level, over the 20% of the maximum load bearing capacity of the column at room temperature.

Table 2. Predicted and measured FRR and maximum axial displacement (δ_{max})

Column specimen	**FRR (min)**		$\xi_{FRR} = \frac{FRR_{test}}{FRR_{NS}}$	**δ_{max} (mm)**		$\xi\,\delta_{max} = \frac{\delta_{max,test}}{\delta_{max,NS}}$
	Test	**Simulation**		**Test**	**Simulation**	
1	57	72	0.79	24.09	24.35	0.99
2	56	75	0.75	20.48	19.25	1.06
3	80	74	1.08	18.13	12.36	1.47
4	102	97	1.05	18.77	16.23	1.16
5	82	68	1.21	20.36	19.30	1.05
6	112	126	0.89	16.40	17.71	0.93
7	133	137	0.97	19.67	18.61	1.06
8	70	70	1.00	5.51	10.35	0.53
	Average		**0.97**	**Average**		**1.03**
	Standard deviation		**0.15**	**Standard deviation**		**0.26**

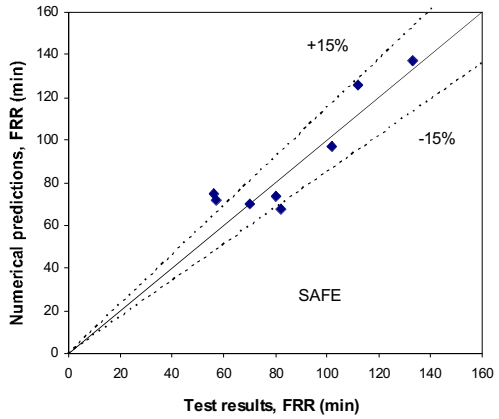

Fig. 2. Comparison of the fire resistance ratings, calculated VS test results

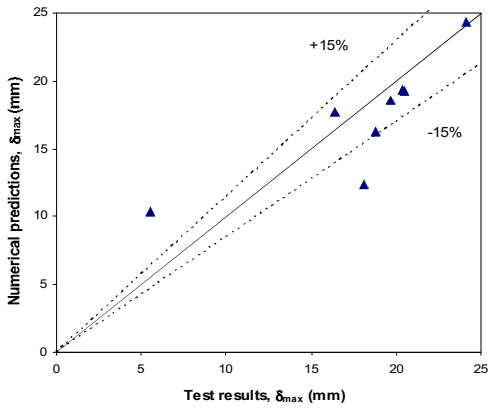

Fig. 3. Comparison of the maximum axial displacement, calculated VS test results

3.2 Comparison with Eurocode 4 simplified calculation model

In this section, the numerical model is compared with the predictions of the EC4 simplified calculation model [6], obtaining the results shown in *Table 3*. It can be seen in *Fig. 4* that the proposed numerical model gives a better prediction of the fire resistance rating, showing a very accurate trend. On the other hand, the EC4 simplified model turns out to be excessively conservative, as shown in the figure. We must note that the EC4 simplified model doesn't take into account the thermal expansion of the materials, nor the air gap at the steel-concrete boundary, what lies on the safe side and gives a very conservative prediction. If we apply these simplifications to our numerical model, smaller values of the fire resistance ratings are obtained, very similar to those predicted by EC4, as shown in *Table 3*. As it can be seen in *Fig. 5*, our predicted values reproduce quite well the results of EC4, except for those tests with fire resistance ratings around 120 minutes, where our numerical model provides more accurate results, what produces a more close to reality trend.

Table 3. Comparison of the numerical model and EC4 predictions with the tests

Column specimen	**FRR (min)**				$\xi_{FRR} = \frac{FRR_{test}}{FRR_{calc}}$		
	Test	**Simulation**	**Simulation (no expansion)**	**EC4**	**Simulation**	**Simulation (no expansion)**	**EC4**
1	57	72	49	49	0.79	1.16	1.16
2	56	75	46	46	0.75	1.22	1.22
3	80	74	52	49	1.08	1.54	1.63
4	102	97	63	61	1.05	1.62	1.67
5	82	68	52	51	1.21	1.58	1.61
6	112	126	118	91	0.89	0.95	1.23
7	133	137	126	96	0.97	1.06	1.39
8	70	70	58	56	1.00	1.21	1.25
				Average	**0.97**	**1.29**	**1.39**
				Standard deviation	**0.15**	**0.25**	**0.21**

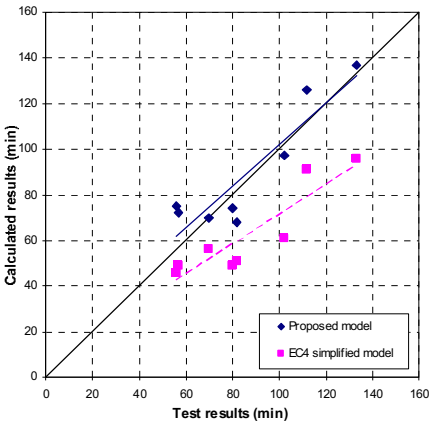

Fig. 4. Comparison of FRR, proposed numerical model VS EC4 model

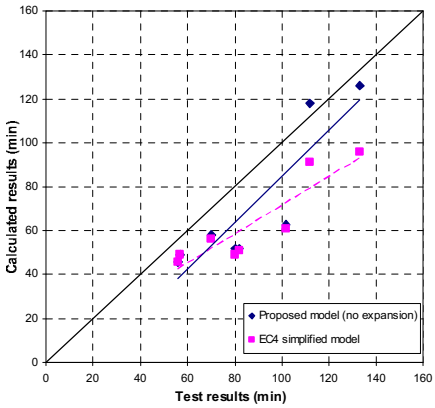

Fig. 5. Comparison of FRR, proposed model (without expansion) VS EC4 model

4. SUMMARY AND CONCLUSIONS

A three-dimensional numerical model for axially loaded slender CFT columns under fire was presented. By means of this model, the behaviour under standard fire conditions of eight column specimens previously tested by the NRCC research group [11] was predicted. The proposed numerical model showed better behaviour for columns with low slenderness and loading levels under 20%. Despite these two aspects, the model shows an accurate response when contrasted with the fire tests.

This study also proved that the predictions of EC4 simplified calculation model [6] can be reproduced with the proposed numerical model by eliminating the thermal expansion of the materials, which lies on the safe side. Nevertheless, if the real behaviour of CFT columns under fire wants to be predicted, this aspect must be taken into account, extending the failure time. The expansion of the steel tube produces an opposed axial strain in the early stages of heating, as well as an opening of the gap in the steel-concrete interface, which delays the heating of the concrete core and thus increases the fire resistance rating.

The proposed numerical model proved to give better predictions than the EC4 simplified model, which turned out to be excessively conservative.

REFERENCES

[1] ABAQUS. ABAQUS/Standard Version 6.6 User's Manual: Volumes I-III. Pawtucket, Rhode Island: Hibbit, Karlsson & Sorenson, Inc.; 2005.

[2] EN (European Committee for Standardisation). EN 1363-1: Fire resistance tests. Part 1: General requirements. Brussels: CEN; 1999.

[3] CEN (European Committee for Standardisation). EN 1991-1-2, Eurocode 1: Actions on structures, Part 1.2: General actions - Actions on structures exposed to fire. Brussels: CEN; 2002.

[4] CEN (European Committee for Standardisation). EN 1992-1-2, Eurocode 2: Design of concrete structures, Part 1.2: General rules – Structural fire design. Brussels: CEN; 2004.

[5] CEN (European Committee for Standardisation). EN 1993-1-2, Eurocode 3: Design of steel structures, Part 1.2: General rules – Structural fire design. Brussels: CEN; 2005.

[6] CEN (European Committee for Standardisation). EN 1994-1-2, Eurocode 4: Design of composite steel and concrete structures, Part 1.2: General rules - Structural fire design. Brussels: CEN; 2005.

[7] CIDECT. Twilt L, Hass R, Klingsch W, Edwards M, Dutta D. Design guide for structural hollow section columns exposed to fire. CIDECT (Comité International pour le Développement et l'Etude de la Construction Tubulaire). Cologne, Germany: Verlag TÜV Rheinland; 1996.

[8] Ding J, Wang YC. Realistic modelling of thermal and structural behaviour of unprotected concrete filled tubular columns in fire. Journal of Constructional Steel Research 2008; 64:1086-1102.

[9] Hong S, Varma AH. Analytical modeling of the standard fire behavior of loaded CFT columns. Journal of Constructional Steel Research 2009; 65:54-69.

[10] ISO (International Standards Organization). ISO 834: Fire resistance tests, elements of building construction. Switzerland: International Standards Organisation; 1980.

[11] Lie TT, Caron SE. Fire resistance of circular hollow steel columns filled with siliceous aggregate concrete: Test results. Internal report No. 570. Ottawa, Canada: Institute for Research in Construction, National Research Council of Canada; 1988.

[12] Lie TT. Fire resistance of circular steel columns filled with bar-reinforced concrete. Journal of Structural Engineering-ASCE 1994; 120(5):1489-1509.

NUMERICAL AND EXPERIMENTAL DETERMINATION OF
residual concrete strength after action of fire

Meri Cvetkovska [a], Petar Cvetanovski[b], Viktor Mihajlov[c]

[a] Ss."Cyril and Methodius" University, Faculty of Civil Engineering, Skopje, Macedonia
[b] Ss."Cyril and Methodius" University, Faculty of Civil Engineering, Skopje, Macedonia
[c] Ss."Cyril and Methodius" University, Faculty of Civil Engineering, Skopje, Macedonia

INTRODUCTION

A reinforced concrete structure exposed to fire should undergo a significant damage. Based on experience and on data collected through detailed visual survey of fired structural elements, the following characteristic damages can be recorded: change of the concrete colour (red, grey-yellow, yellow, fig.1); fissures and cracks inside the concrete mass; cracks along main reinforcement in columns, beams and slabs; crushing of concrete and falling off the concrete parts along the edges of linear elements up to the reinforcement. The possibility for adequate repair of the damaged elements and the measures that have to be done in that case, directly depend on the level of the damages caused during the fire action, as well as in the cooling period. One of the most important factors that directly influence the repairing possibility is the residual compressive strength of concrete. The mechanical properties of the reinforcement decrease as well, but in the cooling phase they increase again.

Temperature over 400^0C causes irreversible reduction of the compressive strength and other mechanical properties of concrete. The compressive strength of concrete does not recover in the cooling phase because of initial degradation and chemical decomposition of the cement past. The residual compressive strength of concrete should be determinate by laboratory tests of specimens taken from the RC elements exposed to fire, but very often this procedure is impractical because additional destruction of the damaged elements is not advisable. Because of the position of the reinforcement in the surface layers of the cross section, taking the specimens from columns and beams is more complicated and is not advisable. In such cases the problem can be solved by using a numerical procedure, based on the nonlinear transient heat flow analysis and the nonlinear stress-strain analysis. When the residual compressive concrete strength is numerically determined, it's value is assumed to be the same as the value that corresponds to the maximum concrete temperature.

The program FIRE solves this problem. This program carries out the nonlinear transient heat flow analysis (modulus FIRE-T) and nonlinear stress-strain response associated with fire (modulus FIRE-S). The solution technique used in FIRE is a finite element method coupled with time step integration.

1 NUMERICAL PROCEDURE FOR RESIDUAL CONCRETE STRENGTH DETERMINATION

The residual concrete strength directly depends on the maximum achieved temperature in the cross section of the fire exposed concrete elements. The temperature distribution in the cross section of the elements can be calculated once the Theory of Heat Transfer is used. The governing differential equation of heat transfer in conduction is:

$$\frac{\partial}{\partial x}(\lambda_x \frac{\partial T}{\partial x}) + \frac{\partial}{\partial y}(\lambda_y \frac{\partial T}{\partial y}) + \frac{\partial}{\partial z}(\lambda_z \frac{\partial T}{\partial z}) = \rho c \frac{\partial T}{\partial t} \quad (1)$$

where: λ is a thermal conductivity (temperature dependent);
ρ is a density of the material (temperature dependant);
c is a specific heat (temperature dependent).

The fire boundary conditions can be modelled in terms of both convective and radiative heat transfer mechanisms. The heat flow caused by convection is:

$$q_c = h_c(T_z - T_f) \tag{2}$$

where h_c is coefficient of convection (for surface directly exposed to fire h_c=25W/m^2 K, and for the unexposed surface h_c=9 W/m^2 K. These values are recommended in EC 2, part 1.2);

T_z is the temperature on the boundary of the element;

T_f is the temperature of the fluid around the element.

The heat flow caused by radiation is:

$$q_r = V\varepsilon\sigma_c({T_{z,a}}^4 - {T_{f,a}}^4) = h_r\left(T_z - T_f\right) \tag{3}$$

$$h_r = V\varepsilon\sigma_c\left(T_{z,a}^2 + T_{f,a}^2\right)\left(T_{z,a} + T_{f,a}\right) \tag{4}$$

where: h_r is coefficient of radiation (temperature dependant);

V is a radiation view factor (recommended $V = 1.0$);

ε is a resultant coefficient of emission $\varepsilon = \varepsilon_f\varepsilon_z$; $\varepsilon_f = 0.8$ is coefficient of emission for the fire compartment; $\varepsilon_z = 0.7$ is coefficient of emission for the surface of the element;

σ_c is Stefan-Boltzmann constant;

$T_{z,a}$ is the absolute temperature of the surface; $T_{f,a}$ is the absolute temperature of the fluid.

Using a typical Galerkin finite element approach *Eq. (1)* assumes the form:

$$\int_V N^T\left[\lambda_x\frac{\partial^2 T}{\partial x^2} + \lambda_y\frac{\partial^2 T}{\partial y^2} + \lambda_z\frac{\partial^2 T}{\partial z^2} - \rho c\frac{\partial T}{\partial t}\right]dV = 0 \tag{5}$$

where the approximation field function is expressed in terms of the interpolation function as:

$$T = N \cdot T_e \tag{6}$$

Integration of *Eq. (5)* by parts yields:

$$\int_V\left(\left[\frac{\partial N}{\partial x}\right]^T\lambda_x\frac{\partial T}{\partial x} + \left[\frac{\partial N}{\partial y}\right]^T\lambda_y\frac{\partial T}{\partial y} + \left[\frac{\partial N}{\partial z}\right]^T\lambda_z\frac{\partial T}{\partial z}\right)dV - \int_S N^T\left(\lambda_x l_x\frac{\partial T}{\partial x} + \lambda_y l_y\frac{\partial T}{\partial y} + \lambda_z l_z\frac{\partial T}{\partial z}\right)ds$$

$$+ \int_V \rho c N^T T dV = 0 \tag{7}$$

where:
$$q = q_c + q_r = (h_c + h_r)(T_z - T_f) \tag{8}$$

Finally, the governing equation takes the form:

$$C\dot{T} + (K_1 + K_2)T + RT = P \tag{9}$$

where: C is a heat capacity matrix (temperature dependent): $C = \int_V \rho c N^T N dV$

K_1 is the conductivity matrix (temperature dependent): $K_1 = \int_V B^T D B dV$

K_2 is the convective matrix: $K_2 = \int_S h_c N^T N dS$

R is the radiative matrix (temperature dependent): $R = \int_S h_r N^T N dS$

P is the external heat flow vector (caused by convection and radiation on the surface of the element and is temperature dependent): $P = \int_S h_c T_f N^T dS + \int_S h_r T_f N^T dS$

$\dot{T}$ is the vector of temperature derivatives

T is the vector of unknown temperatures in the nodal points of the element.

If the heat capacity of the material is taken under consideration and if thermal load is time dependent, the problem becomes transient and for solving the *Eq. (9)* an iterative procedure has to be used. In a small time interval we assumed that the time derivative of the temperature is constant:

$$\dot{T}_t = \dot{T}_{t+\Delta t} = \frac{T_{t+\Delta t} - T_t}{\Delta t} \tag{10}$$

By summarizing *Eq. (9)* for time t and $t + \Delta t$ and assuming that the capacity matrix in small time interval is constant: $C_t = C_{t+\Delta t}$, the heat flow equation for a small time step becomes:

$$\left[K_{t+\Delta t} + \frac{2}{\Delta t} C_t\right] T_{t+\Delta t} = \left[-K_t + \frac{2}{\Delta t} C_t\right] T_t + P_{t+\Delta t} + P_t \tag{11}$$

Eq. (11) together with the initial and boundary conditions completely solves the problem. Taking the radiation into account makes the problem nonlinear. This problem is solved by involving new iterative procedure in every time step. Problem becomes nonlinear too, when temperature dependent physical properties of the materials are assumed. In that case the conductivity and capacity matrix are defined at the beginning of each time step based on the temperature from the previous time step.
The modulus FIRE-T solves the governing differential equation of heat transfer in conduction and in that purpose the following assumptions are made: a fire can be modelled by a single valued gas temperature history: ASTM E119, ISO 834 or SDHI (short duration, high intensity) fire model; no contact resistance to heat transmission at the interface between the reinforcing steel and concrete occurs; the fire boundary conditions can be modelled in terms of both convective and radiating heat transfer mechanisms; the temperature dependant material properties are known (recommended in Eurocode 2, part 1.2); while cracks appear, or same parts of the element crush, the heat penetrates in the cross section easier, but in this study it is neglected. It has been assumed that the heat flow is separable from the structural analysis.
The modulus FIRE-S defines the nonlinear stress-strain response of structure in case of fire. This modulus enables use of temperature dependant $\sigma - \varepsilon$ curves for steel and concrete based on experimental data, or use of theoretical curves. A stress-strain law for concrete under uniaxial loading consists of two parts: a compressive part and a tensile part. Parameters that completely define this curve are temperature dependant and for various temperature intervals they are given in EC 2, part 1.2. The compressive concrete strength "f_c" decreases with temperature, strain at compressive strength "ε_{c1}" increases with temperature and the ultimate crushing strain "ε_{cu}" increases with temperature.

2. TEST EXAMPLE FOR NUMERICAL PROCEDURE

A twenty storey building structure was in fire and two apartments at the seventh and eighth floor were completely burned. Primary, the fire was caused by gas explosion, but the synthetic materials in the apartment were additional fire load, so very high temperatures were reached and the fire time was more than four hours. Thermal and structural response of four-bay, five-story reinforced concrete frame (only one part of the whole frame with defined support conditions) exposed to fire scenario at the two floors only, has been investigated analytically. Elements geometry; support conditions; concrete cover thickness; type of aggregate; compression strength of concrete; steel ratio and defined fire scenario were taken into account while the nonlinear and transient temperature field and the concrete strength reduction in the cross section of the elements exposed to fire were determined.

The most damaged column was incorporated into the wall, so it was exposed to fire only from the inside of the compartment, but the temperature on the other side (in the hall) was raising proportionally to the temperature in the fire compartment (the fire flames were coming out through the open door) and the heating was from the both sides, but not with the same intensity. The dimensions of the cross section of this column are 60· 60cm, the compressive strength of the concrete before action of fire was f_c=40MPa (according to national codes this value corresponds to concrete type MB30).

The concrete strength was reduced as a result of high temperatures in the surface layers of the cross section (*Fig.1*). Calculation results indicate that on the side of the fire, in 4-5cm thick layer, which is 17% of the cross section of the column, the strength reduction is significant and the residual strength of concrete is 15Mpa (MB11) in average (*Fig.2*). These results correspond well with experimental results obtained by laboratory testing of specimens taken from the nearest RC wall (B8, *Table 1*). In the cross section core the strength of concrete is not reduced.

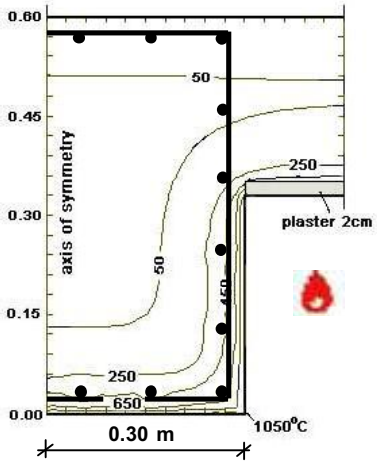

Fig. 1. Temperature distribution in the cross section of the column exposed to fire from two sides

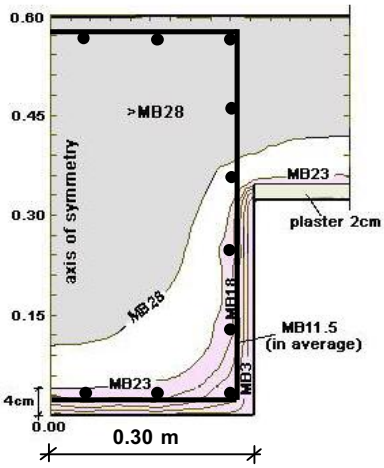

Fig. 2. Residual concrete strength in the cross section of column

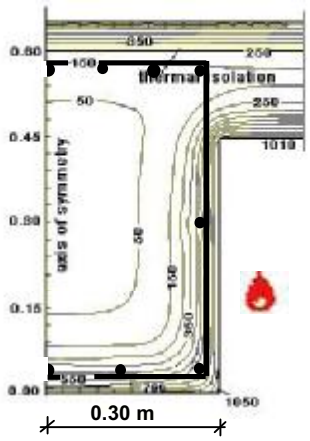

Fig. 3. Temperature distribution in the cross section of the beam exposed to fire from both sides

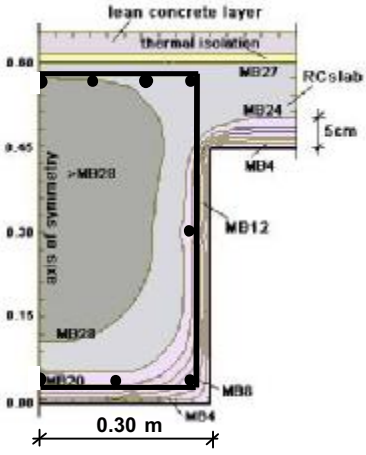

Fig. 4. Residual concrete strength in the cross section of beam

Results obtained by the thermal and static analysis of the frame structure show that fire had the most negative influence upon the beam elements over the 7th floor, where the fire started. These results correspond well with experimental results obtained by laboratory testing of specimens taken from the elements from that floor and with visually recorded changes in concrete colour (V7, G7, D7, E7, *Table 1*). The fire intensity on the 8th floor was less then that of the 7th floor and the degree of damage was less too (for B8 the reduction of concrete strength is less then for the other specimens). Beams over the 7th floor were fire exposed from both sides, but from the upper side, as a part of the RC slabs, they were covered with 1cm thermal isolation and 4cm lean concrete, that directly influenced upon the cross section temperature field (*Fig.3*) and the concrete strength reduction (*Fig.4*).

2. EXPERIMENTAL DETERMINATION OF THE RESIDUAL CONCRETE STRENGTH

The experimental testing of the residual concrete strength after the fire action was done by the Institute for Materials Testing and Development of New Technologies "Skopje"-Skopje. According to the previous Schmidt hammer testing results, the locations of the eight concrete specimens, taken only from RC walls and RC slabs, were defined. Hammer testing of concrete elements from apartments that were not fired confirmed that the compressive strength of the concrete before the action of fire was f_c=40MPa (MB30).

The concrete specimens taken from the RC walls (B8, V7, G7, D7, E7) were exposed to fire from one side. The corresponding surface layers (3-5cm thick) had changed the colour (red, grey-yellow, yellow) and were more deteriorated than the inner layers (*Fig.5*). Before testing all the specimens were divided in two slices. The deteriorated (burned) slices had small height (3-6cm) and rough surface therefore they were specially prepared by adding plaster layers (*Fig.6*). In that case the measured values for the compressive concrete strength were reduced with coefficients depending on the shape and height (h) of the deteriorated concrete specimens [4].

Fig. 5. Change of concrete colour and deterioration of surface layers of specimens

Fig. 6. Deteriorated concrete specimens, prepared for testing

Table 1. Concrete strength testing results

Position	Dimensions of specimens (cm)			Concrete compressive strength (MPa)		Concrete strength (MB)
	total H	h (testing)	D	cylinder	reduc.to cube 20/20/20	
RC wall (B8)	15	9.9	9.9	**26.0**	26.5	**20.0**
(after fire expose)		3.5		**15.8***	16.1	**12.0**
RC slab (MS)	18	10.3	9.9	**33.8**	34.5	**26.0**
(after fire expose)		6.5		**12.5***	12.8	**9.5**
RC slab (SII)	18	9.6	9.9	**38.4**	39.1	**29.4**
(after fire expose)		4		**13.0***	13.3	**10.0**
RC wall (V7)	25	9.9	9.9	**35.4**	36.1	**27.0**
(after fire expose)		5		**14.5***	14.8	**11.0**
RC wall (G7)	19.4	10	9.9	**25.4**	25.9	**20.0**
(after fire expose)		3.5		**14.5***	14.5	**11.0**
RC wall (D7)	18	10	9.9	**30.7**	31.3	**24.0**
(after fire expose)		3.5		**14.5***	14.8	**11.0**
RC wall (E7)	16	10	9.9	**31.9**	32.6	**25.0**
(after fire expose)		3		**14.1**	14.4	**10.5**

* Values are reduced with coefficients depending on the shape and height (h) of the deteriorated concrete specimens.

Results obtained by the thermal analysis and experimental testing of specimens show that during the fire action, as well as in the cooling period, the compressive strength of concrete is continually reduced. Numerically achieved results correspond well with experimental results obtained by laboratory tests of specimens taken from fired elements (RC walls and slabs). All these confirms that the numerical procedure, based on the nonlinear transient heat flow analysis, can be used for defining the residual concrete strength with grate accuracy.

REFERENCES

[1] Cvetkovska M., Nonlinear stress strain behavior of RC elements and RC frames exposed to fire, *Phd. thesis, University St.Cyril and Methodius, Skopje*, 2002

[2] Cvetkovska M., Lazarov Lj., Examination and assessment of degree of damage of fired elements of building structure K2-Karpos IV, *Civil engineering faculty-Skopje,* May 2005

[3] Cvetkovska M., Lazarov Lj., The repair project of the RC structure of the building K2-Karpos IV-Skopje, damaged by fire, *Civil engineering faculty-Skopje,* June 2005

[4] Manov Z., Determination of the residual concrete strength after action of fire on building structure K2-Karpos IV-Skopje, *Institute for materials testing and development of new technologies "Skopje"-Skopje,* May 2005

FIRE RESISTANCE CURVES FOR RC COLUMNS

Meri Cvetkovska [a], Petar Cvetanovski[b], Viktor Mihajlov[c]

[a] Ss."Cyril and Methodius" University, Faculty of Civil Engineering, Skopje, Macedonia
[b] Ss."Cyril and Methodius" University, Faculty of Civil Engineering, Skopje, Macedonia
[c] Ss."Cyril and Methodius" University, Faculty of Civil Engineering, Skopje, Macedonia

INTRODUCTION

The response of complex structure subjected to a real fire loading is estimated by methods of computational modelling of thermo dynamic and thermo mechanical processes. However, the development of various numerical methods for the analysis of the nonlinear response of structures under fire does not reduce the necessity and the importance of the experimental tests. They are necessary to determine the mechanical properties of materials at elevated temperatures, as well as to check the adequacy of the developed computational methods.
The columns as structural elements have an important role in preventing loss of global stability of structures under fire. If these elements do not suffer failure, damages shall be of a local character, which shall enable evacuation and efficient extinguishing of the fire. This paper describes the analytically achieved results for the fire resistance of centrically and eccentrically loaded RC columns incorporated in a wall for separating the fire compartment. The influence of: element geometry, concrete cover thickness, steel ratio and intensity of the axial force and bending moment are analyzed and the results are presented by curves which enable determination of the fire resistance of these columns without use of numeric procedure. For that purpose the program FIRE is used. This program carries out the nonlinear transient heat flow analysis (modulus FIRE-T) and nonlinear stress-strain response associated with fire (modulus FIRE-S). The solution technique used in FIRE is a finite element method coupled with time step integration.

1. FIRE RESISTANCE OF CENTRICALLY LOADED RC COLUMNS

Fig.1a shows a column, fixed at A and free to move vertically at B, allowing a free expansion in longitudinal direction; and *Fig.1b* shows the cross section of the column. The steel ratio is $\alpha = 1\%$. The yield strength of the reinforcing bars is $f_y(20^oC) = 400\ Mpa$ and the strength of the siliceous concrete is $f_c(20^oC) = 30\ Mpa$. The column is exposed to a standard fire only from one side of the wall. At the other side the column is part of a concrete wall, which is not fire exposed.
The column is discretisated by three elements and each element is further discretisated by five subelements. Because of the symmetry of the cross section and the symmetry of the fire load, only one half of the column is analyzed. For the thermal analysis the cross section of the column and the associated part of the wall is discretisated by isoparametric 4 nodes rectangular elements (subslices). In the stress-strain analysis the wall elements are excluded, reducing the number of elements. For the surface layers a finer discrete mesh is adopted because of the high temperature gradient ($\Delta x = 1.0cm$), while for the inner layers the size of the subslices is $2.0 \le \Delta x \le 3.0cm$. The time step is $\Delta t = 0.025h$ and it is adopted to the size of the subslices. Temperature dependent thermal and mechanical properties of concrete and steel are taken as recommended by Eurocode 2, part 1.2.
For the regions with high seismic risk it is recommended stresses in concrete not to exceed: $\sigma_c \le 0.35 f_{cd} \le 0.35 \cdot 0.85 f_c \le 0.3 f_c$. In this research the load ratio is defined as: $\alpha = \sigma_c / f_c(20^oC)$, but its value is varied in more wide range: $0 \le \alpha \le 0.5$. Dimensions of the cross section, concrete cover thickness, steel ratio and intensity of the axial force are varied and the results are presented by curves from which the fire resistance of the column can be determined without any additional calculations.

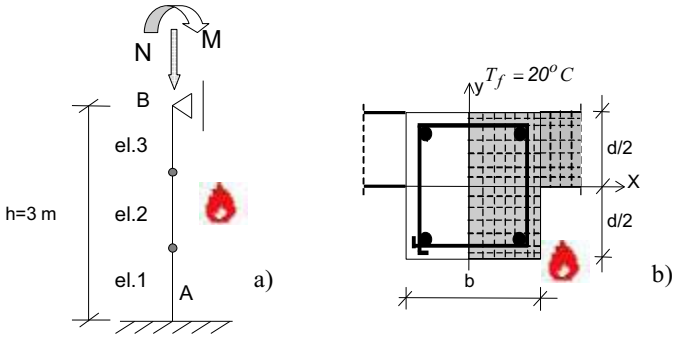

Fig. 1. a) Geometry and support conditions. b) discretization of the cross-section when column is part of a wall for separation the fire compartment

The results of the thermal analysis, in case when the dimensions of the cross section are $30 \cdot 30\,cm$, are presented on *Fig. 2*. Isobars in the cross section at support B, for the case when the load ratio is $\alpha = 0.3$, are shown on *Fig.3*.

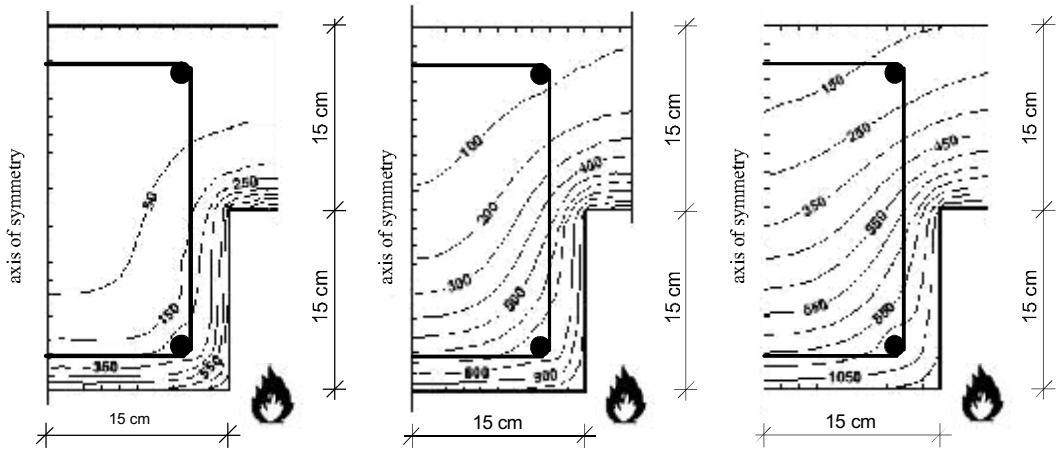

Fig.2: Isotherms in the cross section of a column $30 \cdot 30\,cm$, that is a part of a wall for separation the fire compartment

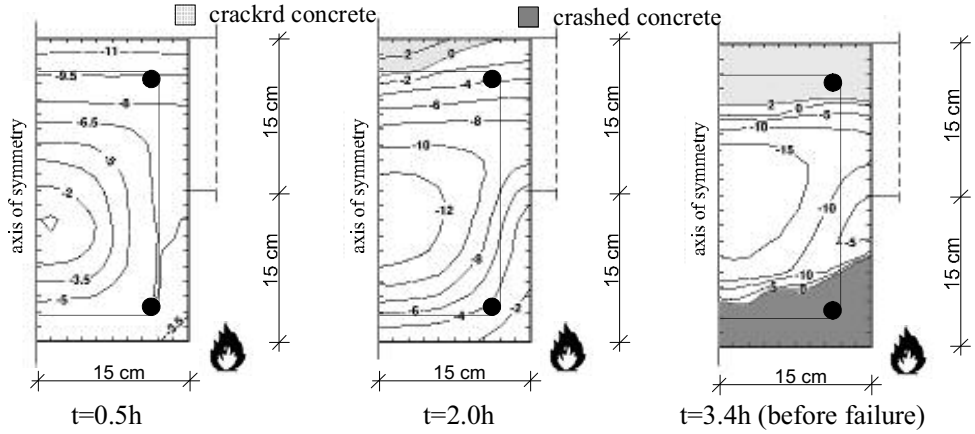

Fig.3: Isobars in the cross section at support B
(load ratio α = 0.3, concrete cover thickness a=2.0 cm)

The differential heating causes the end B of the column to separate from the support thus causing negative reaction. This action results in an initialization of negative moment at support A (*Fig.4*), but after some time the moment changes the sign. The outside reinforcement at support A (el.2A at *Fig.5*) remains cold for a long period of time, its yield strength is not reduced and the axial force produces compressive stresses, so the negative moment can be accommodated. The reinforcing bar that is on the side of the fire (el.1A) is in compression by the axial force, bending moment and the action of the fire. The yield strength is reduced because of the high temperatures, so stresses are close to the yield strength very soon, but after some time the moment changes the sign and the stresses decrease. Element 1B, at support B, is in compression all the time by the axial force and the fire action and yields first. Failure occurs at support B (*Fig.3*, t=3.4h).

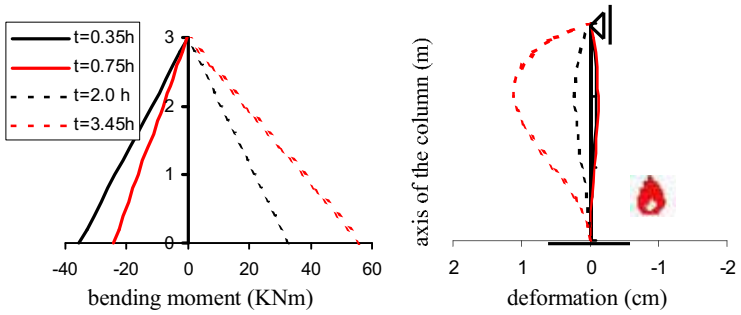

Fig.4: Bending moment and deformation redistribution during a fire exposure, (load ratio $\alpha = 0.3$)

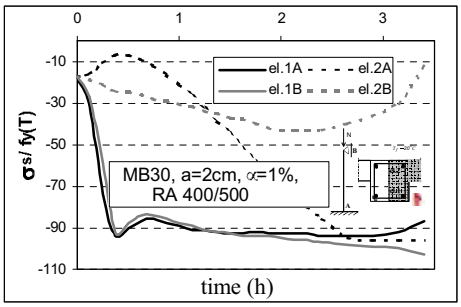

Fig.5: Time redistribution of stresses in the reinforcement at support A and B, $\alpha = 0.3$

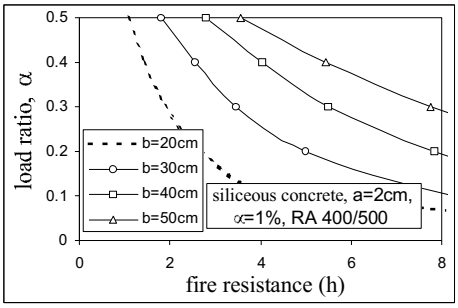

Fig.6: Fire resistance curves for centrically loaded columns

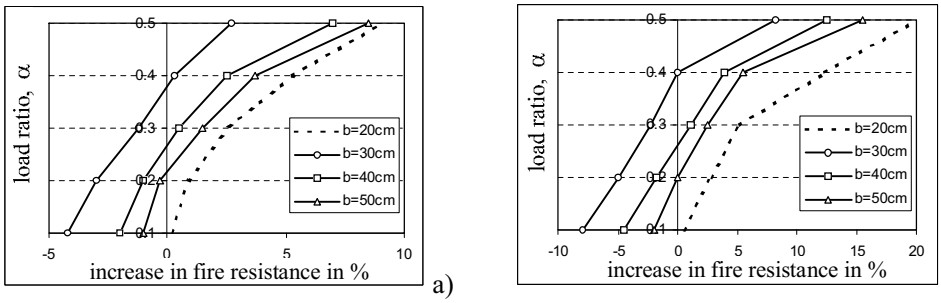

Fig.7: Increase in fire resistance of centrically loaded columns when the concrete cover thickness is increased: a) a=3cm, b) a=4cm, (reference column has a=2cm)

If dimensions of the cross section, intensity of the axial force (load ratio α) and concrete cover thickness are known, fire resistance of centrically loaded column that is part of a wall for separation

the fire compartment, can be directly defined from the diagram presented on *Fig.6*. If the concrete cover thickness is $a = 2cm$, the results are presented on *Fig.6.* For all other cases ($a = 3cm$ or $a = 4cm$) a correction has to be made according to the values on *Fig.7.*

2. FIRE RESISTANCE OF ECCENTRICALLY LOADED RC COLUMNS

Fire resistance of RC columns subjected to eccentric loads is determined in this example. Columns are part of a wall for separation the fire compartment, so they are exposed to ISO 834 standard fire only from the inside of the compartment. This is the most usual case in practice. Geometry and support conditions of the columns analyzed in this example are presented on *Fig.1*. Dimensions of the cross section; concrete cover thickness; steel ratio; intensity of the axial force and bending moment are significant factors affecting fire resistance of these columns.

The differential heating causes redistribution of bending moments (Fig.8). The outside reinforcement remains cold for a long period of time (el.2A, Fig.9), its yield strength is not reduced and the axial force produces compressive stresses, so that the change of the moment sign can be accommodated. The reinforcing bars that are on the side of the fire are all the time in compression by the dominant axial force and the action of the fire (el.1A and el.1B, Fig.9). The yield strength is reduced because of the high temperatures, so they start to yield very soon. Failure occurs at support B where the bending moment and the fire cause the same effect.

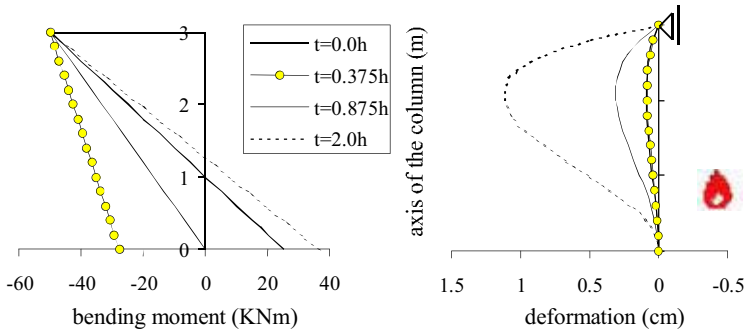

Fig.8. Deformation and bending moment redistribution during fire for column $30 \cdot 30cm$ ($\eta = 0.2$, $\beta = 0.4$, $a = 2cm$, $\alpha = 1\%$)

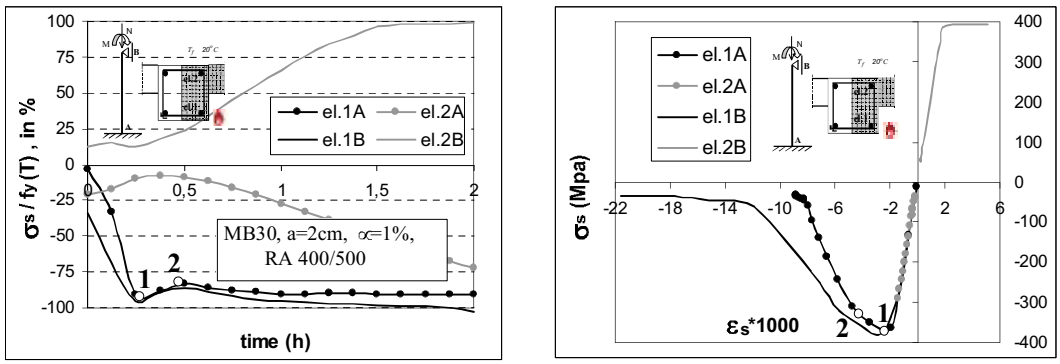

Fig.9. Time redistribution of stresses in a column $30 \cdot 30cm$ ($\eta = 0.2$, $\beta = 0.4$, $a = 2cm$, $\alpha = 1\%$)

Stresses on *Fig.9a* are presented as a per cent of the yielding strength for the corresponding temperature of the reinforcement, but on *Fig.9b* they are presented with the real values, so typical stress-strain diagrams for steel at high temperature are obtained.

If the column is designed according to current design standards, the fire resistance can be directly defined from the diagrams presented on *Fig.10a,* when concrete cover thickness is $a = 2cm$. For

that purpose the M-N diagram of the column at ambient temperatures has to be defined and the load coefficients for the axial force and bending moment to be calculated:

$$\eta = \frac{N}{N_{u,max}} \quad , \quad \beta = \frac{M}{M_u} \tag{1}$$

where: η - load coefficient for axial force
N - axial force before action of fire
$N_{u,max}$ - ultimate axial force when the bending moment is zero (defined from the M-N diagram)
β - load coefficient for the bending moment
M - bending moment before action of fire
M_u - ultimate bending moment corresponding to the ultimate axial force N_u (defined from the M-N diagram according to Equation 2)

$$N_u = N_g \gamma_{ug} + N_p \gamma_{up} = N \gamma_u \Rightarrow M_u = f(N_u) \tag{2}$$

For all other cases ($\propto = 0.6\%$ or $\propto = 1.5\%$; a = 3cm or a = 4cm) a correction has to be made according to the values on *Fig.10b* and *Fig.11*. Such diagrams are obtained for columns $40 \cdot 40$cm and $50 \cdot 50$cm, but they are not presented.

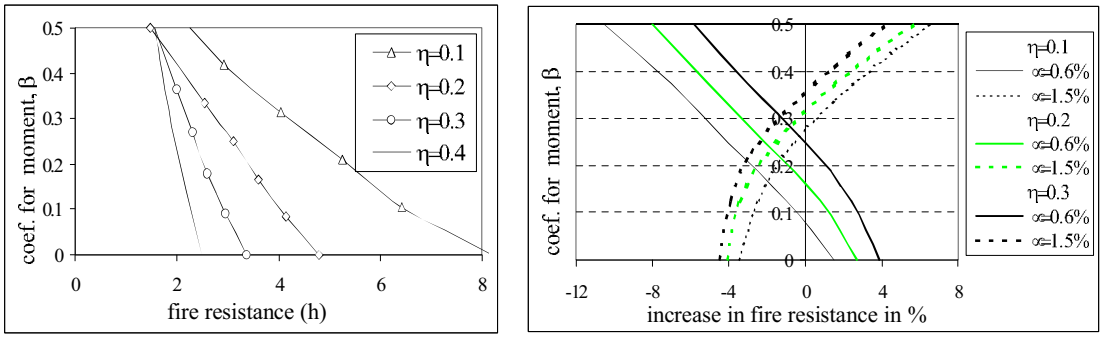

a) *b)*

Fig.10. Effect of a) load intensity b) steel ratio (referent column ∝=1%) upon the fire resistance of eccentrically loaded column $30 \cdot 30cm$ (concrete cover $a = 2cm$)

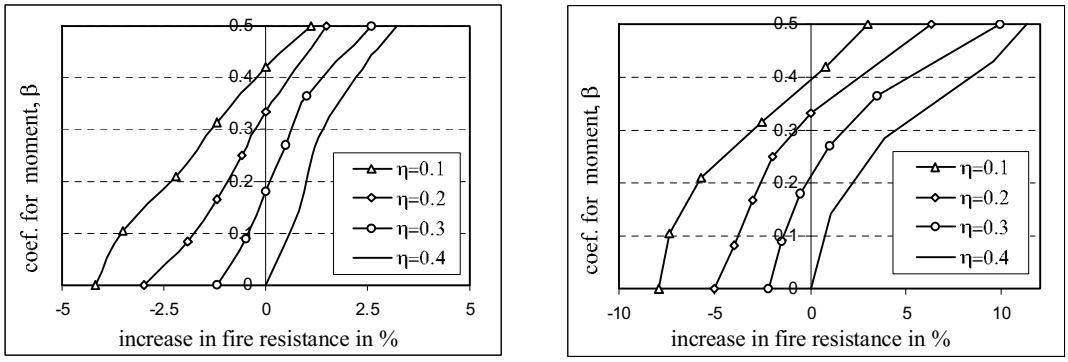

a) *b)*

Fig.11. Increase in fire resistance of eccentrically loaded columns $30 \cdot 30cm$, when concrete cover thickness is increased: a) $a = 3cm$, b) $a = 4cm$, (reference column has $a = 2cm$)

3. SUMMARY AND ACKNOWLEDGMENT

As a result of parametric studies, the following conclusions are made: dimensions of the cross section, intensity of the axial force (load ratio α) and the type of the aggregate (siliceous or carbonate) are significant factors affecting fire resistance of centrically loaded columns exposed to standard fire from all sides. When dimensions of the cross section are small temperature penetrates deeper in a short time period and the fire resistance is lower. When the load ratio is increased, the fire resistance is decreased, and opposite. If load ratio $\alpha = 0.3$ is decreased to $\alpha = 0.2$, the fire resistance is increased for 30%. If carbonate aggregate concrete is used instead of siliceous aggregate concrete, the fire resistance is increased for 30% in average. Experimental results indicate even higher effect, which leads to a conclusion that recommendations for the temperature dependant physical characteristics of carbonate aggregate concrete, given in Eurocode 2 part 1.2, are conservative but are on the side of safety.

With the increase of the strength of concrete, the fire resistance increases in proportion to the assigned load capacity. The steel ratio has a negligible effect on the fire resistance of the centrically loaded columns, exposed to fire from all sides. As e result of that the concrete cover thickness has a negligible effect. Because of the symmetry of the axial load and fire exposure, support conditions and height of the column have no influence on the fire resistance (the used analysis procedure does not account for the effects of large displacements on equilibrium equations). The effect of axial restraint on the fire resistance is negligible. Experimental results indicated that fully restrained column didn't significantly decrease its fire resistance, and only columns with high slenderness ratio failed in buckling.

Eccentrically loaded columns that are part of a wall for separation the fire compartment have the lowest fire resistance. Dimensions of the cross section; concrete cover thickness; steel ratio; support conditions; fire scenario and intensity of the axial force and bending moment are significant factors affecting fire resistance of these columns. The effect of increasing the steel ratio is positive. It was not a case when the column was centrically loaded ($\beta = 0$). When the bending moment is increased and the axial force is decreased the positive effect is more expressive. For optimally loaded columns ($\eta \leq 0.3$) the concrete cover thickness has a positive effect in increasing the fire resistance, but not more than 5% for columns with small dimensions, and up to 10% for larger columns.

REFERENCES

[1] Anderberg, Y. Magnusson, S.E. Pettersson, O. Thelandersson, S. & Wickstrom, U., An analytical approach to fire engineering design of concrete structures. *International Symposium on Concrete and Structures*. *ACI Publications* 1986.

[2] Bazant, Z.P. & Kaplan, M.F., Concrete at high temperature: Material properties and mathematical models. *London: Longman Group Limited*, 1996.

[3] Cvetkovska, M., Nonlinear stress strain behaviour of RC elements and RC frames exposed to fire. *Phd. thesis. Skopje: University St.Cyril and Methodius,* 2002.

[4] Ellingwood, B. & Lin, T.D., Flexure and shear behavior of concrete beams during fires. *Journal of the Structural Engineering.* Vol.117 No.2, 1991.

[5] Iding, R. Bresler, B. & Nizamuddin, Z., FIRES-RC II A computer program for the fire response of structures-reinforced concrete frames. *Report No. UCG FRG 77-8. Berkeley: University of California,* 1977

[6] Lin, T.D. Zwiers, R.I. Burg, R.G. Lie, T.T. & McGrath R.J., Fire resistance of reinforced concrete columns. *PCA Research and Development Bulletin RD101B. Skokie, Illinois: Portland Cement Association,* 1992.

SPALLING OF CONCRETE
Implications for Structural Performance in Fire

Susan Deeny [a], Tim Stratford [a], Rajesh Dhakal [b], Peter Moss[b], Andy Buchanan[b]

[a] The University of Edinburgh, BRE Centre for Fire Safety Engineering, Edinburgh, UK
[b] University of Canterbury, Department of Civil and Natural Resource Engineering, Christchurch, New Zealand

INTRODUCTION

Spalling involves the breaking off of layers or pieces of concrete from the surface during thermal exposure. Spalling can broadly be classified into 3 different types: aggregate spalling, corner spalling (or sloughing off) and explosive spalling. Aggregate spalling and corner spalling are generally not considered to be critical for the performance of concrete structures in fire and are, therefore, not considered further here. Explosive spalling involves the ejection of pieces of concrete from the heated surface at high velocities. It typically occurs in the early stages of the fire when heating rates are high [1, 2]. Explosive spalling (hereafter referred to as spalling for brevity) poses the greater threat to structural stability; it is, therefore, the form of spalling focused upon in this paper.

Current research is predominantly concerned with establishing and modelling the precipitating mechanisms. Prediction of the stress state leading to spalling requires complex hygro-thermal-mechanical modelling; the reliability and accuracy of such models however is not yet sufficient to formulate design guidelines; hence, there is little guidance provided under BS 8110 part 2 [3] and the new Eurocode 2 [4] with regards to protection of concrete structures in the event of spalling. In this paper, a preliminary investigation on the effect of spalling on structural stability is performed through the finite element analyses of a reinforced concrete beam subjected to the Eurocode 1 [5] standard temperature – time curve. It is not the intention of this investigation to model explicitly the hygro-thermal-mechnical processes, rather to develop a framework for consequence modelling of spalling in a finite element analysis.

1 MECHANISMS OF SPALLING

Spalling of concrete can generally be categorised as pore pressure induced spalling, thermal stress induced spalling or a combination of the two. In general terms, pore pressure spalling occurs when migration of evaporated free water from the heated surface leads to increased pore pressure at some distance from the heated surface. Continued heating will result in the pore pressure reaching the tensile strength of the concrete, causing explosive local failure. No pore pressures have yet been measured which would exceed the tensile strength of concrete [6, 7]. Thermal stress induced spalling is thought to occur due to the steep thermal gradients which develop in concrete as it is heated. These gradients induce compressive stresses at the surface due to restrained thermal expansion and tensile stresses in the cooler interior. Surface compression may be augmented by applied loading or pre-stress. It is most likely that spalling results as a combination of the tensile stresses induced by thermal expansions and increased pore pressure. Much debate still surrounds the identification of the key mechanism (pore pressure or thermal stress). However, it is noted that the key mechanism may change depending upon the section size, material composition and moisture content [8].

2 SPALLING MODEL

2.1 Spalling Criteria

From the previous discussion of the governing mechanisms of spalling, it is evident that the stress state within the concrete will dictate whether spalling will occur. The stress state due to moisture migration and thermal stress will be influenced by several parameters; these parameters can be categorised as follows [1, 2]:

- Material Parameters: Initial moisture content, permeability, porosity, presence of cracks, aggregate type and size, amount of reinforcement.
- Geometric Parameters: Section shape and size.
- Environmental Parameters: Heating rate and profile, temperature level and thermal restraint.

It is not the intention of this investigation to model explicitly the hygro-thermal-mechnical processes which determine this stress state leading to spalling. A comprehensive review of the substantial body of research which has sought to characterise the conditions under which spalling occurs has been undertaken to identify critical conditions or parameters for spalling which are applicable within a structural analysis. The fundamental assumption in this analysis is that spalling ***will*** occur, thus it is assumed that the material and geometric conditions which trigger spalling are satisfied.

Assuming that spalling will occur, it is then necessary to define ***when*** spalling will occur during fire exposure. The environmental parameters of heating rate and temperature level are useful indicators in a thermal analysis of when spalling may occur. From the literature it is found that heating rates in the range of 20–32^{o}C/min are significant for spalling [2]. Such high heating rates normally occur in the early stages of the fire which is consistent with the experimental observations. Several researchers have identified critical temperature ranges for the exposed surface at the onset of spalling. Aktaruzzaman and Sullivan [9] have cited exposed surface temperatures in the range of 375–425^{o}C for normal weight concretes.

2.2 Spalling Implementation

A 2-D heat transfer analysis of the member cross section is performed using ABAQUS finite element software [10]. The onset of spalling is triggered when the bottom surface temperature reaches the range of 375-425^{o}C. Spalling is modelled by removing all the elements making up the bottom concrete cover. The analysis is continued and the temperature distribution for the reduced cross section is calculated. Figure 1 presents typical temperature contour plots just prior to and just after spalling and one hour from the beginning of the analysis for the abrupt spalling analysis.

Removing all of the concrete cover instantaneously when the bottom surface reaches a certain temperature greatly simplifies the progressive nature of spalling. Slower and more progressive spalling can also be modelled by employing the same temperature criteria but only removing single layers of elements at time. The thickness of the layers removed will be a function of the element thickness used in the finite element analysis.

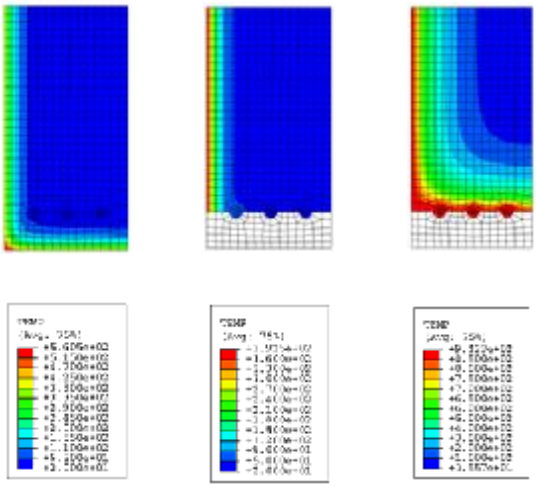

(a) Pre Spalling (b) Immediately post spalling (c) Final temp distribution

Fig. 1. Beam cross section temperature profile (°C) for abrupt spalling.

4 CASE STUDIES

The performance of a simply supported RC beam exposed to the EC1 [5] standard temperature-time curve (Figure 2) and subject to spalling is investigated.

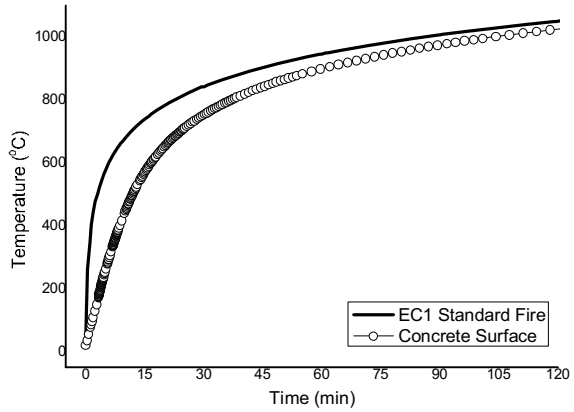

Fig. 2. Eurocode 1 standard temperature curve and concrete surface temperature.

The beam cross section is 600 mm deep by 300 mm. The concrete strength f_{cu} is assumed to be 30 MPa. The beam is reinforced with six 16 mm steel bars of yield strength, f_y = 500 MPa. The cover depth is assumed to be 45 mm. Temperature dependant material properties for both the concrete and reinforcing steel are taken from Eurocode 2

Advantage is taken of symmetry and half of the beam cross section is analysed for the case of no spalling, progressive spalling (8 mm layers) and abrupt spalling. The rapid evolution of concrete surface temperature in Figure 2 would indicate that varying the criterion temperature

between 375°C- 425°C would have little effect on the final temperature distribution therefore the surface temperature criterion for the onset of spalling is taken as a single value of 400°C.

For each case the resulting evolution of temperature in the reinforcement is plotted in Figure 3 (a). The corresponding reduction in reinforcing steel yield strength is plotted according to the reduction factors provided in Eurocode 2 is plotted in Figure 3 (b).

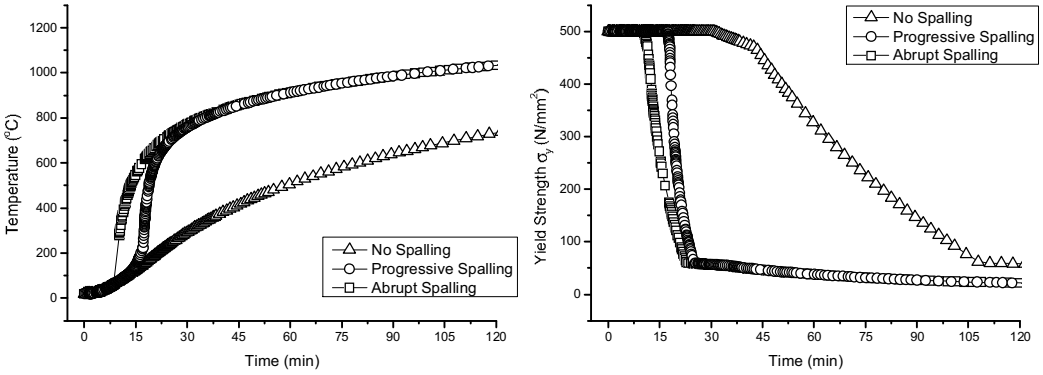

(a) (b)

Fig. 3. (a) Temperature development and (b) reduction in yield stress in reinforcing steel on exposure to the standard fire.

For the case of no spalling the steel temperatures rise gradually, being insulated by the concrete cover. Removal of the concrete cover due to spalling instantly results in a sharp increase in steel temperatures and a corresponding reduction in steel strength.

4.1 Single span simply supported RC beam

For a simply supported beam a single point of failure will result in a stability failure. Thus, failure times can be calculated by comparing the load ratio, $r_{load,}$ with the residual steel strengths. The load ratio, r_{load} , is defined as per Equation 1 below:

$$r_{load} = M^*_{fire} / R_{cold} \quad (1)$$

Where M^*_{fire} Applied bending moment in fire conditions

R_{cold} Ambient ultimate capacity

Table 1. Failure times for simply supported beam under standard heating.

r_{load}	No spalling (min)	Progressive spalling (min)	Abrupt Spalling (min)
0.4	78	21	17
0.45	73	20	16
0.5	71	20	16

The failure times for each scenario and a variety of load ratios representative of those expected in a real building [11] are presented in Table 1. It is apparent that spalling significantly reduces the failure time of the simply supported concrete beam when exposed to the standard fire. Note that the failure time predicted with spalling (even in progressive spalling) is well short of the time when the cooling phase typically starts in 'natural' or

parametric fires (EC1 2002). Hence it can be argued that consideration of the cooling phase will not alter the prediction of failure time.

4.2 Two span simply supported RC beam

Continuous beams generally exhibit improved fire performance due to their ability to maintain stability through alternate load paths (moment redistribution). The fire affected moment capacity is calculated using the simplified method from EC2 [4] which assumes that concrete above 500°C is structurally insignificant and below 500°C the concrete is unaffected, the results can be seen in Table 2.

Table 2. Failure times for a two span RC beam under standard heating.

Spalling		Single steel layer (min)	Double steel layer (min)
Span 1	Span 2		
No	No	177	224
Yes	Yes	24	258
No	Yes	99	188

Figure 4 shows the bending moment distribution for the case of unsymmetrical spalling. Yielding at the mid span and near the support creates a failure mechanism in the spalling affected span.

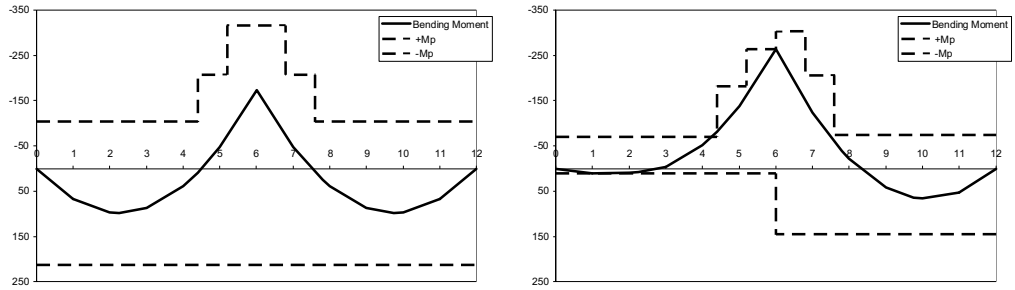

Fig. 4. (a) Ambient BMD (b) BMD at failure

The beam analysed has a 2 hour fire rating according to the requirements of EC2. For the normal design of a single layer of tensile steel failure times in the event of spalling are significant less than prescribed in design. The analysis was repeated using an equivalent quantity of steel but distributed in two layers thus increasing the insulation to 50% of the steel. This simple change significantly increases the performance of the beam.

In both analyses the standard temperature-time curve has been used to define the thermal exposure for the beam. This assumes a uniform thermal exposure along the length and across the width of the beam which, in conjunction with a thermal criterion for spalling predicts spalling affects the entire beam length. In reality this is not the case, because spalling may be localised to regions of high thermal exposure. The effects of localised spalling become more complicated in the case of a continuous multi-span beam or a slab.

6 CONCLUSIONS

Explosive spalling is a very complex phenomenon which poses a great threat to structural performance of some reinforced concrete structures in fire. There is a large body of research

concerning the prediction of whether spalling will occur, but rather less research concerning the implications that spalling has for structural performance. Current design guidance for the consideration of spalling is limited thus spalling is largely ignored in the design process of concrete structures despite its potential consequences.

The results of the analysis of a simply supported beam indicate that spalling threatens stability of the structure by exposure of the reinforcement to high and rapidly rising temperatures. It is shown that under exposure to the standard fire, failure times are significantly reduced for both models of spalling (abrupt and progressive spalling).

Multi-span beams perform better due to their ability to utilise alternate load paths. However, in the presented example, extensive spalling still leads to premature failure. More sophisticated calculation methods considering the effects of end restraint are required to better establish performance in fire and spalling. In the future, the study will be extended to consider spalling implications in a finite element mechanical analysis using non-uniform heating definitions for multi-span beams and slabs.

7 SUMMARY AND ACKNOWLEDGMENT

The authors gratefully acknowledge sponsorship and support of the first author by Buro Happold FEDRA Ltd and EPSRC. Thanks are also due to the Royal Society of Edinburgh Lessells Travel Scholarship without which this collaboration would not have been possible.

REFERENCES

1. Hertz, K.D., Limits of Spalling of Fire-exposed Concrete. Fire Safety Journal, 2003. 38(2): p. 103-116.
2. Khoury, G.A., Effect of fire on concrete and concrete structures. Progress in Structural Engineering and Materials, 2000. 2(4): p. 429-447.
3. BSI, Design of Concrete Structures: General rules - Structural Fire Design. 2004, BSI: London. p. NA to BS EN 1992-1-2:2004.
4. EC2, Design of Concrete Structures; General Rules - Structural Fire Design. 1996, European Committee for Standardisation: London. p. BS EN1992-1-2:1996.
5. EC1, Actions on Structures: General Actions - Actions on Structures Exposed to Fire. 2002, European Committee for Standardisation: Brussels. p. BS EN1991-1-2.
6. Khoury, G.A., Anderberg, Y, Concrete Spalling Review. 2000, Fire Safety Design.
7. Jansson, R., Bostrom, L. The influence of pore pressure in the pore system on fire spalling of concrete. in Structures in Fire - SiF'08. 2008. Singapore.
8. Davie, C.T., Zhang, H., Pearce C.J., Bicanic, N. Computational modelling of concrete exposed to fire: The effects of coupled hydro-thermal-mechanical behaviour of the development of spalling in concrete structures. in Structures in Fire - SiF'08. 2008. Singapore.
9. Akhtaruzzaman, A.A., Sullivan, P.J, Explosive spalling of concrete exposed to high temperature, in Concrete structures and Technology Research Report. 1970, Imperial College: London.
10. Simulia, ABAQUS 6.6-2. 2006, Simulia: U.S.A.
11. Buchanan, A.H., Structural Design for Fire Safety. 2001: John Wiley & Sons. 444.

COMBINED WHILE-DRILLING TECHNIQUES
for the assessment of the fire damaged concrete cover

Roberto Felicetti

Politecnico di Milano, Milano, Italy, roberto.felicetti@polimi.it

INTRODUCTION

Concrete is known to exhibit a good behaviour when submitted to fire, thanks to its incombustible nature and low thermal diffusivity. These qualities guarantee a slow propagation of the thermal transients within the structural elements, but they also trigger very steep temperature gradients within the concrete cover. As a consequence, pronounced variations of the mechanical properties take place in the outer layer of the heated members, making difficult to ascertain the actual depth of the visible damage suffered by the structure.

A number of other properties are affected by the physicochemical transformations experienced by the material, casting the base for the indirect assessment of the effects of fire via the Non-Destructive Testing techniques [1]. Most of these methods are generally meant to smooth the effect of the inherent heterogeneities of the material at the scale of the coarse aggregate, which is also the significant range of the problem at issue. Hence, they can hardly outline more than the average response of the investigated cover layer.

Despite of the possible detriment to the integrity of the structure, a very analytical approach to the assessment of fire damaged concrete is based on the extraction of cores, to be examined as they are (visual observation, colour measurement, ultrasonic scan) or to be cut into slices for subsequent laboratory analyses [1-4]. A number of investigation techniques are available to this latter purpose, involving the mechanical response of each slice (splitting test, punching-load compression, dynamic Young's modulus), their physical and morphological properties (colour, micro-crack density, porosity, air permeability, petrographic and SEM examinations) and their physicochemical features (X-ray diffraction, thermal and chemical analyses). The results pertaining to each slice can then be sorted into a profile depicting the evolution within the concrete cover of the property under study.

This wide assortment of inspection techniques paves the way for the implementation of combined methods, in which an improved accuracy is achieved by properly merging different sets of results. In this perspective, the operation of coring a concrete member can be itself considered as a way of scanning the material soundness at increasing depth, which comes at no cost after having decided to take samples of the deteriorated concrete.

To date, the potential of monitoring the core cutting process, that is a well established practice in geophysical prospection, has not been studied systematically for the assessment of construction materials. On the contrary, several examples of this kind of approach applied to the simple drilling of holes are available in the literature. By means of suitably modified drills, different operational parameters can be surveyed, like the thrust or the torque to be exerted to keep a constant feed rate [5] and the mechanical work spent for a unit penetration of the bit [6]. The attractive pros of this technique are the little time required to run a test, the immediate availability of the results and the limited damage to the member under consideration. Compared to the core extraction, the main limitation is the lack of a material sample to analyse, though the remaining hole and the ensuing ground-concrete powder could be in principle the object of additional investigations.

In this paper a comparison among some drilling and coring resistance indicators is performed first, in order to ascertain the sensitivity of these methods to a steep gradient of the mechanical properties. Further studies aimed to go beyond some limitations of the drilling technique will be also briefly illustrated. Then the potentials of the visual observation of the drilled hole and the of analysis of the ensuing powder are checked, as a way to implement the combination of different assessment techniques even in the absence of an undisturbed concrete sample.

1 CORING AND DRILLING RESISTANCE

In order to monitor the process of cutting a concrete core, a common core drill has been fitted with a set of sensors for measuring the rotational speed, the longitudinal stroke, the exerted thrust and the electric power consumption (Fig. 1a). The most significant parameters that can be worked out for revealing the quality of the material are the specific work (J/mm^3 - work per unit notched volume) and the time spent for a unit advance of the tool (s/mm).

In a first series of tests, the effect of the working variables (bit diameter, exerted thrust, rotation rate) has been studied by coring some ordinary concrete cubes (side = 150 mm, average cubic strength R_{cm} = 50 N/mm^2 - Fig. 2). At the reference rotational speed (600 rpm), the results show a relatively stable specific work consumption for increasing tool size and thrust (Fig. 2), whereas a concurrent reduction of the drilling time and rise of the electrical power input are observed. The same trends have been recognized by increasing the rotational speed (1250 rpm, not reported here). The slower rotation and the intermediate thrust (1.36 N/mm^2) have been adopted in the following series of tests, together with the smallest core bit ($Ø_{int}$ = 44 mm), which has the advantage of a minor damage to the investigated member.

The sensitivity of the two cited coring resistance indicators to the mechanical weakening of a deteriorated material has been ascertained on two sets of cubes, made of an ordinary and a lightweight concrete (average cubic strength R_{cm} = 50 N/mm^2 - max aggregate size = 16 mm). The samples have been tested as they were or after being uniformly damaged by way of a slow thermal cycle (T_{max} = 200÷800°C, heating/cooling rates = 0.5/0.2°C/min, 1 hour spell at T_{max}). Identical samples were used also in other studies in order to compare the effectiveness of a series of ND techniques [1, 7]. Among them, a like method based on the measurement of the drilling resistance via a modified hammer-drill has been also thoroughly deepened (Fig. 1b [6]). A summary of all the results is presented in Fig. 3.

In principle the coring and the hammer-drilling techniques are based on the same micro-fracturing mechanism induced by a hard indenter scratching the concrete surface. However, the diamond-tipped bit of the core drill is fitted with a number of small hard grains, which have the effect of finely milling the material. On the contrary, the bit of a hammer-drill ends with a single large indenter submitted to strong pressure pulses, leading to a deeper propagation of cracks and a coarser fragmentation, especially in stiff and brittle materials like rock and high grade concrete. Hammer-drilling is then far less energy demanding than coring, but a rise of both the drilling work and time can be observed in slightly damaged concretes, when the increased deformability and almost constant fracture energy give way to less efficient penetration mechanisms (plastic crushing and milling rather than chipping [6]).

For this reason, even being the most promising parameter to be monitored in hammer-drilling, the dissipated work proved to be not enough sensitive to low levels of damage. On the other hand, the

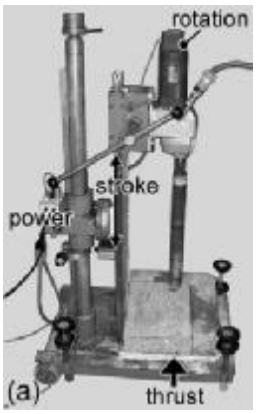

core bits geometry

#	Øint (mm)	thick (mm)	area (mm^2)
1	44	3.5	522
2	54	3.8	680
3	64	3.5	748
4	74	3.5	852
5	100	3.5	1138

#	thrust (N/mm^2)
a	0.69
b	1.36
c	2.05

exerted thrust

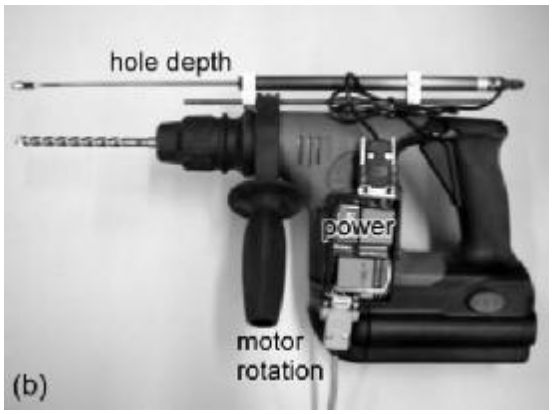

Fig. 1. (a) The core drill fitted with the sensors for monitoring the functioning parameters and investigated variables; (b) modified hammer-drill for measuring the drilling resistance [6].

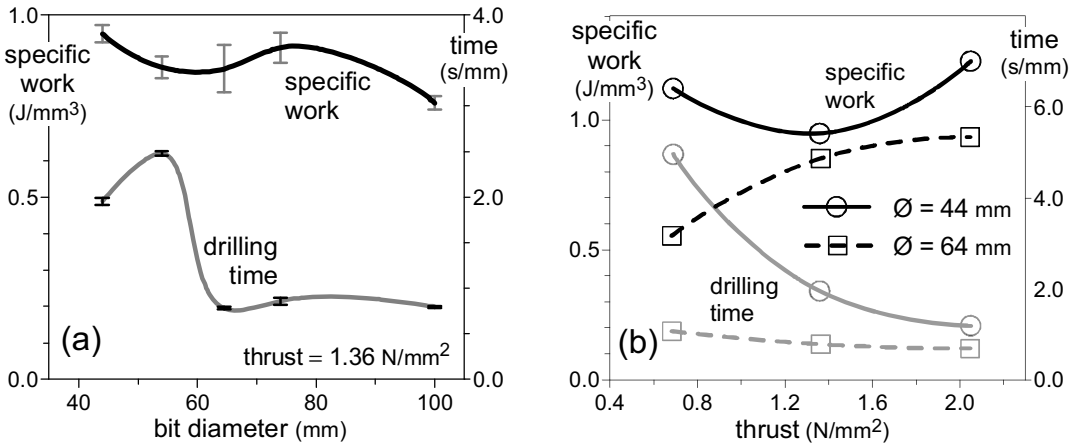

Fig.2 . Results of the preliminary core drilling tests under varying bit diameter and exerted thrust (rotational speed 600 rpm).

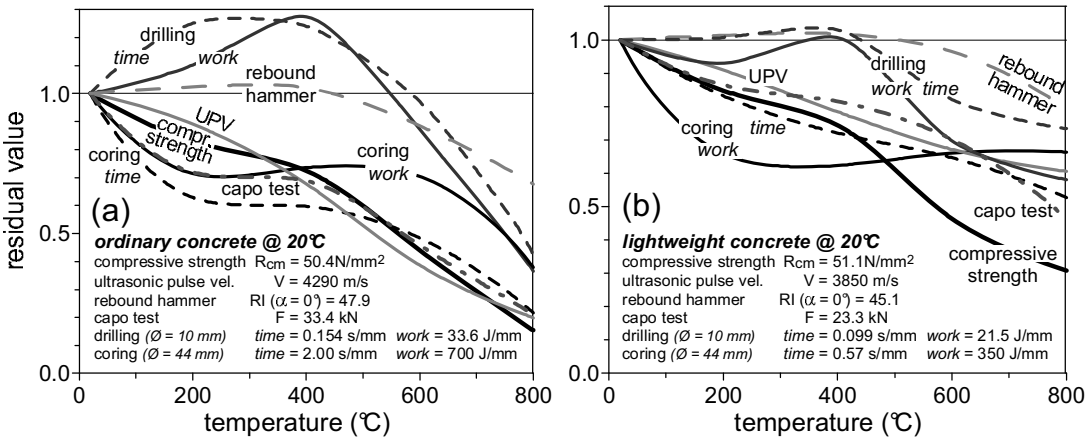

Fig.3 . Sensitivity to a uniform thermal damage of some common ND techniques and of the two drilling methods herein investigated.

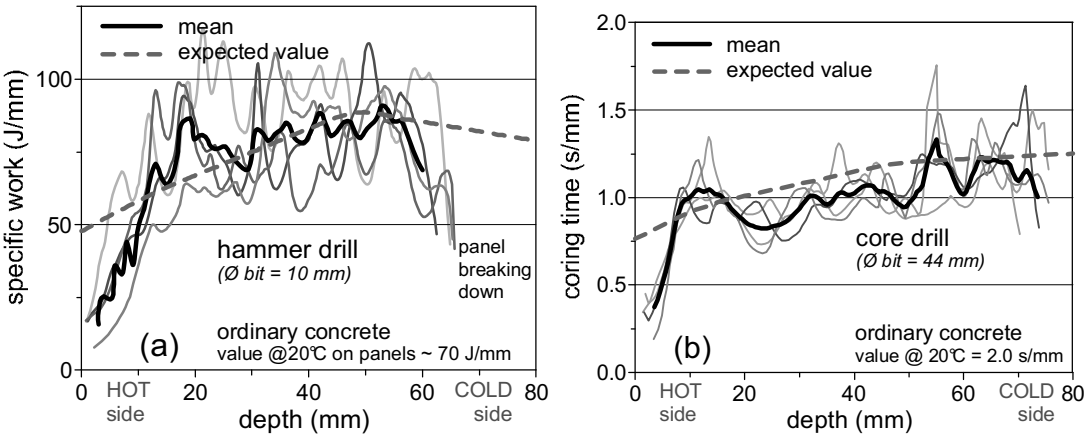

Fig. 4. Profiles of the most significant drilling and coring resistance indicators in the case of a concrete panel exposed to a steep thermal gradient.

elapsed time is the most responsive parameter in core drilling, provided that a careful control of the exerted thrust is performed. The fairly good sensitivity to thermal damage of this latter value can be compared to some well established ND techniques (ultrasonic pulse velocity and capo test) and to the compressive strength itself.

The interesting feature of both the discussed drilling techniques is their ability to continuously scan the material response at increasing depth, even in presence of strong gradients due to the concrete exposure to fire. As an example, Fig. 4 reports the profiles recorded while drilling a ordinary-concrete panel (thickness = 80 mm) that was preliminarily exposed to a steep thermal gradient (675 to 230°C left to right [7]). Based on the maximum temperatures reached in the panel and on the calibration curves of Fig. 3a, the expected drilling resistance profiles have been also worked out for reference. The general good agreement with the measured profiles confirms the reliability of this approach. Other features to be noted are the lower initial resistance due to the settlement of the cutting-tools, the remarkable sensitivity of the core drilling time to low damage levels (a 30% decay compared to unheated concrete is recognized already on the cold side) and the higher influence of the hard aggregate pebbles on the hammer drilling results, which requires to average some tests in order to recognize a clear trend. In the common case of shallow degradation of relatively thick members, a steady resistance value is reached in the end of the drilling process, when the pristine material is inspected. This allows to plot the profiles in relative terms, releasing from the need of specific calibration curves for a first assessment of the damaged depth.

Further studies are in progress, aimed to go beyond the limitation of the hammer-drilling technique in the case of slightly damaged concrete. One direction is focused on the propagation along the bit of the strong pulses induced by the hammering mechanism of the drill. This mechanism (Fig. 5a) is generally based on a crankshaft which activates a cylinder containing a striker (the so called “flying piston”). A quick succession of vacuum and pressure is exerted on the striker on its rebounds against the rammer-bit line, leading to resonance and then considerably boosting the impact energy. The compressive stress-wave generated by the impact propagates towards the tip of the drill bit, where it is partly reflected in the form of a backward tensile stress-wave. This propagation can be effectively captured by means of a couple small dual-grid strain gages glued on the bit shank (Fig. 5b) arranged in a full-bridge scheme and connected to a wide band signal conditioner.

Some preliminary tests have been performed on a concrete block by allowing the striker to drop from 2.2 m height (impact energy = 1 J) on the vertical drill bit and rammer. The results (Fig. 5c) are quite repeatable and in good agreement with those reported in the literature for the case of rock indentation with slender rods [8]. The reflected wave has practically the same amplitude as the incident wave, but the duration and the enveloped area are quite different in the two cases. This is particularly true for stiff and hard materials, being higher the share of impact energy transmitted to the workpiece. The next step will be to monitor the strain-waves propagation during the normal operation of the hammer drill, so to scan the material hardness at increasing depth. The sensitivity of the reflected waves to the material thermal degradation is another open issue to be deepened.

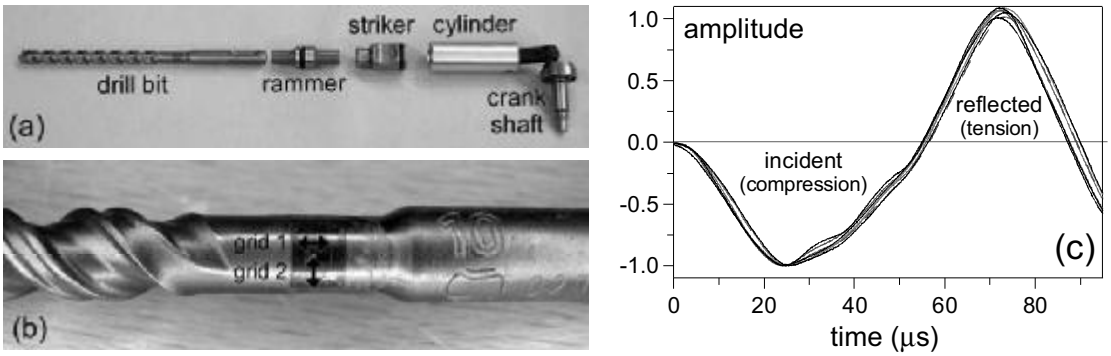

Fig. 5. (a) Components of the pneumatic hammering mechanism of the drill; (b) one strain gauge glued on the bit shank and (c) incident and reflected strain waves induced by one hit of the striker .

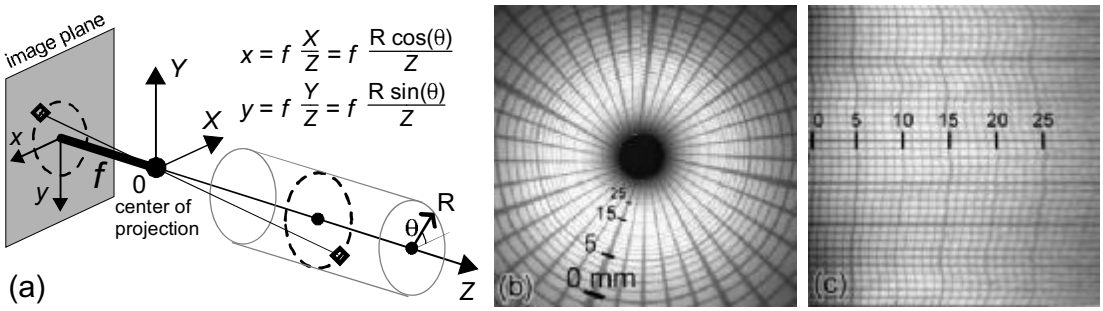

Fig. 6. (a) Endoscopic image projection on the CCD sensor of the digital camera; (b) original and (c) unwrapped views of a rolled graph paper.

2 VISUAL INSPECTION OF THE DRILLED HOLES

One advantage of taking a core from a member, compared to hammer-drilling, is the opportunity to observe the extracted samples for ascertaining the material morphology and condition. Nonetheless, the point of view can be reversed by examining the small-diameter drilled holes through an optical endoscope. The limitation of this instrument is to provide a magnified view of a just a small portion of the cavity, making difficult to gather a complete representation of the inner surface and to preserve the geometrical proportion of the observed details. A number of techniques have been proposed, mainly for medical and surgical applications, aimed at the calibration, projection and merging of the endoscope images.

In this study a rather simple approach has been implemented so to allow a first check on the viability and significance of this kind of observation. A rigid endoscope with frontal view and a wide field of vision (100 deg) has been fitted with a digital USB camera, in order to automatically store a series of digital images at regular steps (generally every 10 mm). The images are processed in order to switch from the central perspective to a front view of the unwrapped cylindrical surface of the hole. The transformation is based on the pinhole-model of the image projection on the CCD sensor of the camera (Fig. 6a [9]). By assuming a fixed radius of the hole (R = 5 mm in this case) and a perfect alignment of the endoscope axis, a simple relationship can be established between the coordinates of the cylindrical surface and the pixels on the image plane. After deciding the resolution of the unwrapped image, an array of target coordinates ($R\cdot\theta_i$, Z_j) is converted into image coordinates and the RGB values are determined from the sampled pixels via a cubic-spline interpolation scheme. A proper adjustment of the focal length *f* allows to match the longitudinal and the circumferential representation scales, as can be checked on the image of a rolled graph paper (Fig. 6b,c). Finally, the unwrapped frames are merged by means of a software for image editing.

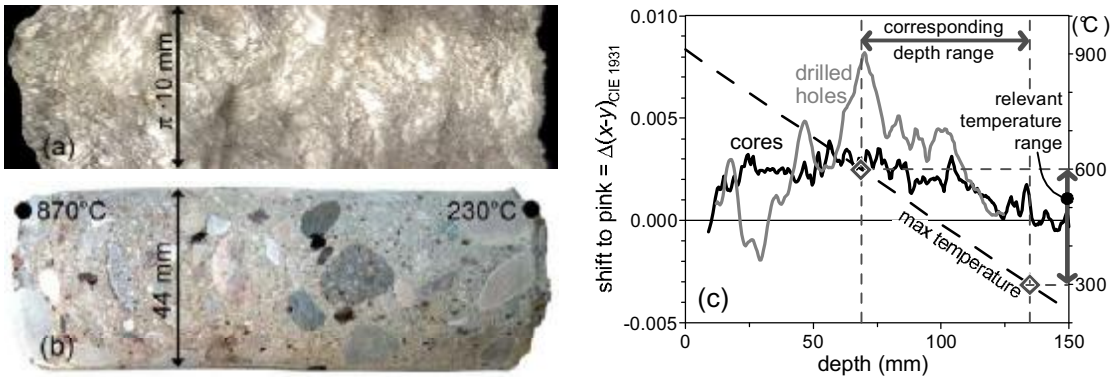

Fig. 7. View of (a) the unwrapped inner surface of a drilled hole and (b) a core taken from the same concrete panel submitted to a thermal gradient; (c) colour alteration profiles within the panel determined via the digital image analysis.

The comparison between the internal image of one hole drilled in a heated concrete panel (Fig. 7a) and the side view of a core taken from the same sample (Fig. 7b) allows to point out the limitations and the potential of this technique. As expected, the limited size of the drilled hole doesn't allow to recognize the material texture nor the shape and nature of the coarse aggregate. Moreover, the significant roughness of the hole produced by hammer-drilling makes the visual recognition of small pores and flaws quite a difficult task.
Nevertheless, some averaged values can still be measured, like the slight discoloration occurring along the hole axis. In a former study, the analysis of the digital images of concrete samples has been regarded as a method for detecting the colour variations induced by the exposure of concrete to high temperature [10]. This technique can be implemented on both kinds of image, though a change of the illuminant generally produces a shift of the chromaticity diagrams (a halogen source and the natural daylight have been used in the two images at issue). However, being significant the colour variation compared to pristine concrete, this bias can be deleted by zeroing the plots in the range pertaining to the undamaged material. It can be observed that the two images provide comparable trends of the pink discoloration which generally affects heated concrete in the range 300-600°C (Fig. 7c). A greater noise characterizes the plot obtained from the drilled hole, which is also more sensitive to the return to whitish-grey taking place at higher temperatures. Far less sophisticated observation techniques are required in case of stronger colour variations, as those produced by the common pH indicators for revealing the carbonation depth.

3 ANALYSIS OF DRILLING-POWDER SAMPLES

Several physicochemical analyses on concrete require a preliminary grinding of the material into a fine powder (X-ray diffraction, chloride-ions content, Differential Thermal Analysis, Thermo-Gravimetric Analysis, etc). Moreover, some tests that are normally performed on the intact samples, may be in principle carried out also on the material in pulverized form (carbonation depth, colour measurement, etc).
This evidence casts the base for merging the results of the hammer-drill perforation test and the following examination of the ensuing powder. Compared to the ordinary laboratory practice, the main limitation is the impracticality of controlling whether to include or not the coarse aggregate in the sample, leading to some uncertainties for small diameter holes. In case of steep variations of the investigated properties with the drilling depth, an important requirement is to preserve the order of extraction, so to obtain a sorted sample of powder. Dividing the drilling operation in regular steps is a viable solution to this problem.
In order to check the viability of this kind of test, different types of analysis have been performed on sorted samples of powder obtained by drilling concrete with a 10 mm diameter bit. The first example concerns again the discoloration of heated concrete. By collecting the powder in a transparent test tube, the slight concrete colour variations induced by the exposure to high temperature can be measured via the digital image analysis technique (Fig. 8), as already discussed

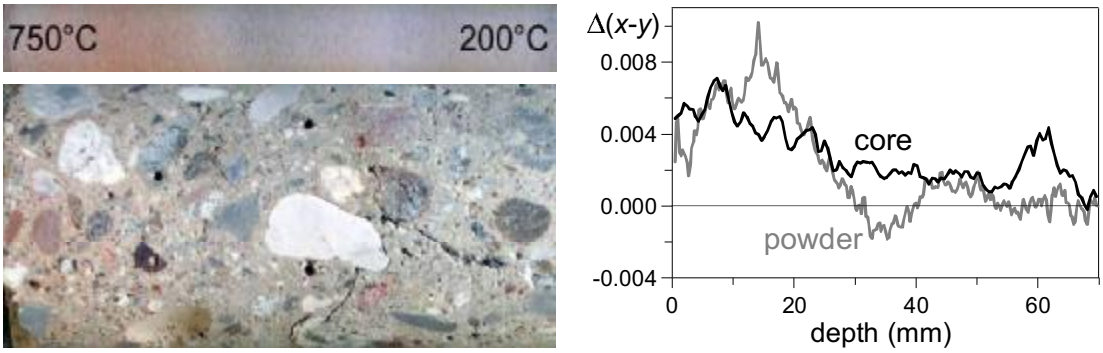

Fig. 8. Discoloration of a powder sample and a core taken from the same heated panel and corresponding colour variation profiles obtained via the digital image analysis.

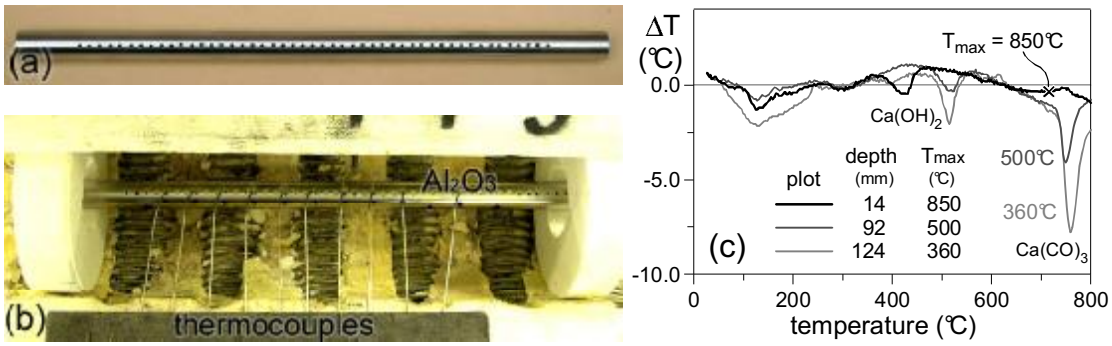

Fig. 9. (a) Nickel-chromium perforated pipe to be filled with a sorted sample of drilling-powder and (b) test setup in the split-tube furnace; (c) temperature differentials pertaining to different depths in a heated panel (see Fig. 7).

in the previous section. After having determined the appropriate scale factor between the hole depth and the length of the powder sample, the discoloration profile can be plotted. Compared to the conventional analysis of cores, an increased noise is observed, probably because of the random influence of the coarse aggregate (see the analogy between Fig. 8 and Fig. 7b). Nonetheless, the relevant features of the material alteration can still be detected.

The second example regards the differential thermal analysis (DTA), that involves the heating a small sample of powdered concrete together with a similar amount of inert material (e.g. aluminium oxide Al_2O_3). Both samples are monitored to trace their temperature difference, which ensues from the transformations occurring in the tested material. This method has been proposed as a way for analyzing fire damaged concrete, because during this second heating minor or different transformations should occur until the maximum temperature experienced during the fire is exceeded [11]. In the case a temperature profile through the cover has to be worked out, the DT analysis has to be repeated on a series of samples taken at increasing depth, which is quite a demanding procedure.

In order to overcome this limitation, a sorted sample of drilling-powder has been collected in a metal pipe, together with a small amount of aluminium oxide. The pipe (Fig. 9a) is made of a thermally stable alloy (nickel-chromium) and it is perforated at regular steps along one generatrix so to allow to vent the developing gases and to reach the inner powder with a series of thin shielded thermocouples (1 mm diameter - Fig. 9b). By heating the pipe in a split-tube furnace (5°C/min) several DT analyses can be performed in one take. Though less rigorous than adopting the standard test procedure and a dedicated device, this method is far less time demanding and still allows to detect the onset of the relevant transformations. The first results (Fig. 9c) pertaining to the same panel already mentioned in Fig. 7 seem in good agreement with the trends reported in the literature [11]. The anticipated dissociation of the calcium-hydroxide resulting from the calcium-oxide rehydration compared to unheated portlandite (350-500°C) and the disappearance of the peak ascribable to the calcium-carbonate dissociation (700-800°C) are the main features to trace on the thermo-differential plots.

4 CONCLUSIONS

In this paper the idea to monitor the resistance encountered while drilling a concrete member and then to analyse the ensuing material has been regarded as a combined method for detecting the deterioration of the concrete cover due to fire exposure. In this perspective, the well established practice of analysing the drilled cores can take advantage of this preliminary scan of the material response, which comes at no cost once the acquisition of samples has been planned. On the other hand, the faster and less invasive monitoring of the hammer-drilling resistance, that in principle is not intended to provide any material sample, can be fostered by the analysis of both the ground-concrete powder and the remaining hole. The results obtained in these different directions can be summarized as follows.

The penetration rate of the core bit, at constant exerted thrust, is the most responsive parameter to be monitored while drilling a concrete member. The sensitivity is comparable to other effective ND techniques, with the additional benefit of a point-by-point analysis at increasing depth. As concerns the hammer-drilling technique, the energy spent to penetrate the material is the most significant parameter to be surveyed, with the limitation of a poor sensitivity to low levels of material damage. Further studies are in progress in order to offset this limitation

A valuable support to the visual inspection of the drilled holes is the proper processing of the endoscopic images, aimed to provide a front view of the unwrapped cylindrical surface of the cavity. However, the limited size and the considerable roughness characterizing the holes produced by hammer-drilling make the recognition of the material texture and the detection of any small flaws quite a difficult task. On the contrary, the analysis of more sketchy features like the pink discolouration of heated concrete may still compete with the traditional inspection of cores.

Collecting the powder produced while drilling a member is a convenient alternative to cores in case the laboratory analyses require a preliminary grounding of concrete into a fine powder. The tests concerning the colour alterations and the physicochemical response of the material seem to confirm the viability of this method. The only drawback is the impracticality of controlling the effect of the coarse aggregate, whose local influence may prevail in relatively small drilled holes.

These results are intended as a first check on the viability and significance of the testing techniques herein proposed. A systematic study on the reliability of the most promising methods will be necessary in order to factually merge different test results in the assessment of the fire damaged concrete cover.

REFERENCES

[1] Felicetti R., Gambarova P.G., Expertise and assessment of structures after fire, in *Fire design of concrete structures - Structural behaviour and assessment*, Fib Bulletin n.46, 2008, p.64-114.

[2] Laboratoire Central des Ponts et Chaussées, Présentation des techniques de diagnostic de l'etat d'un béton soumis à un incendie, Report ME 62, 2005, 114 p. (in French).

[3] Short N.R., Purkiss J.A., Guise S.E., Assessment of Fire-Damaged Concrete, *Proc. of the Concrete Communication Conference*, BCA, 29-30 June, 2000, Crowthorn, UK, pp.245-254.

[4] Dilek U., Leming M.L., Comparison of pulse velocity and impact-echo findings to properties of thin disks from a fire damaged slab, *Journal of Performance of Constructed Facilities*, ASCE, Vol. 21, Nr.1, February 2007, pp.13-21.

[5] Chagneau F., Levasseur M., Contrôle des matériaux de construction par dynamostratigraphie, *Materials and Structures*, Vol. 22, 1989, pp.231-236 (in French).

[6] Felicetti R., The drilling resistance test for the assessment of fire damaged concrete, *Journal of Cement and Concrete Composites*, Vol.28, 2006, pp.321-329.

[7] Colombo M., Felicetti R., New NDT techniques for the assessment of fire-damaged concrete structures, *Fire Safety Journal*, Vol.42, 2007, pp.461-472.

[8] Li, X., Lok, T.S., Summers, D.A., Rupert, G., Tyler, J., Stress and energy reflection from impact on rocks using different indentors, *Geotechnical and Geological Engineering*, Vol. 19, 2001, pp.119-136.

[9] Trucco E., Verri, A., Introductory techniques for 3-D computer vision, *Prentice Hall*, 1998.

[10] Felicetti R., Digital-Camera Colorimetry for the Assessment of Fire-Damaged Concrete, *Proc. Int. Workshop on "Fire Design of Concrete Structures: What now? What next?"*, fib Task group 4.3, 2-3 December, 2004, Milan, Italy, 2005, pp.211-220.

[11] Alarcon-Ruiz L., Platret G., Massieu E., Ehrlacher A., The use of thermal analysis in assessing the effect of temperature on a cement paste, *Cem. and Concr. Res.*,Vol.35, 2005, pp. 609–613.

EXPERIMENTAL ANALYSIS OF CONCRETE STRENGTH AT HIGH TEMPERATURES AND AFTER COOLING

Eike Klingsch, Andrea Frangi, Mario Fontana

Institute of Structural Engineering, Steel, Timber and Composite Structures, ETH Zurich, Switzerland

INTRODUCTION

Since some years, the cement industry invests in the development of new, environmental friendly blended cement products, like e.g. supersulfated slag cement (SSC). This cement is mainly made out of blast furnace slag, a by product of iron making; hence less energy is used during the manufacturing process and less carbon dioxide is produced compared to Portland cement.

The thermal and mechanical properties of concrete change at elevated temperatures. This change of material properties influences the load carrying and deformation behavior of concrete structures in case of fire. The rate of increase of temperature across the section in a concrete element is relatively slow and inner zones are protected against heat. Therefore reinforced concrete structures with adequate structural detailing like minimum dimensions and cover thicknesses of the reinforcement usually reach a satisfactory fire resistance without any additional fire protection [EN 1992-1-2]. However after the fire has been extinguished the heat penetration into the cross section may continue for hours and is inversed during the cooling phase leading to thermal stresses and cracks [Frangi 2006]. Additionally chemical reactions like the reformation of calcium hydroxide during the cooling phase can widen up micro cracks. The combination of these two phenomena may lead to a significant reduction of the compressive strength of concrete after fire [Hertz 2005]. Investigations carried out by Felicetti and Gambarova [CEB 46] find that the minimum strength is reached after the concrete has cooled down to normal temperature.

For general application of concrete made of supersulfated slag cement, there is a lack of basic knowledge on the mechanical behaviour during and after a fire. A research project on the fire behaviour of concrete made of supersulfated slag cement is currently carried out at the Institute of Structural Engineering at ETH Zurich. The research project aims at enlarging the theoretical and experimental data on the performance of concrete made of supersulfated slag cement during and after a fire. An extensive testing program using the IBK electric furnace is performed to study the temperature dependent loss of strength of concrete and to develop temperature dependent stress-strain relationships for concrete made of supersulfated and other types of cement for a complete temperature cycle (including cooling phase). The stress-strain relationships can be used as material input parameters for finite-element analysis and the development of calculation models.

TEST SET UP AND TESTING PROCEDURE

The tests were performed using an electric-powered furnace that can reach a temperature of up to 1000°C. The attainable heating rate at the concrete surface of cylindrical specimens with a diameter of 150 mm and a length of 300 mm can be up to 4.5 K/min. The furnace consists of two U-shaped shells, allowing the test specimen to be placed in the middle of the oven in a metal cage to protect the furnace in case of concrete spalling.

The concrete specimen is loaded with a hydraulic cylinder. At the contact zones a thin layer of gypsum ensures an even and centrical force transmission. The test set-up is shown in figure 3.

All tests were carried out within a very short time-frame and the specimens were kept in a controlled climate (20°C/50%) to reduce the influences of concrete age and moisture content. The tests specimens were heated up slowly to the maximum temperature of 300°C, 500°C and 700°C. After maintaining the temperature level for two hours, the test specimens were cooled down linearly. The compressive strength at maximum temperature (hot strength) as well as the residual strength during the cooling down phase and after being cooled down to ambient temperature of 20°C were measured. The general thermal cycle is shown in figure 1. The corresponding target temperatures for the hot and residual strength are given in table 1.

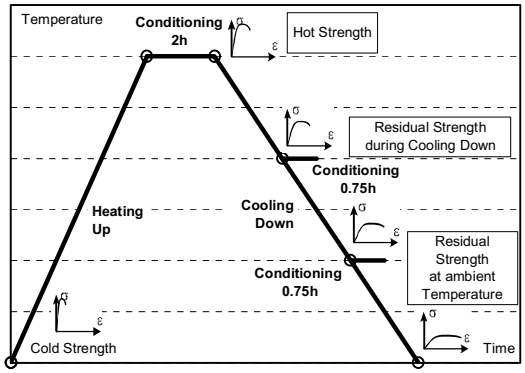

Fig.1 Full thermal cycle

Table 1. Testing Procedure

Testing Series	Max. Temperature	Tests at target temperature (hot and residual strength)			
1	300°C	Hot strength			20°C
2	500°C	Hot strength		300°C	20°C
3	700°C	Hot strength	500°C	300°C	20°C

In order to minimize temperature gradients in the cross section and related thermal stresses slow heating up and cooling down rates and a conditioning time of 2h at maximum temperature were chosen. According to test results presented in [CEB 46], the heating up rate can be as high as 5 K/min while the cooling down rate should not exceed 1.0 K/min, higher values reduce the formation of calcium hydroxide, causing a higher residual strength which decreases within days after cooling down. First simple finite element analysis were carried out to predict the maximum heat gradient during heating up and cooling down. According to this first analysis, literature results and preliminary test, the heating up rate at the surface was chosen as 1.5 K/min and the surface cooling down rate as 0.9 K/min. During the entire heating cycle, the concrete was loaded with a maximum pressure of roughly 0.3 MPa which is less than 0.75% of the cold strength; hence, the cylinders can be assumed as unloaded as the concrete's thermal expansion is not affected by any load effects. The free expansion, internal damages caused by cracks and debonding of the cement matrix lead to a lower hot and residual strength compared to loaded specimens [CEB 46]. A test series with loaded concrete specimens is planned. At the end of the thermal cycle, when reaching the target temperature, the concrete strength was determined inside the furnace. The furnace was not opened; hence the concrete surface temperature remained constant. The load was applied deformation controlled with a constant speed of 0.005 mm/s. The stress-strain curve was continuously monitored and the test was stopped manually post fracture. The concrete cold strength was determined in an analogous manner with the same deformation speed.
After the testing procedure, the specimens were visually inspected with respect to crack formation and spalling. None of the tested concrete specimens showed loose or missing concrete parts caused by spalling. Equalizing the contact zones of the specimens with a thin layer of gypsum lead to proper results, since the fracture pattern was shaped like a truncated cone.

TEST SPECIMENS

The tests were conducted using cylindrical specimens (d=150mm / L=300mm) made of three different concrete mixtures, a superfulfated slag cement (SSC), a Portland-limestone cement (CEM II-A-LL), and a ordinary Portland cement (CEM I). The concrete's mixing properties were identical, apart from the cement used. The cement content was always 300 kg/m^3 with a w/c ratio of 0.55. Common types of carbonate and siliceous aggregates up to 32 mm were used to prepare the test specimens. The fresh concrete density was 2420 kg/m^3, it decreased to 2390 kg/m^3 during conditioning in 20°C/50% atmosphere.

Before concreting, a petro graphic analysis of the aggregates was carried out. The gravel plant is located in the area of an end moraine, hence the main component are based on limestone gravel. The petro graphic analysis shows that roughly 57% of the aggregates consist of carbonate, while 38% of the gravel components are siliceous.

The specimen diameter used in hot material testing, is mostly smaller than 100 mm. These small-scale specimens are insufficient for grading curves with a maximum aggregate size of 32 mm. To ensure adequate compacting of the fresh concrete, cylindrical specimens with a diameter of 150 mm and a height of 300 mm were used.

Fig.2 Thermocouple and formwork

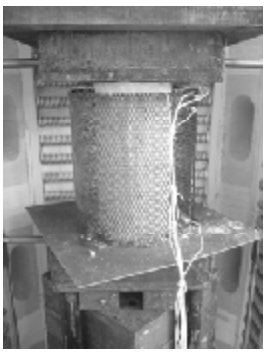

Fig.3. Concrete specimen in furnace

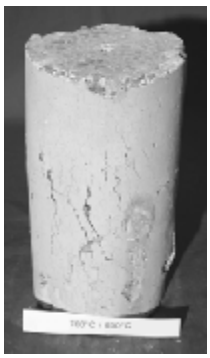

Fig.4. Concrete specimen after the test

The specimens were produced under laboratory conditions. The facilities were climate controlled with a relative humidity of 65% and a temperature of 20°C. As formwork, a non-absorbent plastic cylinder was used. Four thermocouples were placed into this formwork before concreting: two in the core, and additionally two in 30 mm depth, as shown in figure 2 The thermocouples had at least a distance of 30 mm between each other, to minimize perturbation due to electric fields. The thermocouples were fixed to a 2 mm welding wire to ensure that the couples will stay in position during concreting and compacting. This set-up followed generally accepted guidelines [ABM 1990].

The concrete was poured into the formwork in two stages and was compacted after each stage using a vibrating table. Striking times and storage conditions for hardened concrete are respected according to [EN 12390]. According to these regulations, the specimens were cured for three days after concreting; they were then placed either in water or in very humid conditions, i.e. temperature of 20°C and a relative humidity of at least 95% up to the age of 28d from the time of concreting.

According to [EN 1363-1], the specimens have to be conditioned in a dry atmosphere for at least 90d. The surrounding temperature should not exceed 23°C and the moisture level should be around 50% rel. humidity. All cylinders were stored in a 20°C/50% conditioning room; the loss of weight of the concrete was monitored on a weekly basis until the specimen was tested in the furnace. At the time of testing, the specimens showed no significant loss in weight.

TEST PROGRAM

Table 2 shows the test program carried out. While steps one to four are carried out for all cement types, steps five and six are conducted on a few specimens only. The interim values at step four are determined during cooling down cycle (see figure 1). The first temperature in table 2 (step 4 - right) indicates the maximum temperature, while the second temperature is the temperature for testing during cooling down.

Table 2. Testing Program

Step	Measured Category	Temperature Level
1	Cold Strength	20°C
2	Hot strength	300°C ; 500°C; 700°C
3	Residual Strength	After concrete cooled down to 20°C from the three hot strength temperature levels from step 2
4	Interim Values	700°C – 500°C; 700°C – 300°C; 500°C – 300°C
5	Slow heating rate (on CEM II-A-LL cement only)	500°C – hot strength 500°C – 20°C (residual strength after cooling down)
6	Magnetic Resonance Imaging (one CEM I specimen only)	300°C - 20°C

TEST RESULTS

The tested specimens showed no significant difference in strength at room temperature, the average coefficient of variation was less than 5%. The cylindrical cold strength after 90d was 33.1 MPa for the SSC concrete, 34.3 MPa for the CEM II-A-LL concrete and 40.3 MPa for the CEM I concrete.

During the heating cycle, the temperature at the concrete surface and at the core of the specimen was constantly monitored. It was assured that the average temperature gradient between surface and core during the heating cycle was never higher than 1 K/mm.

The measured stress-strain curves for the SSC concrete tests are shown in figure 5. The left picture includes the cold strength stress-strain curve. The interim values during cooling down are presented as well. It could be observed, that at hot stage, the curves' gradient is monotonic, while at residual stage, the gradient shows one inflexion point. This effect increases with increasing maximum temperature and lower cooling temperatures respectively. This is caused by the loss in bond between the aggregates and the cement matrix during cooling down. The stress strain curves for the CEM II-A-LL and the CEM I cement were similar; the SSC showed higher strains at ultimate load.

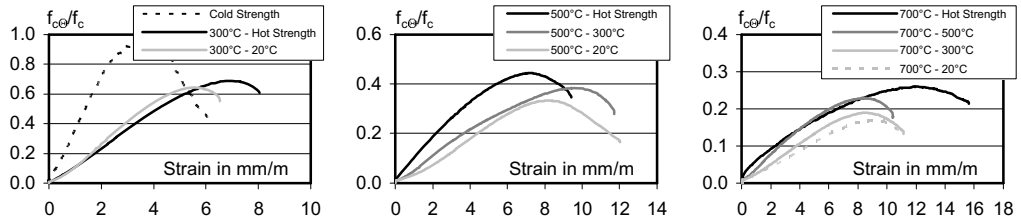

max. temp. level of 300°C (including cold strength) | max. temp. level of 500°C | max. temp. level of 700°C

Fig.5. Stress-Strain relation for the SSC concrete for different heating up levels.

Figure 6 shows the reduction factors for hot and residual strength of the specimen with the three different types of cement used. All results are normalized to the corresponding cold strength before testing (cold strength = 1.0). Starting at the relative cold strength of 1.0 at 20°C, the relative hot strength is given by the continuous line, the dots corresponding to the test results at temperature levels of 300°C, 500°C or 700°C. After reaching the maximum temperature level, the loss in strength during and after cooling down is found by following the dotted line to the left until reaching the residual strength at ambient temperature of 20°C after a full thermal cycle.

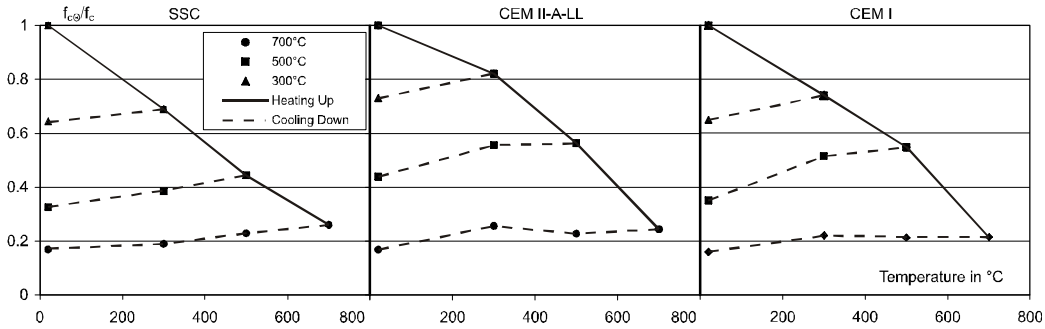

Fig.6. Temperature-Strength relation for three different cements during heating up and cooling down phase

As shown in figure 6, the specimens with SSC show slightly lower hot strength compared to the CEM II-A-LL and CEM I cement at the 300°C and 500°C temperature level. At higher temperature levels, i.e. 700°C, all cements show similar performances. While the loss in strength during cooling down for the SSC was nearly linear CEM I and II show a non-linear residual strength development, with an increased losses in strength while cooling down from 300°C to 20°C.

In general, the losses in strength from hot to residual stage at ambient temperature increase with increasing maximum temperature levels. The concrete specimens cooled down from a maximum temperature of 300°C had an average residual strength of 91% compared to the hot strength. At 500°C it was 72%, and after cooling down from 700°C, the average residual strength was 69%.

Magnetic resonance imaging

Using magnetic resonance imaging the entire concrete cylinder was scanned slice by slice. Higher densities of any scanned objects inside the concrete cylinder, like aggregates, are shown in brighter greyscales, hence, cracks, voids and air pores are shown as black lines or dots in the image.

After heating one CEM I specimen up to 300°C, it was cooled down and inspected by magnetic resonance imaging. The main aim was to study crack formation inside the specimen, and to investigate if any loss in bond between the cement matrix and the aggregates occurred. Scans on SSC and CEM II-A-LL samples are planned.

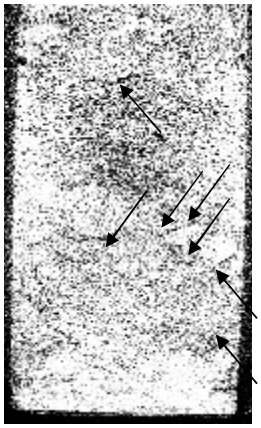

Fig.7. Magnetic resonance imaging

Figure 7 shows that the bond between the aggregates and the cement matrix became loose over the entire cross section. The arrows indicate the zones, where the bond was affected.

CONCLUSIONS

The results of this first series of test on the hot and on the residual strength of concrete after a fire, including cooling can be summarized as follows:

- The difference in strength at hot and residual stage after cooling down to ambient temperature is significant. The losses in residual strength during cooling down increases with higher temperatures.
- During the cooling down phase, a non-linear material behaviour for CEM I and CEM II is observed.
- Even after cooling down from a moderate temperature of 300°C debonding effects between the cement matrix and the aggregates could be observed by magnetic resonance imaging.
- The supersulfated slag cement (SSC) performs not much different compared to ordinary Portland cement.

AKNOWLEDGEMENTS

Thanks to Holcim Group Support Ltd. for the supply of the test specimen.

REFERENCES

[Frangi 2006] A. Frangi, C. Tesar, M. Fontana; Tragwiderstand von Betonbauteilen nach dem Brand; Bauphysik 2006; 28: pp. 170–183

[CEB 46] CEB-FIP state-of-art report bulletin 46; Fire design of concrete structures – structural behaviour and assessment, 2008

[ABM 1990] ABM-Paper 2A by German Federal Institute for Materials Research and Testing, 1990

[EN 12390] EN 12390-2:2008; Testing hardened concrete - Part 2: Making and curing specimens for strength tests

[EN 1363-1] EN 1363-1:1999; Fire resistance tests - Part 1: General requirements

[Hertz 2005] K. D. Hertz, Concrete strength for fire safety design; Magazine of Concrete Research 2005; 57: p. 445-453

[EN 1992-1-2] EN 1992-1-2:2004; Eurocode 2: Design of concrete structures; Part 1-2: General rules - Structural fire design

NUMERICAL ANALYSIS OF CONCRETE COLUMNS IN FIRE
Advanced versus simplified calculation methods

Miguel C. Gonçalves [a], Jean Marc-Franssen [b] , Vitor Abrantes [a] & João Paulo C. Rodrigues [c]

[a] University of Porto, Faculty of Engineering, Porto, Portugal
[b] University of Liège, ArGEnCo, Liège, Belgium
[c] University of Coimbra, Faculty of Sciences and Technology, Coimbra, Portugal

INTRODUCTION

A column is a structural element whose main function is to support axial forces. When these forces are high, lateral deformation will occur, inducing an increment in the bending moment, known as second order effects. These second order effects have a great effect on the behavior of the column in fire and must be taken into account in fire analysis methods.

Two issues are important in the assessment of the fire resistance of concrete columns: for the resistance, the definition the interaction *N-M* diagram of the column, and for the actions, the geometrical and material non-linearity, which are both highly temperature dependent.

The authors describe a simplified calculation method named SimFIRc [1], developed for the analysis of reinforced concrete (RC) columns in fire. The results are compared with those obtained with an advanced calculation method, the finite element program SAFIR, [2]. This program, developed by Jean Marc-Franssen, in the University of Liège, Belgium, can perform the geometric and material non-linear analysis of building elements in fire.

1 CALCULATION PROCESS

The evaluation of the behavior of building structures in fire is very easy using numerical modeling. Two types of model are available in the Eurocodes for that purpose: simplified and the advanced calculation models [3].

1.1 SAFIR

The main objective of analyzing structures is to determine the mechanical behavior of a structure until failure. SAFIR has been developed with the specific aim of modeling structures in fire, with an effort having been made to achieve a wider and more general field of application [2].

The software takes the effects of large displacements into account, using a fiber model where the section is divided into fibers. Each fiber is considered to have a different temperature. The mechanical model was based on a 3D Bernoulli beam finite element.

The thermal and the mechanical analyses are performed separately, in that order, which means that the temperature distribution will obviously deeply influence the mechanical response. However the determination of the temperatures in the fire compartment is a prerequisite of this software, and this can be done with the ISO 834 or some other fire curve.

The program has databases of thermal and mechanical properties for steel, concrete and aluminum and several fire curves.

The thermal analysis

Heat transfer by conduction in solid materials is described by the Fourier equation that is solved in SAFIR according to the standard finite element procedure. The main hypotheses are:

- The materials are isotropic, not submitted to movement, not compressible and have no mechanical dissipation;
- There is no thermal resistance in the interface between adjacent materials.

The local equation describing conduction in solid materials has the form of equation 1 in a Cartesian system of coordinates:

$$K\left(\frac{\partial^2 T}{\partial x^2}+\frac{\partial^2 T}{\partial y^2}+\frac{\partial^2 T}{\partial z^2}\right)+Q-C\rho\frac{\partial T}{\partial t}=0 \qquad (1)$$

Where:

K	= thermal conductivity, W/mK	T	= temperature, K
x, y, z	= coordinates, m	Q	= internally generated heat, W/m^3
C	= specific heat, J/kgK	ρ	= specific mass density, kg/m^3
t	=time, s		

The classical shape functions, N, are used. If the temperature of Equation (1) is replaced by the approximation $T = N_i T$, multiplied by a weighting function and integrated into the volume of the element, then:

$$\int_{element} k\{\nabla N_i\}\langle\nabla N_j\rangle dv T_i + \int_{element} C\rho N_i N_j dv \dot{T}_i + \int_{element} Q N_j dv = \int_{boundary} N_j q_n dS \qquad (2)$$

Where ∇ means $\langle\partial/\partial_x;\partial/\partial_y;\partial/\partial_z\rangle$ and q_n is the heat flux at the boundary of the element.

Finally, when the contributions of all the elements are summed, the matrix (Equation 3) is obtained, describing the equilibrium of heat fluxes in the structure at any given instant of time:

$$[K]\{T\}+[C]\{\dot{T}\}=\{g\} \qquad (3)$$

Where:

$[K]$	= matrix of conductivity	$\{\dot{T}\}$	= vector of temperatures at the nodes
$[C]$	= matrix of capacity	$\{g\}$	= vector accounting for the heat exchange at the boundary.

The fact that the thermal properties are temperature dependent is taken into account in equation 3, which expresses thermal equilibrium at a given time.

The mechanical analysis

The basis of the mechanical analysis of structures that have large displacements is the incremental form of the principal of virtual work. If a total co-rotational configuration is used it as given by equation 4:

$$\int_V \left(\bar{D}_{ijkl} d\bar{E}_{kl}\delta\bar{E}_{ij} + S_{ij}\delta d\bar{E}_{ij}\right)dV = \int_V \left(d\bar{f}_i\delta\bar{u}_i + \bar{f}_i\delta d\bar{u}_i\right)dV \qquad (4)$$

Where:

$V = \bar{V}$ = the undeformed volume of the element

S_{ij} = tensor of the second Pialo-Kirchoff stress

$\overline{D}_{ijkl} = D_{ijkl}$ = tensor defining the incremental constitutive law of the material

$\delta\overline{E}_{ij}$ = Green tensor of the virtual field of displacement

$\bar{f}_i$ = volume forces

$\delta\overline{u}_i$ = virtual field of displacements from the deformed position of the element

In order to solve this equation in a displacement-based finite element formulation, we obtain the matrix equation that governs the iteration from one position to the next position of equilibrium:

$$\int_v B^T DBdVdp + \int_v S^T \delta ledVdp = (K_u + K_s)dp = f^{ext} - f^{\text{int}} \tag{5}$$

Where:

K_u = comprises the linear elastic and the geometric stiffness matrices

K_s = is the stress generated stiffness matrix

f^{ext} = nodal forces energetically equivalent to the applied forces

f^{int} = nodal forces obtained equivalent to the applied forces

1.2 SimFirC

The SimFIRc model was developed for structural elements of reinforced concrete subjected to second order effects with an axial load. It is inspired by the method of nominal stiffness described in EN 1992-1-1, [4].

But there are two aspects to consider in the evaluation of the fire resistance of a column, in analysis at high temperatures:

- For the resistance of the element it is necessary to calculate the diagram of the bending resistance of one section of the RC column (interaction diagram *N-M*), which depends on a great many parameters, such us considerations of material non-linearity as a function of temperature. This diagram establishes the possible domain of the combinations of actions $N_{Rd,fi}$ and $M_{Rd,fi}$ for an RC section subjected to fire at a certain instant of time;

- For the action it is necessary to take into account both geometric non-linearity and material non-linearity (thermal effect). This is accomplished through the method of nominal stiffness.

It will be the intersection of these two curves, calculated for the same instant, that will give the resistance of the column.

The second order effect is calculated with equation 6, which is a function of the first order moment of the critical load and of the load to which the column is subjected.

$$M_{Ed} = M_{0Ed} \cdot (1 + \beta / (N_B / N_{Ed} - 1)) \tag{6}$$

where:

M_{0Ed} = Design value of first order moment, kN.m

β = π^2 / c_0 with $c_0 = 9{,}8$; first order moment (parabolic distribution), -

N_{Ed} = Design value of the axial load, kN

N_B = Buckling load based on the reduction of stiffness, or N_{cr}, kN

The main calculation procedure for SimFIRc is shown in Fig. 1:

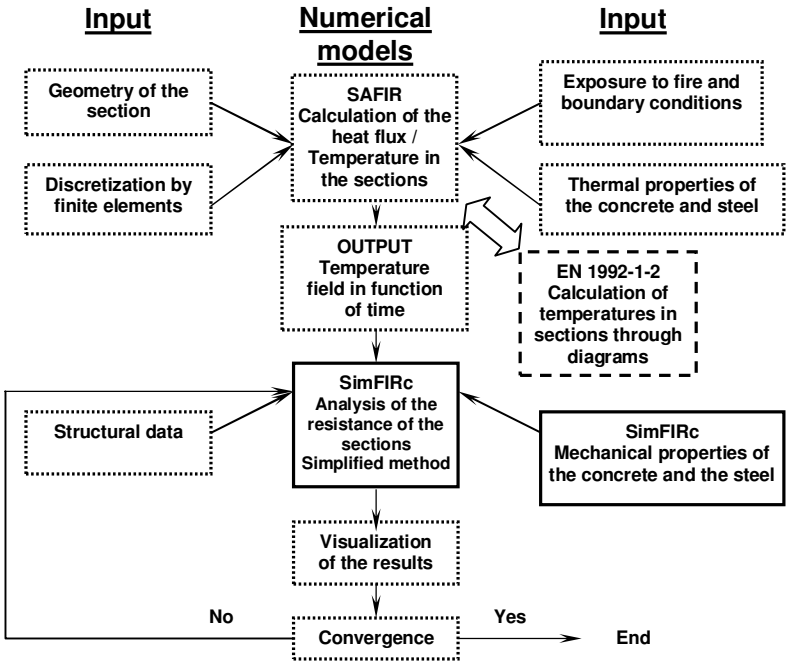

Figure 1. Procedure of calculation of the simplified method "SimFIRc".

The interaction diagram can be created with the equations of equilibrium (7) and (8) established for a certain instant to which correspond certain temperatures in the reinforcement bars and in each of the six zones of concrete.

$$N_{Rd,fi} = \sum_{i=1}^{6} b_{fi} \cdot a_i \cdot f_{cd,fi}\left(\theta_i, \varepsilon_{c,i}\right) + \sum_{j=1}^{m} A_{sj} \cdot f_{sy,fi}\left(\theta_j, \varepsilon_{s,j}\right) \tag{7}$$

With m being the number of reinforcement bars,

$$\begin{aligned} M_{Rd,fi} = & \sum_{i=1}^{3} b_{fi}\left[a_i \cdot f_{cd,fi}\left(\theta_i, \varepsilon_{c,i}\right)\right] \cdot \left[\frac{h}{2} - a_z - \frac{a_i}{2} - a_n\right] \\ & - \sum_{k=4}^{6} b_{fi}\left[a_k \cdot f_{cd,fi}\left(\theta_k, \varepsilon_{c,k}\right)\right] \cdot \left[-\frac{a_k}{2} - a_l\right] \qquad \begin{matrix} n < i \\ , l < k \end{matrix} \\ & + \sum_{j=1}^{m(armad)} A_{sj} \cdot f_{sy,fi}\left(\theta_j, \varepsilon_{s,j}\right) \cdot z_j \end{aligned} \tag{8}$$

and l and k are the number of concrete zones respectively above and below the center of the section. The other variables are presented in Figure 2.

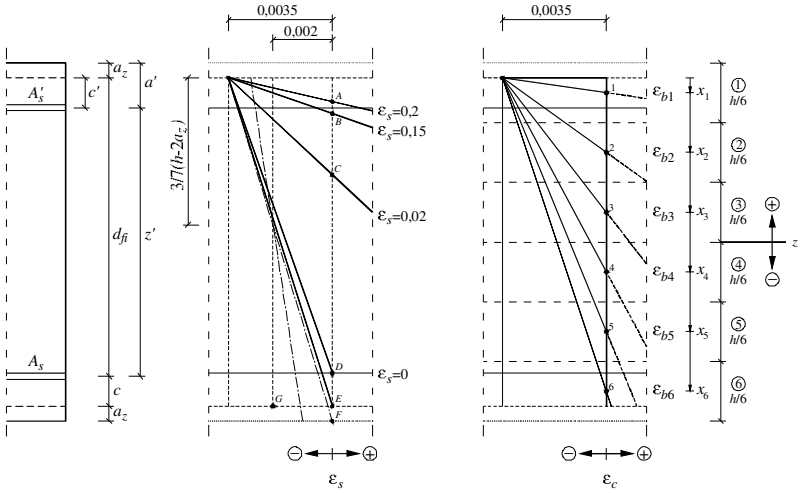

Figure 2. Limit strains in the reinforcement steel bars and in the 6 concrete zones (SimFIRc).

2 EXAMPLE

The RC columns analyzed were made of concrete C35/45 with siliceous aggregate and steel reinforcement bars S500 [3].

Figure 3 shows the mechanical boundary conditions and the accidental eccentricities (a trigonometrical function with maximum value of 2cm at middle height) and the application of the axial load in the top of the column (a). The discretization of the finite elements in the thermal analysis at the level of the section (b) is also given.

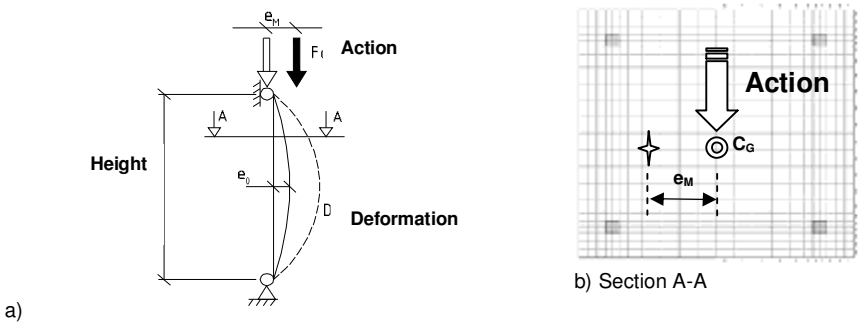

a)

Figure 3. a) Mechanical model; b) Discretization of the section.

2.1 Analysis of the results

Figure 4 shows the values of the interaction graphs $N_{R,fi}$-$M_{R,fi}$ and $N_{S,fi}$-$M_{S,fi}$ obtained by the simplified calculation method (SimFIRc), corresponding to the loadbearing capacity for 30, 60, 90 and 120 minutes (R30, R60, R90 and R120) of an 8 m tall RC column, with a cross-section of 0.3 m x 0.3m and where the distance from the axis of the reinforcement bars to the surface is a=4cm, considering steel reinforcement bars with diameters: 4ϕ12, 4ϕ16 and 4ϕ25,.The values obtained with the advanced calculation method (SAFIR) are also given.

Figure 5 gives the loadbearing capacity for 30, 60, 90 and 120 minutes of an RC with a cross-section of 0.3m x 0.3m, reinforcement bars with diameter 4ϕ25, a=4cm, and 4, 8 and 12 m tall, using the advanced calculation method (SAFIR) and the simplified calculation method (SimFIRc).

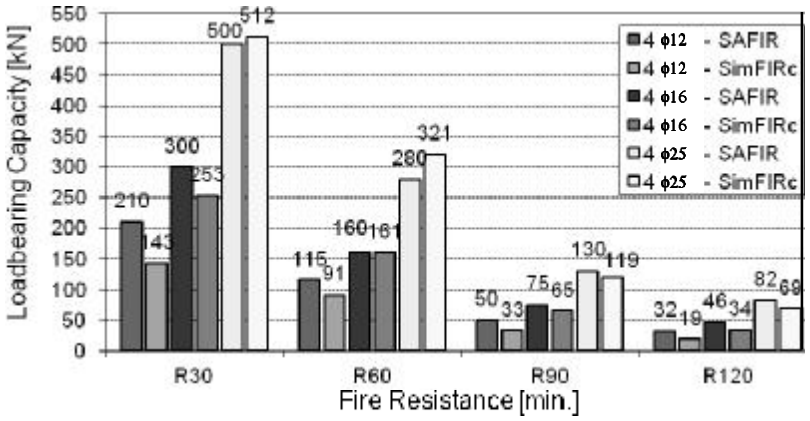

Fgure 4. Loabearing capacity of an RC column 8 m tall for different fire resistances.

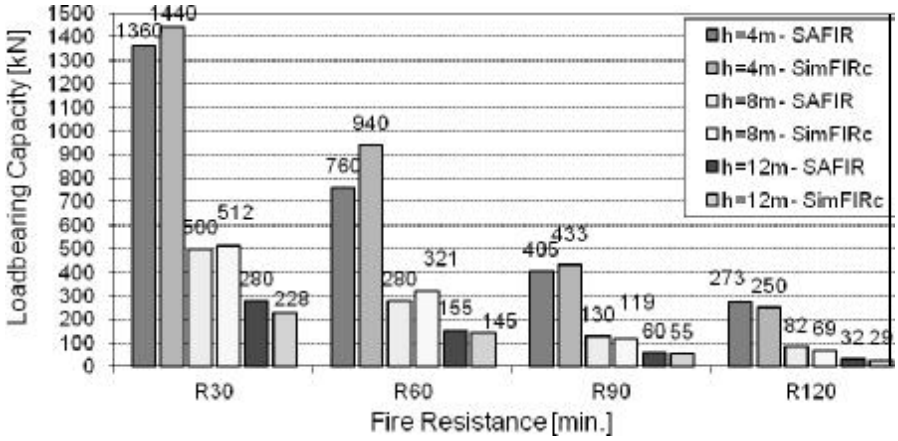

Figure 5. Loabearing capacity of RC columns with 4, 8 and 12 m tall

3. FINAL REMARKS

The formulation of EN 1992-1-1 [4] indicated for the calculation of the resistance of concrete sections at room temperature was suitably adapted by the author [1] to the specificity of thermal action (SimFIRc). The results are at the level of the ones obtained with the advanced calculation models (SAFIR), [2]. A relatively simple and powerful tool has been created which provides results on the side of safety.

REFERENCES

[1.] Miguel Chichorro Gonçalves, *Fire Behaviour of Structural Concrete Elements – Numerical Analysis and Methodology*, Ph.D. Thesis, Faculty of Engineering of the University of Porto, 2006

[2.] Jean-Marc Franssen, SAFIR: *A thermal/structural Program for Modeling Structures Under Fire*, Engineering Journal /Third Quarter/2005

[3.] EN 1992-1-2: *Design of concrete structures, part1-2: General rules - Structural fire design*, European Committee for Standardization, Brussels, 2004.

[4.] EN 1992-1-1: *Design of concrete structures, part 1-1: General rules and rules for buildings*, European Committee for Standardization, Brussels, 2004.

ANALYSIS OF THE BEHAVIOR IN FIRE OF CONCRETE LOADBEARING WALLS

Miguel C. Gonçalves [a], João Paulo C. Rodrigues [c] & Vitor Abrantes [a]

[a] University of Porto, Faculty of Engineering, Porto, Portugal
[c] University of Coimbra, Faculty of Sciences and Technology, Coimbra, Portugal

INTRODUCTION

When a fire occurs in a building, the high temperatures developed introduce important thermal and mechanical actions in the loadbearing elements. Walls are loadbearing elements that are greatly affected, due to the large surface exposed to fire. The boundary conditions, especially at the top, will also influence the performance of walls in fire.

The horizontal elements adjacent to the wall, like the slabs and beams, when heated in fire will apply horizontal forces perpendicular to the wall surface. These forces induce important bending moments and shear forces in the cross-section of the wall. At the same time, the structure surrounding the wall restrains its thermal elongation. The imposed forces and the thermal restraint both have a great influence on the reduction of the fire resistance of walls.

This paper presents the results of numerical simulations for the behavior in fire of loadbearing concrete walls restrained in their thermal elongation. The simulations were performed with the finite element program SAFIR [1], developed by Jean Marc-Franssen, in the University of Liège, Belgium, and the simplified calculation method SimFIRb developed by the authors of the paper. The parameters were considered in the analysis were the thickness of the wall, the height, the load level, the mechanical reinforcement ratio, the distribution of reinforcement in the cross-section, the number of floors adjacent to the walls and the boundary conditions. Walls that were built in at the base, with the top free or restrained against the horizontal displacement were considered.

1 CALCULATION PROCESS

The advanced calculation model used was the finite element program SAFIR [1], which, in addition to determining the ultimate load bearing capacity of the walls after a certain duration of fire, tracks the behavior of the element during the fire. The calculation process of SAFIR is described in other paper submitted by the same authors to this conference [2]. The simplified calculation model SimFIRb is a new model developed by the authors to evaluate the loabearing capacity of concrete beam sections in fire [3].

SimFIRb

The field of temperatures as a function of time can be calculated with the SAFIR model, taking into account the variation of the material properties with the temperature. SimFIRb reads the field of temperatures as input data. The analysis of the bending moment resistance is based on the balance of the forces mobilized in each part of the concrete and the forces mobilized in the steel reinforcement bars (equation 2). Equation 1 makes it possible to determine the height of the concrete compression zone, and consequently the lengths (moment arms) necessary for the calculation of the bending moment resistance in equation 2. The

analysis of the variation of the bending moment resistance of the walls subjected to a certain loading and the standard fire ISO 834, with the time is described by:

$$\sum\left(f_{sy,\theta_i}\cdot A_{s,i}\right)-\sum\left(f_{cd,\theta_j}\cdot A_{c,j}\right)=0 \quad (1)$$

$$M_u=\sum\left(f_{cd,\theta_j}\cdot A_{c,j}\cdot y_j\right) \quad (2)$$

where:

M_u - Bending moment resistance for a field of temperatures [kN.m]

f_{cd,θ_i} - Design value of the compression strength of the concrete j at temp. θ_j [MPa]

θ_j - Temperature of the concrete element j [ºC]

$A_{c,j}$ - Area of the concrete element j subjected to compression [m^2].

f_{sy,θ_i} - Value of the effective yield strength of the reinforcement bar i at temperature θ_i [MPa]

θ_i - Temperature of the reinforcement bar i [ºC]

$A_{s,i}$ - Area of the reinforcement bar i [m^2]

y_j - Moment arm of the resulting force of the concrete element in compression, j [m].

The calculation procedure was as follows:

1 - Determine a strain at the level of the center of gravity of the section: initial value εg=0;

2 - Determine a curvature for the section (initial value K=1x10^{-5} cm^{-1});

3 - Once these two degrees of freedom are defined, just vary εg (expression of the diagram of strain in the section) until the resulting normal force, from the corresponding stresses in the section, balances with the acting normal force (which may be other than 0);

4 - For the balanced position in terms of normal force, calculate the resulting bending moment;

5 - Increase the value of the curvature (initial value of the increment ΔK=2x10^{-5} cm^{-1}) and keep returning to point 3 until one of the following conditions is verified:

- The *M-K* enters a plateau;
- The strains in the concrete and the steel reach limit values;

This process is repeated for each distribution of temperatures in the cross-section, thereby finding the variation of the bending resistance capacity of a section over time (evaluated every 5 minutes).

The iterative process allows the increments, either from the curvature, or from the strain at the level of the center of gravity of the section, to be variable so as to guarantee the desired precision compatible with the discretization of the section with elements.

2 EXAMPLE OF CALCULATION

Concrete C30/32, made with siliceous aggregates, and steel S500 were used in the numerical simulations. Walls built in at the base and with the top free or against to the horizontal displacement (Figure 1a and b, respectively) were analyzed.

The structural evaluation finishes with the analysis of a more complex structure (Figure 1c), which is a wall similar to the previous ones but with adjacent building's floors. This wall has two supports, one at the top and other at mid height, corresponding to the floors.

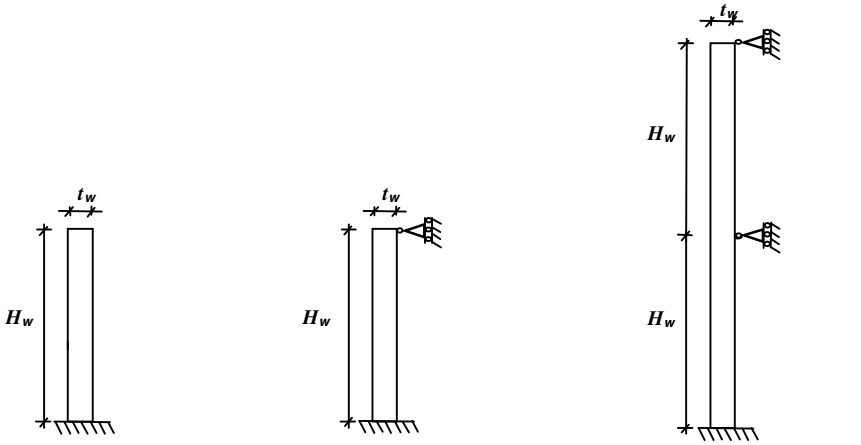

a) Wall built in at the base and free in the top

b) Wall built in at the base ´ and fixed in the top

c) Wall built in at the base with two adjacent floors

Figure 1. Structural models of the RC walls analyzed.

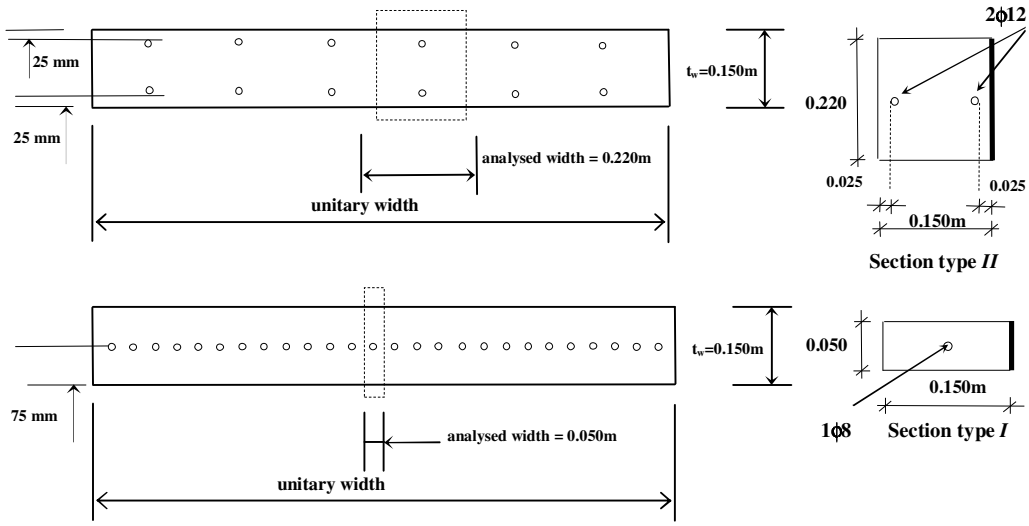

Figure 2. Cross-sections of the RC walls analyzed - sections type.

The cross-sections of the walls analyzed in the numerical simulations, thermal and mechanical analyses, are presented in Figure 2. The wall surface was completely subjected to the ISO 834 fire. The type I section is 0.150 m thick, has steel reinforcement bars ϕ8, spaced 0.050 m

apart. The type II section is 0.150 m thick, two steel reinforcement bars ϕ12, spaced 0.220 m apart with a 0.025 m concrete covering.

3 RESULTS

Simplified calculations were performed in order to determine the expected loadbearing capacity for the sections under analysis. The results are summarized in Table 1.

Table 1 – Bending moment resistance for 0, 30, 60, 90 and 120min, (SimFIRb).

	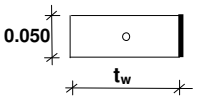				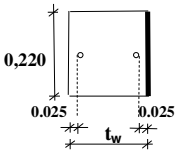				
t_w	0.125	0.150	0.200	0.250	0.150	0.200	0.150		
Reinforcement	1ϕ8				2ϕ12		2ϕ8	2ϕ10	2ϕ16
t [min.]	$M_{r,fi}$ [N.m]								
0	1164	1419	1948	2477	6463	8897	3018	4673	10323
30	1166	1419	1948	2477	5745	7846	2623	4144	9321
60	1081	1375	1949	2477	4840	6485	2150	3424	7915
90	960	1288	1900	2478	4000	5256	1679	2730	6669
120	830	1189	1820	2442	2964	3915	1197	1973	4964

Figures 3 and 4 give the results of the horizontal displacement at the top of the built-in base walls for different wall heights and thicknesses (Figure 3) and for a wall 6 m tall, varying the percentage of steel reinforcement for the type I and II sections (Figure 4).

The main conclusions drawn from Figures 3 and 4 are that, qualitative and quantitatively, the horizontal displacements of the wall are inversely proportional to its thickness and the percentage of steel reinforcement.

Figure 5 shows the horizontal displacements at the mid point of the walls built in at the base and fixed at the top, 6, 8 10 and 12 m tall and 0.125 m, 0.150 m, 0.200 m and 0.250 m thick. From this figure it can be observed that the horizontal displacements at mid height increase as the wall height increases and the wall thickness decreases.

Figure 6 presents the results of the bending moment of a wall with two heights (3 + 3 m) and with loads applied at the two floors, corresponding to a certain percentage of the resistance capacity of the wall at room temperature, and not considering buckling. The bending moment below the first support, in the base of the walls with different levels of axial load, varies with time, as shown in Figure 6. The walls subjected to high axial loads exhibit greater variation of the bending moment in all phases of the fire.

For an instant prior to failure, for F=0% or F=10%+10%, the largest bending moments are mobilized in the sections mentioned below the first support and in the base of the walls. For higher axial loads, the larger bending moments occur in the section that is immediately below the first support. From Figure 6 it can be concluded that the mobilization of bending moments in these two sections is about double for axial loads of 10%+10%.

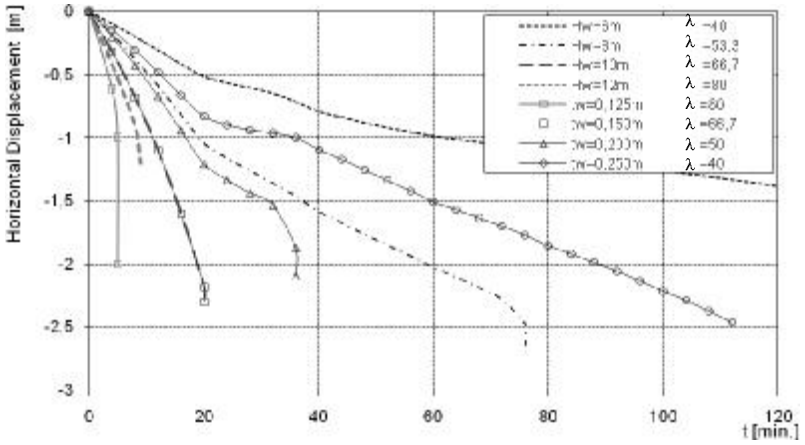

Figure 3. Horizontal displacement in the top of walls built in at the base for different wall slenderness.

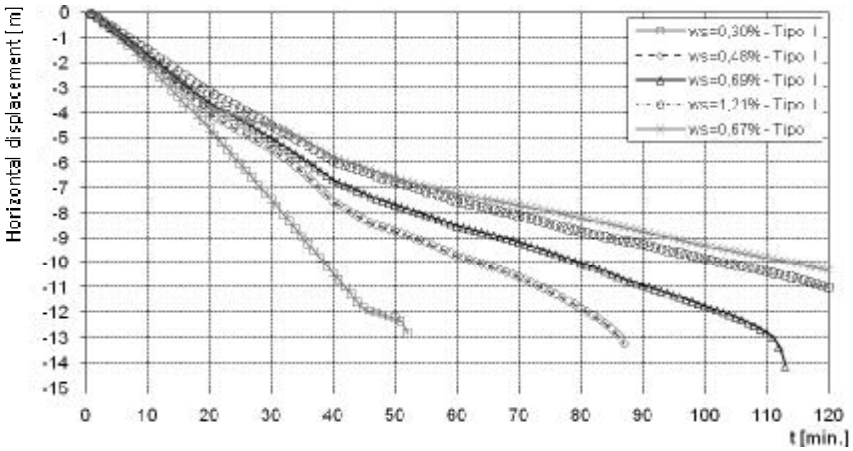

Figure 4. Horizontal displacement at the top of a wall built in at the base, 6 m tall, for different percentages of steel reinforcement.

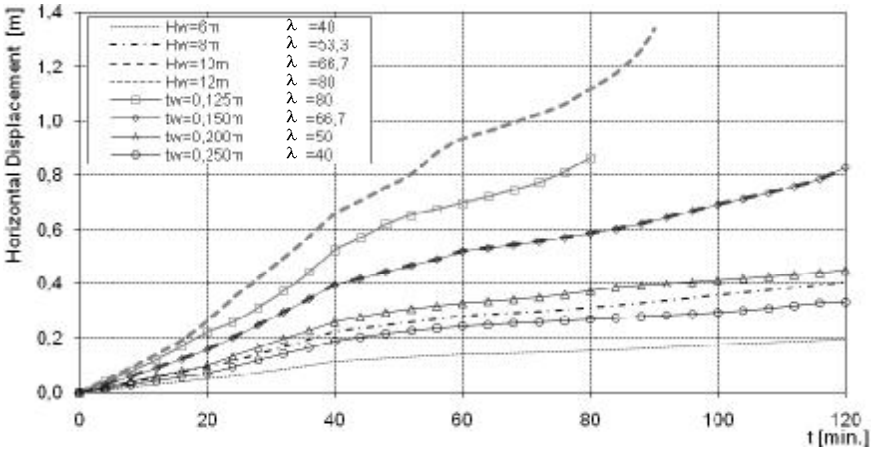

Figure 5. Horizontal displacements at mid height of walls of different heights and thicknesses.

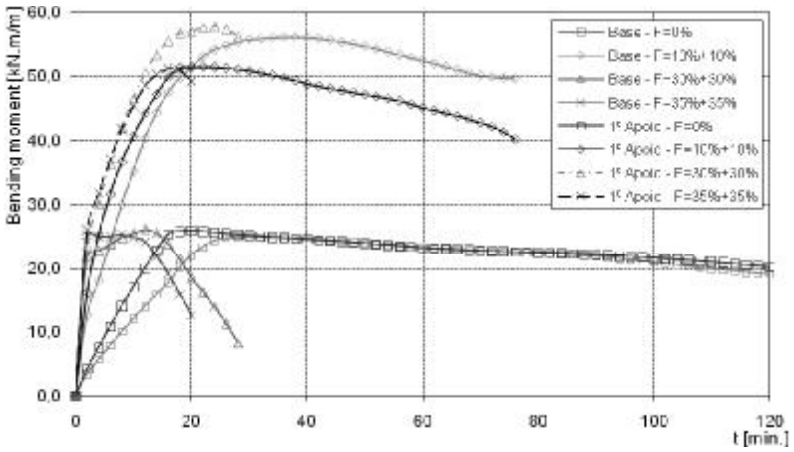

Figure 6. Bending moments at the base and at the first support of walls of 3m+3m tall and subjected to different axial loads

3 CONCLUSIONS

The analyses show that the walls only built in at the base reach great horizontal displacements at the top when subjected to the ISO 834 fire. The percentage of steel reinforcement generally used in normal practice in these walls is inadequate for slenderness ratios higher than 50 because it does not provide enough resistance to bending to avoid large deformations. The major deflections of thermal origin generate large bending moments at the base of the wall. Once the foundation of the walls is adapted, the large displacements cause their collapse by yielding of the steel reinforcement at the base of the wall or by buckling.

Walls built in at the base and with a support at the top present small horizontal deformations. The failure mode of those walls varies between the yielding of the steel reinforcement at the base of the wall due to bending, and buckling. This study shows that the fire resistance of these walls decreases with the increasing wall height. As the height of the walls decreases, the imposed horizontal force in the support due to the thermal curvature increases.

REFERENCES

[1] Jean-Marc Franssen, SAFIR: A thermal/structural Program for Modelling Structures Under Fire, Engineering Journal /Third Quarter/2005.

[2] Miguel C. Gonçalves, Jean Marc-Franssen, Vitor Abrantes and João Paulo C. Rodrigues: Numerical Analysis of Concrete Columns in Fire - Advanced versus simplified calculation methods, Application of Structural Fire Engineering, 19-20 February 2009, Prague, Czech Republic.

[3] Miguel Chichorro Gonçalves, Fire Behaviour of Structural Concrete Elements – Numerical Analysis and Methodology, Ph.D. Thesis, Faculty of Engineering of the University of Porto, 2006.

SELF-COMPACTING CONCRETE AT HIGH TEMPERATURE: A CRITICAL SURVEY AND RECENT TEST RESULTS

Patrick Bamonte, Pietro G. Gambarova

Department of Structural Engineering, Politecnico di Milano, Milan, Italy

INTRODUCTION

Self-Compacting/Consolidating Concrete (SCC) is certainly one the most innovative material used today by the Construction Industry, because of its astonishing workability ensured by large amounts of fine aggregates, special additives and fillers, that characterize its mix compared to traditionally-vibrated concrete – VC. SCC is increasingly used in tunnels, bridges, dwelling houses and office buildings, to reduce the labor cost and to increase the safety of the building site, even if stiffer and stronger shutters are required to withstand the higher pressure exerted by SCC during casting.

Many of the above-mentioned structures are often required to face severe environmental conditions, such as high temperature and fire. While the thermal effects on VC have been extensively investigated in the last 20 years (see for instance [1]) and several studies have been devoted to SCCs spalling in fire (see for instance [2]), scanty attention has been paid so far to the mechanical properties of SCCs at high temperature ("hot" properties) and/or after cooling ("residual" properties) [3-7]. Furthermore, comparing the experimental results coming from different sources is not as simple as one may presume, because of the different heating rates, specimen types, and procedures in data treatment and presentation.

On the basis of a recently-completed project on the hot and residual behavior of a family of Self-Compacting Concretes ("limestone" concretes, 2008; f_c = 50, 80 and 90 MPa, first part of this paper), a survey on the main results published so far on SCC's thermo-mechanical behavior is presented in the second part of this paper, to highlight the general trends, to make comparisons with VC and to check the consistency of the tests.

1 MIX DESIGN AND TEST MODALITIES

The mix design of each concrete is shown in Table 1. The binder is a limestone cement in concrete No.1, and a portland cement in concretes No. 2 and 3.

The tests in compression (to measure the σ_c-ε_c curve, E_c and f_c) were performed on cylinders (d = 100 mm; d/h = ½ in all specimens). Besides the room temperature (T = 20°C), three "reference" temperatures were adopted (T = 200, 400 and 600°C). The temperature 600°C was considered a suitable target since above this temperature both the compressive strength and the elastic modulus rapidly decrease and above 700°C calcination is activated.

The tests were displacement controlled. Both the heating and the cooling processes were performed in a furnace (T_{max} = 1000°C; size of the chamber 300 × 500 × 600 mm) and the heating rate $\Delta T/\Delta t$ was limited to ± 1°C/minute, to avoid dangerous self-stresses.

The tests in 4-point bending made it possible to measure $f_{ct,fl}$ (tensile strength in bending) and G_f (fracture energy) in residual conditions [3]. Prismatic, notched specimens were adopted (size: a × b × L = 150 × 150 × 600 mm; notch at midspan; notch depth / section depth = 0.3).

Table 1. Mix design of the 3 SCCs investigated in this research project.

Concrete No. and type	1 – NSC	2 – HPC	3 – HSC
Cement type	II/A-LL 42.5	I 52.5	I 52.5
Cement content (c) [kg/m^3]	350	480	520
Calcareous filler [kg/m^3]	130	100	100
Acrylic superplasticizer/cement	1.2%	2.0%	2.0%
Water [kg/m^3] (w/c)	175 (0.50)	168 (0.35)	172 (0.33)
Aggregate/d_a [mm]/mass [kg/m^3]	n/16/1700	n/16/1600	n/16/1600
Mass per unit volume [kg/m^3]	2359	2358	2402
f_c [MPa]	51	82	90

n = natural, round river gravel;
concrete age at the onset of testing = 180, 90 and 50 days.

As shown in Fig.1a, in the tests at high temperature two specimens were heated in the furnace, after being insulated with a 20 mm-thick rock-wool blanket, to prevent the specimens from cooling too quickly after the extraction from the furnace. In order to keep the insulated specimens at the reference temperature during the tests, the temperature of the furnace was set to values 5-20% higher than the reference temperatures (240, 480 and 630°C, that were maintained for 2-2.5 hours for T = 200 and 400°C, and for 4-4.5 hours for T = 600°C). Then each specimen was placed in turn between the platens of a press (Fig.1b) and was tested. Between the platens and the end sections of each specimen two pre-heated steel cylinders were inserted (thickness 50 mm), to protect the platens from high temperature and to mitigate the thermal shock in the specimens during the early phase of each test (for more details see [3]). During the first 10-15 minutes of each test the temperature of the specimens was rather constant and close to the reference temperature; this time length (past the extraction from the furnace) was more than adequate to move the specimen from the furnace to the press and to carry out the test up to the peak of the load (the tests were displacement-controlled).
In the hot and the residual tests, slightly different set-ups were used for the 3 LVDTs, that measured the relative displacement of the platens.
In Fig. 2 the stress-strain diagrams in compression are shown both in the "hot" and "residual" conditions, as will be explained later.
The tensile strength was measured in residual conditions, both by splitting and in 4-point bending [3]. The latter tests made it possible to evaluate the residual fracture energy, that turned out to an increasing function of the temperature up to 300-400°C, and then started decreasing [3]. As for the tensile strength, the splitting strength was slightly more temperature-sensitive than the flexural strength, but on the whole the strength decay with the temperature was practically the same in both cases.
Also the thermal diffusivity was evaluated by inserting a couple of thermocouples inside the specimen, in the mid-span section [3]. However, no differences were observed with respect to vibrated concretes. The slight increase with concrete grade was confirmed as well.

2 STRESS-STRAIN CURVES, PEAK STRAINS AND ELASTIC MODULUS

The stress-strain curves in compression are shown in Fig.3a,b,c (T = 400°C), together with the plots of the strain at the peak stress (Figs.3d,e,f). Since the LVDTs are placed between the press platens and are not directly fastened to the specimens, the measured displacements had

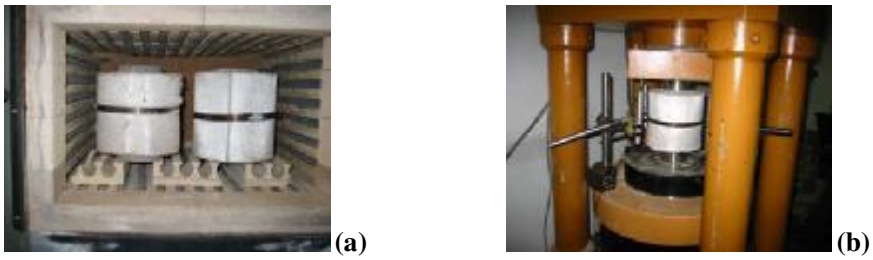

Fig.1. (a) Couple of insulated specimens inside the furnace; and (b) a pre-heated specimen between the press platens, ready to be tested.

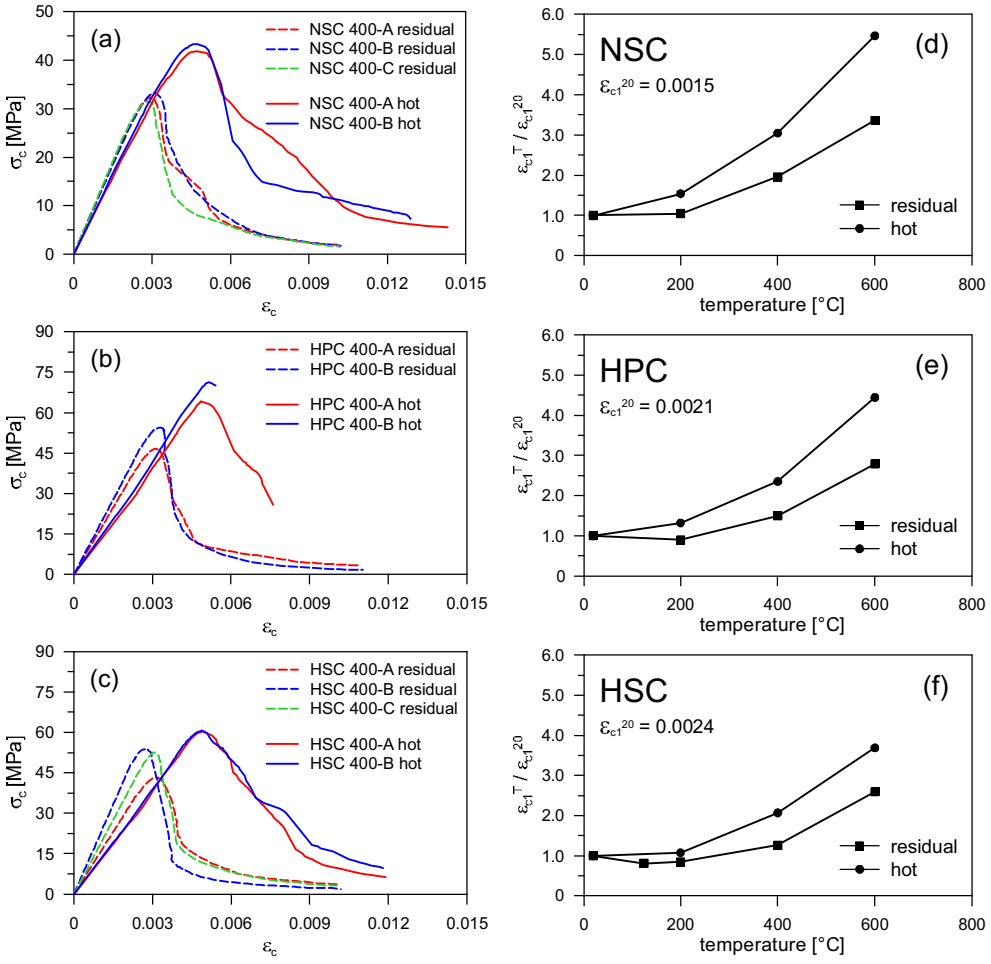

Fig. 2 . T = 400 °C: (a,b.c) Hot and residual stress-strain curves in compression; and (d,e,f) plots of the strain at the peak stress.

to be cleared of the possible disturbances occurring in the end zones. This extra deformability was taken care of by testing a dummy specimen before starting the tests. This procedure was instrumental also in evaluating the elastic modulus.

The relative compressive strength is plotted in Figs.4a,b,c as a function of the temperature. The dashed curves represent the curves indicated by EC-2 for calcareous (top) and siliceous (bottom) concretes. In Figs.4d,e,f, the secant elastic modulus is plotted versus the temperature.

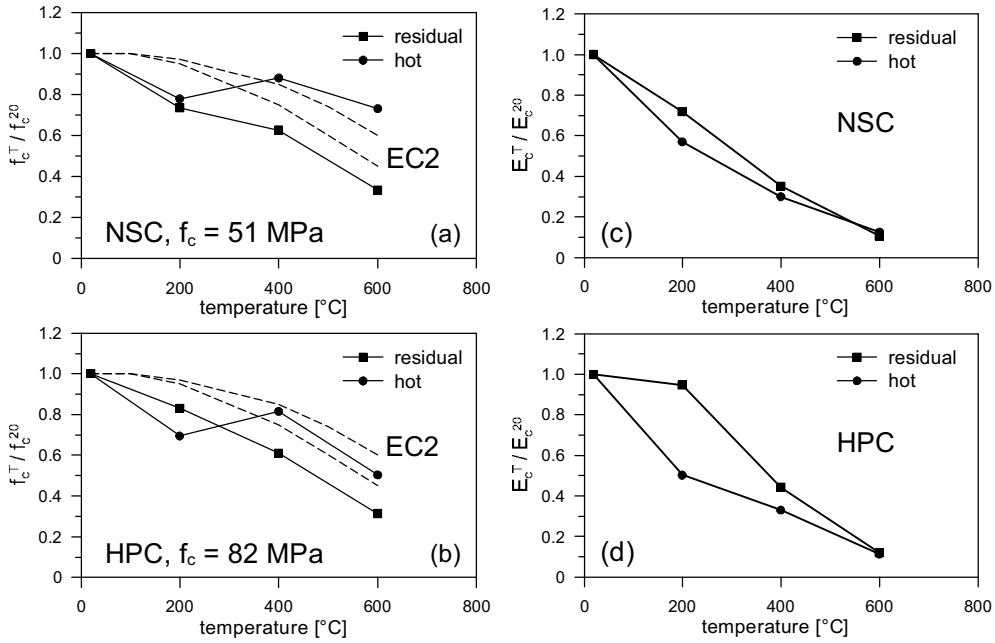

Fig. 3 . SC-NSC and SC-HPC tested in this study: (a,b) normalized compressive strength; and (c,d) normalized elastic (secant) modulus.

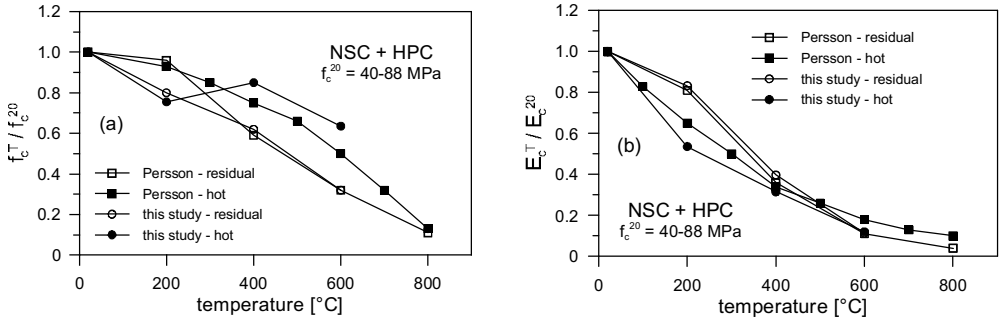

Fig. 4 . Normalized strength (a) and elastic modulus (b): this study and Persson's results [4].

3 COMPARISON WITH AVAILABLE RESULTS

Among the many papers (more than 120) published in 15 international journals in the last 20 years on concrete exposed to high temperature, the authors have found not more than 4 papers dealing with SCC exposed to high temperature and containing well-documented information [4-7]. However, even in these papers scanty results are presented about the "hot" and "residual" stress strain curves in compression, the fracture energy, the tensile strength and the thermal diffusivity. As for the experimental procedures, the heating rate varies between 0.5 and 8°C/minute, the geometry of the specimens is either cylindrical or cubic, the cylindrical

specimens are either cast in a formwork or cored from cubic specimens, the mix designs are different and the materials are NSCs and/or HPCs in the various experimental campaigns.
In the following, the main results presented in the four above-mentioned papers are recalled.

- Persson [4], $\Delta T/\Delta t$ = +4/-1°C/minute, T = 20, 200, 400, 600, 800°C, cylindrical specimens, f_c = 40-88 MPa; hot and residual tests; total number of the mixes 16 (4 VCs and 12 SCCs with/without pp fibers). Here reference is made to 10 SCC mixes (8 with blended cement = limestone cement, and 2 with portland cement, all containing a limestone powder); the aggregates were crushed gneiss and granite. The comparison between the results of this project (SC-NSC and SC-HPC) and Persson's results concerns the mean values of the compressive strength and of the elastic modulus. The agreement is satisfactory above 400°C for the compressive strength (Fig.4a), with no sizable differences compared to VC (EC-2); the agreement is very good indeed for the elastic modulus (Fig.4b).
- Sideris [5], $\Delta T/\Delta t$ = +5°C/minute, T = 20, 100, 300, 500, 700°C, cubic specimens, R_c = 42-75 MPa; residual tests; total number of the mixes 8 (4 VCs and 4 SCCs, without fibers), all containing blended cement and crushed granite aggregates Here reference is made to 2 SCC mixes and 1 VC mix (R_c = 54, 55 e 62 MPa). The comparison with the results of this project concerned the normalized compressive strength of the SC-NSC (Fig.5a). The agreement is rather good. (Sideris' results were corrected, since the ratio of the compressive strengths measured on cylinders and cubes depends on the temperature).
- Noumowé et al. [6], $\Delta T/\Delta t$ = +0.5/-0.5°C/minute, T = 20, 400°C, cylindrical specimens, f_c = 75-81 MPa; residual tests; total number of the mixes 4 (2 VCs and 2 SCCs, with/without fibers, all containing silica fume and calcareous aggregates). Here reference is made to 3 mixes, the first (called "HSC", f_c = 75 MPa) without fibers, the second (called "HSC-F", f_c = 79 MPa) with pp fibers, and the third (called "SC-HSC-F", f_c = 76 MPa) with pp fibers, □△◇ in Fig. 5b. The comparison with the results of this project (mean values for SC-NSC and SC-HPC) was limited to T = 400°C; the agreement is good (Fig.5b).
- Reinhardt and Stegmaier [7], ($\Delta T/\Delta t$ variable between 2 and 8°C/minute), T = 20, 500-600°C, short cylindrical cores, R_c = 33-76 MPa, f_c = 30-68 MPa, residual tests; total number of the mixes 9 (8 SCCs and 1 VC, no fibers). Here reference is made to 5 SCC mixes (f_c = 50-76 MPa, two with $f_c \cong$ 53 MPa - ■, and three with $f_c \cong$ 72 MPa -▲ in Fig. 5b), containing quartzitic aggregates, fly ash and a calcareous powder; two mixes contained also a viscosity agent.
  The cylinders were cored out of large cubes (side 300 mm) subjected for 120 minutes to the standard fire (ISO 834). The length of the cylinders was reduced to 100 mm (h/∅ = 1) by cutting off the extremities that were subjected to very high temperatures (T_{max} = 1038°C). According to the numerical analysis performed in this study, the average temperature reached in the core of the cubes T_{av} was comprised between 450 and 500°C (in [7] a higher temperature was declared = 720°C). The values of the strength measured in [7] were corrected to take care of the differences between "short" cylinders (h/∅ = 1, whose strength is close to that of cubic specimens) and "long" cylinders (h/∅ = 2-3). Even if the results shown in [7] are doubtful, the agreement is very satisfactory (Fig.5b).

CONCLUDING REMARKS

The closeness of the mechanical behavior of Self-Compacting Concrete to the behavior of Vibrated Concrete at high temperature is confirmed by this study, where SCC is shown to

exhibit a markedly linear loading branch in compression and a rather steep softening branch, at any temperature.
The closeness of SCC and VC at high temperature is confirmed by the satisfactory agreement with the results found in the literature, in terms of hot/residual strength and elastic modulus, in spite of the differences concerning concrete mixes, specimen types, heating ramps and concrete grades.

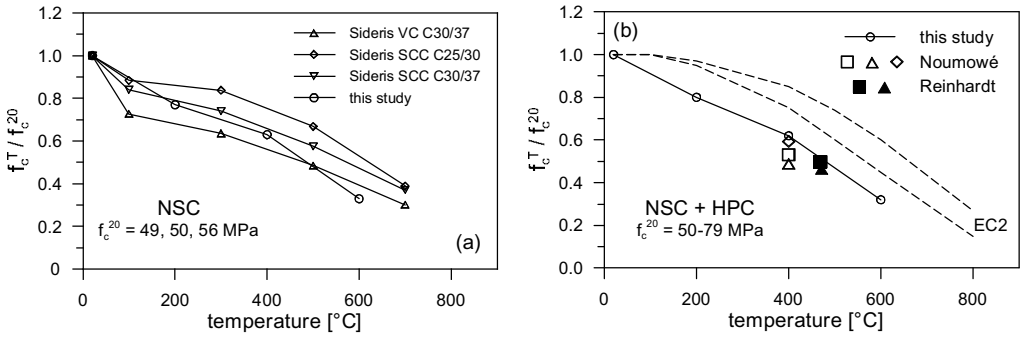

Fig. 5 . This study and Sideris' results [5] (a); and this study and Noumowé's + Reinhardt and Stegmaier's results [6,7] (b), ■ f_c^{20} = 53 MPa; ▲ f_c^{20} = 72 MPa.

ACKNOWLEDGEMENTS

This project was jointly financed by CTG-Italcementi (Bergamo, Italy) and by the Italian Ministry of Higher Education within the National Project–PRIN 2006 "Optimization of Construction Methods and Materials in Tunnel Linings".

REFERENCES

[1] Felicetti R. and Gambarova P.G. Effects of High Temperature on the Residual Compressive Strength of High-Strength Siliceous Concretes. *ACI-Materials Journal, Vol.95, No.4, 1998, 395-406.*

[2] Jansson R. and Boström L. Experimental Investigation on Concrete Spalling in Fire. *Int. Workshop "Fire Design of Concrete Structures: What now? What next?" - fib Task Group 4.3, ed. by P.G. Gambarova, R. Felicetti, A. Meda and P. Riva, publ. by Starrylink (2005, Brescia, Italy), Milan (Italy), December 2004, 109-113.*

[3] Bamonte P., Felicetti R. and Gambarova P.G.: "Mechanical Properties of Self-Compacting Concrete at High Temperature and after Cooling", *Proc. of SCC 2008 - 3nd North American Conf. on the Design and Use of SCC : Challenges and Barriers to Application*, Chicago (USA), November 2008, 6 pp. (in press).

[4] Persson B. Fire Resistance of Self-Compacting Concrete – SCC. *Materials and Structures-Matériaux et Constructions, Vol.37, No.11, 2004, 575-584.*

[5] Sideris K.K. Mechanical Characteristics of Self-Consolidating Concretes Exposed to elevated Temperatures. *ASCE-J. of Materials in Civil Engineering, Vol.19, No.8, 2007, 648-654.*

[6] Noumowé A., Carré H., Daoud A. and Toutanji H. " High-Strength Self-Compacting Concrete Exposed to Fire Test", *ASCE Journal of Materials in Civil Engineering*, Vol. 18, No. 6, 2006, 754-758.

[7] Reinhardt H.W. and Stegmaier M. Self-Consolidating Concrete in Fire. *ACI-Materials Journal, V.103, No.2, 2006, 130-135.*

THE EFFECT OF ELEVATED TEMPERATURES ON AERATED CONCRETE BLOCKS

BRIAN HARDIE [1], ALI NADJAI [1] & FARIS ALI [1]

University of Ulster, School Built Environment, FireSERT, Belfast, United Kingdom brianhardie45@hotmail.com

KEY WORDS: - Concrete Blocks, Elevated Temperatures, Mechanical properties

INTRODUCTION

The tests were part of ongoing experimental research in walling systems at elevated temperatures being carried out at the University of Ulster FireSERT. In the event of a fire, masonry walls in buildings serve as a fire barrier in addition to their architectural and structural functions. Often the subdivision of a building into isolated compartments is achieved by masonry walls in conjunction with fire resisting floors above and below. The dominant factors are the thermal, physical and chemical properties of the constituent masonry units and the joint mortar, the dimensions of the walls, the end restraints and the load conditions.
The role of a single leaf masonry wall in a fire situation is generally seen to be three fold:

a) Firstly a load bearing wall must provide structural stability to prevent collapse. This provision is termed structural adequacy
b) The wall is required to maintain integrity, i.e. prevent the passage of flame from one side of the wall to the other, in an attempt to compartment the fire.
c) The wall must provide adequate insulation properties to prevent excessive temperature on the unexposed face creating further spread of flame.

It is well known that due to their low thermal conductivity [1], masonry walls will experience highly non-linear temperature gradients through their thickness, when subject to fire on one side of the wall. This non-linear temperature will, due to plane-sections-remaining-plane, induce internal thermal stresses [2-3]. To develop performance –based fire design methods, these thermal stresses, together with mechanical stresses (and the influence of transient strains for concrete blocks) need to be estimated and the structural response determined. In order to reliably model walls subjected to fire the mechanical properties at discreet points (temperatures) through the thickness of the wall are required [4].

SPECIMENS AND TESTING EQUIPMENT

Testing procedures were carried out where 15 specimens of aerated concrete block were observed there conduction, and compressive strength at elevated temperature was recorded. The heat flow from one pre loaded and one unloaded specimen was also recorded using infra red camera.
These results were benchmarked with 5N/mm^2 and 7N/mm^2 concrete blocks as well as previously tested prism testing [5]

Specimen sampling and preparation

The specimens were assembled from lightweight aerated block of 3.6N/mm^2 crushing strength. The blocks are constructed utilising pulverised fuel ash, a by product from coal powered electrical generation plant they are very light weight and fuel efficient thus making them particularly attractive material in terms of fuel efficiency, recycling of waste materials, and manual handling. The blocks were selected at random from suppliers and no particular conditioning was carried out prior to the tests. Mortars were mixed utilising ordinary Portland cement, sand and water. The cement and sand was mixed in the portions measured by volume. The water was added to a consistent workable mix and was measured in proportion to the cement, giving a water to cement ratio of 1 to 2. All test samples were placed in the laboratory with a background heat maintaining at least 5^{o}C for 28 days prior to the test, allowing any excess moisture build up to evaporate and the initial 28 day strength of the mortar to be achieved.

Large scale envelope testing

In order to determine the compressive strength at elevated temperatures 15 tests were carried out utilising the 2.5MW gas furnace figure 3 which has an exposed area of 1.5m in length x 1.5m in height. Samples were constructed in the form of three blocks 210mm in length by 100mm in depth, constructed on top of each other thus forming a column. The mortar mix and curing was identical to the prism samples with a 1 in 4 cement sand mix being adopted. The samples top block was drilled to accommodate thermo couples every 25mm into the blocks. Additional thermo couples were placed, two on the surface exposed within the furnace and one on the unexposed face. The samples were placed in a rig detailed (figure 1 and 2) and connected to the furnace. Hydraulic rams were connected to a compressor which had its pressure, prior to the testing, calibrated using a calibration device. 13 of the samples were pre loaded to one third of the designed service load. The time/temperature curve adopted for the furnace was to IS0 834. Once the resultant temperature was attained, the burners in the furnace were switched off and the pressure induced via the hydraulic rams. The failure compression was recorded together with any observations on the type of failure

Fig.1. Testing equipment

Testing equipment used

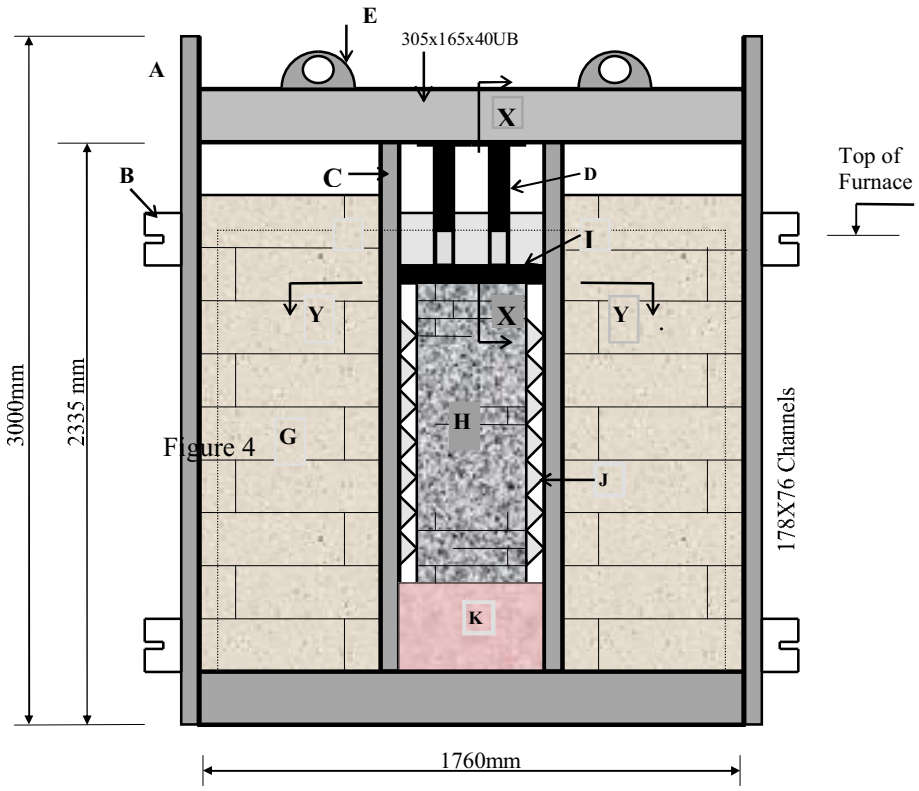

Figure 4

Fig.2. Testing frame details

Key:			
A	Jacking Frame	G	Permanent 150mm thick pre cast concrete with 20mm fibreboard protection to furnace side
B	Bracket Connection to Furnace	H	Test specimen 680 high 210mm wide 100mm thick 3 blocks
C	100x100 L Lateral restraint to panels	I	210mm by 100mm 200mm in height by 10mm thick plate on 3mm fire resisting compressible surface
D	25T Hydraulic Jacks protected with fire resisting material including hoses	J	40mm thick fibreboard with 7mm fire resistant edge seals
E	Lifting eye	K	Pre formed steel framed supports no more than 870mm in height lined with fibreboard

COMPRESSIVE STRENGTH RESULTS

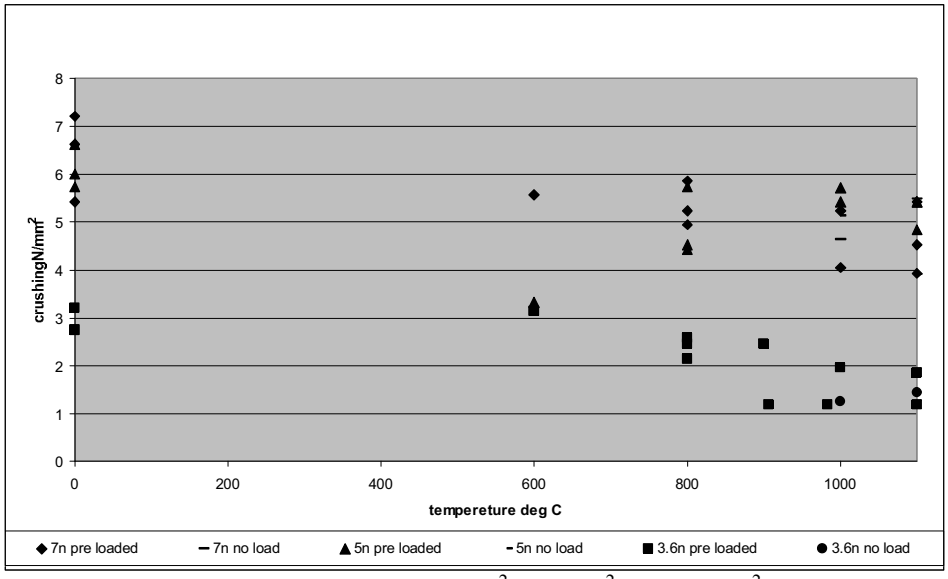

Fig.3. Compressive strength, 3.6N/mm^2, 5N/mm^2 and 7N/mm^2 block work

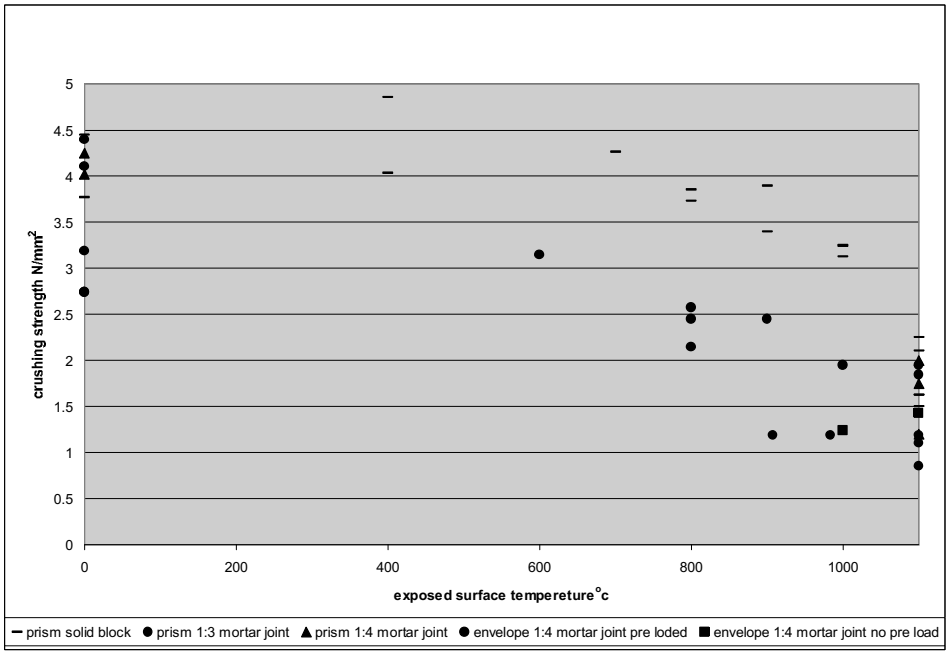

Fig.4. Compressive strength 3.6N/mm^2 blocks (prism samples [5])

Discussion of results

Figure 3 details the results of the aerated block work compared to concrete aggregated block work. At temperature of 900^{o}c, little more than half the designed compressive strength remains within the specimens. Two samples exhibited premature failure with their service load at 900^{o}c and 980^{o}c and were recorded accordingly. From unloaded

and loaded envelopes there was little evidence of a large variation in their results, Figure 4 gives additional benchmarking between the previous prism testing [5] which indicated that the prism samples retained a higher residual compressive strength however the loss in compressive strength, was evident at the requisite temperatures observed in the envelope tests.

RESULTING FAILURE CRACKING

Figure 5 details the crushing results from an aerated block. The picture was taken from the unexposed side with the sample subjected to 1100°c on the exposed face. All blocks tested at and over 1000°c exhibited a sheering parallel to the surface in the bottom two blocks. The sheering varied in the samples from 20mm to 30mm from the unexposed surface. From the conduction data these areas within the block work attained a temperature of 100°c to 367°c. At the lower temperatures the block work failure was evident similar to aggregate concrete block work, where cracking was observed within the base block and extending into the mid block. The exposed face pictured in figure 6 from the same sample in figure 5, exhibited the break down of the block work from an

Fig .5. 1100°c unexposed face

Fig.6. 1100°c exposed face

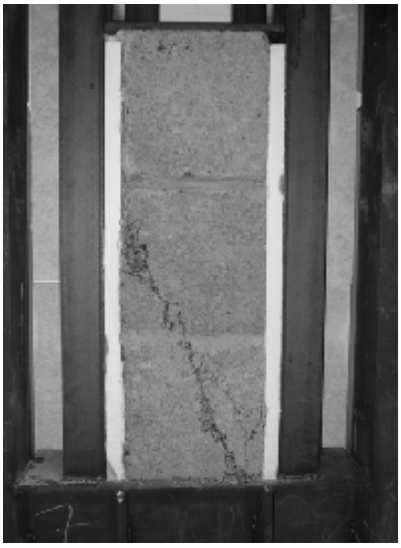

Fig.7. 1100°c concrete block unexposed face

Exposure temperature of 800°c and above a dry shrinkage pattern on the face which extended into the block, not unlike a dried river bed, the depth of penetration varies with temperature. The face remained intact and remained as a barrier to the heat

source. Figure 7 indicates a 5N/mm^2 aggregate. Concrete block which exhibits its typical failure thought the base and partially into the mid block which was typical to all this type of block at all temperatures. These types of block did not disintegrated on the application of the load the cracking was observed but the block remained in place to give some resistance to radiation

CONCLUSION

I. Critical temperature of 900^{o}c was observed as a temperature that triggered a marked loss of compressive strength

II. With temperatures in excess of 1000 ^{o}c there is a risk of spontaneous disintegration on the application of a load at or above one third of the service load.

III. Despite a limited number of samples there was no evidence of different results between unloaded and one third loaded specimens

IV. There is evidence of gains in compressive strength in the cooling phase, as demonstrated in figure 4 residual compressive strength of the prisms as compared with hot crushing of envelopes.

V. There was little evidence of distress in the mortar joints

REFERENCES

1. Cook, GME. Thermal bowing and how it affects the design of fire separating constructio9ns. Interflam 88 – Fourth International Fire Conference. 22-24 March, Church College Cambridge, 1988, pp 230-236
2. Khoury GA, Grainger BN, and Sullivan PJE. Transient Thermal Strain of Concrete: Literature Review, Conditions within Specimen and Behaviour of Individual Constituents. Magazine of Concrete Research, vol 37, No 132, 1985, pp 131-144
3. Anderberg Y, and Thelandersson S. Stress Deformation Characteristics of Concrete at High Temperatures. Division of Structural Mechanics and Concrete Construction, Lund Institute of Technology, Bulletin 54 1076
4. Nadjai A, O' Garra M, and Ali F. A Numerical Model for the Behaviour of Masonry Under Elevated Temperatures, Fire & Materials, Vol 27, pp 163-182, 2003.
5. Hardie B, Nadjai A, and Ali F. concrete block work at elevated temperatures, fib conference proceedings Cabrera Portugal 2007

EXPERIMENTAL AND NUMERICAL STUDY OF HIGH PERFORMANCE CONCRETE COLUMNS SUBJECTED TO FIRE LOADING

Sven Huismann [a], Manfred Korzen [b]

[a] Federal Institute for Materials Research and Testing, Division Building Materials, Berlin, Germany
[b] Federal Institute for Materials Research and Testing, Division Fire Engineering, Berlin, Germany

INTRODUCTION

This paper presents an experimental and numerical study on the thermo-mechanical behaviour of high performance concrete (HPC) columns subjected to fire loading in accordance with ISO 834. The objective is to perform numerical simulations of the thermo-mechanical behaviour of the columns on the basis of the thermo-mechanical material properties which will actually be investigated.

1 EXPERIMENTAL STUDIES

Two HPC square type columns have been tested under ISO 834 fire exposure and mechanical loading of 3200 kN.

1.1 Test Specimens

The two columns had a cross section of 30 x 30 cm² and length of 3.6 m. The longitudinal reinforcing bars of diameter 25 mm and axis distance of 50 mm were welded at end plates of thickness 30 mm. They had an axis distance of 50 mm. The transversal reinforcement has been realized with circular stirrups of 10 mm thickness with a spacing of 150 mm within a distance of 600 mm from the supports, and a spacing of 300 mm in the central part. The ties had 135° bent ends. The column temperatures were measured by 40 thermocouples of type K at 4 measuring stations along the column axis with at least 7 sensors per station. They were positioned inside the concrete and welded at the reinforcements. The concrete mix is shown in Table 1. Column I was made of the concrete HU-9 with a compressive strength of 131.9 MPa (100 mm cube) at the test day and column II of HU-10 with a strength of 124.4 MPa. The age was more than 90 days. The relative humidity was 4.3 % in both columns at the test day.

Table 1. Mix proportions

Materials [kg/m³]		**HU-9**	**HU-10**
Cement CEM I 42,5 R		580	
Water		173	
Aggregates (siliceous)	0 – 2 mm	769	
	2 – 4 mm	231	
	4 – 8 mm	538	
Silica fume		63.8	
Superplasticizer		17.4	
Polypropylene Fibres		2	
Steel fibres		no	100
W/C ratio		0.3	

1.2 Experimental Set-Up

The tests were carried out in a special column-furnace (see Fig. 1) with a loading capacity of 6300 kN. Mechanical and thermal actions are applied through this device to the specimen under test. Six electro-hydraulic control channels equipped with displacement and force sensors are available to influence the mechanical boundary conditions, i.e. two bending rotations each at top and bottom, one axial displacement at the bottom and one horizontal displacement at the top. During the experiments under discussion only the axial load has been applied whereas the other degrees of freedom were fixed. The furnace is operating with six oil burners and the gas temperatures are controlled with plate thermometers according to [2].

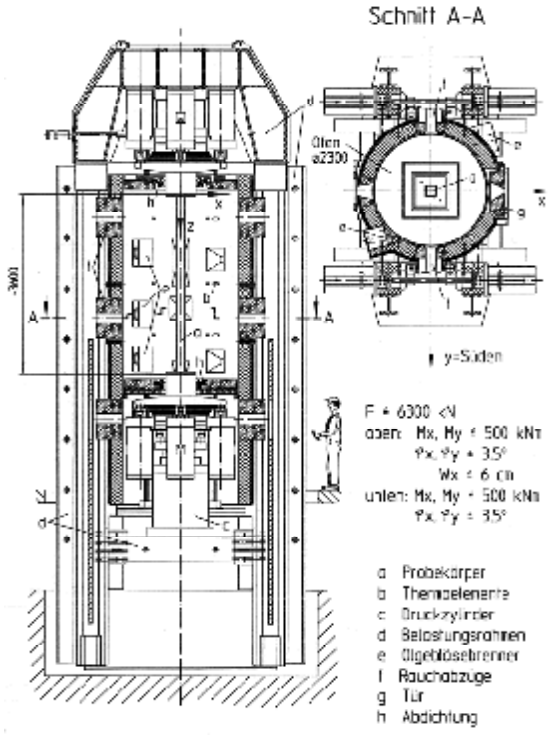

Fig. 1. column-furnace

1.3 Test Conditions and Procedure

The four sided fire loading was in accordance to the ISO 834 standard and in good agreement with EN-1365-1 [2]. Two types of mechanical boundary conditions have been applied to the specimens: Column I fixed at the bottom and with a 25 mm eccentric hinge at the top and column II fixed at both ends. The axial load of 3200 kN, characterized by 75 % of the design load, was kept constant during the tests. The axial displacements as well as the temperatures of the specimens and the gas temperature of the furnace have been measured.

2 RESULTS AND DISCUSSION

2.1 Failure behaviour

Failure of column I and II was observed after 94 minutes and 116 minutes of fire exposure, respectively. The failure mode of column II was compression and not buckling (see Fig.2).

Spalling has been observed only at column I at the side of the concrete charging after 14 minutes. The reason seems to be the abrasion of the fresh concrete at the surface of column I during the production. It was not observed at column II, which was not abraded.

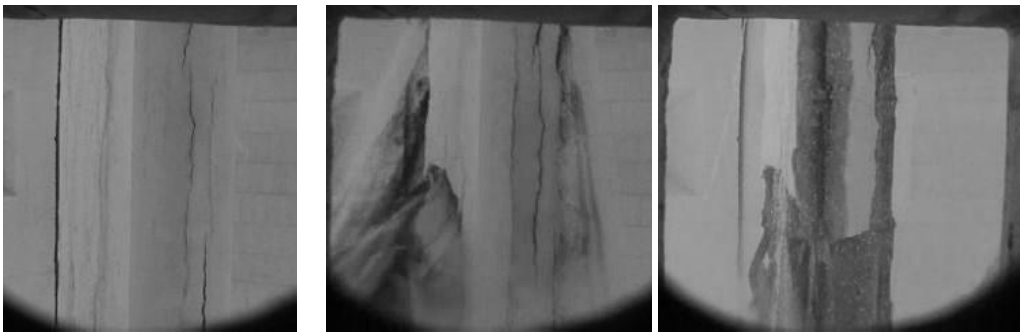

Fig. 2. Failure of column II

2.2 Deformations

The deformations of the two columns are shown in Fig. 3. Both columns expand in the first phase. Column I reached the initial deformation after 30 minutes. In minute 34 was a switch in the deformation of column I, which does not represent the overall failure of the column. This phenomenon is induced by the concentrated load, which results in local failure of the concrete at the top. After the test a large deformation in the top plate was observed. It is not clear in how far this effect contributes to the axial deformation. For this reason the deformation of column I is taken out of the evaluation. Column II reached the initial deformation after 75 minutes.

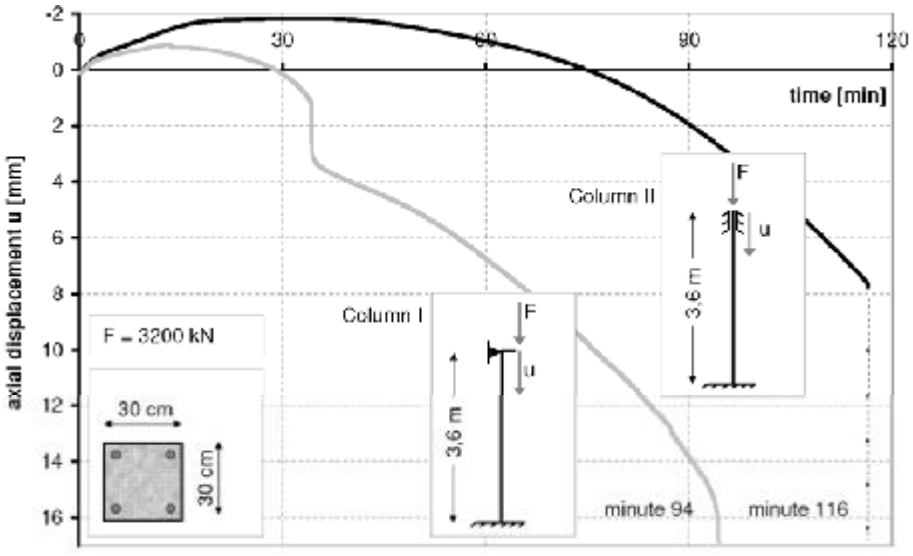

Fig. 3. Axial displacement

2.3 Temperatures

The temperatures were measured in four cross sections at different heights. Fig. 4 shows the temperatures vs. time in the height of 89 cm from the bottom and at middle height of column II.

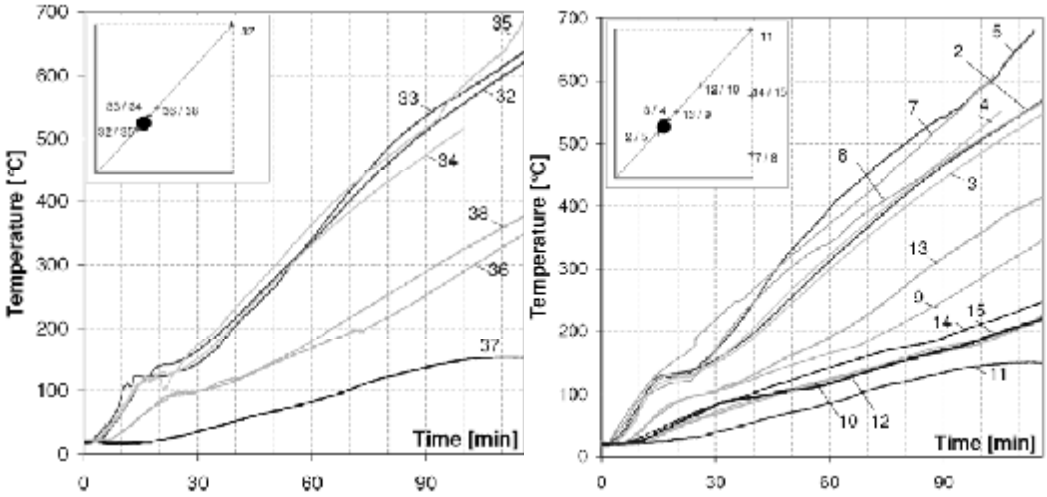

Fig. 4. Temperature in the cross section of column II
(left: 89 cm from the bottom, right: middle-height)

The temperatures at the time of failure in the reinforcement bars and the centre were about 600 °C and about 160 °C, respectively.
The temperatures in column I with additional steel fibres were somewhat higher than in column II. The difference arises mostly at the temperatures of 100 °C to 200 °C when the phase transformation of the water appears.
The temperatures are in good correlation with the calculated temperatures in [2], but they are much higher than in [5]. The reason for this difference is not yet clarified and still under discussion.

2 NUMERICAL STUDIES

2.1 Numerical Model

For the numerical simulation of the thermal and mechanical behaviour of column II the finite element program DIANA from TNO was used. With a three dimensional model a quarter of the cross section which implies that no buckling occurs was simulated. The element size of the twenty node volume element was about 10 mm at each edge.
The longitudinal reinforcement bars were modelled with the embedded reinforcement option without any bond slip. The reinforcement material properties were assumed according to [4]. At the heated surfaces of the column the conditions for the heat transfer with convection and radiation according to [3] were applied. As thermal input heating due to the ISO 834 fire curve was assumed. The mechanical load was set constant to 35.5 MPa which corresponds to the load of 3200 kN.
The thermal conductivity of the concrete is higher than in [3] because of the smaller maximum aggregate size. For this reason the thermal conductivity was set to 2.5 W/mK in the range up to 100 °C and at 150 °C to the lower bound of [3]. Between 100 °C and 150 °C the values were linear interpolated. The heat capacity was also assumed according to [3].

For the temperature dependent stress-strain relations in compression similar curves as defined in [3] were used in which the elastic, plastic and transient creep strains are implied. The tensile behaviour was assumed linear below the tensile strength. After reaching the tensile strength the stress-strain diagram was assumed as constant. All temperature dependent mechanical properties were taken from [3] and related to the measured properties at 20°C. It should be mentioned that the properties in [3] are measured from normal strength concrete.

2.2 Numerical Results

The calculated temperature fields are in relatively good agreement with the measured temperatures. There are differences especially until 150 °C because the finite element program does not consider the change of the thermal properties due to the phase transformation of the water.

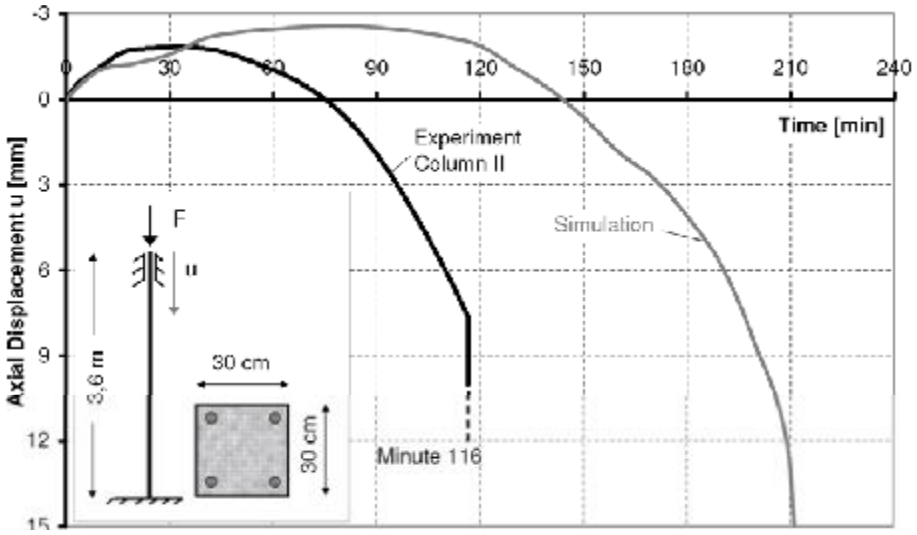

Fig. 5. Comparison of the calculated and measured axial displacement

The results of the axial displacement are presented in Fig. 5. The simulated axial displacement reaches its maximum at about 75 minutes and the initial deformation at about 140 minutes. At 210 minutes failure occurred.
It can be seen that the numerical results of the axial displacement based on material properties according to [3] are not in good agreement with the experimental results. Especially for high strength concrete the transient creep strains are higher than for normal strength concrete [1,6] due to its higher amount of cement. This seems to be the main reason for the difference in the axial displacement predictions in comparison with the experimental results. Therefore more knowledge of the thermo-mechanical properties of high strength concrete is necessary. Material values from ordinary concrete cannot be used. These properties such as strength, thermal expansion and transient creep are currently determined experimentally through a test equipment, which has been specially developed for those purposes. Based on the corresponding identified material properties further simulations will be done.

3 SUMMARY, CONCLUSION AND FUTURE RESEARCH

The subject of this paper was an experimental and numerical study of high strength concrete columns. Two high strength concrete columns were tested under fire conditions. The first one was excluded from evaluation because of its undefined failure. The results of the second test were compared to numerical results. The material properties were assumed according to the Eurocode. But with these properties there was no accordance to the experimental results of the axial displacement. The reason is that the properties according to the Eurocode are related to normal strength concrete. Compared to normal strength concrete the high strength concrete strains are higher. Therefore investigations on the thermo-mechanical properties of the used high strength concrete are in process using recently developed test equipment.

REFERENCES

[1] Diederichs, U. et al., Behaviour of high strength concrete at high temperatures, Report 92, Helsinki University of Technology, Department of Structural Engineering, Espoo, 1989

[2] EN 1363-1:1999 Fire resistance tests - Part 1: General requirements, October 1999

[3] Eurocode 2: Design of concrete structures - Part 1-2: General rules - Structural fire design, EN 1992-1-2:2004, July 2004

[4] Eurocode 4: Design of composite steel and concrete structures – Part 1-2: General rules – Structural fire design, EN 1994-1-2:2005, November 2006

[5] Kodur, V.K.R., Fire Resistance of High-Performance Concrete Columns, Report IRC-IR-834, National Research Council Canada, 2002

[6] Schneider, U. et al., Hochtemperaturverhalten von Festbeton, Sonderforschungsbereich 148 – Brandverhalten von Bauteilen, Technische Universität Braunschweig, Braunschweig, 1987

BEHAVIOUR OF R.C. BEAMS UNDER ELEVATED TEMPERATURE

Lakshmipathy.M [a], Jayasree.G [b] and Santhanaselvi.S [c]

[a] Dean and Professor , [b] Ph.D. Research Scholar , [C] Assistant Professor

School of Civil Engineering, SRM University, Kattankulathur-603 203, Tamil Nadu, India.

1 INTRODUCTION

Concrete is a complex material subjected to a range of heat more severe than that caused by weather. There are important cases in which concrete is exposed to much higher temperatures when subjected to accidental fires in buildings, nuclear reactors, RC chimneys, runways of jet aircraft and rocket launching pads. Such fires or elevated temperatures result in most cases in considerable damages to structures. Generally concrete is thought to have good fire resistance property but the fire resistance capacity of concrete is very complicated because not only is concrete a composite material with components having different thermal characteristics, it also has properties that depend on moisture and porosity. The extensive use of concrete as a structural material had led to the need to fully understand the effects of sustained elevated temperature on concrete. Elevated/high temperature represents one of the most severe exposure conditions and provisions of appropriate resistance of the structural members are the major safety requirements in design.

2 RESEARCH SIGNIFICANCE

From the literature survey it is found that there is a lack of experimental data for concrete heated under a constant preload to simulate the stress conditions in the real field conditions. It is also brought out that data from the stressed test will be of interest, which simulate the conditions of structural elements when exposed to fire in real conditions. The study on the behaviour of RC beams tested under preloaded condition is found limited and there is a scope for attempting studies pertaining to these areas. The dramatic fire accidents/incidents have emphasized the need for safety concerning reinforced concrete (RC) structures made of both ordinary concrete (NSC) and high-strength/ high performance concrete (HPC/HSC). Fire was the main reason in bringing down both of the WTC towers during the tragic event of September 2001 in New York, USA. This has renewed the interest in the area of research on concrete subjected to elevated temperature. A better understanding of behaviour of structural elements under elevated temperature and its implementation will allow improvements to be made in the design of structures for high temperature applications and for accidental exposures. By use of specific concretes, structural configuration and structural detailing the effects of the underlying processes driving this behaviour may be reduced. Such improvements will allow structural safety and consequences of damage due to thermal loading is minimized.

3 OBJECTIVE AND SCOPE OF THE WORK

The main objective and scope of this study is to experimentally investigate the residual characteristics of RC beams subjected to sustained elevated temperature under unstressed and stressed test conditions by considering various aspects given below.

- Grade of concrete : Normal Strength Concrete of grade M20
- Type of beam : Varying % of steel
  : Type I – Steel in one face. (pt%=0.8%, Vst = 1%approx.)
  : Type II–Steel in both faces. (pt%=1.5%,Vst = 2%approx)
- Temperature level : Normal(28°C),100°C,200°C ,300°C, 400°C and 500°C
- Exposure period : Sustained exposure period of 4 hrs

- Test conditions : Residual properties under unstressed test condition and stressed test condition
- Type of loading : Static loading

4 EXPERIMENTAL INVESTIGATIONS

The details of experimental investigations carried out in this work are covered in the following sections.

4.1 Properties of materials used and concrete mix details

Ordinary Portland cement of 53 grade [10] and of specific gravity 3.15 is used. Locally available river sand, which is free from organic impurities and specific gravity 2.60 and of Zone III grading is used. The coarse aggregate of 12.5mm maximum size and specific gravity of 2.65 and conforms to grading of IS383:1970 is used. [7].**C**lean water as available in SRM University campus, which is free from all impurities is used for the entire work of concrete preparation and curing. The yield strength of 8mm and 4mm diameter steel reinforcement bars of Fe 415 and Fe 250 grade steel provided for beams are 397.9N/mm^2 and 238.2N/mm^2 respectively. The concrete of grade M20 is designed as per IS method IS10262-1982.[9] and the mix proportion by weight is 1:1.29:2.28 and w/c ratio of 0.48.

4.2 Casting of R.C. Beams

The dimension of the beam is 120mmx120mmx1500mm and the reinforcement details are shown in Figure1.The R.C beams are provided with reinforcement in the tension zone and without any hanger bars and designated as Type I beams (RCB1) to simulate singly reinforced beam in ideal conditions and it is ensured while casting the beam, the stirrups are held vertical in position and effective in resisting shear. The other set of beams are provided with reinforcement bars on both faces designated as Type II beams (RCB2) [8]. A clear cover of 10mm is provided for the beams. The curing of the specimens are initiated after 10 hours by covering with wet gunny bags and cured in clean water for 28 days.

4.3 Testing of R.C. beams

The details of the testing of the R.C. beams for its residual characteristics under unstressed and stressed test conditions are presented below.

4.3.1 Preloading of R.C. beams in stressed test conditions

It is believed 20 to 40% of the ultimate load act during service load conditions and accordingly 40% of the ultimate load of the R.C. beam is taken for the level of preloading [3]. In the stressed test, the R.C. beams are kept in a simply supported condition in an assembly specially fabricated for the purpose and placed in the Universal testing machine for preloading. The beams are preloaded by applying a concentrated load through the middle threaded rod and the nuts tightened to retain the load. A preload of 5kN and 10kN is applied to the Type I (RCB1) and Type II (RCB2) reinforced beams equivalent to 40% of the ultimate capacity of the beam in normal temperature conditions. After the preload is applied, the nuts are tightened so that the stresses of preload are retained in the beam as shown in Figure2.

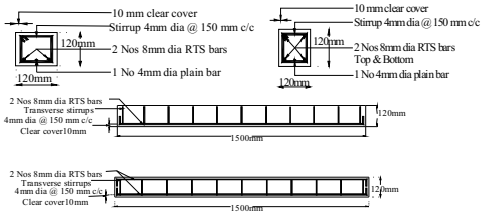

Fig. 1. Reinforcement details of beams

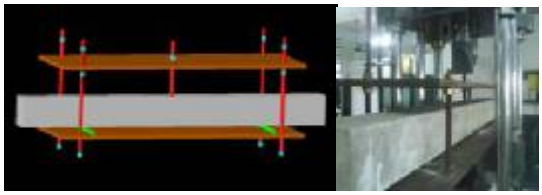

Fig. 2. Preloading of beams

4.3.2 Heating of the specimens

The overall dimension of the oven is 2.26m x 0.36m and 0.57m height and the maximum range of temperature that can be measured is 1000°C and a minimum of room temperature. The beam specimens are heated to the target temperature of 100°C, 200°C, 300°C,400°C and 500°C after the temperature has reached steady state and is sustained for 4 hours of exposure. In the stressed test the beams are exposed to heating in the oven in a preloaded condition. The specimens are then cooled down to room temperature and tested for the residual properties. The heating and the loading histories in unstressed and stressed conditions are shown in Figure3.The heating of the specimens in the oven in unstressed and stressed test conditions are shown in Figure4.

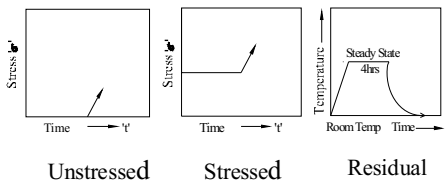

Fig. 3. Heating and loading histories

Fig. 4. Heating of beam specimens in oven

4.3.3 Testing arrangement and instrumentation

The two point bending test is conducted on the R.C. beams in the Universal testing machine of capacity 400kN. To measure the central deflection of the beam, dial gauge of 0.01mm accuracy is fixed to the under side of the beam at mid span. In order to evaluate the behaviour of the R.C. beams, the following behavioral parameters are measured and recorded during testing. (i) Load at initial crack is recorded. (ii) Ultimate load capacity of the beam specimen is noted. (iii) Initial stiffness of the beam is determined from the load-deflection curve of the beams. (iv) Stiffness of the beam at 50% stress level is found from the load-deflection curve of the beam.(v) Failure pattern of the beams are noted and crack pattern is recorded in the beam.

4.4 Results and Discussions

4.4.1 Residual characteristics of beams

The load at initial crack of the R.C. beams at various temperatures 100° C, 200° C, 300° C 400°C and 500°C are compared in Figure 5 for the unstressed and stressed test conditions. The ultimate load at various elevated temperatures are compared with the ultimate load at normal temperature and their ratio T°C/Normal is reported as Residual Strength Ratio (RSR) and compared in Figure6. The damage suffered by the beams are determined as ((1-RSR)*100) due to elevated temperature exposure and expressed in %. The Type II beams are suffering higher % of damage than Type I

beams as more volume of steel in the beam conducts more heat and transfer to the surrounding mass of concrete and causes more damage to the R.C. beams and also due to complex phenomena of loss of bond strength of concrete. The ultimate load at failure determined theoretically for the two types of beams Type I and Type II tested under unstressed test and stressed test conditions are compared with experimental values in Figure7 and Figure8 respectively.

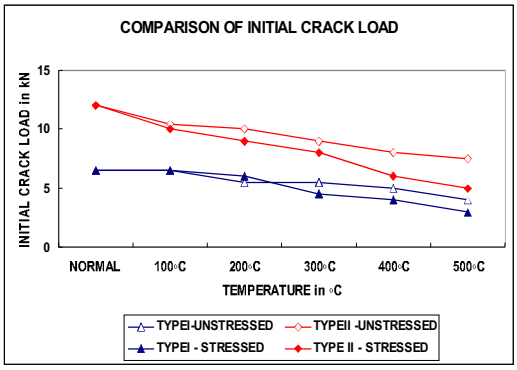

Fig. 5. Comparison of load at initial crack

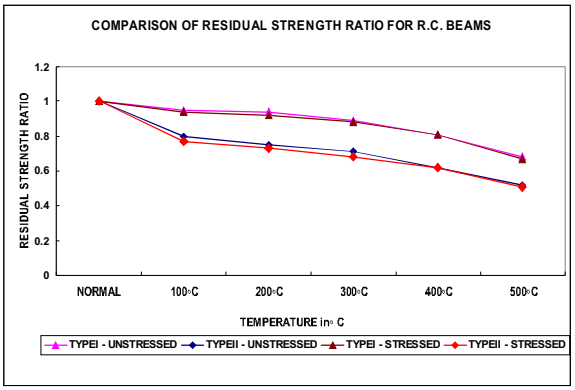

Fig. 6. Comparison of residual strength ratio

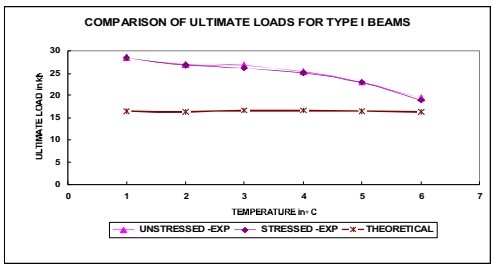

Fig. 7. Comparison of ultimate load Type I beams

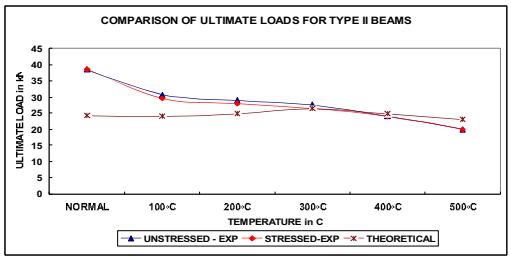

Fig. 8. Comparison of ultimate load for Type II beams

4.4.2 Comparison of stiffness of R.C. beams

The initial stiffness of the beam is determined as slope of the load-deflection curve before initial cracking load. Similarly the stiffness of the beam at 50% of the ultimate load is also determined as slope of the tangent drawn at that point. The stiffness as determined are recorded for the beams in unstressed test condition and stressed condition in Table1 and Table 2 respectively.

Table 1 Comparison of stiffness in unstressed test condition

Type of beam	Temperature (°C)	Initial stiffness kN/mm	Stiffness at 50% load kN/mm	Stiffness degradation (%)	
				Initial	50% Load
Type I Beam (RCB1)	Normal	3.28	1.97	----	----
	100°C	3.47	1.80	+5.8%	-8.63%
	200°C	3.94	1.85	+20%	-6.1%
	300°C	2.176	1.84	-33.66%	-6.6%
	400°C	2.03	1.75	-38.11%	-11.17%
	500°C	1.41	1.0	-57%	-49.23%
Type II Beam (RCB2)	Normal	3.72	2.56	---	---
	100°C	4.025	2.11	+8.2%	-17.6%
	200°C	2.99	1.921	-19.6%	-25%
	300°C	2.136	1.84	-42.6%	-28%
	400°C	2.0	1.75	-46%	-31.64%
	500°C	1.88	1.67	-49%	-35%

Table 2 Initial stiffness and stiffness at 50% of ultimate load in stressed test condition

Type of beam	Temperature (°C)	*Initial stiffness KN/mm	*Stiffness at 50% load KN/mm	Stiffness degradation (%) due to temperature exposure	
				Initial	50% Load
Type I Beam (RCB1)	Normal	3.28	1.97	----	----
	100°C	3.68	1.77	+12.20%	-10.15%
	200°C	3.44	1.93	+4.90%	-2.03%
	300°C	3.20	1.80	-2.44%	-8.63%
	400°C	2.10	1.20	-36%	-39%
	500°C	1.50	0.70	-54%	-65%
Type II Beam (RCB2)	Normal	3.72	2.56	-----	-----
	100°C	3.33	2.52	-10.50%	-1.56%
	200°C	3.19	2.40	-14.2%	-6.25%
	300°C	2.62	2.32	-29.6%	-9.4%
	400°C	1.85	0.88	-50.26%	-65.63%
	500°C	1.00	0.60	-73%	-76.6%

5 CONCLUSIONS

From the results and discussions on the experimental investigations, the following facts are presented.

- At 500°C the initial crack started at lower load and is lower by 38.5% in Type I beams and 37.5% in Type II beams when compared to normal temperature conditions.
- Also the ultimate load decreased and the damage suffered by Type I and Type II beams are to an extent of 32% and 48% respectively in unstressed test condition. In the stressed test condition it is to an extent of 33% and 49% respectively. The reduction in the strength is about 50% at 500°C.
- The ultimate loads from experimental investigations are greater than the theoretical estimation due to the considerations of lower strength of concrete (0.447fck) and yield strength of steel (0.87fy) in theoretical calculations of the moment capacity of the beams.
- The ultimate load at failure of R.C. beams tested in stressed condition are lower marginally by 5% than the beams under unstressed test condition. The amount of preload is smaller in magnitude in the laboratory tested specimens.

- The degradation in initial stiffness and stiffness at 50% load is also nearly 35% to 50% in unstressed test and is about 54 %to 77% in stressed test for the elevated temperature considered in this study.
- All the beams fail in flexure as expected forming cracks in the tension zone.

It can be concluded that the R.C. beams loses its strength and stiffness at higher elevated temperature and is quantified in this study.

ACKNOWLEDGEMENT

The authors expresses their sincere gratitute to the Management, SRM University, for the continuous encouragement and support by providing facilities for conducting the experimental part of this work.

REFERENCES

[1] Crozier, D. A., Sanjayan, J. G. and Liew, E. M., Residual strength of High Strength Concrete beams exposed to high temperatures, *International Conference on HPHSC, Perth, Australia,* 1998

[2] Phan Long, T and Carino Nicholas, J., Review of mechanical properties of HSC at elevated temperature, *Journal of materials in Civil Engineering*, 1998

[3] Phan Long, T. and Carino Nicholas, J., Effect of test conditions and mixture proportions on behaviour of High strength concrete exposed to high temperatures, *ACI Materials Journal, V.99, No.1,*2002

[4] Kodur, V. K. R., World Trade Center building disaster: Stimulus for innovations, *The Indian Concrete Journal,* 2008

[5] Kodur, V. K. R. and Dwaikat, M., A numerical model for predicting the fire resistance of reinforced concrete beams, *Cement and Concrete composites, No.30.*2008

[6] Potharaju, M., Srinivasa Rao, .K, Srinivasa Rao, P.V. and Nalini, M., Theoretical assessment of flexural strength of heated reinforced concrete beams, *Proceedings of the Congress 2008 on Concrete for Fire Engineering, University of Dundee, Scotland,* 2008.

[7] IS: 383-1970, Specification for coarse and fine aggregate from natural sources for concrete (Reaffirmed 1997), *Bureau of Indian standards, New Delhi*

[8] IS:456-2000, Plain and Reinforced concrete–Code of Practice, *Bureau of Indian standards, New Delhi*

[9] IS:10262-1982,Recommended guidelines for concrete mix design(Reaffirmed 1999), *Bureau of Indian standards, New Delhi*

[10] IS:12269-1987, Specification for 53 Grade Ordinary Portland Cement,(Reaffirmed 1999), *Bureau of Indian standards, New Delhi*

SIMPLIFIED LAYERED APPROACH FOR ANALYSIS OF RC SLABS SUBJECTED TO FIRE

Darius Bacinskas [a], Edgaras Geda [a], Gintaris Kaklauskas [a], Viktor Gribniak [a]

[a] Vilnius Gediminas Technical University, Department of Bridges and Special Structures, Vilnius, Lithuania

INTRODUCTION

Around 8 million fire rise on the earth every year. Average losses in EU countries due to fire reach 1% of gross national product [1]. During fire, building structures have to carry mechanical loads to assure safe evacuation of people and safe activities of fire brigades. In most practical cases, behaviour of reinforced concrete structures at fire is assessed by simplified analytical-empirical techniques. However, such simplified analysis makes only a rough assessment of behaviour of concrete structures subjected to fire and mechanical loads. At present time, using advanced finite element software packages such as DIANA, ATENA, ABAQUS etc., it has become possible to assess the influence of various physical phenomena. However, due to complexity of these phenomena, the analysis results (deflections, time of resistance) may differ up to 5–7 times [2]. The reason for that is that presently known thermal and physical models of materials due to lack of experimental investigations are not accurate. Need for huge computing resources is another disadvantage of numerical techniques. Analysis of relatively simple members by standard software packages may last tens of hours.

A new statistically verified constitutive model [3] has been developed for deformational analysis of flexural RC members subjected to short-term loading. The model (called the *Flexural model*) has been developed by means of innovative method [3, 4] aimed at deriving constitutive relationships from flexural tests of RC members. The proposed constitutive relationship in a simple averaging manner (convenient for FE formulation) includes concrete cracking and tension stiffening effects.

In this paper, an attempt has been made to extend application of the *Flexural model* to stress and strain analysis of flexural RC members subjected to high temperature. Constitutive models and key material parameters describing thermo-mechanical behaviour of concrete and reinforcement steel are discussed. A powerful calculation technique based on layered approach is briefly described. Comparison of the experimental [5] and modelling results has shown that the proposed model has satisfactorily captured the load-deflection behaviour of the pre-cast concrete slabs.

1 MATERIAL MODELS

In fire analysis, the material properties have to be considered as temperature-dependent. Mechanical properties of different materials (steel, concrete, aluminium and stone) according to the appropriate *Eurocodes* are presented by Pintea et al [6]. This section briefly describes constitutive relationships for concrete and reinforcement steel used in the present study. Constitutive models are mainly based on *Eurocode 2* specifications [7].

During the last four decades many investigations have been reported on the effect of fire on concrete and concrete structures. The temperature dependent behaviour of concrete was summarized by Schneider and Horvath [8], including most of the test data published on concrete subject during the recent 30 years.

The theoretical stress-strain relationships of compressed and tensile concrete are given in *Fig. 1*. On the compression side, the curve consists of a parabolic branch followed by a

descending curve until crushing occurs. On the tension side, the curve consists of a bilinear diagram. An initial stiffness of concrete in tension is equal to that in compression. At tensile strains greater than this value of ε_{ct} the concrete is assumed to follow the descending branch of the stress-strain curve. Once tensile strains exceed ε_{cu}, the concrete in tension is ignored. It should be noted that behaviour of concrete in tension under fire condition is not fully investigated. So far few investigations have been carried out, mainly aimed to overall and stress-strain behaviour of structures.

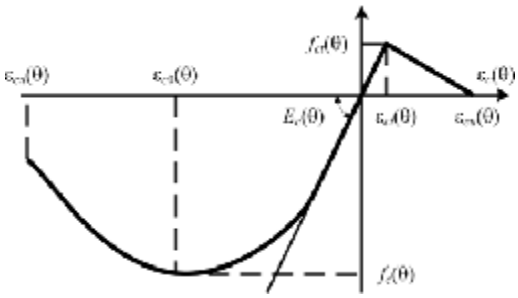

Fig. 1. Theoretical model of the stress-strain relationship of compressive and tensile concrete

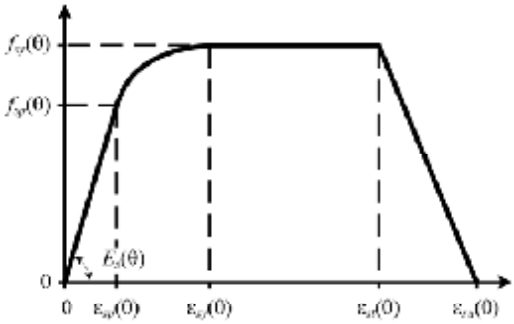

Fig. 2. Stress-strain relationship of steel

Variation of concrete parameters $f_c(\theta)$, $f_{ct}(\theta)$, $E_c(\theta)$, $\varepsilon_{c0}(\theta)$, $\varepsilon_{cu}(\theta)$ under increasing temperatures are defined using *Eurocode* 2 [7]. To the authors' knowledge, investigations regarding the limit strain $\varepsilon_{cu}(\theta)$ of tensile concrete are practically absent. In reference [9] it is taken as $15\varepsilon_{cr}(\theta)$. The same source also notes that the analysis of RC beams at ambient temperature is very sensitive to the assumed tensile behaviour of concrete. In the present study, the limit strain of tensile concrete is expressed as $\varepsilon_{cu}(\theta)=\beta\varepsilon_{cr}(\theta)$ [4]. Parameter β defining the length of the descending branch of stress-strain curve is equal to such tensile strain which corresponds to zero stress. Parameter β is expressed as $\beta=32.8-27.6p+7.12p^2$, where p is reinforcement ratio.

The constitutive model for heated and loaded steel is shown in *Fig. 2*. For a given steel temperature θ, the stress-strain curves are defined by three parameters: the slope of the linear elastic range $E_s(\theta)$ for reinforcement, the proportionality limit $f_{sp}(\theta)$, and the maximum stress level $f_{sy}(\theta)$. The strength and deformation properties of reinforcing steel at elevated temperatures are obtained from [7].

2 ANALYSIS OF RC SLABS SUBJECTED TO FIRE

Modelling of behaviour of structures subjected to high temperature conditions consists of 3 separate steps [10]. The first step is associated with the fire dynamics. Computational fluid dynamics models may be applied to get heat transport from fire source to the boundary of structure. In the second step, heat transfer analysis is performed to get temperature distribution within cross section of the member. Experimental fire tests, tables or graphs, numerical or empirical calculations can be employed for this case. Heat transfer analysis is a link between the first and the final step which is related to the mechanical response of the structure due to simultaneous time-dependent thermal and mechanical loads. Although, some

authors proposed a unified computer model [11], these steps usually, are not integrated, i.e. the thermal calculations are carried out first for the entire duration of the fire and then fed into the mechanical analysis program to produce the stresses and strains for the member.
In this section, a simple iterative technique for mechanical analysis (3rd step) of RC slabs under high temperature is presented. The calculation is based on fundamental techniques of mechanics of materials extended to application of layered approach. As shown in *Fig. 3, a*, a member may contain one or more levels of reinforcement, and is subjected to coupled thermo-mechanical loading. *Fig. 3, c* shows the thermal part of loading. The member's cross-section is divided into a number of horizontal layers corresponding to either concrete or reinforcement (*Fig. 3, b*).

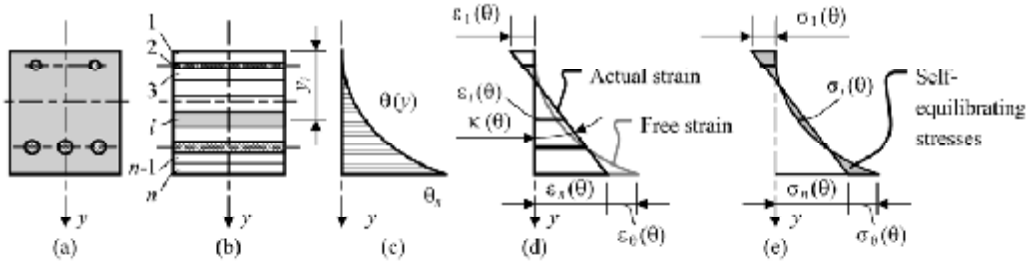

Fig. 3. Stress and strain caused by non-linear temperature gradient: cross-section (a); layered section (b); temperature gradient (c); distribution of strain (d) and distribution of stress across the section (e)

The material properties are assessed in iterative calculation by means of secant deformation modulus and assumed to be constant over the layer thickness. The cross section analysis is performed on the so-called transformed section. The area of bonded steel reinforcement is transformed into an equivalent area of concrete. Thickness of the reinforcement layer is taken from the condition of the equivalent are.
The proposed calculation technique is based on the following approaches and assumptions: 1) smeared crack approach; 2) linear distribution of strain within the depth of the section; 3) perfect bond between concrete and reinforcement; 4) the model is valid only for the ascending temperature regime, i. e. cooling faze can not be assessed.
The strain components can be modelled using the superposition theory whereby the total strain is considered to be the sum of various strain components [12]:

$$\varepsilon_{tot}(T,\sigma) = \varepsilon_{\sigma}(T,\sigma) + \varepsilon_{th}(T,\theta) + \varepsilon_{ttc}(T,\sigma), \quad (1)$$

where $\varepsilon_{\sigma}(T,\sigma)$ is the stress-related strain, $\varepsilon_{th}(T,\theta)$ is the thermal strain, $\varepsilon_{ttc}(T,\sigma)$ is the transient thermal creep strain, θ is the temperature, T is the time, σ is a stress.
Thermal strain of concrete during heating is a simple function of temperature $\varepsilon_{th,i}(\theta) = \alpha_i \Delta\theta_i$, where α_i is the coefficient of thermal expansion of *i*-th layer; $\Delta\theta_i$ is the increment of temperature in this layer. In *Eurocode* 2 [7], empirical expressions for strain ε_{θ} in terms of $\Delta\theta$ are given for concrete and reinforcement.
The transient thermal creep strain of tensile concrete has not been taken into account. Meanwhile the transient creep for each compressive layer is calculated using the relationship proposed by Anderberg and Thelandersson [12]:

$$\varepsilon_{ttc,i}(T,\sigma) = -\varepsilon_{th,i}(\theta)\beta\sigma_i / f_c(20\,^{\circ}\mathrm{C}), \quad (2)$$

where β is a material parameter, σ_i is the stress in the layer, $f_c\left(20^\circ\mathrm{C}\right)$ is the compressive strength of concrete under normal ambient temperature.
As plane sections tend to remain plane, a non-linear temperature gradient and transient thermal creep produces internal, self-equilibrating stresses $\Delta\sigma_\theta$ and $\Delta\sigma_{ttc}$, respectively. These strains of each fibre are restrained by the adjacent fibres resulting in the internal stress distribution. The total restraining axial force $\Delta N = \Delta N_\theta + \Delta N_{ttc}$ and bending moment $\Delta M = \Delta M_\theta + \Delta M_{ttc}$ required to prevent these deformations. These restraining actions are obtained by integrating the internal relaxation stresses $\Delta\sigma_\theta$ and $\Delta\sigma_{ttc}$ and their first moments about the top edge. The restraining forces are added to the external ones ($N = N_{ext} + \Delta N$, $M = M_{ext} + \Delta M$). Thus, the resultant changes in stresses and strains due to high temperature loads are obtained. Expressions for the initial top fibre strain $\varepsilon_1(\theta)$ and curvature $\kappa(\theta)$ in terms of applied axial force N and bending moment M are as follows:

$$\varepsilon_1(\theta) = -\frac{I_{c,eff}N + S_{c,eff}M}{E_c(20^\circ C)\left(A_{c,eff}I_{c,eff} - S_{c,eff}^2\right)},\ \kappa(\theta) = \frac{S_{c,eff}N + A_{c,eff}M}{E_c(20^\circ C)\left(A_{c,eff}I_{c,eff} - S_{c,eff}^2\right)} \tag{3}$$

Here $A_{c,eff}$ is the area of transformed section, $S_{c,eff}$ is the first moment of transformed area, $I_{c,eff}$ is the second moment $I_{c,\,eff}$ of transformed area about the top edge, $E_c\left(20^\circ\mathrm{C}\right)$ is the modulus of elasticity of concrete under normal ambient condition.
Total strain at any point of the section below the top surface is expressed as:

$$\varepsilon_{\sigma,i}(\theta,\sigma) = \varepsilon_1(\theta) - \varepsilon_{th,i}(T,\theta) - \varepsilon_{ttc,i}(T,\sigma) + y_i\kappa(\theta) \tag{4}$$

Based on $\varepsilon_{\sigma,i}(\theta,\sigma)$, the stress at any fibre of cross section is obtained according to the respective material model (steel or concrete). A computer program for the mechanical problem has been developed for assessing stress and strain state of a beam as well as for calculation of curvatures and deflections. For a given external moment, the computation is performed in iterations. For deflection calculation *Mohr's* integral technique has been applied.

3 COMPARISON TO TEST DATA

This section presents a comparison between the computed (using the described procedure) and the measured RC slab deflections reported by Cook [5]. Totally 14 pre-cast concrete floor slabs were exposed to standard ISO 834 and Norwegian Petroleum Directorate (NPD) fires (*Fig. 4*, *a*). Present paper includes results of modelling of six slabs, namely S1, S2, S3, S5, S6 and S10 data of which was reported in [5]. The specimens were 4700 mm long, 150 mm (S1÷S3) and 250 mm high (S5, S6, S10) and 925 mm wide. All slabs were simply supported at 4.5 m centres. The fire exposed length was 4.0 m. The slabs were cast of concrete mixes with siliceous aggregates and designed to have characteristic cube strength of 30 MPa. The moisture content of slabs varied between 3.5 and 4.5% by weight. The reinforcing steel bars were of high yield ribbed bar having yield strength of 460 MPa. Slabs S1÷S3 were reinforced with 10 bars of 8 mm diameter, whereas slabs S5, S6, S10 were reinforced with 6 bars of 8 mm diameter. The reinforcement cover was 25 mm.
Experimental temperature distributions within cross section of slabs after 30, 60, 90 and 120 min fire exposure are presented in *Fig. 4, b and c*. These temperature profiles were used for the respective time-deflection analysis. As temperature dependent material properties were not given in the reference [5], they were assumed according to *Eurocode* 2 [7]. Loading of

slabs S1, S3, S5, S10 was due to selfweight, whereas slabs S2 and S6 were additionally subjected to live distributed load of 1.5 kN/m^2.

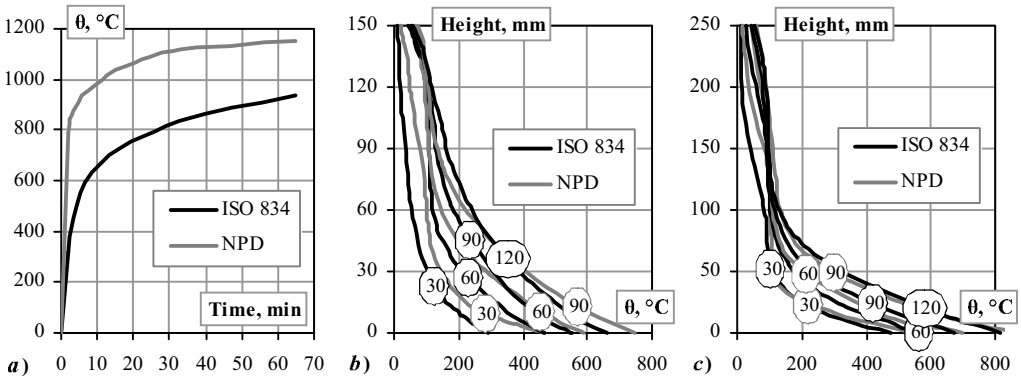

Fig. 4. Temperature-time curves used in tests (a) and temperature profiles for S1÷S3 (b) and S5, S6, S10 (c) slabs

The modelled time-deflection diagrams along with the experimental curves are presented in *Fig. 5* in terms of normalized deflections, $f / f_{\max}$. Here $f_{\max}$ is the maximal deflection at the end of fire exposure. It can be seen from *Fig. 5* that the shape of the experimental load-deflection diagrams was well captured in the present analysis. Agreement of the calculated and measured deflections is within reasonable limits.

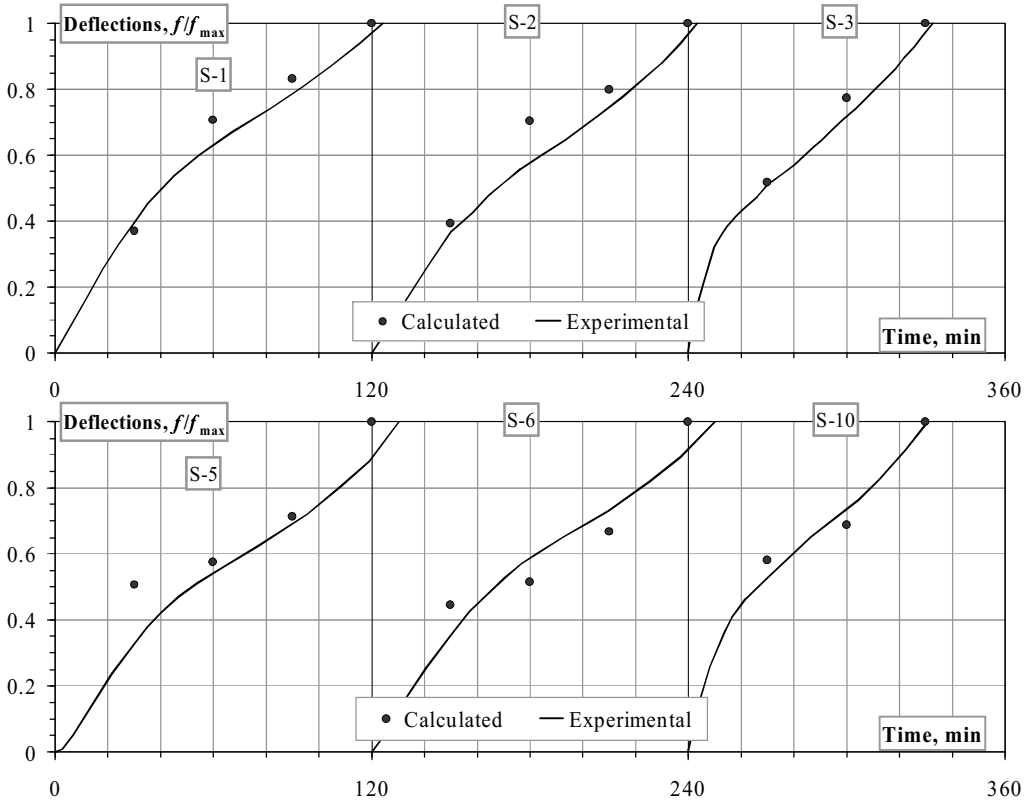

Fig. 5. Comparison of calculated deflections to test results [5]

4 CONCLUDING REMARKS

In this paper, an attempt has been made to extend application of the *Flexural model* to stress and strain analysis of flexural reinforced concrete members subjected to high temperature. Constitutive models and key material parameters describing thermo-mechanical behaviour of concrete and reinforcement are discussed. A powerful calculation technique based on layered approach has been developed. Variation of material properties within the section due to different loading and temperature gradient was assessed in the analysis. Restrained thermal deformations as well as transient thermal creep were modelled by means of fictitious equivalent forces. Comparison of the experimental and modelling results has shown that the proposed model has satisfactorily captured the load-deflection behaviour of the pre-cast reinforced concrete slabs.

5 ACKNOWLEDGMENT

The authors wish to express their gratitude to the *European Community* and the *Agency of International Programs of Scientific and Technology Development in Lithuania* for the financial support provided under the COST action C26. The authors also gratefully acknowledge the financial support provided by the *Lithuanian State Fund of Research and Studies*.

REFERENCES

[1] World Fire Statistics, Report N 10, second edition. *International Association of Fire and Rescue Service (CTIF).* Available online http://www.ctif.org.

[2] Cervenka, J., Surovec, J., Fellinger, J., Feron, C., Wageneder, J., Kaklauskas G., Corsi, F. FE Simulations of a Suspending Ceiling. Comparison of Fire Test Analyses. *UPTUN Report 441*, 2005.

[3] Kaklauskas, G., Ghaboussi, J. Stress–Strain Relations for Cracked Tensile Concrete from RC Beam Tests. *ASCE Journal of Structural Engineering 127(1)*, 2001, pp. 64–73.

[4] Kaklauskas, G. Flexural Layered Deformational Model of Reinforced Concrete Members. *Magazine of Concrete Research 56(10)*, 2004, pp. 575–584.

[5] Cooke, G. M. E. Behaviour of Precast Concrete Floor Slabs Exposed to Standardised Fires. *Fire Safety Journal 36(5)*, 2001, pp. 459–475.

[6] Pintea, D.; Zaharia, R.; Kaliske, M.; Kaklauskas, G.; Bacinskas, D.; Gribniak, V.; Torok, A.; Hajpal, M. Mechanical Properties of Materials. Proceedings of International COST C26 Symposium, Malta, 23-24 October 2008, *Datasheet No. 1.5*, 2008, pp. 28–33.

[7] EN 1992-1-2. Eurocode 2: Design of Concrete Structures – Part 1.2: General Rules – Structural Fire Design. *European Committee for Standartization*, Brussels, 2004.

[8] Schneider, U., Horvath, J. Behaviour of Ordinary Concrete at High Temperatures. *Research Report, Vol. 9*. Vienna University of Technology, 2003.

[9] Cai, J., Burgess, I., Plank, R. A Generalised Steel/Reinforced Concrete Beam-Column Element Model for Fire Conditions. *Engineering Structures 25(6)*, 2003, pp. 817–833.

[10] Wang, Y. C.; Wald, F. Heat Transfer Analysis. Proceedings of International COST C26 Symposium, Malta, 23-24 October 2008, *Datasheet No. 1.4*, 2008, pp. 22–27.

[11] Ren, A., Shi, J., Shi, W. Integration of Fire Simulation and Structural Analysis for Safety Evaluation of Gymnasiums – With a Case Study of Gymnasium for Olympic Games in 2008. *Automation in Construction 16(3)*, 2007, pp. 277–289.

[12] Anderberg, Y.; Thelandersson, S. Stress and Deformation Characteristic of Concrete at High Temperatures. Part 2: Experimental Investigation and Material Behaviour Model. *Bulletin 54*, Lund University of Technology, 1976.

PERFORMANCE BASED FIRE DESIGN OF CONCRETE-FILLED STEEL COLUMNS

Venkatesh Kodur [a], Rustin Fike [b]

[a] Michigan State University, Professor of Civil and Environmental Engineering, E. Lansing, MI, USA
[b] Michigan State University, Ph.D. Candidate Civil and Environmental Engineering, E. Lansing, MI, USA

1 INTRODUCTION

Steel hollow structural sections (HSS) are very efficient in resisting compression, torsional and seismic loads, and are widely used as compressions members in the construction of framed structures. Fire safety is one of the primary considerations in the design of high-rise buildings, and hence, building codes specify fire resistance requirements for HSS columns to maintain overall structural stability in the event of fire. Providing such external fire protection to HSS columns involves additional cost, reduces aesthetics, increases weight of the structure, and decreases usable space. Also, durability of fire proofing (adhesion to steel) is often a questionable issue, and hence, requires periodic inspection and regular maintenance, which in turn, incurs additional cost during the lifetime of the structure [1,2].

Often these HSS sections are filled with concrete (CFHSS) to enhance the stiffness, torsional rigidity and load-bearing capacity. The two components of the composite column complement each other ideally at ambient temperatures. In addition, high fire resistance can be obtained without using external fire protection for the steel. Further, a wide range of fire resistance can be obtained by selecting different types of concrete filling, namely plain concrete (PC) steel fiber reinforced concrete (FC) and bar reinforced concrete (RC) [8]. Design guidelines for achieving fire resistance through concrete filling have been incorporated into codes and standards [3-5]. However, the current fire guidelines are limited in scope and restrictive in application since they were developed based on standard fires (ASTM E-119 and ISO 834) [6,7]. Hence, they are valid only for the standard fire exposure conditions, and for column parameters (length, load, etc.) dictated by the capacity of available testing furnaces.

To overcome some of the drawbacks in current design specifications a numerical study is carried out on a set of CFHSS columns exposed to various fire and loading scenarios. The analysis was carried out using finite element based computational model SAFIR, wherein the material and geometric non-linearity, and stability-based failure criterion are considered. Results from the analysis are used to present a framework for a performance-based fire engineering methodology. It is demonstrated that required fire resistance for HSS columns in the practical range can be achieved through concrete filling.

2 PERFORMANCE BASED DESIGN

Recently there has been an increased impetus on moving toward a performance-based approach for fire safety design [7]. This is mainly due to the fact that the current prescriptive-based approach has serious limitations and does not provide alternate, cost effective and innovative solutions. One of the key components in performance based design is the use of a rational approach for evaluating fire resistance. Numerical/computational simulations can be used to evaluate the structural performance under fire conditions. The most important factors to be considered in any performance-based fire safety design are fire scenario, load level, failure criterion and geometric conditions [9]. Research efforts in the last two decades have

lead to inclusion of recommendations for the use of design fire scenarios, load level, and failure criterion in codes and standards [10]

3 FACTORS GOVERNING FIRE RESISTANCE

Fire resistance of CFHSS columns depends on a number of factors. While the effects of critical factors under standard fire exposure are well understood [11], the influence of critical parameters under realistic fire, loading, and failure criterion are not well understood. To investigate the influence of different parameters on fire resistance of CFHSS columns, a set of numerical studies were carried out using the computer program SAFIR. For the parametric studies, 20 CFHSS columns were selected. Fourteen of the selected columns were the ones tested at the National Research Council of Canada [12,13], while the remaining six columns were variations of the test columns selected to cover a wider range of column variables. In order to fully investigate the effect of length on fire resistance, columns with 3.81, 5, 6, 7, 8, 9 and 10 m (12.5, 16.4, 19.7, 23.0, 26.3, 29.5 and 32.8 ft) length were modeled for each cross-section. Fire exposure was assumed on all four sides with the bottom and top 5% of the column length unexposed to fire. The applied loads on the column were modified to maintain a constant load ratio for all of the lengths modeled for a specific cross-section according to the AISC analysis procedure [4]. The applied load on the composite column takes into account the contribution of different types of concrete filling with steel fiber and bar reinforced concrete-filled HSS columns having higher load capacity. Each of these cross section-length combinations were modeled under seven fire scenarios. Five of the scenarios are shown in Figure 1, the remaining two fire scenarios were also design fires. This parametric study generated a total of 980 numerical simulations covering a wide range of load, geometry, concrete types, and fire scenarios. Detailed results from the parametric studies are presented elsewhere and only the main highlights of the most important parameters are addressed below [11]. The trends (results) discussed below were observed for all of the filling types (plain, bar and steel fiber reinforced) considered unless otherwise noted.

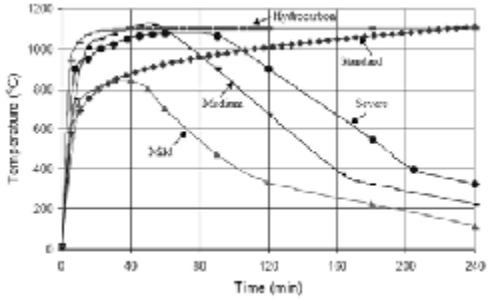

Fig. 1. Time-temperature relationships for various fire scenarios

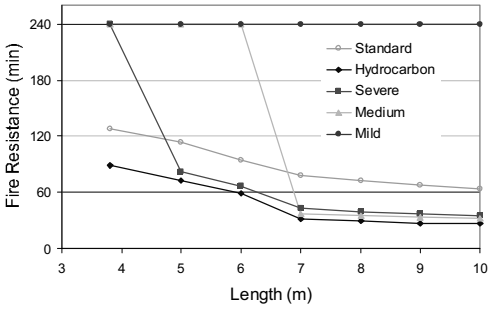

Fig. 2. Fire resistance as a function of length for a PC-HSS under different fire scenarios

3.1 Effect of Fire Exposure

Results from parametric studies indicate that the fire resistance of a column increases as the fire severity decreases. It can be seen in Figure 2 that fire resistance of four hours or more can be obtained for columns up to 10m long under mild fire conditions. However, for other fire exposures, fire resistance decreases with an increase in length. A closer look at Figure 2 reveals that fire resistance of a 5 m (16.4 ft) long CFHSS column ranges from sufficient to withstand compartment burnout for medium and mild fire exposure, to 68 minutes under severe exposure. The reason for this decreased fire resistance with increased fire severity can

be attributed to the higher internal temperatures attained in the concrete under severe fire exposure. Consequently, the column looses its strength and stiffness at a faster rate leading to early failure.

3.2 Effect of Length

Results presented in Figure 2 can also be used to demonstrate the effect of length on the fire resistance of CFHSS columns. As would be expected, fire resistance for a given fire exposure decreases with an increased length of the column. This is due to higher slenderness that accompanies the increased length which in turn governs the failure pattern of the column. Fire resistance is drastically reduced when the failure mode switches from crushing to buckling with increased length. This is most pronounced for the "medium" and "severe" fire exposure as can be seen in Figure 2. Fire resistance under the "medium" fire drops from 240 to 45 minutes when length is increased from 5 to 7 m (16.4 to 23 ft). Under severe fire exposure, the fire resistance decreases from 240 to 75 minutes for an increase in length from 3.81 to 5 m (12.5 to 16.4 ft). However, under mild fire exposure, fire resistance remains high for all cases, and the length does not have any influence. This study clearly illustrates that length has a significant influence on the resulting fire resistance, specifically under severe fire exposures.

3.3 Effect of Concrete Filling

The effect of the type of concrete filling on fire resistance is illustrated in Figure 3. HSS columns with different concrete filling types were analyzed under standard fire exposure and the fire resistance evaluated. As was the case with the effect of length, the applied load was modified according to AISC analysis procedures [4] to account for the higher strength capacity resulting from FC and RC filling. As seen in Figure 3, the fire resistance decreases with an increase in length for all of the filling types. However, columns with RC or FC filling demonstrate higher fire resistance than PC-filled columns at all lengths. This can be attributed to the increased load carrying capacity of the concrete core provided by the inclusion of reinforcement, and also due to the slower loss of strength in RC and FC filled columns resulting from the presence of reinforcement in the concrete core. These results indicate that it is possible to significantly enhance the fire resistance of CFHSS columns by changing the type of concrete filling. The required fire resistance in most practical situations can be obtained for columns up to 10 m (32.8 ft) in length by simply altering the type of concrete filling.

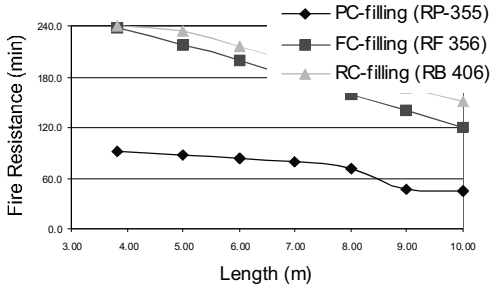

Fig. 3. Effect of length and concrete filling on fire resistance of CFHSS columns

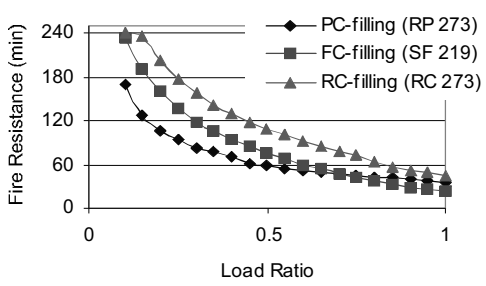

Fig. 4. Effect of load ratio on the fire resistance of CFHSS columns

3.4 Effect of Load Ratio

The effect of load ratio on fire resistance was investigated by analyzing three CFHSS columns under standard fire with load ratios ranging from 10% to 100% (0.1 to 1.0). Load ratio is defined as the ratio of the load on the column under fire conditions to the ambient temperature capacity of the column. The analysis was carried out for three types of concrete filling, namely: PC, FC, and RC, and the results are shown in Figure 4. A RC-filled HSS column withstood the ASTM E-119 [6] fire for 240 minutes with a load ratio of 10% (0.1). The FC and PC-filled columns lasted for 234 and 170 minutes respectively. The fire resistance decreases rapidly with an increase in load ratio up to 0.4. After which point the rate of decrease in resistance is slower as seen in Figure 4. This can be attributed to the fact that concrete filling generally provides a load bearing contribution of about 30%-40% of the overall composite column capacity. In a fire scenario, the steel shell looses its strength very quickly, and concrete carries most of the load. Thus, for load ratios higher than 40%, the concrete filling has to be strengthened either through the use of bar-reinforcement, or through the use of steel fibers to achieve higher fire resistance.

3.5 Effect of Aggregate Type

Results from the analysis indicate that the type of aggregate has a moderate influence on the fire resistance of CFHSS columns. The two common types of aggregate used in concrete are: carbonate (mainly consisting of limestone) and siliceous (mainly consisting of quartz) aggregate. Carbonate aggregate concrete typically demonstrates higher fire resistance than siliceous aggregate concrete [14,15]. This is due to an endothermic reaction occurring in carbonate aggregate at 600-800 °C, in which the dolomite within the aggregate dissociates. Consequently, the heat capacity of carbonate aggregate increases significantly and is approximately 10 times higher than siliceous aggregate in the same temperature range. As a result, there is a slower increase in temperature in the carbonate aggregate concrete, and thus, a slower loss of strength. Therefore, the fire resistance of CFHSS columns filled with carbonate aggregate concrete is about 10% higher than siliceous aggregate concrete-filled HSS columns.

3.6 Effect of Failure Criterion

The two limit states generally considered for defining failure of steel columns under fire conditions are: critical steel temperature and stability (strength) of the column. ASTM E-119 [6] defines fire resistance as the time it takes to reach a maximum average section temperature of 538 °C, or a maximum point temperature of 649 °C. On the contrary, stability-based failure criterion are based on the duration of time during which a column maintains structural stability (strength) during fire exposure. In the case of CFHSS columns, use of critical temperature criterion does not reflect realistic fire resistance since CFHSS columns derive fire resistance primarily from the concrete core. As an illustration, a PC-filled HSS column that has a fire resistance of 128 minutes as per SAFIR analysis (based on strength limit state), only has a fire resistance of 38 minutes when critical temperature criterion is applied. Clearly, thermal failure criteria do not reflect the contribution of the concrete filling to the fire resistance of CFHSS columns. As such, it is necessary to employ stability-based failure criterion for the evaluation of the fire resistance of CFHSS columns.

4 STRATAGIES FOR REALIZING UNPROTECTED CFHSS COLUMNS

In recent years, the performance-based approach to fire safety design has become popular since cost-effective and rational fire safety solutions can be developed using this approach [8]. One of the key aspects in any performance-based design is the fire resistant design of

structural members. Through the application of a performance-based approach, and by utilizing different concrete filling types, the full benefits of CFHSS columns can be realized. For developing such strategies, numerical models that can simulate the response of CFHSS columns under realistic fire, loading and restraint scenarios have to be used. The main steps involved in undertaking a rational approach for performance-based fire design of CFHSS columns are: 1) identifying proper design (realistic) fire scenarios and realistic loading level on the column, 2) carrying out detailed thermal and structural analysis by exposing the column to fire conditions; and 3) developing relevant practical solutions, such as the use of different types of concrete filling, to achieve the required fire resistance.

4.1 Development of Fire Scenario and Loading

The design fire scenarios for any given situation can be established either through the use of parametric fires (time-temperature curves) specified in Eurocode 1 [16] or through design tables [17] based on ventilation, fuel load and surface lining characteristics. To use the design tables, the ventilation factor, F_v, has to be established using $F_v = \frac{A_v}{A_t}\sqrt{H_v}$. Where A_v is the area of the window opening (m^2), A_t is the total internal area of the bounding surface (m^2), and, H_v, is the height of the window opening (m) [18]. The fuel load in the compartment is determined by considering the total bounding surface (not just the floor surface area). Typical fuel loads for common compartment types are available [9,18]. Figure 1 shows typical design fire curves that can be generated using performance-based fire safety design. The presence of sprinklers can also be accounted for in the development of design fire scenarios.
The loads that are to be considered on concrete-filled HSS columns under fire conditions should be estimated based on the guidance given in ASCE-07 standard or Eurocode, [16, 19] (1.2 dead load + 0.5 live load) or through actual calculations based on different load combinations.

4.2 Structural Analysis Under Fire Exposure

Once the fire scenarios and load level are established, the next step is to avail of a computer program for the analysis of CFHSS columns exposed to fire. The computer program should be able to trace the response of the CFHSS column in the entire range of loading up to collapse under fire. Using the computer program, a coupled thermal-structural analysis shall be carried out at various time steps. In each time step, the fire behavior of a CFHSS column is estimated using a complex, coupled heat transfer/strain equilibrium analysis, based on theoretical heat transfer and mechanics principles. The analysis shall be performed in three steps: namely, calculation of fire temperatures to which the column is exposed (as detailed in 4.1), calculation of temperatures in the column, and calculation of resulting deflections and strength, including an analysis of the stress and strain distribution.
The temperatures (in the concrete, and reinforcement), strength capacities, and computed deflections of the column shall be used to evaluate failure of the column at each time step. At every time step, the failure of the column shall be checked against a pre-determined set of failure criteria. The time increments continue until a certain point at which the strength failure criterion has been reached, or the axial deformations reach their limiting state. At this point, the column becomes unstable and will be assumed to have failed. The time to reach this failure point is the fire resistance of the CFHSS column.

4.3 Development of Practical Alternatives

Results from the above analysis can be utilized to develop practical solutions for achieving the required fire resistance in CFHSS columns. The most feasible solution is through the use

of appropriate concrete filling (PC, FC, and RC). Other factors, such as reinforcement in the column or load level can be varied to achieve the required fire resistance in HSS columns. Once the parameters are selected, a detailed analysis can be carried out to assess the fire resistance of the column under a specific fire and loading scenario. The analysis is repeated until the required fire resistance is obtained for the CFHSS column. As an example, while PC-filling can provide one-two hours of fire resistance in HSS columns, by switching to FC or RC-filling, up to three hours of fire resistance can be obtained even under severe design fire scenarios. It should be insured that stem vent holes are provided at the top and the bottom of compartment elevations to alleviate the steam pressure generated inside the HSS column [20].

5 CONCLUSIONS

Based on the results of this study, the following conclusions can be drawn:

- Type of fire exposure has a significant influence on the fire resistance of CFHSS columns. The fire resistance of CFHSS columns under most design fire scenarios is higher than that under standard fire exposure.
- Apart from fire exposure, the other significant factors that affect the fire resistance of CFHSS columns are length, type of concrete filling, load ratio and failure criterion.
- It is possible to achieve unprotected CFHSS columns up to 10m (32.8 ft) in length, capable of withstanding complete compartment burnout through the use of different types of concrete filling.
- Through the use of a performance-based design approach, it is possible to significantly enhance the fire resistance of CFHSS columns by varying parameters such as load level, concrete filling type, and type of aggregate in the concrete.
- The limiting criterion, used for determining failure, has a significant influence on the fire resistance of CFHSS columns. The conventional failure criterion, such as limiting steel temperature can not be applied to CFHSS columns. Strength and deformation failure criteria should be considered for evaluating fire resistance of CFHSS columns.

6 ACKNOWLEDGMENTS

The research, presented in this paper, is primarily supported by the American Institute of Steel Construction through AISC Faculty Fellowship Award to Prof. Kodur. Any opinions, findings, and conclusions or recommendations expressed in this paper are those of the authors and do not necessarily reflect the views of the sponsors.

7 REFERENCES

[1] FEMA, “World Trade Center Building Performance Study: Data Collection, Preliminary Observations, and Recommendations”, Federal Emergency Management Agency, Washington, DC. 2002

[2] NIST, “Final Report of the National Construction Safety Team on the Collapse of World Trade Center Towers”, NCSTAR1, National Institute of Standards and Technology, Gaithersburg, MD 20899. 2005

[3] ASCE/SFPE 29, “Standard Calculation Method for Structural Fire Protection”, American Society of Civil Engineers, Reston, VA. 1999

[4] AISC, “Steel Construction Manual 13th Edition”, American Institute of Steel Construction, Chicago, IL. 2005

[5] NBC, “National Building Code of Canada”, National Research Council of Canada, Canada. 2005

[6] ASTM, “Standard Methods of Fire Test of Building Construction and Materials”, Test Method E119-00, American Society for Testing and Materials, West Conshohocken, PA. 2007

[7] ISO 834, “Fire Resistance Tests – Elements of Building Construction”, International Organization for Standardization, Geneva, Switzerland 1975,

[8] Kodur, V.K.R., “Performance-based Fire Resistance Design of Concrete-filled Steel Columns”, *Journal of Constructional Steel Research Institute*, Vol. 51, pp. 21-36. 1999

[9] Parkinson, D.L. and Kodur, V.K.R., “Performance-Based Design of Structural Steel for Fire Conditions – A Calculation Methodology”, *International Journal of Steel Structures* Vol. 7, No. 3, pp. 219-226. 2007

[10]Eurocode 4, ENV 1994 1-2: "Design of Composite Steel and Concrete Structures" European Committee for Standardization 2005.
[11]Kodur, V.K.R. and Fike, R.F. "Performance-Based Fire Resistant Design for Concrete-Filled HSS Columns" Proceedings of the 2008 Annual Stability Conference, Nashville TN April 2-5, 2008
[12] Kodur, V.K.R. and Lie, T.T., "Fire Performance of Concrete-filled Hollow Steel Columns", *Journal of Fire Protection Engineering*, Vol. 7, No. 3, pp. 89-98. 1995
[13] Lie, T.T. and Chabot, M., "Experimental Studies on the Fire Resistance of Hollow Steel Columns Filled With Plain Concrete", IRC Internal Report No. 611, National Research Council of Canada. 1992
[14] Kodur, V.K.R. and Lie, T.T., "Fire Resistance of Circular Steel Columns Filled With Fiber-reinforced Concrete", *Journal of Structural Engineering*, ASCE Vol. 122, No. 7, pp. 776-782. 1996
[15] Kodur, V.K.R. and Lie, T.T., "Evaluation of Fire Resistance of Rectangular Steel Columns Filled With Fiber-Reinforce Concrete", *Canadian Journal of Civil Engineering*, Vol. 24, pp. 339-349. 1997
[16] Eurocode 1, ENV 1991 1-2: "General Actions – Actions on Structures Exposed to Fire", European Committee for Standardization. 2002
[17] Magnusson, S.E. and Thelandersson, S., "Temperature-Time Curves of Complete Process of Fire Development; Theoretical Study of Wood Fuel Fires in Enclosed Spaces", *Civil Engineering and Building* Series 65, Acta, Polytechnica, Scandinavia. 1970
[18] Buchanan, A.H., "Structural Design for Fire Safety", John Wiley and Sons Ltd., New York, NY. 2005
[19] ASCE 7-05, "Minimum Design Loads for Buildings and Other Structures", American Society of Civil Engineers, Reston, VA. 2005
[20] Kodur, V.K.R. and Mackinnon, D.H. " Design of Concrete-Filled Hollow Structural Steel Columns for Fire Endurance" *American Institute of Steel Construction Engineering Journal* Vol. 37 pp. 13-24 2000

FIRE RESISTANCE OF FIBER REINFORCED CONCRETE COLUMNS

João Paulo C. Rodrigues [a], Luís Laím [a], Georgina Mihailovschi [b]

[a] Faculty of Sciences and Technology, University of Coimbra, Coimbra, Portugal
[b] INTI-Construciones, Buenos Aires, Argentina

INTRODUCTION

In this paper are presented results of fire resistance tests on fiber reinforced concrete columns. The concrete used has a mixture of polypropylene (pp) and steel (st) fibers. The pp fibers have the function to control the spalling while the st fibers have the function to give the concrete the capacity to resist the thermal stresses generated in fire and increase the ductility of the concrete.

The percentage of st fibers varied in the different mixtures studied according to the percentage of steel reinforcement. In other words, it was done a replacement of steel reinforcing bars by steel fibers, maintaining in each column the same quantity of steel reinforcement (st fibers + steel reinforcement). The columns were then tested in fire resistance tests.

The studies developed in the area of fire behavior in fiber reinforced elements are still very premature. Nevertheless, for concrete material, with and without fibers, there are already a lot of tests by Kalifa et al [1] and Han C.G et al (2004) [2]. The most important findings of those studies were that in case of fire the pp fibers will volatize and micro-channels will be formed in the concrete which served as a way for the release of water vapor to the outside, and, consequently, they allowed a reduction in the spalling of concrete. Another important finding is that the use of st fibers or a mixture of both fibers (pp + st) reduces the loss of residual compression strength and elastic modulus of concrete at high temperatures.

1. FIRE RESISTANCE TESTS ON FIBRE CONCRETE COLUMNS

The main objective of this work was to study the behavior of fiber concrete columns when exposed to fire, being the steel reinforcement partially replaced by st fibers. Four fire resistance tests were carried out, one in a column without fibers (reference test) and three others with a fixed quantity of pp fibers and a variable quantity of st fibers. In these three tests, the steel reinforcing bar of the columns was replaced partly by st fibers so that the total amount of steel in the column (st fibers + steel reinforcing bars) was always the same.

1.1. Composition of concrete

The concrete was constituted by cement type I 42,5 R (C), superplasticizer (SP), calcareous filler (CF), fine (FS), middle (MS) and coarse sand (CS), grain of rice (GR), fine (CS1: 5-12 mm) and middle crushed stone (CS2: 14-20 mm), polypropylene fibers (PP) and steel fibers (ST), being the respective quantities of each column described in Table 1. Relatively to the total amount of steel in each column the percentage of steel fibres varied between 36% (Column C3) and 84% (Column C1).

Table 1. Composition of concrete columns [per m^3]

Column	C [kg]	SP [% CEM]	CF [kg]	FS [kg]	MS [kg]	CS [kg]	CS [kg]	CS1 [kg]	CS2 [kg]	PF [kg]	SF [kg]	W/C
1	200.0	3.0	100	539	-----	-----	407	319	422	1.5	38.80	0.67
2	200.0	3.0	100	539	-----	-----	407	319	422	1.5	27.24	0.67
3	200.0	3.0	100	539	-----	-----	407	319	422	1.5	16.56	0.67
4	190.0	2.9	100	260	380	250	-----	940	----	-----	-----	0.59

Table 2 presents the quantities of st fibers and steel reinforcement bars in each column.

Table 2. Quantity of steel fibers and steel reinforcement bars in columns

Column	Dia. of steel bars	Steel reinforcement bars [kg]	Steel fibers [kg]	Total steel [kg]
C1	4 ϕ 10	7.40	38.80	46.20
C2	4 ϕ 16	18.96	27.24	46.20
C3	4 ϕ 20	29.64	16.56	46.20
C4	4 ϕ 25	46.20	---------	46.20

Table 3 presents the compression strength of the concrete at 28 days, where f_{cm} and f_{ck} are the mean and the characteristic value of the compressive strength of concrete, respectively.

Table 3. Compression resistance of concrete at 28 years

Column	f_{cm} [Mpa]	f_{ck} [Mpa]	Class resistance
C1	23.8	16.0	C12/15
C2	27.0	19.0	C12/15
C3	25.1	17.1	C12/15
C4	29.4	21.4	C16/20

1.2. Columns

The columns tested presented all a square section 250 mm x 250 mm with 3 meters high. The longitudinal steel reinforcing bars varied according to the values presented in Table 2, while the stirrups had in all columns 8 mm of diameter (Fig. 1).

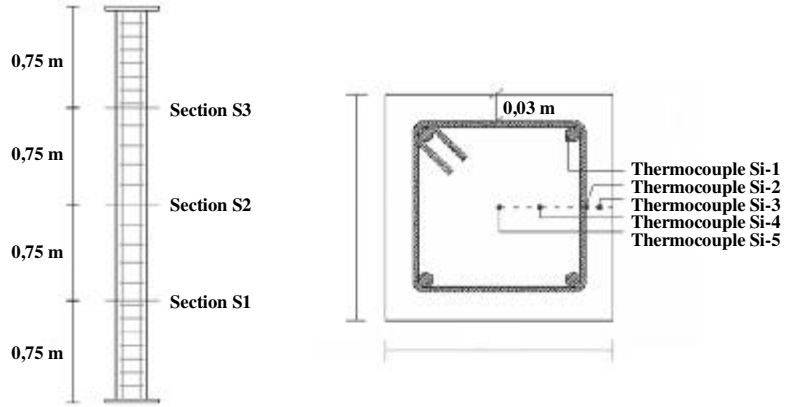

Fig. 1. Scheme of the columns and localization of the thermocouples

The temperature was measured with type K (chromo-alumel) thermocouples located at different depths in three sections of the column as represented in figure 1. Thermocouples Si-1 and Si-2 were welded in steel reinforcing bars, while thermocouples Si-3, Si-4 and Si-5 were embedded in the concrete.

1.3. Test procedure

In the experimental tests was used a new test set-up for fire resistance test of columns with restrained thermal elongation, that has been developed in development in the Faculty of Sciences and Technology of the University of Coimbra (Fig. 2). This system is composed by a restraining frame of variable stiffness (1), although in these tests was adopted a stiffness of 13 KN/mm (stiffness determined experimentally). This restraining frame had the function to simulate the stiffness of the surrounding structure to the column when exposed to fire.

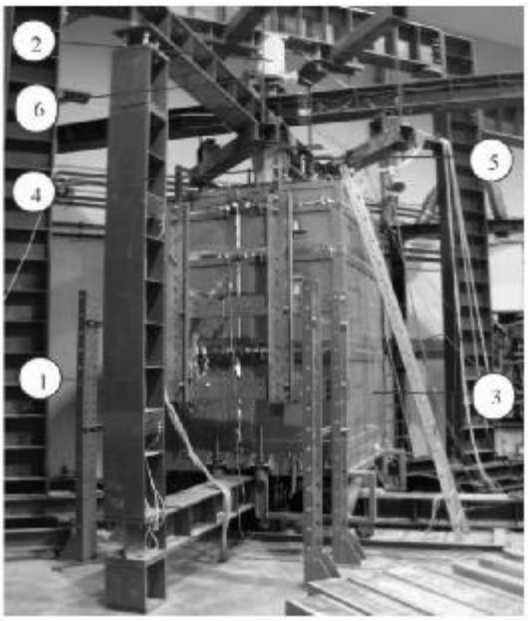

Fig. 2. Test set-up for fire resistance tests on building columns

The columns were subjected to a constant compressive load, during the whole test, of 686 KN. This load was controlled by a load cell of 1 MN, located on the head of the piston of hydraulic jack (6). The applied load corresponded to 70% of the design value of buckling resistance of the column at room temperature. This load was calculated to the reference column C4, through the method of the nominal stiffness, according to EC 2 part 1-1 [3]. Thus, it was pretended to simulate the serviceability load of the column when part of a real structure. The load was applied by an hydraulic jack (2) controlled by a servo hydraulic system.

The thermal action was applied by a modular electric furnace (3) and followed nearly the ISO 834 fire curve [4].

The restraining forces generated in the column due to heating were measured by load cell of 3 MN located into a steel piston (4). This piston was placed between the testing column and the restraining frame, as shown in figure 2.

The axial displacements and rotations on top and base of the column were also measured by displacement transducers (5) orthogonally arranged in three different points, forming a deformation plan.

Besides, as noted, the temperatures in different sections and depths in the cross section of the column and the temperatures of the column were measured.

1.4. Results

Figure 3 presents the furnace temperature during the four tests. The temperature followed nearly the ISO 834 fire curve and was very uniform in the four tests.

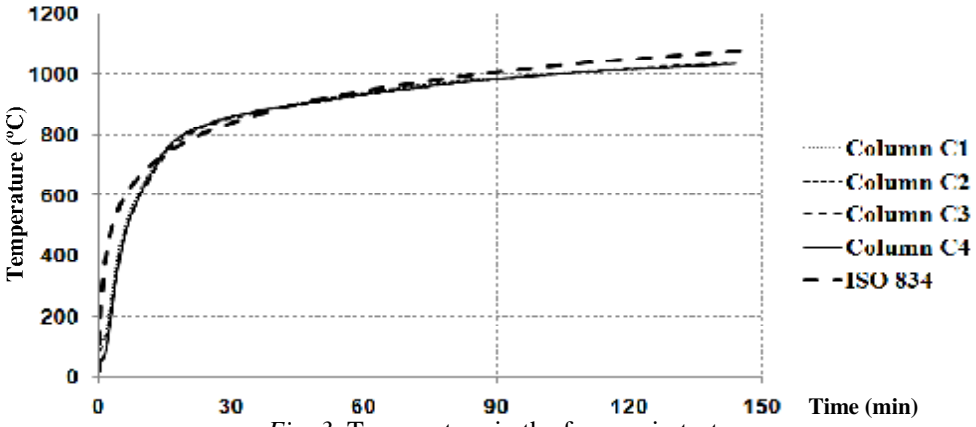

Fig. 3. Temperature in the furnace in tests

Figure 4 shows, as example, the evolution of temperature at different points in section S3 and figure 5 the temperature along the height of column C2.

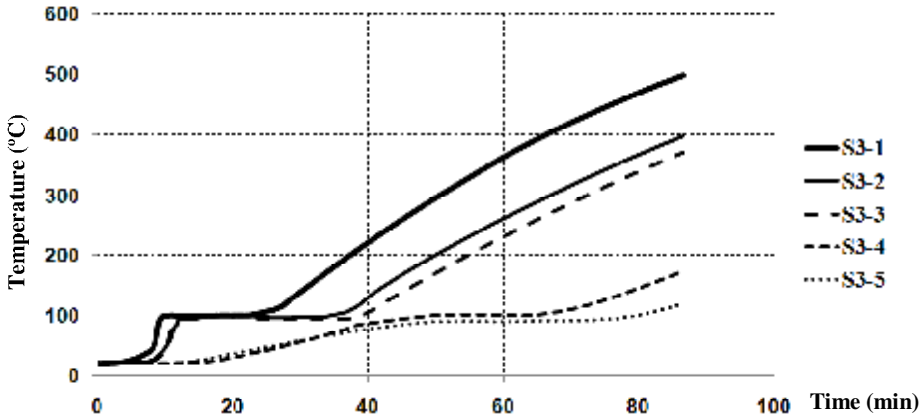

Fig. 4. Evolution of temperature in section S3 of column C2

In figure 4 it can be observed that the temperature remained practically unchanged up to nearly 40 min and then started to increase more in thermocouples near the surface. The temperature in the thermocouples did not exceed 500 ºC while the temperature of the furnace reached around 1100ºC. The difference of temperatures between the surface and inner thermocouples was more than 400ºC, showing a very big thermal gradient along the cross-section of the concrete column. The low thermal conductivity of the concrete associated to the maintenance of the integrity of the element due to the use of pp fibers in the concrete was the responsible for this fact [5].

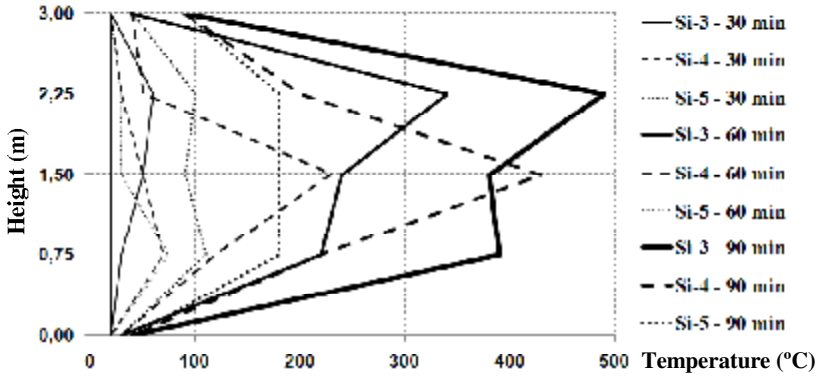

Fig. 5. Evolution of temperature in concrete along the height of the column 2

The thermal gradients in height were also strong and increased throughout time as shown in figure 5.

Figure 6 shows the restraining forces in columns throughout time. In this graph it can be observed that column C1 presented a small increasing in restraining forces. The higher the percentage of steel reinforcement bars the higher was the increasing in restraining forces and the fire resistance. Column C3 with steel reinforcing bars dia. 20 mm and an amount of 16,56 Kg/m^3 of steel fibers presented a development of restraining forces similar to column C4 (reference column). Column C4 had steel reinforcing bars dia. 25 mm and no st fibers.

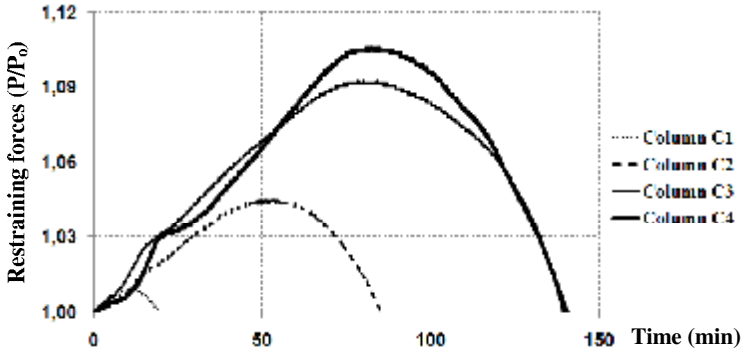

Fig. 6. Restraining forces in columns throughout time

Concerning the displacements and rotations in the ends of the columns (top and bottom) they were very small as expected for a concrete column (Figs. 7 and 8).

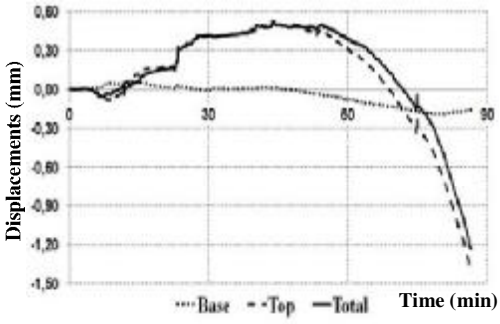

Fig. 7. Axial displacements in column C2

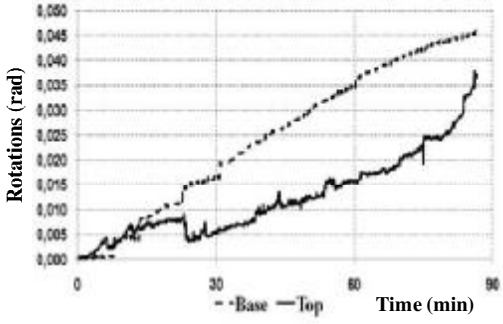

Fig. 8. Rotations in column C2

The columns made of concrete with pp fibers (fig. 9) didn't show any spalling after test in opposition to the reference column C4 (fig. 10) that showed the detachment of big pieces of concrete in the edges of the cross-section and in the more compressed areas of the column.

Fig. 9. Colum C1 after test

Fig. 10. Column C4 after test

2. CONCLUSIONS

As main conclusions of this work, we may see that the use of pp and st fibers in concrete improves the fire behavior of the columns. The pp fibers volatilize and create paths where the water vapour generated inside the concrete can escape, while the steel fibers give the concrete the capacity to resist to the thermal stresses developed in fire.

A day after the test, the reference column showed extensive spalling, exposing the steel reinforcing bars, while the columns with pp and st fibers were not altered. Thus, the use of pp fibers and a small quantity of st fibers in concrete can provide benefits in controlling the spalling of concrete.

The replacement of steel reinforcing bars by steel fibers in big quantity didn't show a significant advantage in the fire behavior of the columns, since the columns that had greater fire resistance were those with steel reinforcing bars with bigger diameter.

REFERENCES

[1.] Kalifa, P., Chéné, G. e Gallé, C. (2001). "High-temperature behaviour of HPC with polypropylene fibres from spalling to microstructure". Cement and Concrete Research. Vol. 31, pp. 1487–1499.

[2.] Cheon-Goo Han, Yin-Seong Hwang, Seong-Hwan Yang & N. Gowripalan (2004). "Performance of spalling resistance of high performance concrete with polypropylene fiber contents and lateral confinement". Science Direct 35 (2005), pp 1747–1753.

[3.] EN 1992-1-1: Design of concrete structures, part 1-1: General rules and rules for buildings, European Committee for Standardization, Brussels, 2004.

[4.] EN 1992-1-2: Design of concrete structures, part1-2: General rules - Structural fire design", European Committee for Standardization, Brussels, 2004.

[5.] Zeiml, M., Leithner, D., Lackner, R. e Mang, H. A. (2006). "How do polypropylene fibers improve the spalling behavior of in-situ concrete?". Cement and Concrete Research, Vol. 36, pp. 929–942.

FIRE RESISTANCE TESTS ON CONCRETE COLUMNS WITH RESTRAINED THERMAL ELONGATION

Alberto Miguel B. Martins [a], João Paulo C. Rodrigues [a]

[a] Department of Civil Engineering, Faculty of Sciences and Technology, University of Coimbra, Portugal

INTRODUCTION

The high temperatures experienced in a fire, lead to thermal elongation of the structural members. However, other parts of the structure may remain at lower temperatures and this will restrain their thermal elongation. The result is to increase stresses in the elements and, if these exceed their buckling resistance the elements will collapse. It is therefore important to analyze the influence of the restraint of the structure on the behaviour of structural elements in the event of fire.

The effect of the boundary conditions on the fire behaviour of reinforced concrete columns has not yet been sufficiently studied [1], [2], [3]. In a recent experimental study [2] it was found that the values of the restraining forces generated were less than 15% of the column's design load. The test models used in this study were small scale, however, (cross-section of 125×125 mm^2 and 1800 mm in height), and were made of high-strength concrete. Thus it cannot be stated with certainty that the results can be extrapolated for larger elements made of other types of concrete.

The Eurocodes allow the use of simplified calculation methods to guarantee that the structures offer appropriate fire resistance, instead of using traditional fire resistance tests. But those methods fail to take account of all the parameters present in real fires in which a structural element may be involved. One parameter not considered is the restraint of the structure according to the thermal elongation of the element.

The main objective of the work described in this paper was to study the fire behaviour of reinforced concrete columns with restrained thermal elongation.

1 EXPERIMENTAL PROGRAMME

Several fire resistance tests were carried out on reinforced concrete columns. The variables studied in the experimental tests were the longitudinal steel reinforcement ratio, the slenderness of the column and the stiffness of the structure surrounding the column.

1.1 Experimental models

The specimens tested were reinforced concrete columns 3000 mm long, with cross-sections of 250×250 mm^2 and 160×160 mm^2, with S355 steel plates measuring 450×450×30 mm at their ends. These plates were used to fix the testing column to the restraining frame in the tests.

The columns were connected to the steel end plates out by welding the longitudinal steel reinforcement bars to the steel plates prior to casting.

Table 1. Characteristics of the columns

Column Reference	Cross-section		Longitudinal Reinforcement		Reinforcement Ratio A_s/A_c [%]
	h × b [mm] × [mm]	Area, A_c [mm^2]	Number and Diameter	Area, A_s [mm^2]	
P16-10-k13	160 × 160	25600	4ϕ10	314.2	1.23
P16-10-k45	160 × 160	25600	4ϕ10	314.2	1.23
P16-16-k13	160 × 160	25600	4ϕ16	804.2	3.14
P16-16-k45	160 × 160	25600	4ϕ16	804.2	3.14
P25-16-k13	250 × 250	62500	4ϕ16	804.2	1.27
P25-16-k45	250 × 250	62500	4ϕ16	804.2	1.27
P25-25-k13	250 × 250	62500	4ϕ25	1963.5	3.14
P25-25-k45	250 × 250	62500	4ϕ25	1963.5	3.14

Table 1 gives the characteristics of the columns tested. In this table the first column indicates the label of each column tested. Thus the label P25-16-k13 indicates that the dimensions of the cross-section are 250 mm×250 mm, the longitudinal steel reinforcement are 16 mm diameter bars and the stiffness of the surrounding structure in the test was 13 kN/mm.

The strength classes of the materials used to make the columns were C20/25 for the concrete and A500 NR for the steel.

1.2 Experimental set-up

This comprised a large number of pieces arranged in a very complex system that is described in the following sections. Figure 1 gives a general view of the experimental set-up.

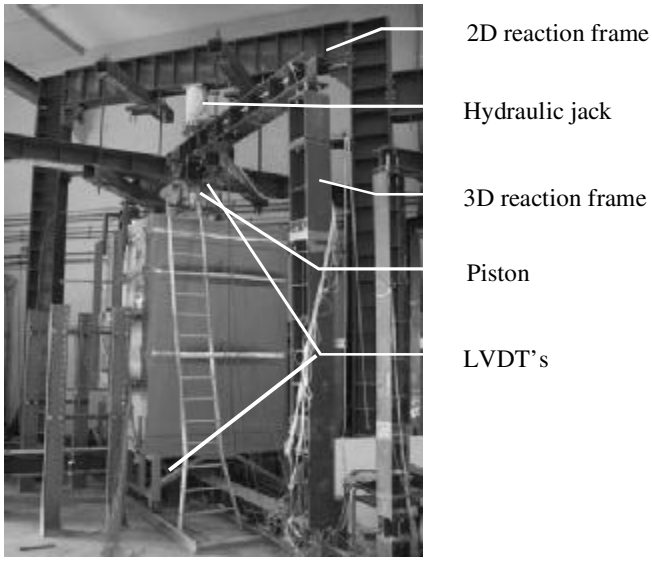

Fig. 1. Experimental set-up

1.3 Boundary conditions

The boundary conditions for the tests were formed by two steel frames: a 2D reaction frame and a 3D reaction frame. This latter frame is hereunder referred to as the "restraining frame".

The 2D reaction frame consisted of two S355 steel HEB500 columns and an HEB600 beam of the same material, connected with bolts M24 class 8.8.

The 3D reaction frame consisted of four HEB300 columns and four HEB 300 beams made of S355 steel, arranged orthogonally. The purpose of this restraining frame was to simulate the effect of the stiffness of the building structure surrounding the column, in a fire. All the elements were connected with bolts M24 class 8.8.

It was possible to change the position of the columns and beams of the 3D restraining frame so that the column being tested could have different stiffness values. Stiffness of 13 kN/mm (*k13*) and 45 kN/mm (*k45*)were tested.

1.4 Mechanical action

The mechanical action imposed on the models was a compression force, applied by a hydraulic jack with 3 MN maximum capacity, fixed in the beam of the 2D reaction frame. The hydraulic jack was controlled by a servo-hydraulic control unit.

This load simulated the serviceability load of the column when part of a real structure. This load was 70% of the value of the column's design load at room temperature, calculated according to EC2-1-1 [4, 5].

1.5 Thermal action

The thermal action on the experimental models was applied by a modular electric furnace with internal dimensions of 1.5m×1.5m×2.5m capable of temperatures up to 1200ºC and fire curves with different heating curves.

In all tests the heating curves applied were close to the standard curve ISO 834.

1.6 Instrumentation and data acquisition

The applied load was recorded by a compression load cell of 1 MN. The load cell was placed on the top of the hydraulic jack.

The restraining forces that developed due to the heating of the column were measured by a load cell of 3 MN placed inside a cylindrical piston made of high stiffness steel.

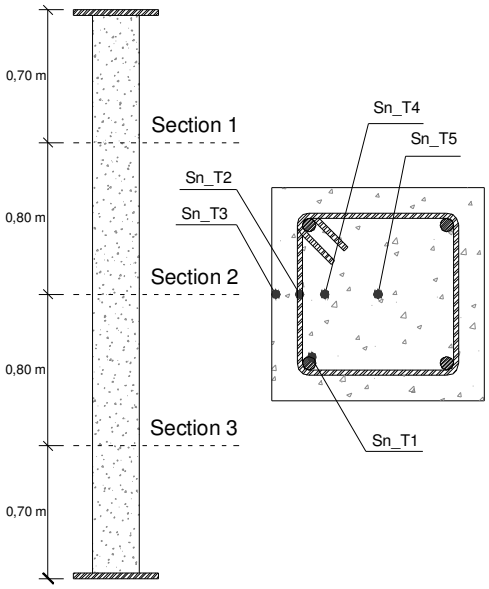

Fig. 2. Location of the thermocouples
(n indicates the section number)

The axial displacements were measured at the top with 3 LVDTs and at the bottom with 4 LVDTs placed orthogonally to form a plane of deformation. The LVDT model used was TML CDP-100.

The temperatures were measured by type K chrome-alumel thermocouples in three sections along the length of the column. Five thermocouples were used in each section, two welded to the steel reinforcement bars and the others embedded in the concrete at various depths (one

nearer the surface Sn_T3, another in the center of section Sn_T5 and the third midway between these two Sn_T4) (Fig. 2).

All parameters were recorded with datalogger model TML TDS-530.

2 TEST RESULTS

2.1 Temperatures

As an example Fig. 3 shows the temperature distribution in the top cross-section S1_Ti of column P25-16-k45 as a function of time. The very high thermal gradients between the inner parts of the concrete and the surface can be seen.

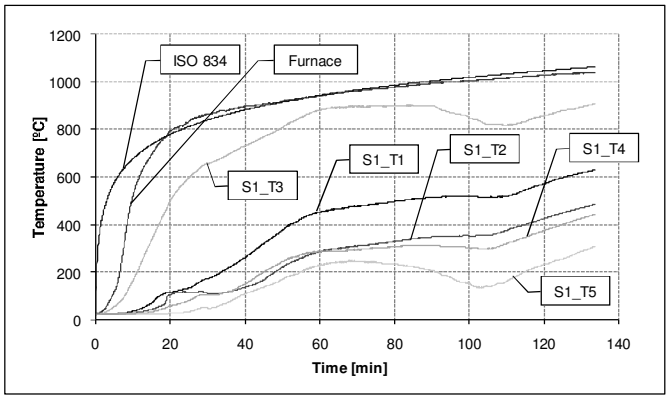

Fig. 3. Temperature in the thermocouples as a function of time (column P25-16-k45)

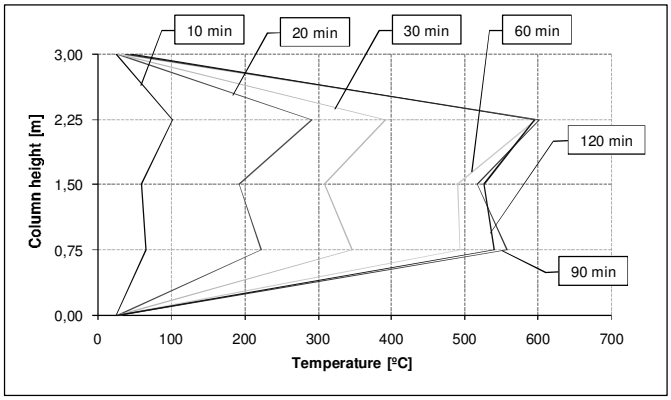

Fig. 4. Thermal gradients in height as a function of fire duration (column P25-16-k45)

Figure 4 shows the thermal gradients vertically in the column, as a function of the heating time. The large thermal gradients registered between the central part of the column and the ends were due to the fact that the ends were protected and not exposed directly to the heating. On the other hand, the graph shows that after 60 min the temperatures in the central part are almost unchanged.

2.2 Restraining forces and fire resistance

Figures 5 and 6 give the graphs for the variation of the restraining forces as a function of time. These graphs show the influence of the longitudinal steel reinforcement ratio and the stiffness of the surrounding structure on the restraining forces and on the fire resistance of the columns

All the results are summarized in Table 2.

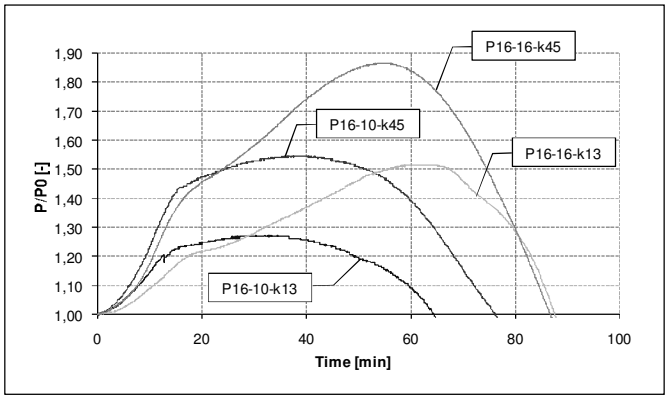

Fig. 5. Restraining forces *versus* time for columns 160×160 mm^2

The increase in the steel reinforcement ratio led to an increase in the fire resistance of 29.9% and 13.4%, for the 160×160 mm^2 columns, and an increase of 5.4% and a reduction of 10.4%, for the 250×250 mm^2 columns, respectively for stiffness *k13* and *k45* of the surrounding structure.

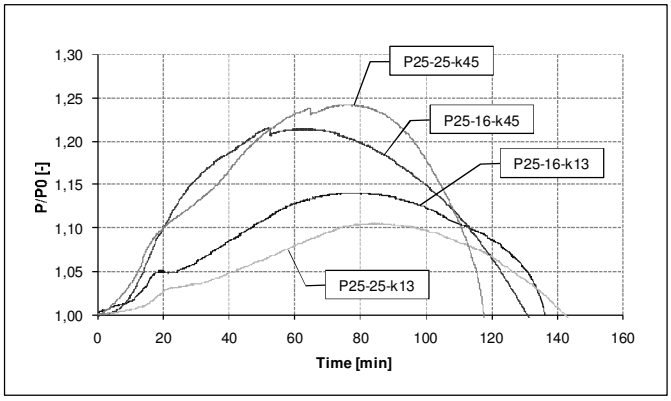

Fig. 6. Restraining forces *versus* time for columns 250×250 mm^2

The increasing of the steel reinforcement ratio led to an increase in the restraining forces of 23.8% for stiffness *k13* and 31.7% for stiffness *k45*, in the 160×160 mm^2 columns, while for the 250×250 mm^2 columns a reduction of 3.3% for stiffness *k13* and an increase of 2.7% for stiffness *k45* was observed. The increased stiffness of the surrounding structure also showed an increase in the restraining forces from 27.4% to 35.4%, for the 160×160 mm^2 columns, and from 7.5% to 13.5% for the 250×250 mm^2 columns, respectively for the smaller and higher steel reinforcement ratio.

Table 2. Experimental results for the restraining forces and fire resistance

Column Reference	P_0 [kN]	P_{rest} [kN]	P_{rest}/P_0 [–]	Fire resistance [min]
P16-10-R1	143.82	39.43	27.4%	64.70
P16-10-R2	152.29	83.52	54.8%	76.58
P16-16-R1	181.06	92.72	51.2%	87.73
P16-16-R2	184.71	159.89	86.6%	86.87
P25-16-R1	494.71	68.85	13.9%	136.22
P25-16-R2	507.40	108.78	21.4%	131.67
P25-25-R1	656.34	69.36	10.6%	143.53
P25-25-R2	675.32	162.81	24.1%	118.02

P_0 – Applied load; P_{rest} – Maximum value of the restraining forces.

3 CONCLUSIONS

The main conclusions of this work are:

- Increasing the longitudinal reinforcement ratio has a beneficial effect on the fire resistance of the columns, but the use of 25 mm diameter bars contradicts this tendency [6];

- Increasing the stiffness of the surrounding structure led to an increase in the generated restraining forces;

- Increasing the slenderness leads to a reduction in the fire resistance, with that reduction being more significant for columns with a smaller longitudinal reinforcement ratio;

- If the thermal restraint is increased a general tendency towards reduction of the fire resistance is observed;

- Spalling occurred in all tests but explosive spalling occurred in just one case;

- Spalling occurred mainly in the compressed zones and at the edges of the columns.

REFERENCES

[1] Benmarce, A., Guenfoud, M., Behaviour of axially restrained high strength concrete columns in fire, *Construction and Building Materials*, article in press, 2005;

[2] Fletcher, I.A., Welch, S., Torero, J.L., Carvel, R.O., Usmani, A., The behaviour of concrete structures in fire, *Thermal Science*, Vol. 11, No. 2, 2007, pp. 37-52

[3] Correia Rodrigues, J.P., Valente, J.C., Cabrita Neves, I., Experimental research on the critical temperature of compressed steel elements with restrained thermal elongation, *Fire Safety Journal*, 35, 2000, pp. 77-98

[4] CEN, Eurocode 2: Design of Concrete Structures – Part 1-1: General rules and rules for buildings, CEN – Comité Européen de Normalisation, Brussels, April 2004;

[5] CEN, Eurocode 2: Design of Concrete Structures – Part 1-2: General rules – Structural Fire Design, CEN – Comité Européen de Normalisation, Brussels, December 2004;

[6] Dotreppe, J.-C., Franssen, J.-M., Bruls, A., Baus, R., Vandevelde, P., Minne, R., van Nieuwenburg, D. and Lambotte, H., Experimental research on the determination of the main parameters affecting the behaviour of reinforced concrete columns under fire conditions, *Magazine of Concrete Research*, 49, No. 179, 1997, pp. 117-127

COMPRESSIVE STRENGTH OF FIBRE REINFORCED CONCRETES

Susana O. Santos [a], João Paulo C. Rodrigues [a], Romildo Toledo[b]

[a] Faculty of Science and Technology of University of Coimbra, Portugal
[b] Federal University of Rio de Janeiro, Department of Civil Engineering, COPPE, Rio de Janeiro, Brazil

INTRODUCTION

During the last 20 years, concrete has been developed to have better performances for normal and extreme actions. The changes made in the composition of the mixtures (reduction of water content, use of superplasticizers, optimization of grain size distribution, use of particles with pozzolanic activity, addition of fibers, etc.) lead to striking improvements in many properties such as strength, reology of fresh concrete, ductility and compactness. The latter yields in most cases a better durability, but it may also lead to a brittle behavior of high-performance concrete (HPC) in fire conditions. Under certain thermal and mechanical stresses, HPC may spall. [1]

Spalling can be defined as the violent or non-violent breaking off of layers or pieces of concrete from the surface of a structural element when it is exposed to high and rapidly rising temperatures, as experienced in fires [2]. It results from two concomitant processes: (i) the thermo-mechanical process associated with the thermal expansion/shrinkage gradients that occur within the element being heated and (ii) the thermo-hydral process that generates high-pressure fields of gas (water vapour and enclosed air) in the porous network [3]

During last year, in Europe, fires occurred in several tunnels which caused loss of lives as well as significant damages in the concrete structure. Some of these tunnels such as the "Channel Tunnel" and "Great Belt Tunnel" were recently built, which shows that spalling phenomenon is not yet completely known in order to be prevented in the construction process.

This paper intended to contribute to the understanding of concrete behavior at high temperatures, and to the characterization of the spalling phenomenon, through the development of concretes with improved fire behavior. Thus, it is presented a Portuguese and a Brazilian study carried out to develop fiber concrete compositions with better fire behavior.

2 EXPERIMENTAL STUDIES

2.1 Portuguese Tests

In the Laboratory of Testing Materials and Structures of the University of Coimbra, studies are being carried out to develop a high-strength concrete (HSC) with improved fire behavior. So, three compositions of concrete were developed, one without fibers, one with steel and polypropylene fibers together and a third one with glass fibers. Compressive strength tests at high temperatures were carried out in cylindrical specimens made from these three different concrete compositions [4].

Concrete compositions

In *Table 1* are presented the three compositions developed. All compositions had cement Portland (CEM) type II 42,5R, superplasticizer (SP) SIKA 3002 HE, limestone filler (LF) and four different aggregates: fine sand (FS) with a fineness modulus of 1.87, coarse aggregate

(CA) with maximum size of 9.5mm and two calcareous crushed stone (CS1 and CS2 with maximum sizes of 12.5 mm and 25 mm, respectively).

Table 1. Concrete compositions (per m^3)

	CEM [kg]	*CS1 [kg]*	*CS2 [kg]*	*CA [kg]*	*FS [kg]*	*LF [kg]*	*W/C*	*SP [%CEM]*	*PF [kg]*	*SF [kg]*	*GF [kg]*
HSC	400	600	321	230	470	200	0.3	2.9	-	-	-
HSCSPF	400	600	321	230	470	200	0.3	11.6	1	70	-
HSCGF	400	600	321	230	470	200	0.3	11.6	-	-	1.5

The compositions differ only in the fiber type, or lack of them. For the first composition (HSC) fibers were not incorporated, in the second there were used steel fibers (SF) DRAMIX RC ZP305 with length of 30 mm, diameter of 0.55 mm, relation length/diameter of 55, tensile strength of 1100MPa, together with polypropylene fibers (PF) DURO-FIBRIL, with diameter of 31 μm and length of 6 mm (HSCSPF); in the third composition were used glass fibers (GF) VIMACRACK, with length of 12 mm and diameter of 14 μm (HSCGF).

In *Table 2* are presented the resistance classes for each concrete composition, obtained through the European Standard EN 206-1 (2000) by the realization of compressive strength tests at room temperature, after 28 days. This table also incorporates the values correspondent to the compression load of $0.7f_{cd}$ applied in the compressive strength tests of concrete at high temperatures.

Table 2. Compressive resistance classes

	f_c (MPa)	*f_{cm} (MPa)*	*f_{ck} (MPa)*	*Resistance Class*	*Compression load ($0.7f_{cd}$) (kN)*
HSC	73.04 72.25 68.69	71.33	63.33	**C50/60**	130.5
HSCSPF	75.79 77.18 75.65	76.21	68.21	**C55/67**	140.6
HSCGF	65.19 57.04 70.23	64.16	56.16	**C45/55**	115.8

The polypropylene fibers, when exposed to high temperatures, form pathways that allow the output of steam, thereby reducing the pressure accumulated in the porous network of the concrete element, while the steel fibers increase the ductility of the concrete, thus allowing a more mechanically and thermally resistant concrete. The aim of include glass fibers in concrete composition was to assess to which point these fibers can replace the polypropylene and steel fibers, taking into account the concrete strength at high temperatures.

Specimens

The specimens were cylinders of 75 mm diameter (∅) and 225 mm height (h), where the ratio h/∅ is 3.

Five thermocouples type K (Cromo-Alumel), with diameter of 0.5 mm, were placed within the specimen and its surface to measure the temperature during high temperatures tests.

The location of thermocouples was defined according to the recommendations of RILEM TC-200 HTC [5].

Test procedure

The test system used is presented in *Fig. 1*, comprising a press machine AMSLER with a capacity of 5 MN (a), a cylindrical furnace with a inner diameter of 90 mm and 300 mm of height and capacity to reach temperatures up to 1200°C (b) and a datalogger TML TDS-601 for data acquisition (force, displacement, and furnace and specimens temperature) (c).

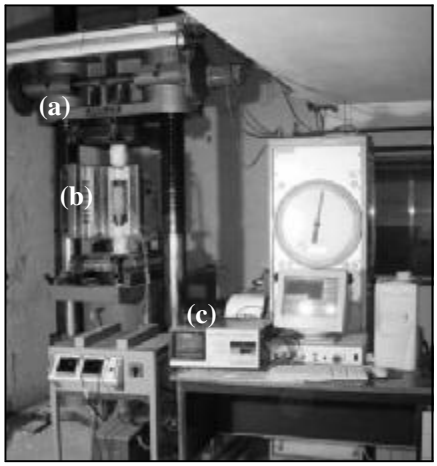

Fig. 1. Test system

The tests procedures were adopted according to the recommendations of the RILEM TC-200 HTC [5]. The specimen was initially loaded with a load equal to 70% of the design value of concrete compressive strength at room temperature ($0{,}7f_{cd}$). When the load level was reached, the specimen was heated at a heating rate of 3ºC/min, until the desired level of temperature. Three levels of maximum temperature were experimented (300°C, 500°C and 600°C). The level of temperature was reached when the average temperatures on the three specimen thermocouples of the surface match the temperature of the furnace. The specimen was then kept at that temperature for an hour to stabilize. The difference of temperatures inside and outside the specimen, given by thermocouples at the same level, was also verified. This difference should not be above 20°C.

Results

In *Fig. 2* is presented a graph with the variation of concrete compressive strength versus the maximum temperature that specimens were subjected in the experimental tests.

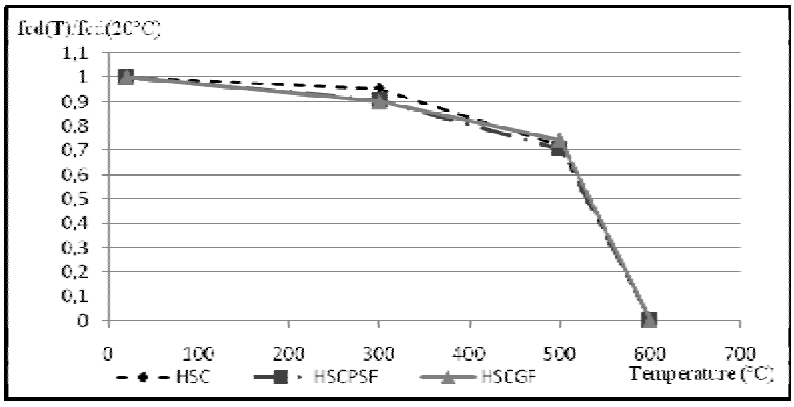

Fig. 2. Concrete compressive strength *vs* maximum temperature.

In tests carried out up to 300 ° C, all specimens had a slight loss of strength. However, the samples of HSC had a smaller loss of strength (5%) that those made of HSCPSF and HSCGF (10%).

In the 500ºC tests, the HSC and HSCPSF specimens lost about 30% of its strength at room temperature while the samples made of HSCGF suffered a strength decrease of approximately 26%.

In the maximum temperature tests, 600ºC, all the specimens collapsed before reaching the stabilization of the temperature.

It was observed a less explosive failure in HSCPSF specimens confirming the effectiveness of steel fibers in obtaining more ductile concrete and control of cracking.

Explosive spalling was not observed in any of the heating-cooling tests, only some cracks. It was verified an aggravation of cracking, for tests up to 500ºC. For this level of temperature, the HSCSPF specimens suffered exfoliation at the top.

In tests for 300ºC, the HSC specimens showed only some surface cracks.

2.2 Brazilian Tests

Tests to assess the stress-strain behavior of polypropylene fiber reinforced high performance concrete exposed to ambient temperature (27ºC) and to temperatures of 400, 650 and 900ºC, were carried out in the Laboratory of Structures of COPPE of the Federal University of Rio de Janeiro [6].

The residual compressive strength and elastic modulus were determined after allowing the samples to cool down to room temperature.

The role of polypropylene fiber to control the spalling of high performance concrete (HPC) was also investigated.

Concrete composition

In specimens composition was used Portland cement (CPIII-40), sand with a fineness modulus of 2.70, crushed syenite with a maximum size of 9.50 mm and a specific weight of 2.70 g/cm^3, naphtalene sulphonate based superplasticizer (SP) with a total amount of solid particles of 40% and silica fume. The polypropylene fibres (PP) were 40 mm long and had a specific weight of 0.91 kg/dm^3 and an elastic modulus value of 3500 MPa.

The mixtures were produced in order to reach compressive strength levels at 28 days of 65 MPa (C65) and 85 MPa (C85). They were reinforced with 0.25% and 0.5% by volume of polypropylene fibers (C65PP0.25/C85PP0.25 and C65PP0.5/C85PP0.5 series, respectively).

The mix proportions of the mixtures are summarized in *Table 3*.

Table 3. Mix proportions for the polypropylene fiber reinforced concrete -HPC (per m^3)

Series	*Cement [kg]*	*Silica [kg]*	*Sand [kg]*	*Agg. [kg]*	*Water [l]*	*SP [l]*	*Fibres [kg]*
C65	365	37	780	857	156	8.30	-
C85	414	42	694	895	151	8.49	-
C65PP0.25	365	37	780	857	156	8.30	2.28
C65PP0.5	365	37	780	857	156	8.30	4.56
C85PP0.25	414	42	694	895	151	8.49	2.28
C85PP0.5	414	42	694	895	151	8.49	4.56

Specimens and test procedure

In the compression tests were used cylindrical specimens with 100 mm x 200 mm. These tests were carried out in a 2500 kN MTS testing machine, at a loading rate of 0.00078mm/s. Three samples were tested for each mixture. Average values were taken as representative for each analyzed mixture.

Prismatic specimens (150 mm x 260 mm x 100 mm) were used in the spalling and total porosity studies. They were heated in a computer-controlled electric furnace at a rate of 10ºC/min. Three maximum temperatures (400ºC, 650ºC and 900ºC) were chosen. After the peak temperature was reached, it was maintained for one hour and then cooled down at a rate of 0.4-0.5ºC/min until room temperature.

Total porosity was measured by means of water absorption tests on cylindrical specimens (60 mm height, with a diameter of 25.4 mm) extracted from the prismatic samples.

Results

Typical compressive stress-strain curves for the HPC matrices and polypropylene fiber reinforced-HPC, at room temperature and after exposure to high temperatures, are presented in *Fig. 3*.

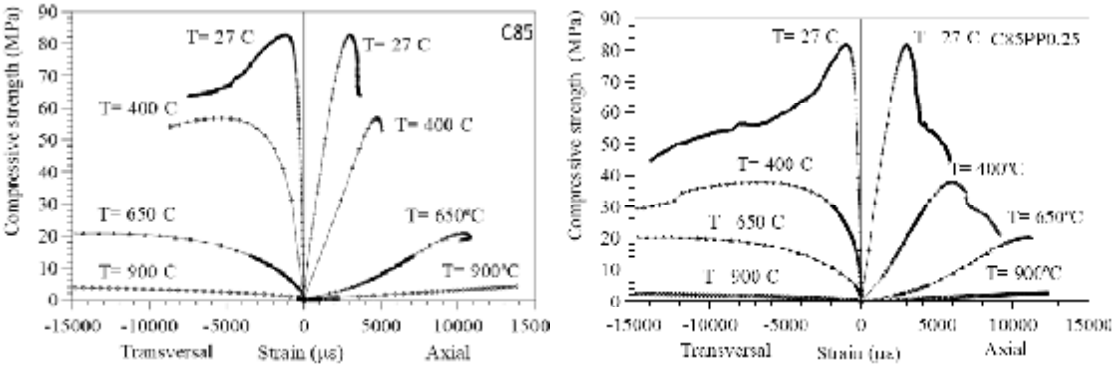

Fig. 3 Compressive stress-strain curves at room temperatures after exposure to high temperatures: (a) Concrete series C85; (b) Composite series C85PP0.25

At room temperature, the addition of small volume fractions of polypropylene fibers did not change significantly the behavior in compression of the matrices.

The results indicate that at the temperature of 400°C, the concrete specimens reinforced with polypropylene fiber show a strength and rigidity loss more pronounced than those observed to the plain HPC mixtures. At higher temperatures (650°C and 900°C) all specimens experienced a similar strength and rigidity loss, independently of the presence of fibers in the mixtures.

The worst behavior of the reinforced concrete specimens is associated with the melting of polypropylene fibers at about 170ºC. During the melting process occurs a slight dilatation of about 10% [3] of the polypropylene generating extra pore-pressure in the concrete leading to a crack density higher than that observed in the plain concrete. The fiber beds led in the matrix after fiber melting can also help in the nucleation of cracks locally as they have sharp angles favoring the distribution of microcraking.

In this study, spalling was observed in prismatic samples of concrete C85 when they were being heated to the temperature of 400ºC. The spalling of the HPC prismatic sample occurred at about 200-220ºC. The addition of 0.25% by volume of polypropylene fibers to the C85 matrix prevented concrete spalling.

3 CONCLUSIONS

In the Portuguese studies, it could be concluded that the inclusion of PP fibers in the concrete compositions avoided spalling. The specimens of concrete with steel and polypropylene fibers had better performance than those with glass fibers. It has been observed a small detachment of concrete surface in the last ones.

In compression tests, it was noticed a more explosive rupture in specimens without fibers as well as those with glass fibers. It was confirmed the benefit of steel fibers in the crack control.

The incorporation of steel fibers with a lower length and a lower amount of polypropylene fibers conferred greater strength to the concrete specimens.

In this study, in compression tests, the glass fibers have an identical behavior to the polypropylene and steel fibers. The loss of strength of HSCGF specimens, at high temperatures, was only slightly lower than the HSC and HSCPSF ones. Thus, it was concluded that glass fibers not had the intended effect, the effect of winning the mechanical and thermal stresses, which are developed in the concrete at high temperatures. However, further studies in this area have to be performed, given the small number of tests performed in this experimental work.

In the Brazilian studies it was concluded that at high temperatures, the concrete specimens reinforced with PP fiber showed a strength and rigidity loss more pronounced than those observed to the plain HPC mixtures. The increase in porosity was also higher for the reinforced specimens. This behavior can be associated with melting of polypropylene fibers at about 170ºC.

In this study, it could also be concluded that the addition of polypropylene fibers to the C85 matrix prevented concrete spalling.

Given these findings, we can state that polypropylene fibers prevent the spalling occurrence. These fibers melt at approximately 170ºC being then partially absorbed by the microcracked cement matrix leaving a pathway for gas, reducing the intensity of the pore pressure.

REFERENCES

[1]Kalifa, P., Menneteau, F. and Quenard D. (1999); “Spalling and pore pressure in HPC at high temperatures”, Cement and Concrete Research, Vol. 30, pp. 1915-1927.
[2]Khoury, G. A. (2000); “Effect of fire on concrete and concrete structures”, Prog. Struct. Engng Mater., Vol 2, pp. 429-447.
[3]Kalifa, P., Chene, G., Galle, C. (2001); “High-temperature behaviour of HPC with polypropylene fibres. From spalling to microstructure.”, Cement and Concrete Research, Vol 31, pp 1487-1499.
[4]Santos, S. and Rodrigues, J. P. (2008); “Spalling on concrete structures”, Proceedings of the National Conference on Structural Concrete, Guimarães, Portugal.
[5]Recommendations of RILEM TC 200-HTC (2005); “Mechanical concrete properties at high temperature – Modeling and applications”. Materials and Structures, V. 38, pp. 913-919.
[6]Velasco, R. V., Toledo, R. D., Fairbairn, E. M. R., Lima, P. R. L. and Neumann, R.; “Spalling and stress-strain behaviour of polypropylene fibre reinforced HPC after exposure to high temperatures”.

NUMERICAL EVALUATION OF LOAD INDUCED THERMAL STRAIN IN RESTRAINT STRUCTURES

Calculation of a tunnel cross section subjected to fire

Ulrich Schneider [a], Martin Schneider [b], Jean-Marc Franssen [c]

[a] Univ. of Techn. Vienna, Karlsplatz 13/206, 1040 Vienna, Austria, ulrich.schneider+e206@tuwien.ac.at
[b] Univ. of Techn. Vienna, Karlsplatz 13/206, 1040 Vienna, Austria, e0527948@student.tuwien.ac.at
[c] Univ. of Liege, 1, Ch. des Chevreuils, 4000, Liège, Belgium, jm.franssen@ulg.ac.be

INTRODUCTION

Calculations to predict the deformation rate and load bearing capacity of concrete structures at high temperatures are often based on material models according to the model of the Eurocode 2 (EC2-Model). In Europe most of the calculations of structures are based on this model. The model is very usable and provides a high level of safety for members under bending and standard fire test conditions. It has not been tested for natural fire conditions which include decreasing temperature conditions.
The load bearing capacity of concrete structures can be optimized with models representing a transient material behaviour. Models which are approximated by transient data are more realistic. The following investigation describes the potential when using a new transient concrete model. This model considers thermal induced strain with external load or internal restraint load during heating up. For this model, a realisation of all components of concrete strain is needed. The concrete behaviour is influenced by transient temperature and load history.
A material model for calculation of siliceous concrete is given in [1]. This new model is based on a Thermal-Induced-Strain-Model (TIS-Model) and is called advanced transient concrete model (ATCM). Transient conditions during the whole calculation routine are taken into account. The transient load and the real temperature development are considered. Generally an ATCM can be used for every type of concrete; only some parameter must be changed. This examination is based on ordinary concrete with siliceous aggregates. Using this model, the finite element analysis (FEA) is applied to the calculation [2].
Both concrete models, EC2-Model and ATCM based on material properties according to TIS-Model (see equation (1)), show a very different behaviour for deformation and restraint stresses during calculation. The influence of load during heating is essential [3]. A cut and cover rectangular-shape reinforced concrete tunnel is calculated with the new model in the followed paper.

1 GENERALS ADVANCED TRANSIENT CONCRETE MODEL

It is generally agreed that the total strain ε_{tot} comprises the following parts:

$$\varepsilon_{tot} = \varepsilon_{el} + \varepsilon_{pl} + \varepsilon_{tr} + \varepsilon_{th} \tag{1}$$

where:

ε_{tot} total strain, ε_{el} elastic strain, ε_{pl} plastic strain, ε_{tr} total transient creep strain, ε_{th} thermal dilatation

It is therefore convenient to write for the pure mechanical strain:

$$\varepsilon_{m} = \varepsilon_{el} + \varepsilon_{pl} + \varepsilon_{tr} = \varepsilon_{tot} - \varepsilon_{th} \tag{2}$$

According to [4], in this case the term ε_m is called „load inducted thermal strain“. It consists of transient creep (transitional thermal creep and drying creep), basic creep and elastic strains. The shrinkage during the first heating is accounted for by the observed thermal strain (load 0%).
Eq. 3 is used to calculate the thermal induced creep strain:

$$\varepsilon_{tr}(T,\alpha) = \frac{\varphi * \sigma(t)}{E(T)} - \varepsilon_{pl}(T,\alpha) - \Delta\varepsilon_{el}(T,\alpha) \text{ with: } \Delta\varepsilon_{el}(T,\alpha) = \varepsilon_{el}(T) - \varepsilon_{el}(T,\alpha) \quad (3)$$

$\varepsilon_{tr}(T,\alpha)$ is called “thermal induced creep strain“ but the definition is different compared to [4]. The pure transient creep will not be calculated numerically within the proposed calculation procedure described above, but the exact extended relationship is given in equation (3).
The φ-function is calculated by the equation (4). It utilizes new parameters, those were obtained by recent scientific results [5, 6] based on ongoing research.

$$\varphi = C_1 * \tanh \gamma_w * (T - 20) + C_2 * \tanh \gamma_0 * (T - T_g) + C_3 \quad (4)$$

with: $C_1 = 2.50$, $C_2 = 0.70$, $C_3 = 0.70$, $\gamma_0 = 7.5*10^{-3}\ C^{-1}$, $T_g = 800°C$ for quarzit concrete [7].

The moisture content of concrete is taken into account using equation (5).

$$\gamma_w = 0.3*10^{-3} * w^{0.5} + 2.2*10^{-3} \text{ with } \gamma_w \le 2.8*10^{-3} \quad (5)$$

It is concluded that the irreversible character of the main material properties must be incorporated in a calculation model to ensure a realistic consideration of the behavior of concrete.

2. CALCULATION OF A TUNNEL CROSS SECTION

2.1 Model of the calculation of a tunnel cross section

In general, calculation methods have two separate arithmetic steps: a thermal and a mechanical analysis. For further information, please see the references [8].

In the following example, a single-bay frame is calculated. It is a model of a tunnel taken from a research project, shown in Figure 1 [9].

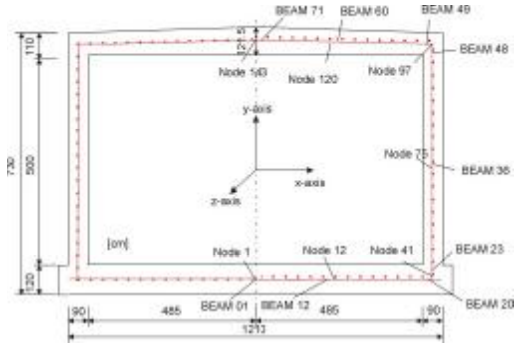

Fig. 1: Principle sketch of the tunnel; according to [9].

The simulation calculates a tunnel cross section with an exposition of a HCI curve. Derived from the Hydrocarbon curve, the maximum temperature of the HCI curve is 1300ºC instead of the 1100ºC, standard HC curve. Such fires may in accidents of tank trucks.

The arithmetic model is based on a section with a width of 1 meter. General calculations utilize the semi-probabilistic concept of the Eurocode 1. The bedding is considered with the help of a spring component under every beam element of the ground plate. The used material is ordinary siliceous concrete C25/30 and steel BSt500. The heating is calculated for transient heating. Before the structure is subjected to fire, the basic combination must be used to determine the amount of reinforcement, which is to be used for comparison purposes during the fire exposure. It is assumed that no spalling occurs during the fire.

2.2 Results of the Calculation of a tunnel cross section

The various displacements demonstrate the whole structure responds during heating. The system's stiffness is changing as a function of time [10]. Most of the deformations show a lower deformation with the ATCM. Only in node 1 the deformation in y-axis is a little bit larger with the ATCM than with the EC2-Model. These results show the effect of the higher load utilisation of the new model. Without considering the load history the influence of the load under temperature exposure is not sufficient reflected in the calculation of deformation of the structure. The figures 2 to 3 show the results of the deformation with the EC2-Model with the maximum value of PSS and with the ATCM.

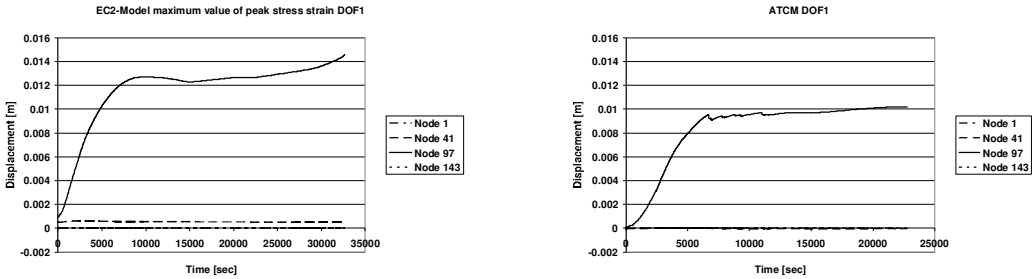

Fig. 2: Displacement in x - axis in various nodes.

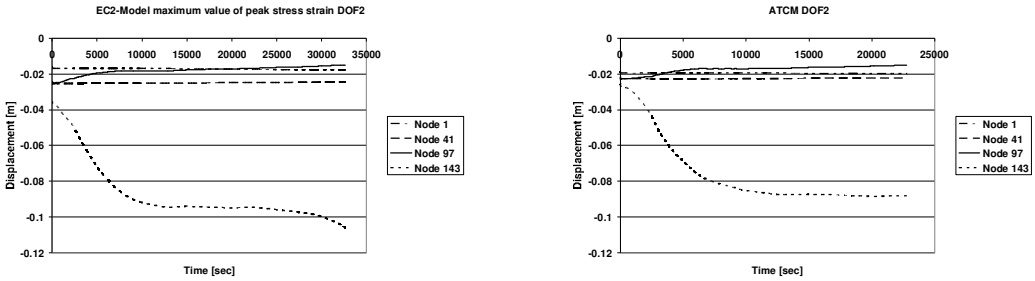

Fig. 3: Displacement in y - axis in various nodes.

The axial forces of the ground plate, the wall and the ceiling are generally higher according to simulations with the EC2-Model compared to the ATCM. Due to the lower deformation in the ATCM lower axial forces occur. An insignificant difference between the two models is seen in the calculation of the bending moment. The positive bending moments are lower with the ATCM than with the EC2-Model. The negative bending moments are higher with the ATCM than with the EC2-Model. The next figures show these mechanical properties of the structure with respect to the axial forces and the bending moments.

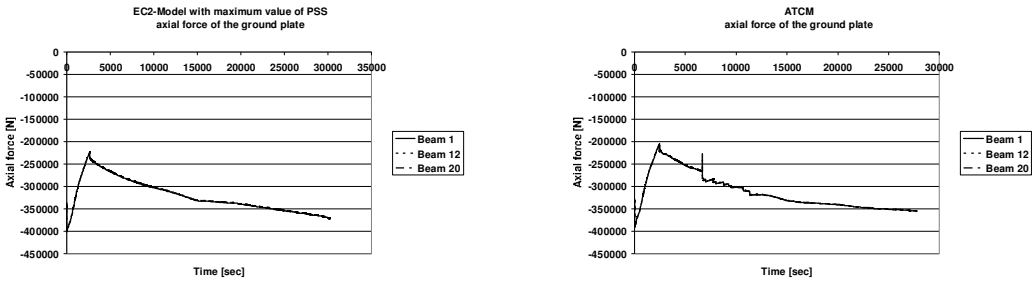

Fig. 4: Axial forces in various beams in the ground plate.

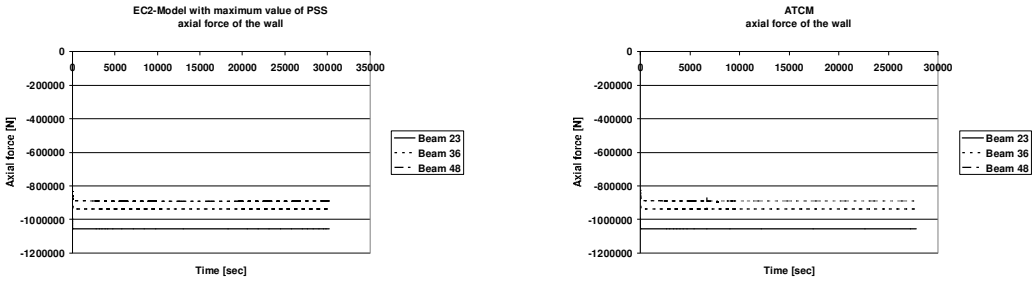

Fig. 5: Axial forces in various beams in the wall.

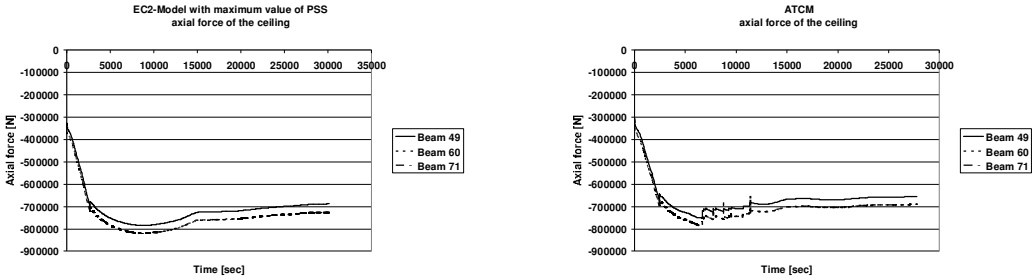

Fig. 6: Axial forces in various beams in the ceiling.

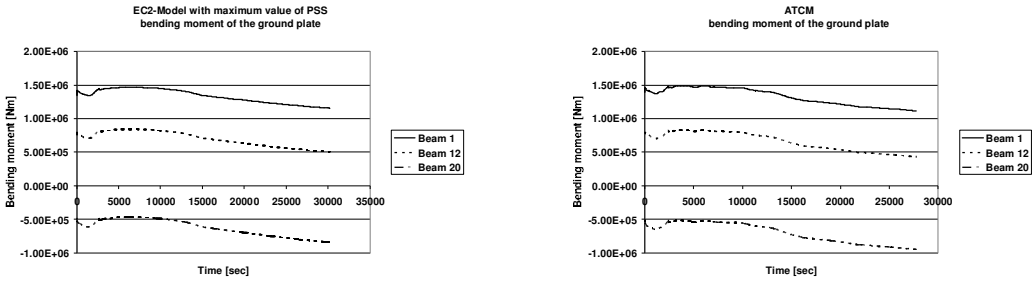

Fig. 7: Bending moments in various beams in the ground plate.

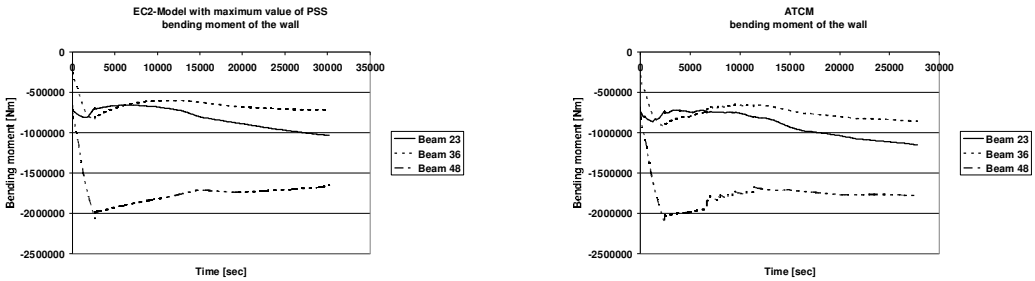

Fig. 8: Bending moments in various beams in the wall.

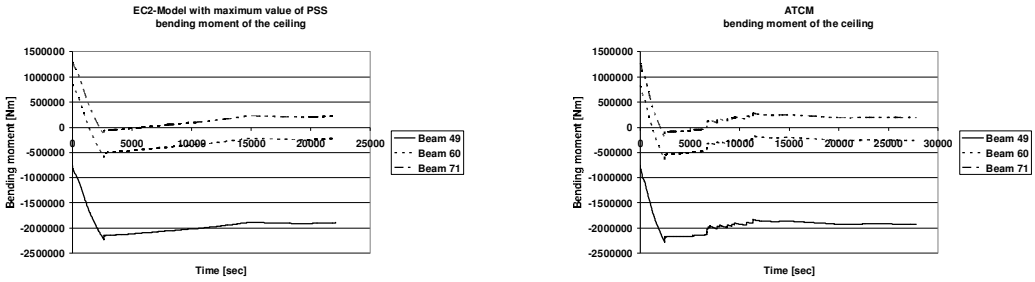

Fig. 9: Bending moments in various beams in the ceiling.

3 DISCUSSION OF THE RESULTS

For the calculation of the load bearing capacity and behaviour of structures subjected to fire, new material equations for the most important material properties of ordinary concrete were developed [1, 4]. This model was developed to complete the existing concrete model of EC2 with respect to the transient thermal creep and the effect of load history. It is possible with this new model to consider the load history in all phases of thermal exposure. With this complex model one can calculate total strain taking into account a wide range of variations of load history and temperatures. Different parts of deformations are approximated with discrete equations interacting in the new concrete model. This technique is usable to calculate realistic behaviour of structures, especially in the case of restraint.

By considering the load history during heating up in several cases an increasing load bearing capacity due to a higher stiffness of concrete may be obtained. With this model it is possible to consider the thermal-physical behaviour of material properties for the calculation of reinforced concrete structures. By applying this model instead of the calculation system of EC2 this will lead to a better evaluation of the safety level. This opens space for optimizing reinforced concrete structures under temperature exposure.

A calculation of a tunnel cross section of cut and cover single bay frame was performed and presented above. Lower deformations are calculated in all parts of the structures using the new advanced transient concrete model (ATCM). Due to this lower deformation a lower axial force during heating occurs.

The results of the calculation of the bending moments show a lower moment at the inside of the tunnel surface and a higher bending moment outside of the tunnel if one compares results of the ATCM with those of EC2-Model. The differences between the calculations are very small. Here we don't observe a significant difference in this structure by using the new model of concrete.

4 CONCLUSION

It is shown that the recommended model of EC2 doesn't calculate realistic values of deformations of concrete structures under high temperature if one compares to the results of an advanced transient concrete model (ATCM) which is based on measured data. A maximum value of peak stress strain is necessary for describing a relatively realistic behaviour of the structure. For calculation of tunnels with concrete with siliceous aggregates the EC2-Model should be taken with the maximum value of the peak stress strain. For calculation a higher load bearing member the ATCM should be applied. Note, only with the TIS-Model with the equations of the ATCM the full concrete behaviour is used in the structure.The calculation with the ATCM has a high potential for optimizing concrete structures, more than the EC2-Model. The reliability of the load bearing capacity is higher with the ATCM because the deformations are lower than with the EC2-Model. The calculated axial forces with the ATCM are close to the EC2-Model.A potential is observed for more detailed calculations of complex structures. In the concept of structures it may be applied with lower safety factors, i.e. lower excess charges may be used in the design.

5. REFERENCES

[1] Schneider, U.; Schneider, M.; Franssen, J.-M.: Consideration of nonlinear creep strain of siliceous concrete on calculation of mechanical strain under transient temperatures as a function of load history. Proceedings of the *Fifth International Conference – Structures in Fire SIF 08, pp. 463-476, Singapore 2008*

[2] Franssen J.-M.,: SAFIR. A Thermal/Structural Program Modelling Structures under Fire, *Engineering Journal, A.I.S.C., Vol. 42, No. 3 (2005), 143-158*

[3] Schneider, U.; Schneider, M.; Franssen, J.-M.: Numerical evaluation of load induced thermal strain in restraint structures compared with an experimental study on reinforced concrete columns, Proceedings of the *11th International Conference and Exhibition, FIRE AND MATERIALS 2009, 26th - 28th January 2009, Fisherman's Wharf, San Francisco, USA*

[4] Khoury, G.A.; Grainger, B.N.; Sullivan, P.J.E.: Transient thermal strain of concrete: Literature review, conditions with specimens and behaviour of individual constituents, *Magazine of Concrete Research Vol. 37 No. 132, 1985*

[5] RILEM TC HTC 200: Mechanical Concrete Properties at High Temperature – Recommendation Part 1: *Mat. & Struct., Vol. 44, Paris, June 2007*

[6] Schneider, U.: Ein Beitrag zur Frage des Kriechens und der Relaxation von Beton unter hohen Temperaturen, *Habilitationsschrift, Institut für Baustoffe, Massivbau und Brandschutz, TU Braunschweig, Heft 42, Braunschweig, 1979*

[7] Schneider, U.; Lebeda, C.; Franssen, J.-M.: Baulicher Brandschutz, *Bauwerk Verlag GmbH, Berlin, 2008*

[8] Franssen, J.-M.: Contributions à la Modélisation des Incendies dans les Bâtiments et leurs Effets sur les Structures, *Université de Liège, Belgium 1998*

[9] Franssen, J.-M.; Hanus, F.; Dotreppe, J.-C.: Numerical Evaluation of the Fire Behaviour of a Concrete Tunnel Integrating the Effects of Spalling in Proceedings *fib Workshop – Ciombra, November 2007*

[10] Schneider, U.; Horvath, J.: Brandschutz – Praxis in Tunnelbauten, *Bauwerk Verlag GmbH, Berlin, 2006*

Application of Structural Fire Engineering, 19-20 February 2009, Prague, Czech Republic

STRUCTURAL SAFETY ASSESSMENT OF TUNNELS SUBJECTED TO FIRE LOADING

Thomas Ring [a], Matthias Zeiml [a], Roman Lackner [b]

[a] *Institute for Mechanics of Materials and Structures, Vienna University of Technology, Karlsplatz 13/202, 1040 Vienna, Austria*
[b] *Material-Technology Unit, University of Innsbruck, Technikerstraße 13, 6020 Innsbruck, Austria*

1 STATE OF THE ART

Tunnel structures have to fulfill requirements as regards their bearing capacity and serviceability before as well as during/after fire accidents. Currently, the determination of the structural safety of tunnels subjected to fire loading is based on the so-called equivalent-temperature concept, assuming linear-elastic material behavior. As illustrated in [1], the equivalent-temperature load is calculated from the real (nonlinear) temperature distribution within a clamped (layered) beam, using the stress-resultants N_{equ} and M_{equ} (see Fig. 1):

$$T_m = \frac{N_{equ}}{\alpha E_{equ} A} \quad \text{and} \quad \Delta T = \frac{M_{equ}}{\alpha E_{equ} I} \,. \tag{1}$$

In Eq. (1) and (2), A [m^2] and I [m^4] are the cross-sectional area and the moment of inertia, respectively, whereas α [K^{-1}] is the thermal expansion coefficient of concrete. E_{equ} [MPa] is the equivalent Young's modulus, given by

$$E_{equ} = \sum_{i=1}^{N} \frac{E_{c,i}(T_i) A_i}{A} \,, \tag{2}$$

where $E_{c,i}(T_i)$ [MPa] and A_i [m^2] are Young's modulus and cross-sectional area of the i-th layer (with N [–] as the number of layers). The parameters T_m [°C], ΔT [°C/m], and E_{equ} serve as input for the linear-elastic analysis.
In this paper, selected results from a structural safety assessment of different tunnel cross-sections under fire are presented. Hereby, the influence of different material models and modes to consider fire loading (equivalent temperature loading or nonlinear temperature distribution) is investigated.

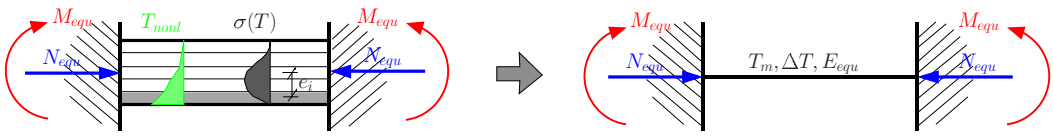

Fig. 1. Model for determination of equivalent temperature loading (T_m and ΔT) [1], giving the same stress resultants N_{equ} and M_{equ}

2 NUMERICAL MODEL

The finite-element analyses are performed using thick (layered) shell elements (see Fig. 2 and [2–4]). The layer concept enables for (i) assignment of different temperatures and, hence, of temperature-dependent material parameters to the respective layers and (ii) consideration of spalling by de-activation of the respective near-surface layers. Concrete and steel are considered by separate layers, the reinforcement bars are transformed into a homogeneous steel layer of

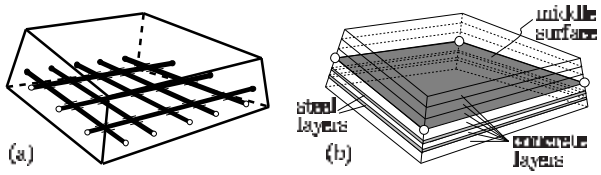

Fig. 2. Illustration of employed layer concept [2–4]: (a) real cross-section, (b) layered finite element

equivalent thickness. As mentioned in [4], a plane-stress plasticity model for concrete is used, whereas the steel reinforcement is simulated by a 1D plasticity model formulated in the direction of the reinforcement bars. The temperature-dependent material parameters are taken from national/international standards [5,6].

3 APPLICATION

3.1 Geometric properties and loading conditions

The numerical model described in the previous section is used to analyze different double-track railway tunnel cross-sections (see Fig. 3). Hereby, the mechanical load consists of the self-weight of the tunnel, earth load with an overburden of 1.50 and 1.75 m, respectively, and the traffic load resulting from a road crossing above the tunnel. The bottom of the tunnel is covered by a gravel layer as rail bedding which is considered to protect this part of the tunnel structure from fire loading. Therefore, temperature loading (representing a fire of stacked car tires) is applied only at the side wall and the top of the tunnel. The duration of the fire load is set to 180 min with an increase of the surface temperature up to 900°C within the first 20 min and a constant surface temperature of 900°C until the end of the fire load (see [1] for details). In addition to fire load, different spalling scenarios are considered, with a final spalling depth d_s^∞ [m] to be reached after 30 min of fire loading (with $d_s^\infty = 0$ m, $d_s^\infty = 0.1$ m, and $d_s^\infty = 0.2$ m,

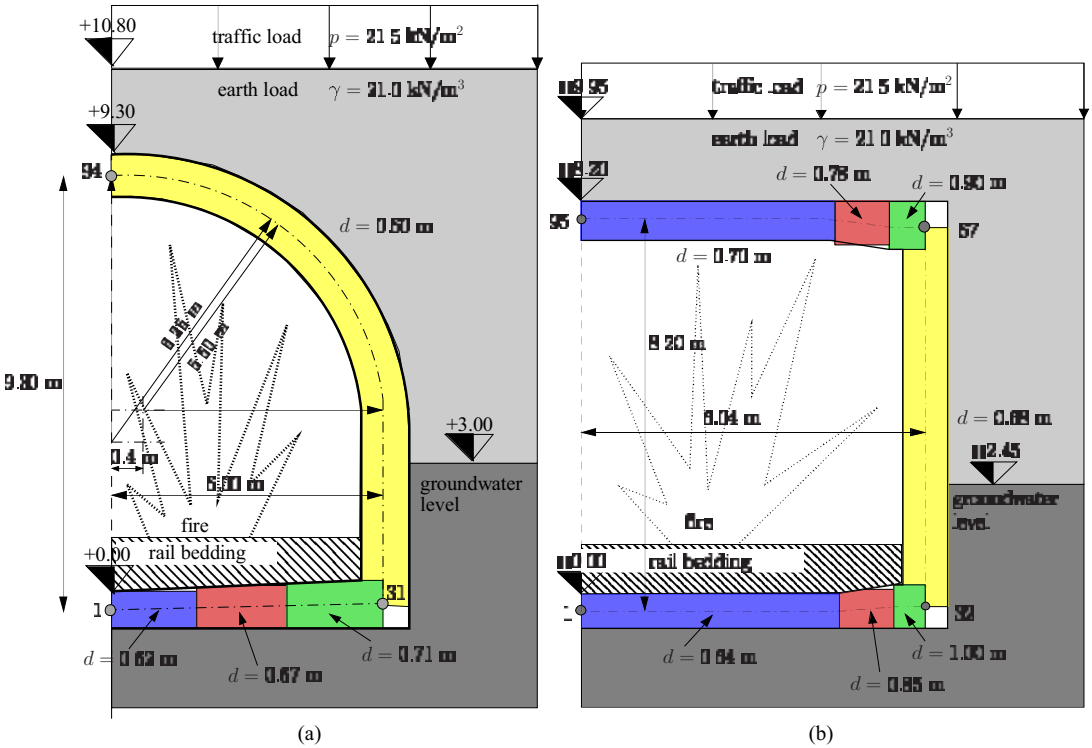

Fig. 3. Investigated concrete structures: (a) circular and (b) rectangular tunnel cross-section

see [3] for details). Furthermore, different material models and modes of temperature loading are employed, i.e.,

- Linear-elastic material behavior and equivalent temperature (LE – T_m, ΔT), and
- Linear-elastic/ideal-plastic material behavior and nonlinear temperature (LE/IP – T_{nonl}).

3.2 Results – circular tunnel cross-section

In the following, representative numerical results are presented. In order to determine whether the reinforcement steel exhibits plastic behavior, the level of loading L [–] is determined at significant sections of the tunnel cross-section (e.g., upper corner, shoulder), with L defined as the ratio between the actual steel stress σ_s [MPa] and the (temperature-dependent) yield strength $f_y(T)$ [MPa]. In case of $L = 0$, the steel reinforcement is unloaded, whereas $L = 1$ indicates that the maximum possible loading is reached. Additionally to L, the bending-moment distribution over the tunnel cross-section is presented for selected time instants (before fire and after 180 min of fire loading). Finally, the relative top displacement v_{rel} [cm] is shown in order to evaluate the compliance of the tunnel.
In Fig. 4, the level of loading of the reinforcement at the shoulder of the tunnel cross-section is presented. Hereby, the consideration of linear-elastic/ideal-plastic material behavior and the nonlinear temperature distribution (LE/IP – T_{nonl}) leads to significantly higher steel stresses. In case of spalling ($d_s^{\infty} = 0.1$ m and 0.2 m), the inner reinforcement layer is lost and, lateron,

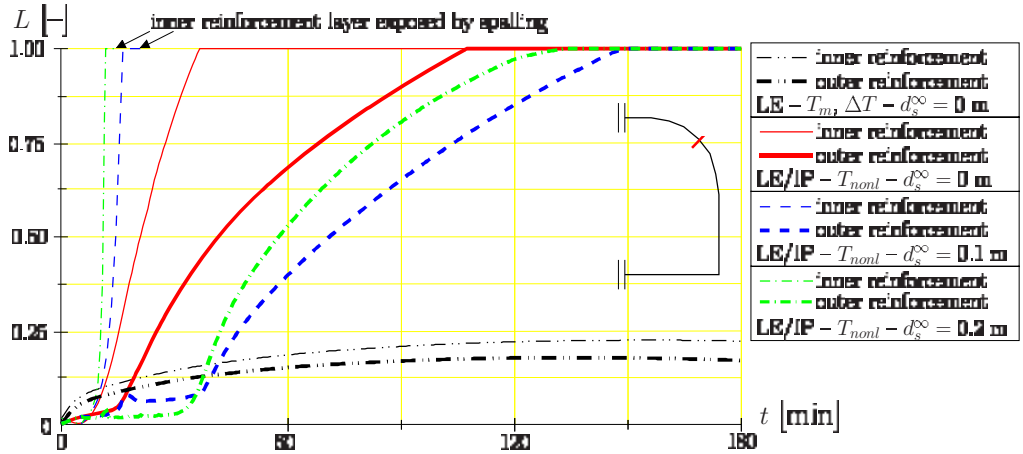

Fig. 4. Circular cross-section – level of loading of reinforcement at the tunnel shoulder for different material models and spalling scenarios

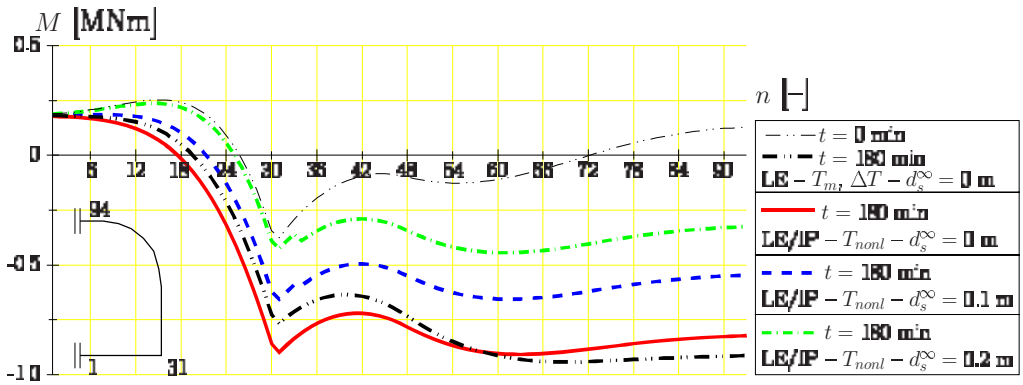

Fig. 5. Circular cross-section – distribution of bending moment for different material models and spalling scenarios before ($t = 0$ min) and after 180 min of fire loading

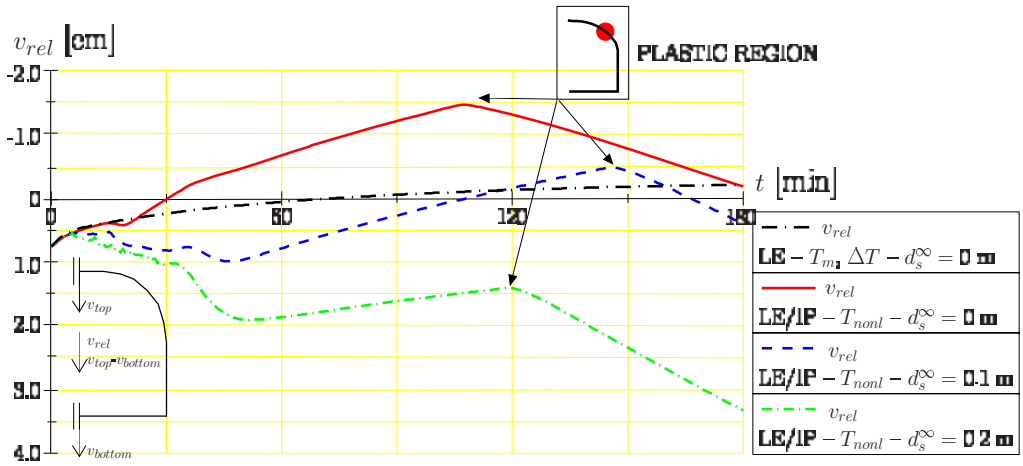

Fig. 6. Circular cross-section – vertical convergence for different material models and spalling scenarios

the outer reinforcement experiences plastic deformations.

The bending-moment distributions (see Fig. 5) indicate a significant increase of the bending moment at the fire-exposed regions. The differences between cases LE – T_m, ΔT and LE/IP – T_{nonl} are small (see results for $d_s^\infty = 0$ m). In case of LE/IP – T_{nonl}, however, the redistribution of forces in consequence of changing stiffness from the fire-exposed towards the unexposed parts of the cross-section (lower corner and bottom) can be observed. In general, the reduction of the cross-section in consequence of spalling resulted in a reduction of the bending moments.

The history of the vertical convergence of the tunnel cross-section is presented in Fig. 6. In case of the analysis using a linear-elastic material behavior and the equivalent temperature distribution (LE/IP – T_m, ΔT), a continuous decrease of convergence in consequence of heating of the cross-section is observed. In case of LE/IP – T_{nonl}, the upward deformation of the cross-section is even more pronounced. After about 105 min of fire loading, a plastic hinge is formed, leading to a continuous increase of deformations. The development of this plastic hinge was already indicated in Fig. 4, where both the inner and the outer steel layer exhibits $L = 1$ after 105 min of fire loading. Consideration of spalling leads to an increase of the compliance and, thus, of the downward motion of the top of the tunnel.

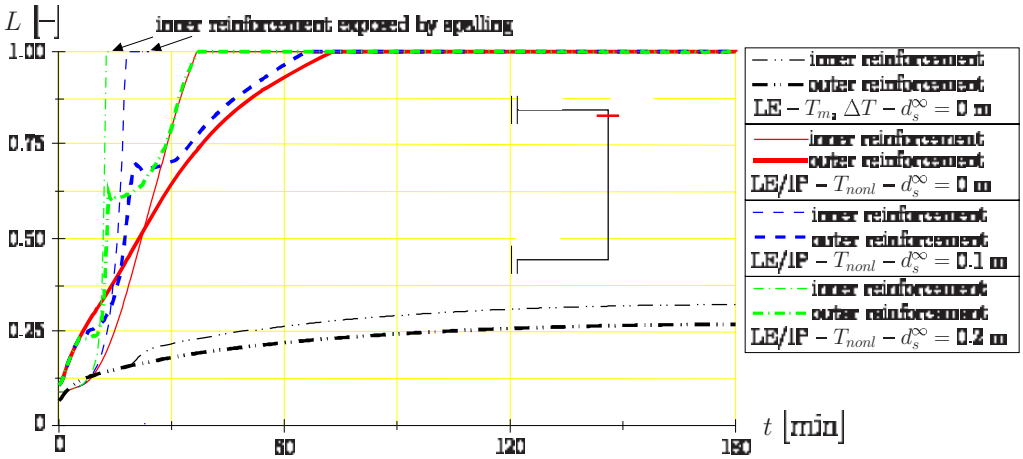

Fig. 7. Rectangular cross-section – level of loading of reinforcement at the upper corner for different material models and spalling scenarios

3.3 Results – rectangular tunnel cross-section

Fig. 7 depicts the level of loading of the reinforcement in the upper corner of a rectangular cross-section. Similar to the case of the circular cross-section, the analysis characterized by LE/IP – T_{nonl} leads to significantly higher stresses (compare with LE – T_m, ΔT for $d_s^{\infty} = 0$ m). The stresses, however, increase faster and plastic deformations occur earlier than in case of the circular cross-section. When spalling is considered, the inner steel layer is deactivated at a certain time instant and plastic deformations of the outer reinforcement occur even earlier as in case of no spalling.

The bending moment depicted in Fig. 8 indicates a shift of loading from the fire-exposed upper tunnel corner to the bottom corner when plastic deformation and the nonlinear temperature distribution are considered (compare with LE – T_m, ΔT for $d_s^{\infty} = 0$ m). Again, spalling leads to a reduction of the bending moment, explained by the reduced cross-sections inducing smaller thermal constraints.

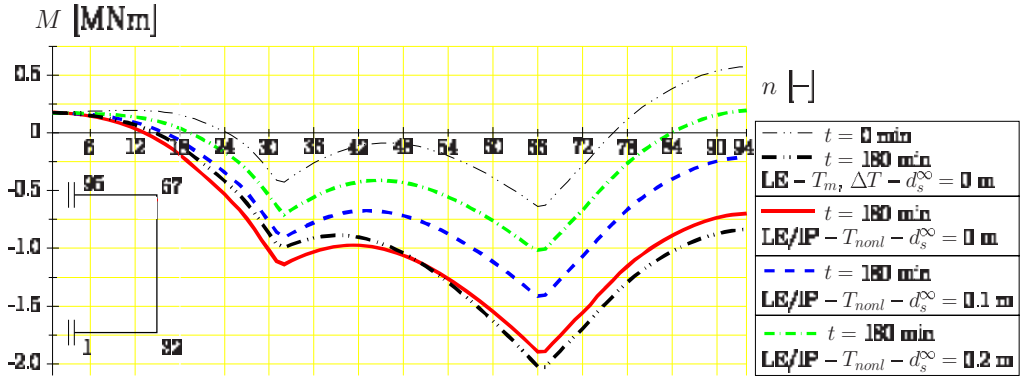

Fig. 8. Rectangular cross-section – distribution of bending moment for different material models and spalling scenarios before ($t = 0$ min) and after 180 min of fire loading

The vertical convergence of the tunnel (see Fig. 9) illustrates the influence of the underlying material model on the compliance of the tunnel lining (compare cases LE – T_m, ΔT and LE/IP – T_{nonl} for $d_s^{\infty} = 0$ m with increased deformations in the latter case). Comparison of the results of the two considered cross-sections for LE/IP – T_{nonl} and $d_s^{\infty} = 0$ m (Fig. 6 and 9) shows a higher structural safety of the circular cross-section. This difference is more pronounced in case of spalling. For $d_s^{\infty} = 0.2$ m, the increase in deformations of the rectangular cross-section is

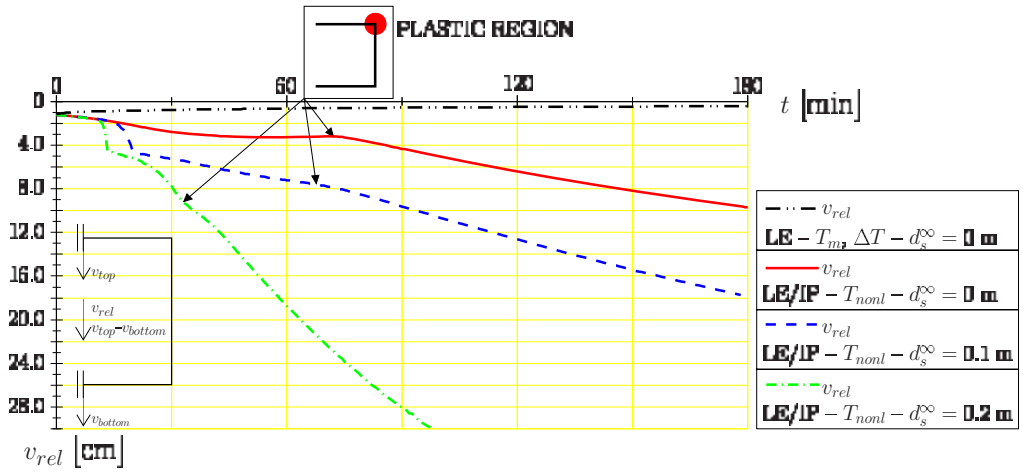

Fig. 9. Rectangular cross-section – vertical convergence for different material models and spalling scenarios

significantly higher as for $d_s^{\infty} = 0$ m and 0.1 m (see Fig. 9) because of a positive bending moment in the tunnel ceiling (see Fig. 8) and deactivation of the inner reinforcement in consequence of spalling. However, collapse of the tunnel is not observed (even for $d_s^{\infty} = 0.2$ m) which would result in a sudden and steep increase of deformation. Moreover, collapse would require the development of a second plastic hinge.

4 CONCLUSIONS

As illustrated by results for different tunnel cross-sections, the structural safety of tunnels subjected to fire loading strongly depends on the considered material model and whether spalling is taken into account. In contrast to the state-of-the-art analysis mode, characterized by linear-elastic material behavior and the so-called equivalent temperature loading, the application of linear-elastic/ideal-plastic material models and consideration of the real (nonlinear) temperature distribution leads to force redistribution within the tunnel cross-section. For the investigated cross-sections and loading conditions, however, the difference in stress resultants (e.g., bending moment) is small. The level of loading of the steel reinforcement, on the other hand, reveals large differences between the two different modes of analysis. A realistic prediction of plastic deformations within the reinforcement requires consideration of linear-elastic/ideal-plastic material behavior allowing the formation of plastic hinges and, hence, the realistic determination of tunnel deformations.
The geometric properties of the tunnel cross-section have a significant influence on the sensitivity of the structure to fire loading. The analyses showed that the rectangular cross-section is more sensitive to fire loading than the circular cross-section because of the more efficient geometry of the latter. Consideration of spalling leads to an increase of the compliance of the lining, with the rectangular cross-section again being more sensitive.
Ongoing research focuses on the improvement of the employed material model, considering the influence of combined thermal and mechanical loading on the strain behavior of heated concrete, giving numerical results in better agreement to reality.

REFERENCES

[1] W. Kusterle, W. Lindlbauer, G. Hampejs, A. Heel, P.-F. Donauer, M. Zeiml, W. Brunnsteiner, R. Dietze, W. Hermann, H. Viechtbauer, M. Schreiner, R. Vierthaler, H. Stadlober, H. Winter, J. Lemmerer, E. Kammeringer, Brandbeständigkeit von Faser-, Stahl- und Spannbeton [Fire resistance of fiber-reinforced, reinforced, and prestressed concrete], Tech. Rep. 544, Bundesministerium für Verkehr, Innovation und Technologie, Vienna, in German. (2004).

[2] K. Savov, R. Lackner, H. A. Mang, Stability assessment of shallow tunnels subjected to fire load, Fire Safety Journal 40 (2005) 745–763.

[3] M. Zeiml, R. Lackner, F. Pesavento, B. A. Schrefler, Thermo-hydro-chemical couplings considered in safety assessment of shallow tunnels subjected to fire load, Fire Safety Journal 43 (2) (2008) 83–95.

[4] T. Ring, Finite element analysis of concrete structures subjected to fire load considering different element types and material models, Master's thesis, Vienna University of Technology, Vienna, Austria (2008).

[5] CEB, Fire Design of Concrete Structures, Bulletin d'Information 208, CEB, Lausanne, Switzerland (1991).

[6] ÖNORM EN1992-1-2, Eurocode 2 – Bemessung und Konstruktion von Stahlbeton- und Spannbetontragwerken – Teil 1-2: Allgemeine Regeln – Tragwerksbemessung für den Brandfall [Eurocode 2 – Design of concrete structures – Part 1-2: General rules – Structural fire design], European Committee for Standardization (CEN), in German (2007).

A NUMERICAL MODEL FOR PREDICTION OF SPALLING OF CONCRETE EXPOSED TO ELEVATED TEMPERATURES

Honglin Zhang[a], Colin T. Davie[a], Chris J. Pearce[b] and Nenad Bićanić[b]

[a] School of Civil Engineering and Geosciences, Newcastle University, Newcastle upon Tyne, UK
[b] Department of Civil Engineering, University of Glasgow, Glasgow, UK

1 INTRODUCTION

When concrete structures are exposed to elevated temperatures, extremely complex phenomena, such as dehydration of cement paste, evaporation of water in pores and restrained thermal expansion of the structures will occur, which result in build-up of pore pressure and thermally induced stresses inside the structures. If high enough, pore pressure or thermally induced stresses could lead to spalling of the structures, i.e., the fracturing and loss of material from the surface of concrete elements. The increase in temperature will also cause decrease in strength and stiffness of concrete, further facilitating the occurrence of spalling.

In the last few decades, extensive experiments have been performed to gain a better understanding of the spalling mechanism [1-3]. Meanwhile, several numerical models were presented for simulation of the complex phenomena at different levels of simplification [4-9]. The past research suggests that spalling is influenced by a combination of heating rate, section shape and size, moisture content, permeability and restraint of concrete structure. However, as for the driving force of spalling, there still exists controversy. Some researchers state that pore pressure is the most importance factor, some emphasise the significance of thermally induced stresses, while others believe spalling is caused by the combination of these two factors.

In this paper, taking a one-dimensional and a two dimensional benchmark problem as examples, the significance of pore pressure and thermally induced stresses for spalling of concrete with different permeability and moisture content is investigated using a finite element method solution procedure, which can capture the coupled hygro-thermo-mechanical behaviour of concrete exposed to elevated temperatures.

2 MATHEMATICAL MODELLING

In the mathematical formulation, concrete is treated as a multiphase system consisting of solid, liquid and gas phases. The solid skeleton is assumed to undertake isotropic elastic-damage deformations under mechanical and thermal loadings. The liquid phase is considered to include adsorbed water and the gas phase to be a mixture of dry air and water vapour, both of which are assumed to behave as ideal gases. The material parametric relationships are given based on the work conducted by previous researchers. The complete description of the mathematical formulation was given in [10]. Here, only governing equations, mechanical constitutive equation and damage model were briefly described in the following.

The model is composed of four governing equations, defining the conservations of mass of dry air, mass of moisture, energy and momentum Eqs. (1) - (4).

$$\frac{\partial(\varepsilon_G \tilde{\rho}_A)}{\partial t} = -\nabla \cdot \mathbf{J}_A \tag{1}$$

$$\frac{\partial(\varepsilon_G \tilde{\rho}_V)}{\partial t} + \frac{\partial(\varepsilon_L \rho_L)}{\partial t} - \frac{\partial(\varepsilon_D \rho_L)}{\partial t} = -\nabla \cdot (\mathbf{J}_V + \mathbf{J}_L) \tag{2}$$

$$\underline{(\rho C)}\frac{\partial T}{\partial t} - \lambda_E \frac{\partial(\varepsilon_L \rho_L)}{\partial t} + (\lambda_D + \lambda_E)\frac{\partial(\varepsilon_D \rho_L)}{\partial t} = \nabla \cdot (k \nabla T) + \lambda_E \nabla \cdot \mathbf{J}_L \tag{3}$$

$$\nabla \cdot (\boldsymbol{\sigma}' - P_{Pore}\mathbf{I}) + \mathbf{b} = 0 \tag{4}$$

Mechanical strains are developed by way of an isotropic damage model, which accounts for the loss of the elastic stiffness that is caused by the micro-fracturing of concrete that develops under loading and under heating. The classical mechanical damage formulation is modified to include a second thermal damage parameter in a multiplicative form Eq. (5).

$$\boldsymbol{\sigma} = (1-\omega)(1-\chi)\mathbf{E_0} : \boldsymbol{\varepsilon}^{\mathrm{e}} = \mathbf{E}_{\mathrm{sec}} : \boldsymbol{\varepsilon}^{\mathrm{e}} \tag{5}$$

The mechanical damage parameter, ω, is defined by the temperature dependent function shown in Eq. (6)

$$\omega = 1 - \frac{\kappa_0^{md}(T)}{\kappa^{md}} \mathrm{e}^{-\gamma(T)\left(\kappa^{md} - \kappa_0^{md}(T)\right)} \tag{6}$$

where, K_0^{md}, which defines the onset of fracturing, is a function of the tensile strength, $f_t(T)$, and elastic modulus, $E(T)$.

$$\kappa_0^{md} = \frac{f_t(T)}{E(T)} \tag{7}$$

The thermal damage parameter is defined by the temperature dependent function shown in Eq. (8), which is derived from the degradation of the elastic modulus that results from increased temperatures, $E(T)$.

$$\chi = 0.2\theta - 0.01\theta^2 \tag{8}$$

3 NUMERICAL PROCEDURE

Employing the Galerkin weighted residual method and application of the divergence theorem the weak form of the governing equations (1) - (4) is obtained and may be expressed in matrix-vector form as (9).

$$\mathbf{C}\dot{\mathbf{x}} + \mathbf{K}\mathbf{x} = \mathbf{f}^{ext} \tag{9}$$

where, the coefficient matrices, **C** & **K**, and the array of nodal variables, **x**, are given below for the chosen set of primary variables (10).

$$\mathbf{C} = \begin{bmatrix} 0 & 0 & 0 & 0 \\ 0 & \mathbf{C}_{TT} & \mathbf{C}_{TP} & \mathbf{C}_{TV} \\ 0 & \mathbf{C}_{AT} & \mathbf{C}_{AP} & \mathbf{C}_{AV} \\ 0 & \mathbf{C}_{MT} & \mathbf{C}_{MP} & \mathbf{C}_{MV} \end{bmatrix}; \quad \mathbf{K} = \begin{bmatrix} \mathbf{K}_{uu} & \mathbf{K}_{uT} & \mathbf{K}_{uP} & \mathbf{K}_{uV} \\ 0 & \mathbf{K}_{TT} & \mathbf{K}_{TP} & \mathbf{K}_{TV} \\ 0 & \mathbf{K}_{AT} & \mathbf{K}_{AP} & \mathbf{K}_{AV} \\ 0 & \mathbf{K}_{MT} & \mathbf{K}_{MP} & \mathbf{K}_{MV} \end{bmatrix}; \quad \mathbf{x} = \begin{Bmatrix} \mathbf{u} \\ \mathbf{T} \\ \mathbf{P}_G \\ \boldsymbol{\rho}_V \end{Bmatrix} \tag{10}$$

The governing equations are discretised using the standard finite element approximation and the chosen primary variables of displacements, u, temperature, T, gas pressure, P_G, and vapour content, $\tilde{\rho}_V$, are expressed in terms of their nodal quantities Eq. (11).

$$u = \mathbf{N}_u \mathbf{u}; \quad T = \mathbf{N}_T \mathbf{T}; \quad P_G = \mathbf{N}_P \mathbf{P}_G; \quad \tilde{\rho}_V = \mathbf{N}_\rho \boldsymbol{\rho}_V \tag{11}$$

The formulation is completed with the following boundary conditions. Transfer of heat across the boundary is described by Eq. (12).

$$\frac{\partial T}{\partial n} = \frac{h_{qr}}{k}(T_\infty - T) \tag{12}$$

Transfer of water vapour across the boundary is described by Eq. (13).

$$\frac{\partial \tilde{\rho}_V}{\partial n} = -\frac{K_{VT}}{K_{VV}}\frac{h_{qr}}{k}(T_\infty - T) + \frac{\beta}{K_{VV}}\left(\tilde{\rho}_{V,\infty} - \tilde{\rho}_V\right) \tag{13}$$

Finally, the gas pressure on the boundary is given by Eq. (14).

$$P_G = P_{G,\infty} \tag{14}$$

4 ONE-DIMENSIONAL PROBLEM

The significance of pore pressure for the development of spalling can be investigated by application of the model to the analysis of the one-dimensional problem as shown in Fig. 1, which may be considered as a simplified representation of a concrete wall exposed to fire from one side. One (left) side is constraint-free and heated by the standard ISO834 fire, far-field temperature of which can be expressed as Eq. (15).

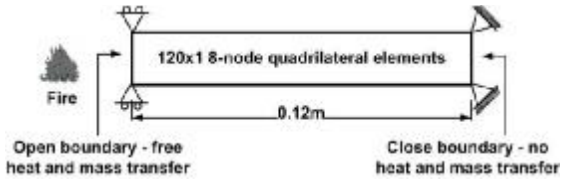

Fig. 1 Schematic diagram of the 1D problem

$$T_\infty = 20 + 345\log_{10}(8t + 1) + 273.15 \tag{15}$$

In the simulation, the initial internal temperature, gas pressure and porosity of the concrete are 293K, 0.1MPa and 12.2%. Initial Young's modulus, tensile strength and Poisson's ratio are 30GPa, 3MPa and 0.2, respectively. As the magnitude of gas pressure built-up in concrete during heating is significantly affected by the permeability and moisture content of the concrete, different levels of initial permeabilities in combination with different levels of initial relative humidities were used in the analysis.

Fig. 2 gives distributions of mechanical damage and gas pressure at different times for an initial permeability of $1\text{x}10^{-17}\text{m}^2$ and a relative humidity of 10%. The occurrence of mechanical damage starts from the surface after about 1200s, developing towards the inside. The maximum built-up gas pressure, as seen in the figure, is much lower than the tensile strength of concrete. Moreover, the advancement of the damage zone front falls behind the advancement of the peaks of gas pressure. Therefore, the development of damage is not due to the build-up and transport of pore pressure. Rather, it is mainly caused by the degradation of the elastic modulus due to high temperature, which results in high strains.

Fig. 3 gives distributions of mechanical damage and gas pressure for an initial permeability of $1\text{x}10^{-19}\text{m}^2$ and a relative humidity of 65%. As compared to Fig. 2, the occurrence of mechanical damage starts earlier (i.e., at about 800s), with the higher maximum built-up gas pressure reaching as high as 2.3MPa. This indicates that pore pressure accelerates the occurrence of damage.

Similarly, Fig. 4 shows distributions of mechanical damage and gas pressure for an initial permeability of $5\text{x}10^{-21}\text{m}^2$ and a relative humidity of 90%. As can be seen, the maximum pressures are higher than 3.2MPa, and the advancement of the damage zone front is almost synchronous with that of the peak of gas pressure. It should also be noticed that mechanical damage does not start from the surface as in the previous cases, but a few centimetres beneath the surface.

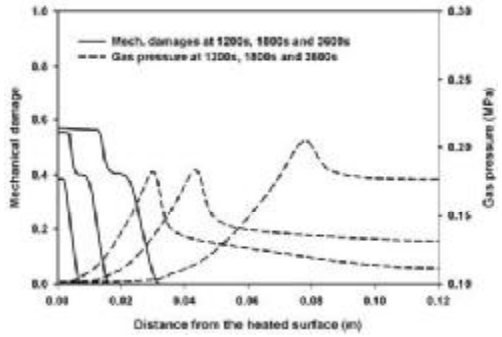

Fig. 2 Distributions of mech. damage and gas pressure. Perm. = $1x10^{-17}m^2$; R.H. = 10%

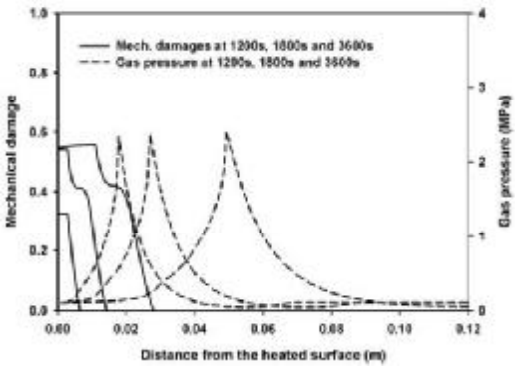

Fig. 3 Distributions of mech. damage and gas pressure. Perm. = $1x10^{-19}m^2$; R.H. = 65%

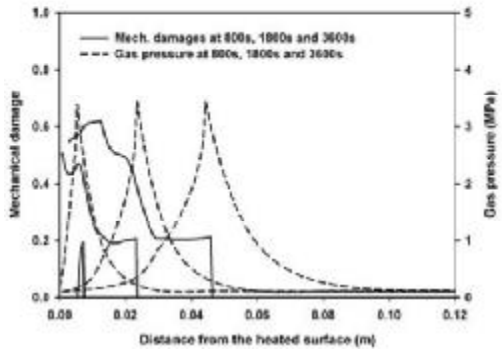

Fig. 4 Distributions of mech. damage and gas pressure. Perm. = $5x10^{-21}m^2$; R.H. = 90%

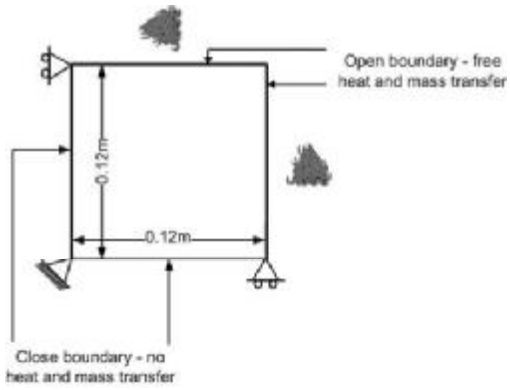

Fig. 5 Schematic diagram for the 2D problem

5 TWO-DIMENSIONAL PROBLEM

The significance of thermally induced stresses, in addition to the presence of pore pressures, is now investigated by application of the model to the analysis of the two-dimensional problem as shown in Fig. 5. This problem may be considered a simplified representation (in quarter symmetry) of a cross-section through a concrete column exposed to fire on all sides. Similarly to the one-dimensional problem, the top and right-hand sides of the concrete column are heated by the standard ISO834 fire while the other two sides are isolated. Unless explicitly stated otherwise, the material properties of the concrete are the same as those used in the one-dimensional problem.

Figures 6-8 give the development of mechanical damage, first principal stress and gas pressure for the concrete with permeability of $1x10^{-19}m^2$ and relative humidity of 65%. The most severely damaged zone occurs almost at the same location as the maximum stress, but in a different location to the maximum gas pressure. Moreover, the maximum stress (i.e., about 8MPa) is much higher than gas pressure (~1MPa). Therefore, the damage is mainly caused by the thermally induced stress and not by the gas pressure.

For further investigation of the role played by thermally induced stresses, another case using extremely low relative humidity (10%) and high permeability ($1x10^{-17}m^2$) was run. As seen in Fig. 9, very low gas pressure is built-up since the low moisture content is easily transported and dissipated.

However, the damage pattern is almost the same as the former case (see Fig. 6). This means that thermally induced stresses can themselves lead to the occurrence of damage, even for concrete where pore pressure build-up is very small, because thermally induced stresses can be built-up rapidly to a higher value than the tensile strength of the concrete.

To illustrate the importance of pore pressure for concrete of low permeability and high relative humidity, where higher pore pressure is expected to build-up, simulation using a relative humidity of 80% and a permeability of $1x10^{-21}m^2$ was performed (Fig. 10). As can be seen, although a higher maximum gas pressure is built-up, it seems not to have significant effect on the damage pattern.

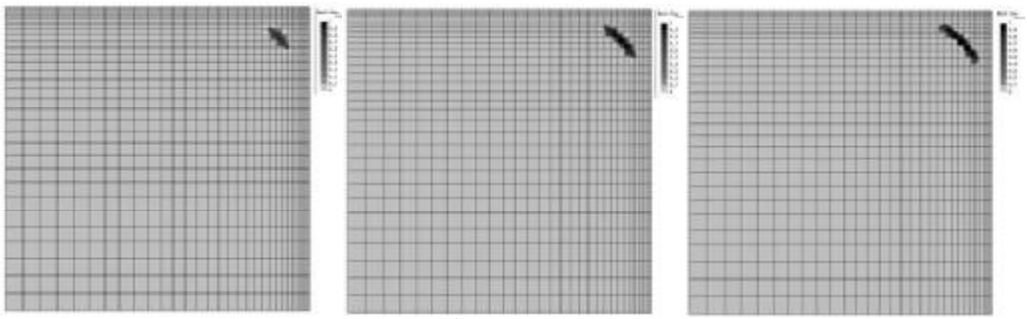

Fig. 6 Evolution of damage. Perm. = $1x10^{-19}m^2$; R. H. = 65%; at (a) 160s; (b) 180s and (c) 200s

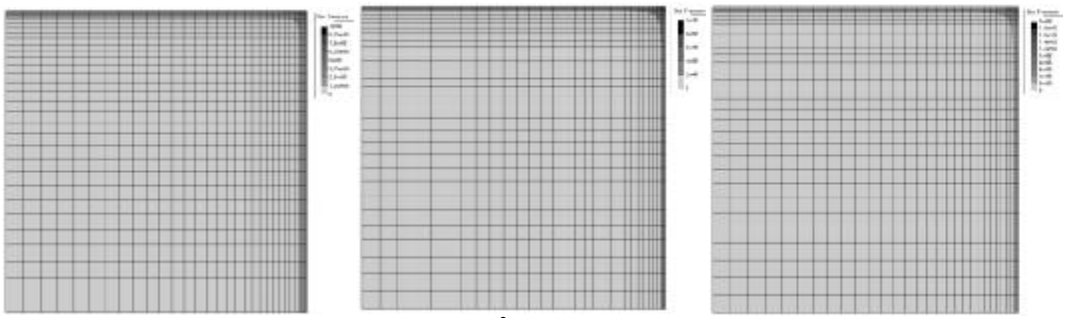

Fig. 7 Evolution of gas pressure. Perm. = $1x10^{-19}m^2$; R. H. = 65%; at (a) 160s; (b) 180s and (c) 200s

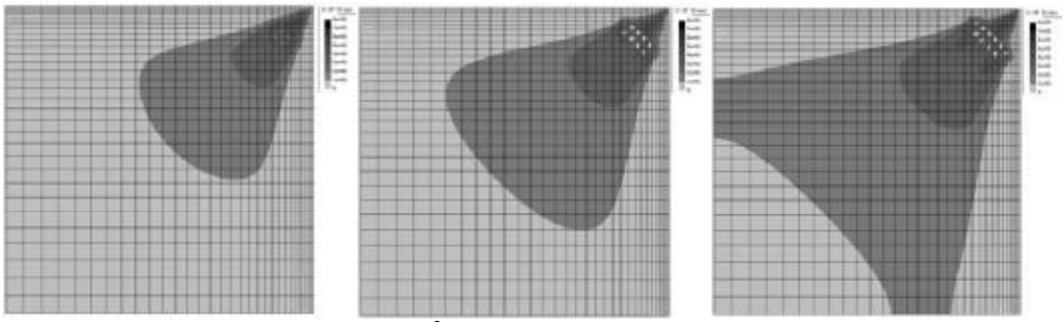

Fig. 8 Evolution of stress. Perm. = $1x10^{-19}m^2$; R. H. = 65% at (a) 160s; (b) 180s and (c) 200s

Fig. 9 Distributions of: (a) mech. dam; (b) gas pre. (c) stress. Perm.=$5x10^{-17}m^2$; R.H.=1%; t=200s

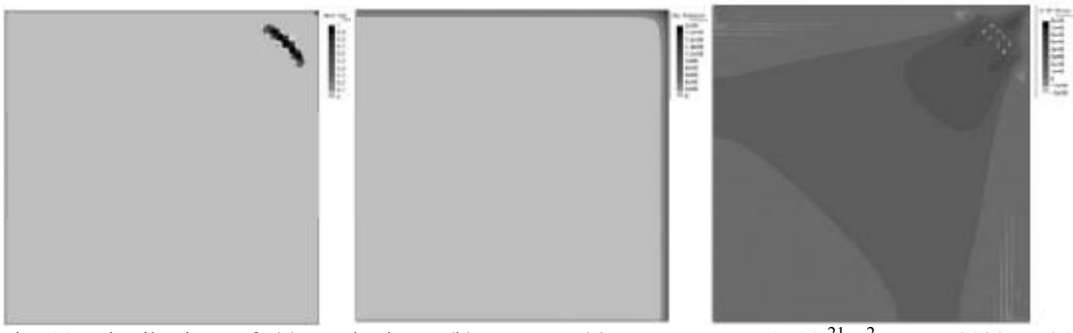

Fig. 10 Distributions of: (a) mech. dam.; (b) gas pre.; (c) stress. Perm.=$1x10^{-21}m^2$; R.H.=80%; t= 200s

REFERENCES

[1] Anderberg, Y. (1997). "Spalling phenomena of HPC and OC." International Workshop on Fire Performance of High-Strength Concrete, Gaithersburg, MD.

[2] Kalifa, P., Menneteau, F.-D., and Quenard, D. (2000). "Spalling and pore pressure in HPC at high temperatures." *Cement and Concrete Research* 30 1915-1927.

[3] Phan, L. T. (1996). "Fire performance of high-strength concrete: A report of the state-of-the-art." NIST, Gaithersburg, MD.

[4] Gawin, D., Majorana, C. E., and Schreßer, B. A. (1999). "Numerical analysis of hygro-thermal behaviour and damage of concrete at high temperature." *Mech. Cohes.-Frict. Mater.*, 4, 37-74.

[5] Stabler. (2000). "Computational modelling of thermo-mechanical damage and plasticity in concrete," PhD, The University of Queensland.

[6] Khoury, G. A., Majorana, C. E., Pesavento, F., and Schrefler, B. A. (2002). "Modelling of heated concrete." *Magazine of Concrete Research*, 54(2), 71-101.

[7] Tenchev, R., and Purnell, P. (2005). "An application of a damage constitutive model to concrete at high temperature and prediction of spalling." *Int.l J Solids Struct*, 42 (26), 6550–6565.

[8] Gawin, D., Pesavento, F., and Schrefler, B. A. (2006). "Towards prediction of the thermal spalling risk through a multi-phase porous media model of concrete." *Comput. Methods Appl. Mech. Engrg.* , 195 5707–5729.

[9] Davie, C. T., Pearce, C. J., and Bicanic, N. (2006). "Coupled heat and moisture transport in concrete at elevated temperatures - effects of capillary pressure and absorbed water." *Numerical Heat Transfer, Part A*, 49, 733-763.

[10] Davie, C. T., Zhang, H. L., Pearce, C. J., and Bicanic, N. (2008). "Computational modelling of concrete exposed to fire: the effects of coupled hygro-thermal-mechanical behavour on the development of spalling in concrete structures." The 5th International Conference for Structures in Fire, Singapore.

A THEORETICAL MODEL FOR RC COLUMNS SUBJECTED TO NATURAL FIRE

Yao Yao[a], *Tan Kang Hai[b]

[a]ExxonMobil Upstream Research Company, Houston, Texas, USA

[b]Nanyang Technological University, School of Civil and Environmental Engineering, Singapore

(*corresponding author)

INTRODUCTION

In the European and the American codes, the design of reinforced concrete (RC) columns exposed to fire is generally based on the national and international code recommendations. They are largely derived from empirical test results under the standard ISO 834 or ASTM E119 fire curves. In view of the current global trend towards performance-based design, it is helpful and necessary to develop a simple, robust and yet rational design method for structural engineers to calculate the fire resistance of RC columns under natural fire conditions. Drawing from the limitations of standard fire curve, it is important to extend the Rankine method for RC columns under natural fire conditions. This takes account of actual fire load, ventilation conditions and thermal characteristics of compartment walls. It should be noted that failure of a particular column in a fire scenario does not in itself signify the collapse of an entire structure.

1 FIRE MODELLING ANALYSIS FOR RC COLUMNS

Generally, there are three phases in the fire resistance calculations, viz. fire modeling, heat transfer and structural analysis. The benchmark tests consist of fire modeling using either Ozone software or parametric fire curves. Through the heat transfer process, the predicted thermal field is then input into finite element software SAFIR to determine the mechanical responses of RC columns subject to elevated temperature. In the same sequence, for heat transfer analysis, the authors adopt a time-equivalence approach coupled with empirical formulas (Tan and Yao 2003). This is then followed by the application of Rankine method for fire resistance calculations. A well-established finite element computer code SAFIR is available for the simulation of the mechanical response of steel, concrete, and composite structures under elevated temperatures (Dotreppe et al. 1999). Since the software has been validated with extensive test data, in the absence of available test results for columns subjected to natural fire conditions, the authors used SAFIR as a numerical tool for the development of the proposed methodology. This paper presents a framework to deal with the fire resistance of RC columns in a natural compartment fire. The emphasis is on the proposed methodology and simplifications based on Rankine method. Thus, it represents a performance-based approach taken at the member level.

For design purpose, a formula recommended in Eurocode 1 (1994) can be applied. The equivalent time of exposure to ISO 834 fire test t_e (min) is given by:

$$t_e = k_b w Q_f \tag{1}$$

where k_b (min m2/MJ) is a parameter to account for different compartment linings; it depends on thermal conductivity k, density ρ, and specific heat c of compartment materials, and the value of k_b is given in Table 1; Qf is the fire load (MJ/m2) of floor area and the ventilation

factor w is given by: $w = \left(\frac{6.0}{H_c}\right)^{0.3}\left[0.62 + \frac{90(0.4-\alpha_v)^4}{1+b_v\alpha_h}\right] > 0.5$; Hc is the compartment height (m); αv =Av/Af=BvHv/L1L2 for $0.05 \le \alpha_v \le 0.25$; αh =Ah/Af =BhHh/L1L2 for $\alpha_h \le 0.20$; if there is no horizontal opening, $\alpha_h = 0$; L1, L2 are the length and width of fire compartment, respectively; Bv, Hv are the width and height of vertical opening, respectively; Bh, Hh are the width and height of horizontal opening, respectively, and $b_v = 12.5(1+10\alpha_v - \alpha_v^2)$; Af is the floor area (m2) of the compartment; Av is the total area (m2) of vertical wall openings; Ah is the total area (m2) of horizontal roof openings.

It is instructive to compare the temperature-time predictions of fire gas in the compartment using time equivalence, zone modeling, and parametric fire curves, since temperature has a direct effect on fire resistance calculations. For a compartment which has geometrical and thermal conditions given in Table 1, the respective equivalent time t_e and gas temperature T_{ISO} corresponding to different fire loads and ventilation factors are given in Table 2a. Table 2b and Table 2c show the time t_d when a fire reaches its maximum temperature T predicted by parametric fire curves and Ozone, respectively. Comparing Table 2a with Table 2b and 2c, it shows that the time equivalence formula consistently gives higher estimates of equivalent ISO 834 temperature, thus leading to conservative lower column fire resistance. Besides, the applicable range of time equivalence (Table 2a) is limited compared with the parametric fire curves (Table 2b) and Ozone (Table 2c). However, for fire load equal to 200 MJ/m^2, the parametric fire predictions are not comparable with time equivalence and Ozone predictions.
To verify the approach for design purpose, a range of generalized design fire curves are presented with geometry and materials defined in Table 2. It should be noted that Ozone can only be used to calculate the temperature-time relation of single compartment and sprinklers are assumed to be out of order. The following fire load and compartment parameters are used in Ozone: Fire load density of 200, 400, 800, 1200 MJ/m^2 of floor area; Vertical ventilation factors $A_v\sqrt{h}/A_t$ of 0.02, 0.04, 0.08 and 0.12 m$^{0.5}$; Horizontal ventilation factor $\alpha_h = 0$; Compartment construction – concrete.

Table 1. Geometrical and thermal conditions of analyzed compartment

Compartment Length L_1	5.0 m
Compartment Width L_2	5.0 m
Compartment Height H_c	3.0 m
Ventilation Opening Height H_v	2.0 m
Ventilation Opening Width B_v	0.778, 1.556, 3.111, 4.667 m
Enclosing Boundary	Walls, ceiling and floor all of heavy concrete Density ρ 2300 kg/m^3 Specific Heat c 1230 J/kg K Thermal Conductivity k 1.3 W/mK Thickness 0.200 m

Table 2a. Equivalent time and peak temperature of the gas temperature

Time Equivalence	Q_f = 200 MJ/m^2		Q_f = 400 MJ/m^2		Q_f = 800 MJ/m^2		Q_f = 1200 MJ/m^2	
	t_e(min)	T_{ISO}(℃)	t_e(min)	T_{ISO}(℃)	t_e(min)	T_{ISO}(℃)	t_e(min)	T_{ISO}(℃)
v_f = 0.02	25	815	49	915	98	1019	147	1079
v_f = 0.04	15	739	30	842	61	948	92	1009
v_f = 0.08	9	663	18	766	36	869	54	930
v_f = 0.12 (note: not applicable)								

Table 2b. Peak temperature/time of Eurocode parametric fire curves

Parametric Fire curve	Q_f = 200 MJ/m^2		Q_f = 400 MJ/m^2		Q_f = 800 MJ/m^2		Q_f = 1200 MJ/m^2	
	t_d(min)	T (℃)	t_d (min)	T (℃)	t_d(min)	T (℃)	t_d (min)	T (℃)
v_f = 0.02	27	384	55	559	109	699	164	754
v_f = 0.04	20	261	27	700	55	788	82	841
v_f = 0.08	20	261	20	593	27	882	41	944
v_f = 0.12	20	261	20	593	20	806	27	1006

Table 2c. Peak temperature/time of zone modeling analysis (Ozone)

Parametric Fire curve	Q_f = 200 MJ/m^2		Q_f = 400 MJ/m^2		Q_f = 800 MJ/m^2		Q_f = 1200 MJ/m^2	
	t_d(min)	T (℃)	t_d (min)	T (℃)	t_d(min)	T (℃)	t_d (min)	T (℃)
v_f = 0.02	23	540	40	600	100	740	138	780
v_f = 0.04	17	640	21	730	45	860	65	930
v_f = 0.08	15	740	17	800	27	920	37	990
v_f = 0.12	12	760	16	840	25	990	35	1060

Note: v_f=0.02, α_v=0.062; v_f=0.04, α_v=0.124; v_f=0.08, α_v=0.249; v_f=0.12, α_v=0.373; (the idea of time equivalence is not applicable)

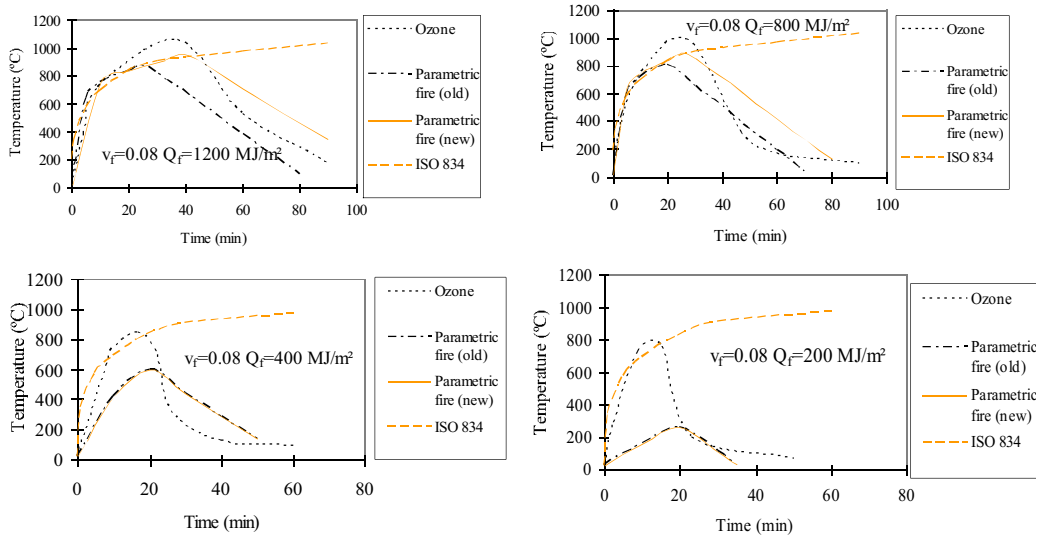

Fig. 1. Gas time-temperature relationship predictions by Ozone and Parametric fire curve

Due to the limit of paper length, only part of the comparison is presented here, as shown in Fig. 1, in which Q_f is the fire load and v_f is the ventilation factor. Basically, it is found that the predicted heating curves by different zone modeling and parametric fire equations are similar

for Q_f greater than 200 MJ/m^2; the higher the fire loads, the greater the similarity in predictions by zone modeling and parametric fire curve equations. However, for fire loads equal or smaller than 200 MJ/m^2, Ozone gives very conservative predictions compared with parametric fire equations. It should be noted that for Q_f less than 200 MJ/m^2, most columns will not fail and therefore, the comparisons are only academic. Moreover, it can be found that predictions of modified parametric fire curves in the new edition (EC1 2003) are closer to Ozone predictions compared with the old version (EC1 1994) for higher fire loads (say above 400 MJ/m^2). And for smaller fire loads (say less than 400 MJ/m^2), the two versions of the parametric fire curves give similar predictions. However, for fire loads smaller than 200 MJ/m^2, both editions of parametric fire curves have significant differences compared with Ozone predictions. From comparison, it can be concluded that for most cases, the new parametric fire curves and Ozone give similar predictions to temperature-time relationship of the compartment. Thus, both methods can be applied to verify the time equivalence approach.

2 STRUCTURAL ANALYSIS

Having presented the fire modeling calculations, this section presents the comparison of fire resistance calculations using Rankine method and finite element program SAFIR. SAFIR accommodates various elements for different idealizations, calculation procedures, and various material models for incorporating the stress-strain behavior. The stress-strain material laws are generally linear-elliptic for steel and nonlinear for concrete. SAFIR can be used for performing two different types of calculation, namely, thermal and structural analyses.
The Rankine formula has the following form:

$$\frac{1}{P_R} = \frac{1}{P_p} + \frac{1}{P_e} \tag{2}$$

where P_R, P_p and P_e are the Rankine load, plastic collapse load, and elastic critical load, respectively.

Although it is derived for ambient-temperature analysis, the Rankine formula can be extended to columns in fire conditions by taking account of the deterioration of material properties at elevated temperatures (Tang et al. 2001). Thus, Eq. (2) can be expressed as:

$$\frac{1}{P_R(t)} = \frac{1}{P_p(t)} + \frac{1}{P_e(t)} \tag{3}$$

where t is the time of fire exposure.

The capacity of a real column in fire conditions may be less than that expected from Eq. (2), as both the plastic collapse load and elastic critical load are over-estimated by ignoring secondary effects such as load eccentricity and initial crookedness. The reduced plastic collapse load $P_{pr}(t)$ and the reduced elastic critical load $P_{er}(t)$ are introduced to account for secondary effects. Thus, if the secondary effects are significant, a modified form of Rankine formula can be used:

$$\frac{1}{P_{Rr}(t)} = \frac{1}{P_{pr}(t)} + \frac{1}{P_{er}(t)} \tag{4}$$

where $P_{Rr}(t)$ is the reduced Rankine load for imperfect columns.
The following equations are useful in dealing with the modified Rankine formula:

$$P_{pr}(t) = u_{pr} P_p(t) \text{ and } P_{er}(t) = u_{er} P_e(t) \tag{5}$$

where u_{pr} and u_{er} are the plastic load reduction factor and elastic critical load reduction factor,

respectively. The values can be obtained from the method recommended by Tang et al. (2001).

There are 4 steps in the Rankine method to determine the fire resistance of RC columns (Tan and Yao 2003). The first step is to determine the equivalent ISO 834 fire exposure time. The second step is to calculate the plastic squashing and elastic buckling loads of columns, followed by the third step to determine the imperfection parameter which explicitly includes secondary effects such as load eccentricity. The last step is to calculate column failure loads. Although the proposed method is developed based on standard fire curve, for general conditions, different heating rates can be incorporated into the proposed method by applying the time equivalence formula. . To verify the proposed method, a series of case studies for RC columns is conducted in the following section.

3 CASE STUDY FOR RC COLUMNS UNDER NATURAL FIRE

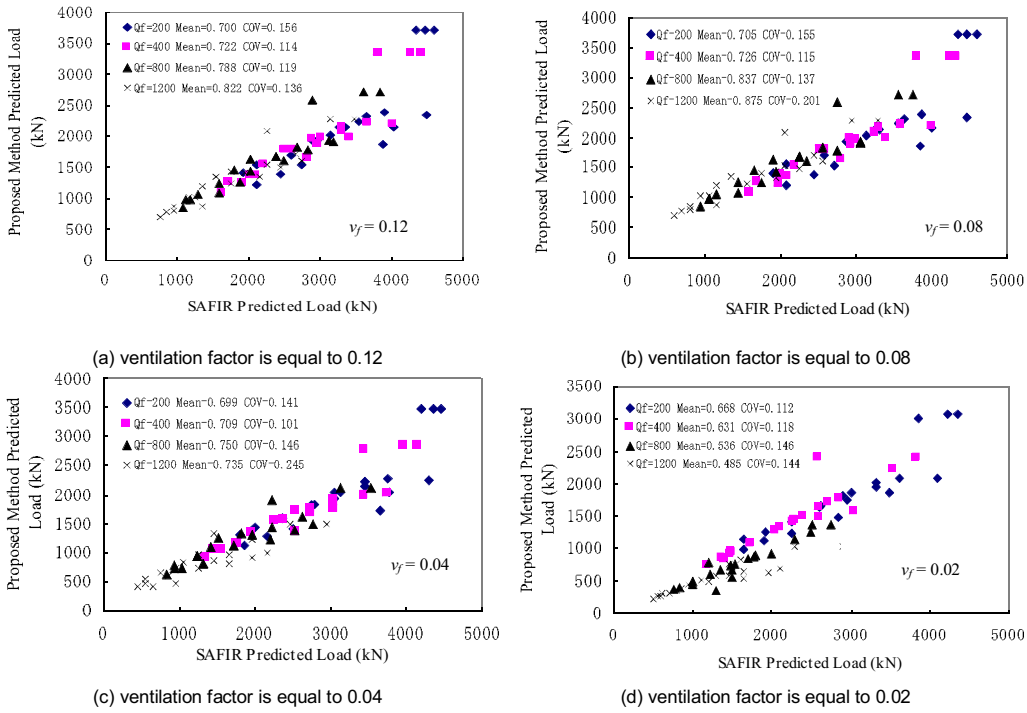

Fig. 2. Comparison of RC columns failure load under different heating conditions predicted by the proposed method (with Euro code formula) and SAFIR (with Ozone modeling); fire loads from 200 to 1200 MJ/m2

For more general heating conditions, the predictions of the proposed method are compared with SAFIR and Ozone. The fire resistance predictions of a large pool of RC columns with different slenderness ratios (from 20 to 100), load levels (from 20 to 80% of design load) (100 to 4500 kN), load eccentricities *e/h* (from 0 to 0.4), cross section areas (from 200×200 to 600×600mm^2), concrete strengths (from 20 to 80 MPa), and concrete covers (from 20 to 60mm) were analyzed. The comparisons between the proposed approach (using Eq. (1) to

predict equivalent ISO 834 fire exposure time t_e) with Ozone and SAFIR predictions corresponding to fire loads from 200 to 1200 MJ/m^2, and ventilation factors from 0.02 to 0.12 are given in Fig. 2. From the comparison study, the predictions by the proposed method are consistent and conservative with a mean value ranging from 0.699 to 0.875, and a COV of 0.101 to 0.245 for ventilation factors ranging from 0.04 to 0.12. The conservative predictions of the proposed method may be due to the physical meaning of the concept of time equivalence as discussed before. Thus, the approach is suitable for design purpose under natural fire conditions. However, it should be noted that when the ventilation factor is 0.02, the predictions by the approach are too conservative. This is partly because the predictions by zone modeling may not be accurate within this range.

4 CONCLUSION

A theoretical model based on Rankine method is proposed to predict the fire resistance of RC columns. Comparison between zone modeling, parametric fire curves, and time equivalence are first conducted. Based on time equivalence formula recommended in the EC 1 (1994), the Rankine method can be applied to different fire curves. A large pool of columns with different slenderness ratios, load levels, eccentricities, cross sectional areas, material strengths and concrete covers have been analyzed with Zone modeling, parametric fire curves and Finite Element program SAFIR. Comparisons of predictions between the Rankine method (combining with the Eurocode time equivalence formula) and SAFIR (with fire curves predicted by Ozone) are performed. The results show that the proposed method can be safely applied for design purpose for most natural fire curves and for different thermal boundary conditions in a compartment fire. Only when the ventilation factor is equal to 0.02, the proposed method is too conservative.

5 ACKNOWLEDGEMENT

The authors would like to acknowledge funding support from the Ministry of Education, Singapore, for research project titled “Failure modes and ultimate strength of tubular joints under elevated temperatures” with account number ARC 2/07.

REFERENCES

[1] Dotreppe, J.C., Franssen, J.M. and Vanderzeypen, Y. “Calculation Method for Design of Reinforced Concrete Columns under Fire Conditions,” ACI Structural Journal, 1999, V. 96, No. 1, 9-18.

[2] Eurocode 1 (1994). “Basis of design and Actions on Structures. Part 2-2: Actions on structures Exposed to Fire,” European Committee for Standardization.

[3] Eurocode 1 (2003). “Basis of design and Actions on Structures. Part 2-2: Actions on structures Exposed to Fire,” European Committee for Standardization.

[4] Tan, K.H. and Yao, Y. (2003). “Fire Resistance of Four-Face Heated Reinforced Concrete Columns”, J. of Struct. Engrg. ASCE, 129(9), pp. 1220-1229.

[5] Tang, C. Y., Tan, K. H. and Ting, S. K. (2001). “Basis and Application of a Simple Interaction Formula for Steel Columns under Fire Conditions,” J. of Struct. Engrg., ASCE, 127(10), 1214 –1220.

DIFFERENT TYPES OF PRE-STRESSED HOLLOW CORE PANELS
And their fire resistance according to Eurocodes

Radim Čajka[a], Pavlína Matečková[a]

[a] VSB – Technical University Ostrava, Faculty of Civil Engineering, Ostrava, Czech Republic

INTRODUCTION

Calculation of the fire resistance demands apposite determination of temperature distribution in the cross-section (heat-exposure model) and analysis of mechanical responses of the structure exposed to increased temperature (structural response model).
The transient thermal array was solved numerically using FEM analysis and appropriate computer program.
Mechanical response of pre-stressed cross-section was analysed on the basis of published dependences of thermal and mechanical characteristics of concrete and pre-stressing steel on temperature.
The temperature distribution in the cross-section, mechanical behaviour of the structure and final fire resistance are compared with test results (if available).

1 HEAT-EXPOSURE MODEL

1.1 Air in hollow core

Analysis of transient thermal array in hollow core cross-section demands setting up of boundary conditions and thermal characteristics of concrete and air in hollows. Boundary conditions are given in Eurocode 1 [2] by standard time-temperature curve and parameters of convection and radiation. Thermal characteristics of concrete are given in Eurocode 2 [3]. Thermal characteristics of air in hollows were determined on the basis of inverse analysis. Several reports about testing the fire resistance of pre-stressed panel are available. During the fire resistance testing both the temperatures on unexposed side and the temperatures in cross-section were measured.
The basis of inverse analysis were thermal properties of air. Comlex process of convection in hollow cores is defined in a simplyfied way through substitutive coefficient of thermal conductivity [4].

1.2. Comparison of measured and calculated temperatures

In the Table 1 calculated and measured temperatures are presented. Temperatures on the bottom of hollow and temperatures on unexposed side are compared for pre-stressed panel Spiroll 250 mm. Measured and calculated temperatures on the bottom of hollow respond with acceptable divergence, calculated temperatures on unexposed side are significantly higher then measured temperatures. Inverse analysis was elaborated so that the measured and calculated temperatures respond together, but the temperatures on the bottom of hollow in preference because it is nearer the reinforcement. Besides, measured temperatures are represented with average values and measured temperatures have wide variance, even temperatures measured on particular panel.

Table 1. Spiroll 250 mm, calculated and measured temperatures

	Temp. on the bottom of hollow			Unexposed side		
	calculation	measurement		calculation	measurement	
Time	EN	panel 1	panel 2	EN	panel 1	panel 2
min	°C	°C	°C	°C	°C	°C
0	20	12	11	20	11	11
15	112	92	46	21	12	11
30	202	225	115	32	14	15
45	261	347	162	55	23	34
60	307	413	238	84	33	49
90	379	472		148	53	

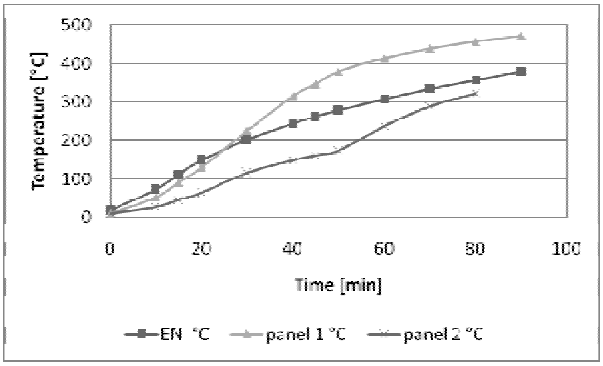

Fig. 1. Spiroll 250 mm, calculated and measured temperatures

1.3. Comparison of different types of panel

In the Table 2 calculated temperatures for different types of hollow core panels are presented. Temperatures in reinforcement and temperatures on unexposed side are compared for pre-stressed panel, thickness 200 mm, type Echo with oval hollow core and type Elematic with circle hollow core, see Fig.2. Temperatures both in reinforcement and on unexposed side are more favourable for panel Echo due to higher portion of concrete in cross-section. Insulation limit state is 90 minutes for panel type Echo and 60 minutes for panel type Elematic.

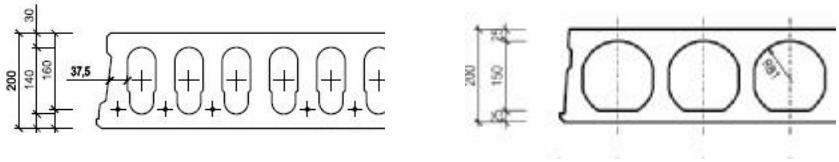

Fig. 2. Different types of pre-stressed panel, Echo 200 mm, Elematic 200 mm

Table 2. Temperatures in cross-section, Echo 200 mm, Elematic 200 mm

	Echo		Elematic	
Time	reinfor.	unexposed	reinfor.	unexposed
min	°C	°C	°C	°C
0	20	20	20	20
15	119	21	118	25
30	246	31	261	55
45	333	57	362	102
60	396	90	438	151
75	447	126	498	196
90	489	160	549	237

2 STRUCTURAL RESPONSE MODEL

2.1 Load bearing capacity and fire resistance

Mechanical response of pre-stressed cross-section was analysed on the basis of published dependences of concrete and pre-stressing steel mechanical characteristics on temperature. In the Table 3 fire resistance 40 minutes of pre-stressed panel Elematic is determined according to final version of Eurocode 2 [3], see Fig. 3. As the thermal properties of concrete and parameters of heat transfer are more favourable according to P ENV version of Eurocode, the fire resistance according to P ENV version was stated to value 45 minutes. Laboratory testing of fire resistance was quitted for panel 1 after 65 minutes and for panel 2 after 74 minutes, fire resistance on the basis of laboratory testing was settled 45 minutes.
In the Table 4 fire resistance determined for panel Echo and Elematic is compared and again is more favourable for panel type Echo. In the Table 4 the concrete cover is also analysed. Higher concrete cover responds to mildly decrease of load bearing capacity for permanent design situation but significant increase of fire resistance.

Table 3. Fire resistance, Elematic 200 mm

Time	reinforcement		concrete		$M_{Rd,fi}$	$M_{ed,fi}$
min	Temp °C	Strength MPa	Temp °C	Strength MPa	kNm	kNm
0	20	1593	20	41,67	66,24	40,22
15	118	1543	25	41,67	64,19	40,22
30	261	1241	55	41,67	51,91	40,22
45	362	889	102	41,64	37,39	40,22
60	438	575	151	40,62	24,31	40,22
75	498	328	196	39,68	13,91	40,22
90	549	257	237	38,04	10,92	40,22

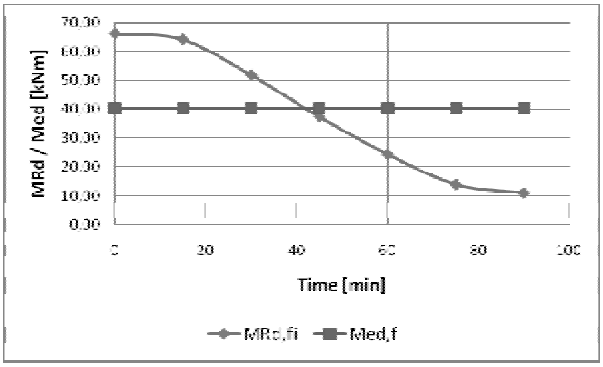

Fig. 3. Elematic 200 mm, fire resistance determination

Table 4 . Fire resistance, Echo 200 mm, Elematic 200 mm

Type of panel	Elematic		Echo	
Reinforcement	5 x cable 9,3 mm		6 x cable 9,3 mm	
Weight [kg.m^{-2}]	240		315	
Concrete cover [mm]	35	40	35	40
Bearing capacity [kNm]	57,5	55,7	68,56	66,41
Fire resistance [min]	40	50	45	60

2.2 Decrease of pre-stressing force

Decrease of pre-stressing force during the fire influences especially deformation of particular panel. Owning to irregular decrease of pre-stressing force and reinforcement strength the bearing capacity of pre-stressing panel could be exceeded. Decrease of pre-stressing force in fire resistance calculation was considered according to *Eq. (1):*

$$P(\theta) = A_s.\varepsilon_s(\theta).E_s(\theta) \tag{1}$$

where $P(\theta)$ pre-stressing force versus temperature
A_s area of reinforcement
$\varepsilon_s(\theta)$ specific thermal elongation of reinforcement versus temperature
$E_s(\theta)$ modulus of elasticity of reinforcement versus temperature

Specific thermal elongation versus temperature is creasing function and modulus of elasticity versus temperature is descending function. After multiplying those functions the result $P(\theta)$ form local minimum. Decreasing values of pre-stressing force for Elematic 200 mm are sequenced in the Table 5.

Table 5 . Decrease of pre-stressing force, Elematic 200 mm

Time	Temp.	ε	E	ΔP	P
min	°C		Gpa	kN	kN
0	20	0,000000	195	0,00	284,76
15	118	0,001034	190	50,80	233,96
30	261	0,002675	177	122,38	162,38
45	362	0,003946	163	166,36	118,40
60	438	0,004946	138	176,36	108,40
75	498	0,005767	106	158,74	126,02
90	549	0,006490	93	155,94	128,82

3 SUMMARY

In the paper the fire resistance of pre-stressed hollow core panels is analysed. Calculation of transient thermal array in cross-section is based on inverse analysis and measured and calculated temperatures confrontation. Field of temperature and final fire resistance is compared for different types of pre-stressed panel, Echo 200 mm with oval hollow core and Elematic 200 mm with circle hollow core. Calculated temperatures and final fire resistance are more favourable for panel Echo due to higher portion of concrete in cross-section. Concrete cover was also analysed. Higher concrete cover responds to mildly decrease of load bearing capacity for permanent design situation but significant increase of fire resistance. Decrease of pre-stressing force is also mentioned.

ACKNOWLEDGMENT

This outcome has been achieved with the financial support of the Ministry of Education, Youth and Sports of the Czech Republic, project No. 1M0579, within activities of the CIDEAS research centre.

REFERENCES

[1] Zidkova, P., Fire resistance calculation of concrete slab structures with respect to physical and geometrical non-linearity, *PhD. thesis*, 2004 (in Czech)

[2] CSN EN 1991-1-2: Eurocode 1: Actions on structures, part 1-2: Action on structures – Action on structures exposed to fire, CNI, 2004

[3] CSN EN 1992-1-2, Eurocode 2: Design of concrete structures, part 1-2: General rules – Structural fire design, CNI, 2006

[4] Sazina, M., Kmonicek, V.: Heat, SNTL, Prague 1989 (in Czech)

EFFECT OF TEMPERATURE ON THE BEHAVIOUR OF CONFINED FIBER REINFORCED HIGH STRENGTH CONCRETE

U.K. Sharma, C.R. Babu , P. Bhargava and V.K. Gupta

Deaprtment of Civil Engineering, Indian Institute of Technology Roorkee, Roorkee, India

INTRODUCTION

With the development and application of high strength concrete (HSC), understanding of its behavior when subjected to elevated temperature in the event of fire is needed to insure its safe application [1]. HSC exhibits superior performance in many aspects e.g. possesses high strength, duarability and workability. Given the many benefits of HSC and its increased use in structural applications, it is essential that the fundamental behavior of HSC at elevated temperatures be understood to ensure that structural fire design involving HSC will be safe. Recently, some studies have been conducted to investigate the performance of HSC at elevated temperature [2-3].

In the structural design, inelastic deformability to the structural elements is ensured by providing sufficient amount of lateral confining steel. The requirements of confinement are well established now at ambient temperature, however, it remains to be seen that how confined concrete would behave after having exposed to elevated temperature. Further, the use of fibers in concrete at ambient and elevated temperature has also picked up recently [4]. In view of the above, the present study aims to establish the behavior of confined fibre reinforced HSC after exposure to a single cycle of high temperature.

1. EXPERIMENTAL PROGRAM

1.1 Test specimens

One hundred specimens of 100 mm diameter and 200 mm height cylinders were cast (Table 1). These included plain and hoop reinforced cylinders in two grades of concrete with discrete polypropylene fibers at 0.1%, 0.2% and 0.3% by volume. The transverse reinforcement was provided in the form of 4 mm tor steel hoops at various spacings. The spacing varied from as small as 34 mm to as large as 85 mm so as to achieve a very light to heavy confinement. Longitudinal reinforcement of 4 numbers of 4 mm tor steel was provided for holding the transverse reinforcement in the position. Plain concrete specimens (S0V0 and V0S0) were also cast as control specimens.

1.2 Properties of materials

Two grades of High Strength Concrete of compressive strength 60 MPa and 80 MPa were designed and used in this study. The control cubes and cylinders were cast in all the two mixes to determine the compressive strength of cubes and cylinders. The specimens were cured under water (28 days) and in air (28 days) and tested after 56 days. The details of the designed concrete mixes along with the 28 days compressive strengths are given in Table 2. Ordinary Portland Cement 43 grade (OPC 43) from a single lot was used throughout the course of the investigation. Locally available river sand was used as fine aggregate. Locally available crushed stone aggregate of maximum nominal size of 10 mm was used as coarse aggregate. Commercially available high range Superplasticizer (Glenium 51) based on modified polycarboxylic ether and conforming to ASTM C494 type F and IS: 9103-1999 with specific gravity as 1.09 was used throughout the investigation. Micro Silica was obtained

from M/S Elkem (India) Private Limited was used in the present study. A fly-ash obtained from combined fields of the electrostatic precipitator of the thermal power plant at Dadri was used. Polypropylene fibers were used throughout the investigation. Physical properties of Polypropylene fibers are 0.3 mm diameter, 20 mm length and 150-170^0 C melting point.

Table 1-Details of Test Specimens

Mix	f_{ck} (f_c') (MPa)	Specimen Label	Pitch of Transverse Hoop (mm)	Fibers Volume (%)
M60	73.52 (66.33)	S0V0	-	-
		S1V1	34	0.1
		S2V1	57	0.1
		S3V1	85	0.1
		S1V2	34	0.2
		S2V2	57	0.2
		S3V2	85	0.2
		S1V3	34	0.3
		S2V3	57	0.3
		S3V3	85	0.3
M80	93.09 (83.97)	V0S0	-	-
		V1S1	34	0.1
		V1S2	57	0.1
		V1S3	85	0.1
		V2S1	34	0.2
		V2S2	57	0.2
		V2S3	85	0.2
		V3S1	34	0.3
		V3S2	57	0.3
		V3S3	85	0.3

Table.2 Concrete Mix Proportions

Mix	Cement (Kg/m^3)	Sand (Kg/m^3)	Aggregate (Kg/m^3)	Water (Kg/m^3)	Silica Fume (Kg/m^3)	Fly Ash (Kg/m^3)	Super-plasticizer (Kg/m^3)	28 days Cylinder Compressive Strength* f'$_c$ MPa	28 days Cube Compressive Strength* f_c MPa
M60	535	688	1085	166	27	0	5.35	61.63	68.61
M80	555	700	868	155	55.5	63	11.07	78.36	86.72

1.3 Heating of specimens

The tests to determine residual properties of confined fiber reinforced High Strength Concrete after subjecting to thermal loads were conducted at room temperature (27^o approx., 100^o, 200^o, 400^o, 800^o. A digitally controlled electric furnace was used to heat the specimens. After the specimens reached to desired temperature, the same temperature was maintained for 60 minutes in order to achieve steady state condition. After that, furnace was switched off in order to bring the heated specimen to room temperature. After the fire resistance test, spalling was examined with the naked eye, and weight reduction ratio was calculated by measuring the weight of specimens before and after the fire resistance test. The real time-temperature curve of the furnace and specimens are shown in Fig.1. The specimen is heated without preload at a prescribed rate to the target temperature, which is maintained until a thermal steady state is reached within the specimen. The specimen is then allowed to cool.

1.4 Residual Testing of specimens

All specimens were tested after 56 days of ageing, under axial compression. Before testing, the cylinders were capped with a rich cement paste to ensure parallel loading faces and constant height of the test specimens. The complete load-displacement and stress-strain response of confined fiber reinforced concrete was obtained by testing the specimens in a 2500 kN capacity INSTRON make Universal Testing Machine. Displacement controlled in-plane loading was applied at a relatively slow rate of 0.2 mm per minute until the specimens fails. The load is applied from top collar and all precautions are taken to avoid loading eccentricity on the specimens.

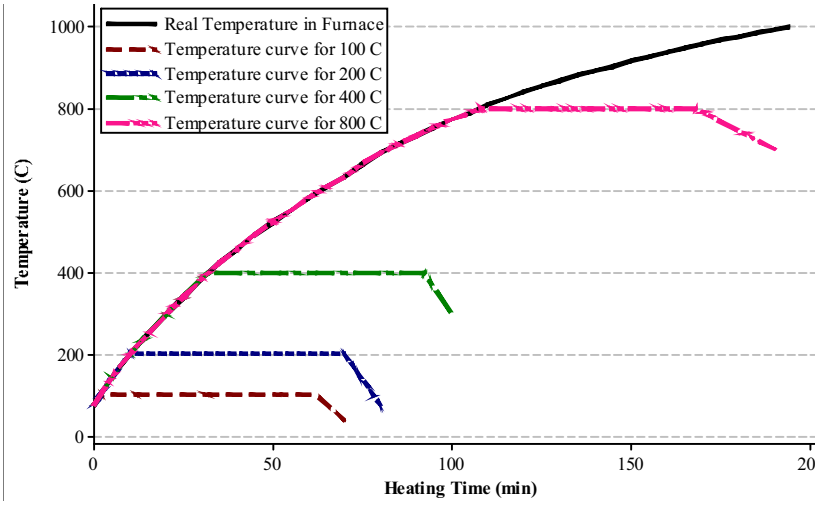

Fig.1 Temperature Curve for Electric Furnace

Before testing, the specimens were loaded and unloaded once or twice up to 5% of the expected maximum load to take care of all loose joints and reduce as much as possible the curvilinear response that would otherwise distort the initial portion of the load displacement curve. The shape of uniaxial load-displacemet curve is strongly affected by the testing conditions namely stiffness of testing machine, size and shape of specimens, rate of loading etc. and concrete characteristics like water/cement ratio, aggregate type etc. To minimize the effects of testing conditions, careful attention was exercised to avoid variation in the testing setup.

2. TEST RESULTS

The test programme included measurement of axial load, displacements and mass loss after fire test. The test results of all the specimens are given in Table 3. The discussion presented below focuses on the residual load-displacement behavior of confined fiber reinforced high strength concrete, comparing the effects of temperature, amount of transverse reinforcement, fiber volume fraction and concrete strength. Crack patterns at the time of fire test and the failure modes after the compression test are also discussed below.

2.1 Observations and Failure modes

When the specimens were heated to 100^{o} C and 200^{o} C, no cracks were found on the surface of the specimens. The specimens heated to 400^{o} C, minor cracks appeared in the specimens containing confinement and polypropylene (PP) fibers. Same minor cracks appeared, but the number of cracks was more on plain concrete specimens. At 800^{o} C, major cracks were formed on the surface for the specimens containing confined PP fiber concrete and the plain concrete specimens disintegrated completely especially for M80 plain concrete specimens. The spalling was observed in plain concrete specimens only. However, when PP fiber percentage was more than 0.1% with confinement, spalling did not occurr in any of the specimens. There are two reasons for this behavior: one is that as PP fiber in concrete melts at the high temperature (at about 170 ^{0}C) and vapor pressure is relieved. The other reason may be that lateral confinement pressure provided by the confining material is higher than the pressure induced by the internal vapor pressure. On surface of the specimens; black spots were formed after heating to 400^{o} C due to melting of PP fibers, whereas colure of the surface became ash white after heating to 800^{o} C. After the fire test the weight reduction ratios were recorded.

In the case of specimens without PP fiber and confinement, the weight reduction ratio is high as compared to the specimens with PP fiber and confinement. At 100^{o} C and 200^{o} C temperatures for M60 grade concrete specimens as the mixing ratio of PP fibers is increased there is more or less no change in the weight reducing ratios. But at 400^{o} C and 800^{o} C the weight reducing ratio is high at 0% of mixing ratio of PP fibers. When the mixing ratio of PP fibers is increased from 0% to 0.1% the weight reducing ratio is decreased. At this point it is observed that for 800^{o} C rate of decreasing of weight reducing ratio is more than that of 400^{o} C. As the mixing ratio of PP fibers is increased from 0.1% to 0.3% there is more or less no change in the weight reducing ratio both for 400^{o} C and 800^{o} C. From the Table 3, it can be observed that M80 grade concrete specimens also follow the same trend as the M60 grade concrete specimens. These results corroborate the cracking/spalling observation mentioned in previous paragraph. The effect of confinement was negligible on weight reduction ratio due to its high melting temperature. The temperature was one of the primary variables investigated extensively in the test programme. The specimens exposed to 100^{0} C and 200^{0} C, behavior and strengths are more or less same as the specimens tested at room temperature.

After 200^{o} C as the temperature was increased to 800^{o} C the displacement increased but the axial load decreased for both M60 and M80 grade concrete specimens. As the temperature increases from 200^{o} to 400^{o} C, strength ratio decreased to 0.78 and 0.85 for plain concrete and confined fiber reinforced concrete respectively. When the temperature increased from 400^{o} to 800^{o} C, strength ratio reduced drastically upto 0.2 in the plain concrete specimen, but the confined fiber reinforced concrete showed much better improvement in the behavior and strength ratio reduced to 0.4. At 0.1%, 0.2% and 0.3% volume fraction of fibers, the variation of strength ratio with the temperature is almost same.

3 SUMMARY

At high temperature, the weight reduction ratio increases as the grade of concrete increases for both plain and fiber reinforced concrete. Addition of polypropylene fibers to the concrete reduces the weight reduction ratio. The effect of fibers in reducing the weight reduction is more at high temperatures. Upto 200^0 C, the effect of temperature on the strength of concrete is negligible for both plain and confined polypropylene fiber reinforced concrete. As the temperature increases, the strength of concrete decreases.

Table 3 Test Results

		M60			M80		
Specimen Label	Tempe-rature (^{0}C)	Displace-ment (mm)	Axial Load (kN)	% Mass Loss	Displace-ment (mm)	Axial Load (kN)	% Mass Loss
S0V0	27	1.314	520.92	0	1.221	659.52	0
	100	1.287	506.15	0.248	1.319	663.43	0.253
	200	1.361	528.28	0.500	1.261	682.13	0.496
	400	1.811	404.29	5.434	1.593	501.85	5.477
	800	1.125	109.98	11.073	---	---	12.039
S1V1	27	1.465	684.40	0	1.497	814.38	0
	100	1.424	692.96	0.238	1.603	826.00	0.243
	200	1.482	688.24	0.477	1.239	830.09	0.496
	400	2.191	577.90	4.513	2.461	694.84	4.523
	800	2.964	261.30	6.398	3.055	307.56	7.747
S1V2	27	1.512	655.10	0	1.558	813.20	0
	100	1.660	649.45	0	1.583	817.91	0.254
	200	1.625	652.35	0.714	1.642	821.06	0.525
	400	2.050	558.50	3.941	1.807	691.47	4.500
	800	2.677	246.77	6.573	2.802	321.70	6.863
S1V3	27	1.494	650.78	0	1.673	802.52	0
	100	1.312	658.09	0	1.702	810.69	0.241
	200	1.620	650.15	0.246	1.626	809.12	0.512
	400	2.163	544.12	4.276	2.268	684.32	4.077
	800	2.774	238.29	6.566	2.977	315.10	6.835
S2V1	27	1.768	645.13	0	1.555	774.95	0
	100	1.524	643.01	0.239	1.704	783.28	0
	200	1.613	652.90	0.450	1.684	771.58	0.521
	400	2.161	558.26	4.282	2.197	672.93	4.847
	800	2.902	252.98	6.651	2.357	313.06	6.699

Table 3 (Contd.)

Specimen Label	Tempe-rature (^{0}C)	Displace-ment (mm)	Axial Load (kN)	% Mass Loss	Displace-ment (mm)	Axial Load (kN)	% Mass Loss
S2V2	27	1.565	606.64	0	1.548	753.67	0
	100	1.521	612.14	0.254	1.533	759.24	0.254
	200	1.447	614.73	0.515	1.601	755.63	0.522
	400	2.617	528.18	4.293	2.354	660.98	4.381
	800	2.960	232.63	6.398	2.717	288.48	6.718
S2V3	27	1.735	610.49	0	1.676	756.42	0
	100	1.398	601.77	0.238	1.534	762.70	0
	200	1.723	610.10	0.487	1.753	763.96	0.249
	400	2.314	518.91	4.208	2.304	644.18	4.381
	800	2.901	239.86	6.147	2.914	287.77	6.806
S3V1	27	1.566	575.46	0	1.626	680.39	0
	100	1.519	561.01	0.232	1.667	692.25	0.243
	200	1.482	566.51	0.500	1.617	685.10	0.514
	400	2.261	471.08	4.167	2.292	578.37	4.556
	800	3.094	209.39	6.527	2.671	244.27	6.983
S3V2	27	1.381	524.10	0	1.726	665.15	0
	100	1.538	537.68	0	1.613	659.73	0
	200	1.453	527.63	0.253	1.644	657.69	0.748
	400	2.133	413.20	4.167	2.064	553.08	4.106
	800	2.193	200.90	6.599	2.940	243.00	6.959
S3V3	27	1.308	526.92	0	1.466	657.61	0
	100	1.366	530.77	0	1.498	653.06	0.258
	200	1.232	518.24	0.723	1.572	656.83	0.480
	400	1.809	450.90	4.239	2.506	551.90	4.639
	800	2.453	205.62	6.733	2.750	257.85	6.700

At 400^0 C, the compressive strength decreases to 75 to 80% for plain concrete. Whereas for concrete containing polypropylene fibers and confinement, the compressive strength reduces to approximately 90%. At 800^0 C, compressive strength reduces to approximately 20% for M60 grade plain concrete, but for M80 grade concrete the reduction is still more. Whereas for concrete containing polypropylene fibers and confinement the average compressive strength reduces to approximately 40% for both M60 and M80 grade of concrete.

REFERENCES

1. Kodur, V.K.R., and Sultan, M.A., Effect of temperature on thermal properties of high-strength concrete, Journal of Materials in Civil Engineering, ASCE,2003, pp. 101-107.

2. Phan, L.T., Lawson, J.R. and Davis, F.L., Effects of elevated temperature exposure on heating characteristics, spalling, and residual properties of high performance concrete, Materials and Structures/Materiaux et Constructions, Vol. 34, March 2001, pp 83-91.
3. Wu, B., Su, X., Li, H. and Yuan, J.,Effect of High temperature on Residual Mechanical Properties of Confined and Unconfined High-Strength Concrete, ACI Materials Journal, Vol. 99, No.4 2002, pp. 399-407.
4. Sharma, U., Bhargava, P. and Kaushik, S.K., Behavior of Confined High Strength Concrete Columns under Axial Compression, International Journal of Advanced Concrete Technology, Japan Concrete Institute, Vol. 3. No. 2, pp. 267-281, June, 2005.

RECOVERY BEHAVIOR OF HYBRID FIBER REINFORCED HIGH STRENGTH CONCRETE AFTER FIRE EXPOSURE

Takashi Horiguchi [a], Sofren Leo Suhaendi [b]

[a] Hokkaido University, Faculty of Engineering, Sapporo, Japan
[b] STO Singapore Transportation Office, Singapore

INTRODUCTION

High-strength concrete shows particular characteristic behaviour at elevated temperatures, such as explosive spalling, that is rarely observed in normal-strength concrete. This behaviour has been attributed to the very dense concrete matrix usually associated with high-strength concrete [1-3]. Recently the addition of polypropylene fibres into high-strength concrete was reported to be very effective against the explosive spalling [4,5]. As heating increases, the fibres in the cement matrix start to melt at about 160 C and increase the total pore area. This melting effect mitigates the explosive spalling as it provides pore space in which moisture vapour can accumulate at lower vapour pressures. However, it is hopeless to maintain the residual strength and the fracture toughness when the fibres melt. Steel fibre reinforcement can help to maintain the residual strength and fracture toughness after heated.
In this point of view, authors have proposed the hybrid fibre reinforcement systems with the combination of polypropylene and steel fibres for improving the residual strength as well as the residual fracture characteristics after heating [6,7]. This paper investigates the residual properties as well as recovery possibility of heated hybrid fibre reinforced high-strength concrete.

1 EXPERIMENTAL PROCEDURE

1.1 Materials

The cement was a normal Portland cement, and river gravel (Sand stone) (5 - 20 mm of particle size) was used as the coarse aggregate and river sand was used as the fine aggregates. A maleic acid based super-plasticizer (SP), air entraining agent (AE), and bubble cutter agent (BC) were used. For bubble cutter agent, this chemical admixture was used only in the concrete mix containing fibres since this particular mix had the tendency to form more additional air bubble.
Steel and polypropylene fibres with the properties as shown in Table 1 were added into concrete mix in this study. The steel fibres came in bundles where each bundle consisted of 10 to 12 single steel fibres bound by special glue that would dissolve in water. As for polypropylene fibres, they came in fine fibrillated bundles that would disperse into monofilament fibres inside the concrete mix.

Table 1. Properties of polypropylene and steel fibres

Fiber material	Length (mm)	Shape	Denier	Effective diameter (mm)	Aspect ratio (l/d)	Specific gravity
Polypropylene	6	Fibrillated	20	0.06	100	0.9
	30				500	
Steel	30	Straight-hooked	-	0.6	50	7.8

1.2 Mix Design of Concrete

There were eleven series of concrete mix as shown in Table 2 to be tested in this experimental study. These are plain concrete, four series of polypropylene fibre reinforced concrete (PFRC), two series of steel fibre reinforced concrete (SFRC), and four series of hybrid fibre reinforced concrete (HFRC). In this mix proportions, all series had the same value of these factors: water to cement ratio (W/C) of 0.3, sand to aggregate ratio (s/a) of 60 %, and unit water content of 170 kg/m^3. The main factor differentiated each series of concrete mix was the fibres. The valuable included fibre material (polypropylene fibre, steel fibre, and combination of the two fibres), fibre volume fraction (Vf), fibre length (lf), and Vf composition. The Vf composition in hybrid fibre reinforced concrete was selected intentionally so that correlation between single type fibre reinforced concrete and hybrid fibre reinforced concrete could be maintained.

Table 2. Mix design of plain and fibre reinforced high-strength concrete

Series	Code	w/c	s/a (%)	Fiber volume (%)		SP[1] (% x c)	AE[2] (A)	BC[3] (T)
				pp	steel			
Plain	Plain	0.3	60	~	~	1.3	7	~
PFRC 6 - 0.25	P6-0.25			0.25	~	1.3	3	1
PFRC 6 - 0.5	P6-0.5			0.5	~	1.3	3	1
PFRC 30 - 0.25	P30-0.25			0.25	~	1.7	3	2
PFRC 30 - 0.5	P30-0.5			0.5	~	1.9	3	2
SFRC 30 - 0.25	S30-0.25			~	0.25	1.3	3	1
SFRC 30 - 0.5	S30-0.5			~	0.5	1.3	3	1
P_6-0.25 S_{30}-0.25	H1			0.25	0.25	1.35	3	2
P_6-0.25 S_{30}-0.5	H2			0.25	0.5	1.3	1	4
P_6-0.5 S_{30}-0.25	H3			0.5	0.25	1.4	1	4
P_6-0.5 S_{30}-0.5	H4			0.5	0.5	1.5	1	4

[1] Superplasticizer= Paric FP300U

[2] Air entraining agent= Flowric AE200, 1A= 0.004% x cement (by weight)

[3] Bubble cutter agent, 1T= 0.0002% x cement (by weight)

1.3 Experimental test procedures

For fresh concrete, the performed tests included slump and air content tests. Some features of the hardened concrete like density, voids, and ultrasonic pulse velocity (UPV test according to ASTM C 597-83) were also conducted. The mian tests in this study consisted of compressive strength (ASTM C 39-86 and ASTM C 469-87a), splitting tensile strength (ASTM C 496-90), and permeability test (modified DIN 1048).
Specimens were heated using computer-controlled electric furnace. The heating rate was set at 10 ^{o}C per minute with peak temperature maintained at 200 ^{o}C and 400 ^{o}C for 2 hours.

2 TEST RESULTS AND DISCUSSION

2.1 Residual properties of heated concrete

Fig.1(a) shows the heating effect on quality of concrete based on UPV test as it detect the presence of cracks, voids, and other imperfections inside the concrete.

Fig. 1(b), and (c) show the heating effect on relative compressive strength and relative tensile strength of heated concrete, respectively. Similarly, heating effect on relative Young's modulus and relative permeability coefficient were shown in Fig. 1(d) and (e).

Generally, concrete properties will tend to undergo further deterioration with the increase in maximum temperature. In mechanical point of view, modulus of elasticity decreases very significantly compared to compressive and splitting tensile strength. Average reduction of 30%, 20%, and 15% was observed in modulus of elasticity, splitting tensile strength, and compressive strength, respectively, for specimens heated up to 200°C. For specimens heated up to 400°C, average reduction in modulus of elasticity of 70% was observed while both compressive strength and splitting tensile strength showed an average reduction of 40%.

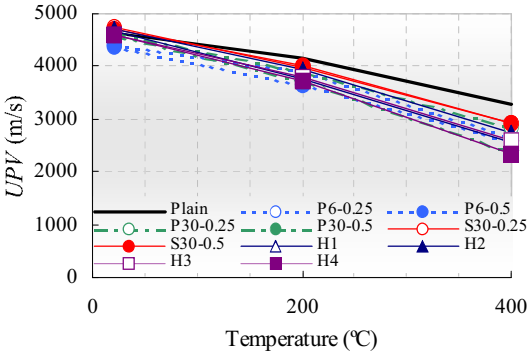

(a) Relative UPV value

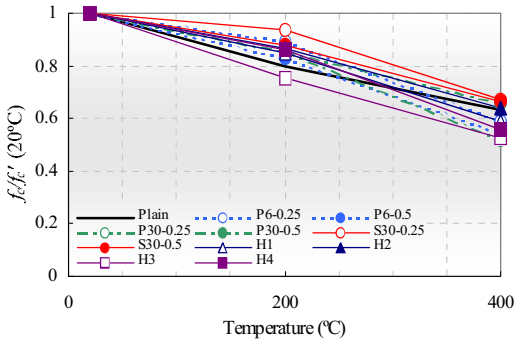

(b) Relative compressive strength

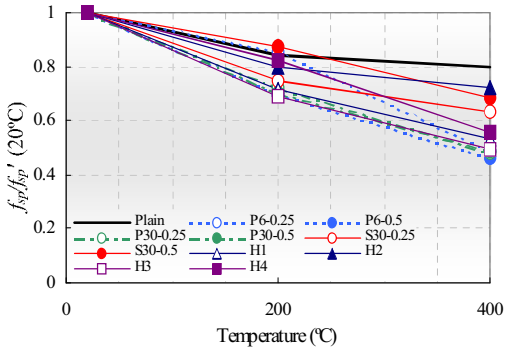

(c) Relative splitting tensile strength

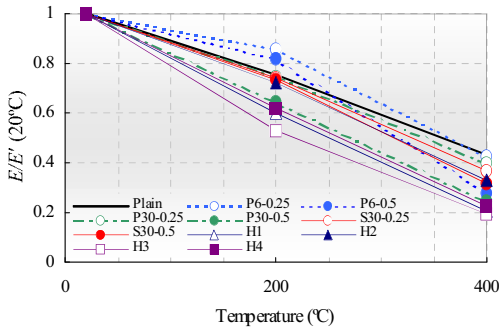

(d) Relative Young's modulus

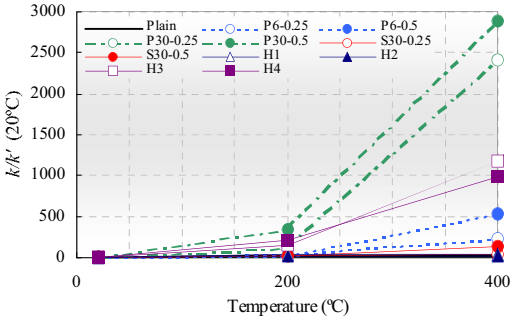

(e) Relative permeability

Fig. 1. Relative residual properties of plain and fibre reinforced concrete after heat exposure

As polypropylene fibers melted at its fusion point of 160-170°C, PFRC showed more reduction in its residual properties compared to SFRC. More inclusion of polypropylene fibers will tend to reduce most of PFRC and HFRC residual properties.
As shown in the Fig.1(c), more inclusion of steel fibers may improve the splitting tensile strength of SFRC and HFRC, especially at 400°C. Inclusion of 0.5% of steel fibers might lead to a better performance in modulus of elasticity compared to inclusion of 0.25% of steel fibers at both 200°C and 400°C, in both series also containing 0.25% and 0.5% of polypropylene fibers.
In residual permeability performance, more inclusion of polypropylene fibers will tend to reduce most of PFRC and HFRC residual permeability performance as shown in the Fig.1(e). More inclusion of steel fibers was found to be quite effective in the series also consisting 0.25% of polypropylene fibers in the HFRC, at both 200°C and 400°C. For PFRC, fiber length significantly affected the residual water permeability coefficient. The longer the fiber, the higher the residual water permeability coefficient

2.2 Recovery properties of heated concrete

Fig.2 to Fig.5 show the properties of heated concrete after being cured under ambient temperature (dry curing) and under water (saturated curing), respectively.
The compressive strength, tensile strength and Young's modulus do not seem to recover clearly in the case of heated concrete specimens being cured under ambient temperature. Meanwhile, for heated concrete specimens that had been cured under saturated curing, the recovery in UPV, compressive strength, tensile strength and Young's modulus can be observed as shown in Fig.2 to Fig.4. This might indicate that re-hydration of heated concrete had taken place for the heated specimens cured under saturated condition. The recovery rate under saturated curing showed a rapid increase in the first 2 months and slows down after that.
As shown in the Fig.5, recovery in permeability performance was observed significantly in the case where heated concrete specimens were cured under saturated condition while no significant change in these properties on heated concrete specimens under ambient temperature.

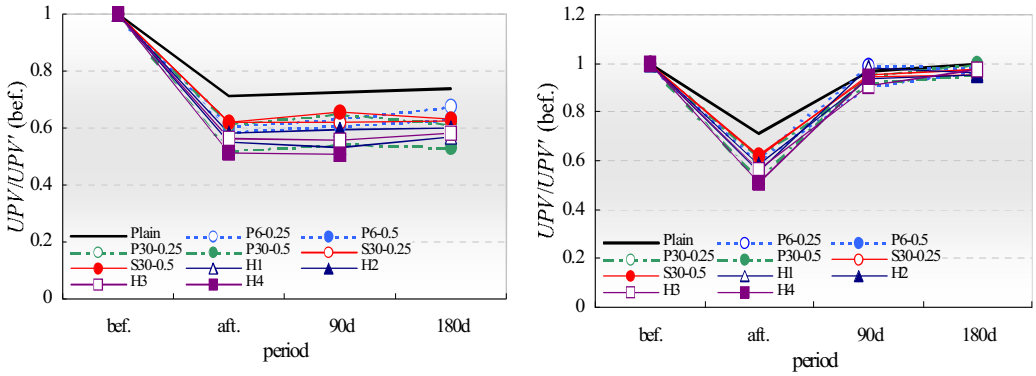

(a) Under dry curing (b) Under saturated curing

Fig. 2. Relative UPV value before and after heat exposure under dry curing

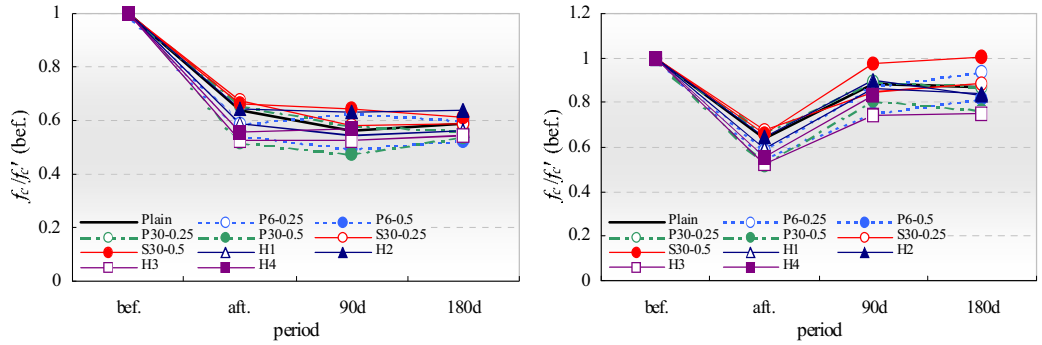

(b) Under saturated curing

(a) Under dry curing

Fig. 3. Relative compressive strength before and after heat exposure

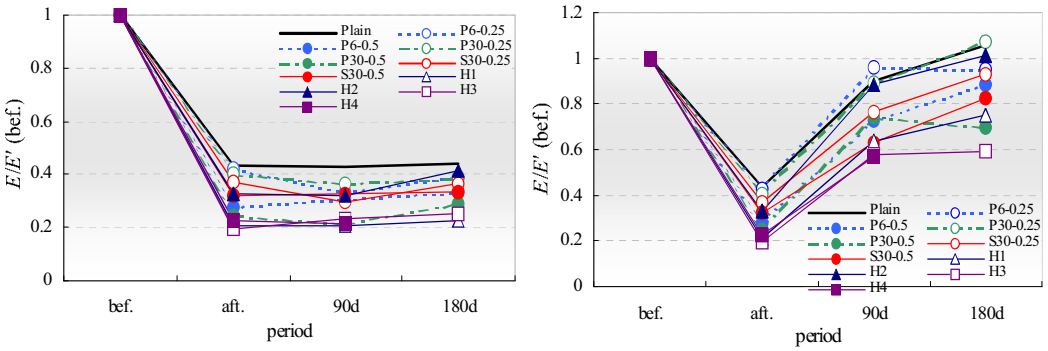

(a) Under dry curing

(b) Under saturated curing

Fig. 4. Relative Young's modulus before and after heat exposure

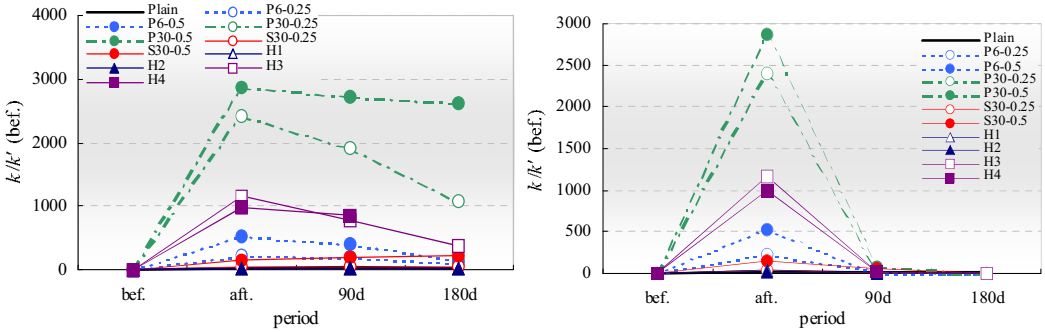

(a) Under dry curing

(b) Under saturated curing

Fig. 5. Relative permeability coefficient before and after heat exposure

3 SUMMARY

From the experimental test results, the following conclusions were made:

1. Average reduction of 30%, 20%, and 15% was observed in modulus of elasticity, splitting tensile strength, and compressive strength, respectively, for specimens heated up to 200°C. For specimens heated up to 400°C, average reduction in modulus of elasticity of 70% was observed while both compressive strength and splitting tensile strength showed an average reduction of 40%.

2. As polypropylene fibers melted at its fusion point of 160-170°C, polypropylene fiber reinforced concrete (PFRC) showed more reduction in its residual properties compared to steel fiber reinforced concrete (SFRC). More inclusion of polypropylene fibers will tend to reduce most of PFRC and HFRC residual properties, especially its residual permeability performance. On the other hand, more inclusion of steel fibers may improve the splitting tensile strength of SFRC and HFRC.

3. In residual permeability performance, more inclusion of steel fibers was found to be quite effective in the series also consisting 0.25% of polypropylene fibers in the HFRC, at both 200°C and 400°C. For PFRC, fiber length significantly affected the residual water permeability coefficient. The longer the fiber, the higher the residual water permeability coefficient

4. Properties recovery was observed significantly on heated concrete specimens cured under saturated condition compared to the ones cured under ambient temperature.

5. The recovery rate showed a rapid increase in the first two months on heated concrete being cured under saturated condition and slowed down after that

REFERENCES

[1] Ali, F.A., Connolly, R. and Sullivan, P.J.E., "Spalling of High Strength Concrete at Elevated Temperatures," Journal of Applied Fire Science, Vol.6, No.1, pp.3-14, 1996-97

[2] Phan, L.T., "Fire Performance of High-Strength Concrete: A Report of the State-of-the-Art," NISTIR 5934, NIST 1996

[3] Khoury, G.A. and Algar, S., "Mechanical behavior of HPC and UHPC concrete at high temperatures in compression and tension, "ACI International conference on State-of-the-Art in High Performance Concrete, Chicago, 1999

[4] Takano, T., Shimura, K., Horiguchi, T. and Saeki, N., "Fire Resistance of High-strength Mortars with Several Types of Fibers and Polymers," 3rd Joint Symposium on the Structural Materials between Korea & Japan, pp.65-72, 2000

[5] Horiguchi, T., Takano, T., N. Saeki, T. D. Lin, "Effect of Fiber Reinforcement on Residual properties of high strength concrete under elevated temperature," American Concrete Institute, ACI SP-209, 53-64, 2002

[6] Suhaendi, S. L. and Horiguchi, T.: Effect of short fibres on residual permeability and mechanical properties of hybrid fibre reinforced high strength concrete after heat exposition, Cement and Concrete Research, Vol.36, Issue 9, pp.1672-1678, 2006.

[7] Horiguchi, T., Watanabe, K. and Suhaendi, S. L. : Study on fracture toughness of hybrid fiber reinforced high strength concrete at high temperature environment, Proceedings of 11th International Conference on Durability of Building Materials and Components, 11dbmc, pp.117-124, 2008